# Tribology and Rheology of Biopolymer Mixtures

**Kwan Mo You**

Submitted in accordance with the requirements for the degree of

Doctor of Philosophy

The University of Leeds

School of Food Science and Nutrition

MAY 2023

The candidate confirms that the work submitted is his/her own, except where work which has formed part of jointly-authored publications has been included. The contribution of the candidate and the other authors to this work has been explicitly indicated below. The candidate confirms that appropriate credit has been given within the thesis where reference has been made to the work of others. Details of the jointly-authored publications and contribution of each authors are outlined on the next page.

Further details of the jointly-authored publications and the contributions of the candidate and the other authors to the work are included below:

**Chapter 2**

You, K.M. and Sarkar, A., 2021. Oral tribology of polysaccharides. In *Handbook of Hydrocolloids* (pp. 93-124). Woodhead Publishing.

**Chapter 3**

You, K.M., Murray, B.S. and Sarkar, A., 2021. Rheology and tribology of starch+ $\kappa$-carrageenan mixtures. *Journal of Texture Studies*, 52(1), pp.16-24.

**Chapter 4**

You, K.M., Murray, B.S. and Sarkar, A., 2023. Tribology and rheology of water-in-water emulsions stabilized by whey protein microgels. *Food Hydrocolloids*, 134, p.108009.

**Chapter 5**

You, K.M., Murray, B.S., Connell, S.D., and Sarkar, A., Fabrication and Lubrication Performance of Sustainable Pickering-like Water-In-Water Emulsions Using Plant Protein Microgels. *Advanced Materials Interfaces*, This paper has been submitted in a peer-reviewed journal.

# Details of authorship contributions:

**Kwan-Mo You**: designed the experiments and conducted the measurements, data analysis and interpretation as well as drafted and edited the manuscripts and replied to the comments from reviewers.

**Anwesha Sarkar** and **Brent S. Murray**: provided supervision, feedback and contributed to the proofreading and editing of the manuscript and to the comments from the reviewers.

**Simon D Connell**: provided methodology, writing reviewing and editing

# List of accepted conference abstracts

## Poster presentations:

**Kwan-Mo You,** Brent Murray and Anwesha Sarkar," Novel water-in-water emulsion droplets stabilized by proteinaceous microgels" Bragg, Leeds, 2022.

**Kwan-Mo You,** Brent Murray, Simon Connell and Anwesha Sarkar, "Fabrication and Lubrication Performance of Sustainable Pickering-like Water-In-Water Emulsions Using Plant Protein Microgels ", UK SPM/AFM User Meeting 2023, Leeds, 2023.

**Kwan-Mo You,** Brent Murray, Simon Connell and Anwesha Sarkar, "Fabrication and Lubrication Performance of Sustainable Pickering-like Water-In-Water Emulsions with protein particles: whey and pea proteins", SCI Formulation Forum 4th Annual Event, Lodnon 2023.

## Oral presentations:

**Kwan-Mo You**, Brent Murray and Anwesha Sarkar, "Tribology and rheology of thermodynamically incompatible biopolymer mixtures" Physics in Food and Manufacturing Conference, Leeds, UK, 2020

**Kwan-Mo You,** Brent Murray and Anwesha Sarkar, "Oral tribology and rheology of starch + κ-carrageenan mixtures", 34th EFFoST International Conference, Online, 2020.

**Kwan-Mo You**, Brent Murray and Anwesha Sarkar, "Investigation on Rheology and Tribology Properties of Starch + κC Mixtures" FOOD ORAL PROCESSING FOP2021, online, 2021

# Acknowledgements

This PhD has been a genuinely life-changing experience for me, and it would not have been possible without the help and advice of many others. First of all, I would like to express my sincere gratitude to my supervisors, Professor Anwesha Sarkar, whose excellent counsel and assistance in all areas made this possible. Their vision, genuineness, and determination have profoundly inspired me and given me confidence in my talents. Their encouragement and suggestions have aided in the development of my professional career and advancement as a scientist. Also, I would like to express my heartfelt gratitude to Professor Brent S. Murray, who have instructed and helped me a for their instructive advice and useful suggestions on publications.

I gratefully acknowledge Horizon 2020 European Research Council (ERC) Project "LubSat: Unravelling Multi-scale Oral Lubrication Mechanisms (macro-to-nano): A Novel Strategy to Target Satiety" for the financial support during my PhD course.

Many thanks to colleagues and staff at the School of Food Science and Nutrition, especially those in the Food Colloids group, for their help and encouragement during my study and for making my life in the laboratory pleasurable. I am really happy to be a member of this team. I would like to thank Dr. Efren Alberto Andablo Reyes, Dr. Stephen D. Evans. Dr. Andrea Araiza-Calahorra, Dr. Nataricha Phisarnchananan, Ben Kew, Neil Rigby, and Miles Ratcliffe in particular for their aid and support during my PhD.

Last but not least, I would want to thank my parents and friends for always being there for me and helping me in their own unique manner throughout my career. Words cannot explain how thankful I am to my amazing family for their unending love and support. This thesis is dedicated to each and every one of you!

# Abstract

The thesis discusses the field of tribology and its growing recognition in the context of oral processing of structured biopolymer mixtures. The tribological properties of polysaccharides, particularly starch and non-starch polysaccharides which are often added as thickeners in processed foods can play a critical role in altering the mouthfeel of foods and beverages. To date, there is lack of understanding on lubrication mechanism of biopolymers and combinations thereof have. Therefore, the study started experiments on rheological and tribological properties of biopolymer mixtures having the possibility of designing natural lubricants. Specifically, thermodynamically incompatible biopolymer mixtures with phase separation i.e. water-in-water (W/W) emulsions present the possibility of acting as fat-replacers which have never been investigated for their tribological properties. These W/W emulsions suffer from poor stability, which has led to the use of particles as stabilizers, including microgel particles. This study explores the potential of using both animal and plant protein-based microgels to design Pickering W/W emulsions for both stability and tribology, which has not been previously explored.

The key finding of this thesis presents the rheological, microstructural and tribological properties of W/W emulsions formed from gelatinized starch and polysaccharides (κ-carrageenan or xanthan gum) stabilized with protein microgel particles. The results show that the W/W emulsions had different rheological and tribological properties than the individual biopolymer, i.e., increasing viscosity and lowering friction at specific concentrations of the biopolymers and the microgels present at the interface compared with the corresponding weight average of the values of the individual equilibrium phases. The contribution of the water droplets in the emulsion systems, and the sizes and shapes of droplets might affect the rheological and tribological properties. In addition, the presence of microgels affected the tribological properties of the emulsions, with plant protein microgels offering higher boundary lubrication properties compared to dairy protein microgels explained by elasticity, size, softness and adhesives interaction with the surface.

Overall, the results from this thesis highlight the importance of tribology in biopolymer mixtures and shows the unique properties of sustainable Pickering W/W emulsion system with improved lubrication performance. The findings contribute to the development of eco-friendly water-based systems with potential applications in food, biomedicine, and biocatalysts

# Table of Contents

# List of Tables

# List of Figures

# List of Abbreviations

| | |
|---|---|
| $\kappa$C | kappa-carrageenan |
| CS | Corn starch |
| GS | Gelatinized starch |
| XG | Xanthan gum |
| GG | Gellan gum |
| WPI | Whey protein isolate |
| WPM | Whey protein microgel particles |
| PPM | Pea protein microgel particles |
| CLSM | Confocal laser scanning microscope |
| AFM | Atomic force microscopy |
| SPM | Scanning probe microscopy |
| QMC-D | Quartz crystal microbalance with dissipation monitoring |
| Cryo-CEM | Cryo-scanning electron microscopy |
| LVER | Linear viscoelastic region |
| DLS | Dynamic light scattering |
| PDMS | Polydimethylsiloxane |
| W/W | Water-in-water |
| O/W | Oil-in-water |
| RCF | Raw correlation function |
| PDI | Polydispersity index |
| SE | Secondary electrons |
| BSE | Backs-scattered electrons |
| MTM | Mini traction machine |
| SRR | Slide-to-roll ratio |
| MTD | Mounted tribological device |
| OTC | Optical tribological configuration |
| NSPs | Non-starch polysaccharides |
| RB | Rhodamine Blue |
| AO | Acridine Orange |
| FG | Fast green |
| EHL | Soft-elastohydrodynamic lubrication |

# List of Symbols

| | |
|---|---|
| $\Delta G$ | Gibbs free energy |
| $\gamma$ | Interfacial tensions |
| R | Particle radius |
| $h$ | Gap width |
| A | Area |
| $F$ | Shear force |
| $v$ | velocity |
| $\eta$ | Viscosity |
| $\tau$ | Shear stress |
| $\dot{\gamma}$ | Shear rate |
| $\gamma$ | Strain amplitude |
| G' | Storage modulus |
| G" | loss modulus |
| $D$ | Translational diffusion coefficient |
| $q$ | scattering vector |
| $k_B$ | Boltzmann's constant |
| $f$ | Frequency |
| D | Dissipation |
| $\mu$ | Friction coefficient |
| $F_R$ | Frictional force |
| $F_L$ or $W$ | Normal load |
| V | Moving speeds |
| $\delta$ | Film thickness |
| $U$ | Entrainment speed |
| $\eta_\infty$ | High shear rate limiting viscosity |

# Chapter 1
# General Introduction

## 1.1.     Research Motivation

The World Obesity Atlas (2023) predicts that more than half of the global population will be either overweight or obese by 2035 unless significant preventative actions are taken. There is thus growing interests in food industries and research community to design reduced fat or low fat foods to reduce the overall calorie intake in diets in order to address the growing rise in food-linked obesity and associated non-communicable diseases. Often biopolymers such as starches and non-starch polysaccharides in various combinations are used as thickeners to replace calorie-dense fat and modify the textural properties of food. However, often they do not provide the necessary mouthfeel that fat tends to offer and suffer from consumer acceptability. Also, the real food physics behind such mouthfeel performance is rarely studied. Among various food colloidal strategies, oil-free "water-in-water emulsion" is a promising template where biopolymers can be mixed to design droplets dispersed in a water phase replicating the behaviour of fat droplets. However, their kinetic stability is an important challenge to address. Of more importance, their mouthfeel properties remain principally unexplored. Hence, providing insights into stabilization and lubrication performance of water-in-water emulsions can help to design next generation low calorie food. It may also provide new insights into cosmetic, and pharmaceutical industries, among others where designing oil-free stable water-based emulsions are of growing interests to address biocompatibility and sustainability.

**Thesis objective:** This PhD thesis aims to investigate the rheological and tribological properties of biopolymer mixtures, with a specific focus on understanding the interplay between the two components and how it affects the overall behaviour of water-in-water (W/W) emulsions. A key challenge to address in these 'oil-free' W/W emulsion systems is a lack of lubrication performance compared to 'oily' systems. Lubrication from oil droplets has a major effect on sensory perception, including sensory descriptors as "cream", "fatty" and "smooth" *etc.* Replacing oil droplets with aqueous solutions can be challenging. However, one could hypothesize improving the lubrication performance of such aqueous systems by structuring structured with biopolymers, taking inspiration from nature-engineered lubricants such as tears,

synovial fluids, saliva, *etc* (Jin et al., 2016a, Limbert et al., 2019, Mann and Tighe, 2016a, Sarkar et al., 2019c). However, often these 'oil-free' W/W emulsions suffer from poor kinetic stability. Low-molecular-weight surfactants are not able to offer any additional stabilization because the interfacial tension are orders of magnitude smaller compared with that of a typical oil-water interface. Therefore, "Pickering stabilization, *i.e.*, using particles as stabilizers, including microgel particles offers a promising strategy to improve their stability. Hence, choosing an optimized type and concentration of hydrocolloids for W/W emulsion, as well as designing relevant biocompatible particles and understanding how presence of such particles at the W/W interface offers lubricity in addition to stability, is our key objective. In summary, our goal is to provide multiscale understanding on the lubrication behaviour of mixed hydrocolloid systems, especially Pickering-like W/W emulsions stabilised my microgel particles which have never been reported in the literature to date.

**Thesis hypothesis**: We hypothesis that W/W emulsions exhibit better lubrication properties than each pure hydrocolloid in single phase by virtue of their viscous properties and aqueous lubrication.

## 1.2. Background

### 1.2.1. Mixed hydrocolloid systems

Hydrocolloids are an important category of natural biopolymers that are widely used in different industrial sectors to perform certain functions such as thickening, gelling, structuring, stabilization, encapsulation, *etc*. The combined use of two or more hydrocolloids is even more common than the simple use of an individual hydrocolloid. This is because an individual hydrocolloid cannot often provide the required properties and functionalities, especially when the design of processed food products (Gao et al., 2017). Therefore, understanding the behaviour of mixed hydrocolloid systems, including their molecular interactions, phase behaviour, microstructures, and resulting properties and functionalities, are important for extending the utilities of existing hydrocolloids and imparting novel functionalities for improved product formulation.
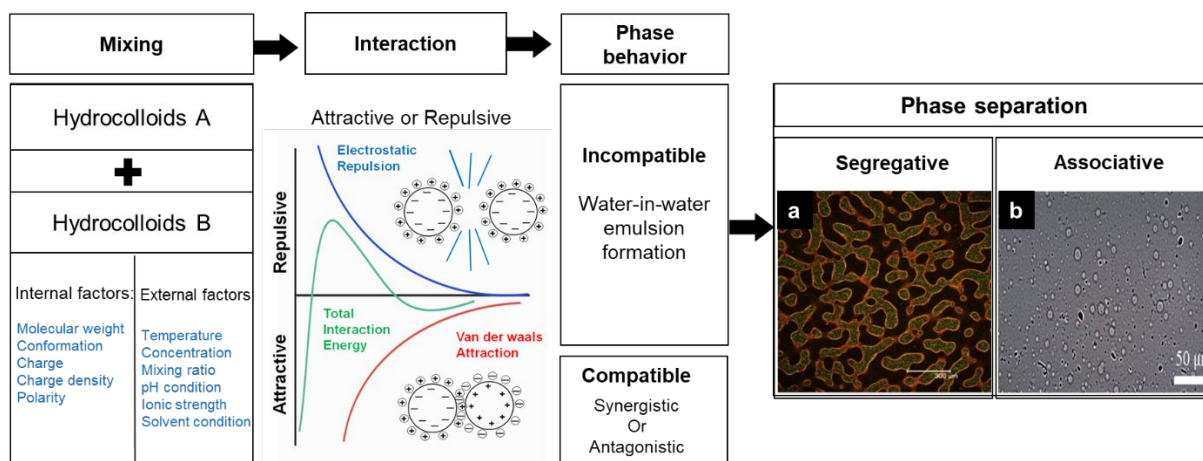
**Figure 1.1** Diagram of a general guide to understanding the interactions and phase behaviour of mixed hydrocolloid systems. **Fig. 1.1a** shows CLSM image illustrating segregative phase-separating mixture of 8% starch + 9% gelatin at 40 °C in a 24 h old (adapted from Firoozmand et al. (2009)) and **Fig. 1.1b** shows optical micrographs of water droplets inside 1 wt% GS + 0.3 wt% $\kappa$C phase separating W/W emulsions (**Chapter 4**).

**Figure 1.1** provides a general guide to the behaviour of mixed hydrocolloid systems and illustrates the factors and approaches that could be utilized to control the behaviour. Intrinsic molecular parameters and external experimental factors together dictate the nature (attractive vs repulsive) and magnitude of molecular interactions between two hydrocolloids when mixed in different max ratio. This results in different phase behaviour, including compatible and incompatible (associative vs segregative) mixtures. For compatible mixtures, the two hydrocolloids mix homogeneously at the molecular level and could produce two effects, that is, synergistic vs antagonistic effects. For incompatible mixtures, depending on the phase composition and temperature, the mixture undergoes phase separation via two different mechanisms, that is, nucleation and growth vs spinodal decomposition. The different phase separation mechanisms normally lead to different microstructures, which can be further deformed and frozen/entrapped by applying different physical and chemical approaches, such as shearing, gelation, *etc*. (Turgeon et al., 2003). Phase separation provides rich opportunities for designing and optimizing properties and functionalities of mixed hydrocolloid systems. In phase-separating mixtures, synergistic and antagonistic effects are even more complex than in compatible mixtures, as they are not only determined by molecular interactions but also are greatly influenced by the phase behaviour.

The large number of available hydrocolloid combinations provides tremendous possibilities for modern product design in the food, cosmetic, and pharmaceutical industries, *etc*. To

understand the resulting properties and functionalities of mixing hydrocolloid systems, it is important to clarify their molecular interactions and phase behaviour. The fundamental knowledge of the thermodynamics and kinetics of mixed hydrocolloid systems, together with the knowhow of processing conditions and parameters, enable the development of advanced applications for microstructure design, purification, thickening, gelation, emulsification, foaming, encapsulation, film formation, *etc*. In this thesis, we designed the biopolymer mixtures *via* specific hydrocolloids particularly using starch as they are orally responsive with the high possibility of synergism when mixing with other hydrocolloids such as $\kappa$-carrageenan and xanthan gum, which is discussed later.

### 1.2.2. Water-in-water Emulsions

Water-in-water (W/W) emulsions are colloidal dispersions composed of two thermodynamically incompatible immiscible aqueous phases (Esquena, 2016). These emulsions consist of droplets of one aqueous phase distributed in another aqueous phase. They are generated in aqueous mixes of at least two water-soluble compounds that are incompatible in solution. Water-water phase separation occurs in a wide range of systems, such as aqueous combinations of polymers, polymers and surfactants, polymers and electrolytes, and surfactant solutions (Wang et al., 2022, Dickinson, 2019). It is well-known, for instance, that the addition of salting-out electrolytes to hydrophilic polymer solutions may result in the formation of two immiscible aqueous solutions: a polymer-rich phase and a salt-rich phase (Bulgariu and Bulgariu, 2013). The phase separation typically observed in micellar solutions of non-ionic surfactants at temperatures over the cloud point of the surfactant is another classic example of an aqueous biphasic system. Typically, phase separation in aqueous two-phase systems occurs between seconds to a few hours. Due to the lack of considerable inter-droplet repulsion forces, the colloidal stability of droplets in such systems is weak, and as a result, emulsions in many aqueous biphasic systems are frequently severely unstable (Esquena, 2016, Dickinson, 2019). With the inclusion of particles, it is possible to generate Pickering-like stable water-in-water emulsions, since the colloidal stability may be significantly modulated (Nicolai and Murray, 2017). The phenomena of phase separation in aqueous mixes of two hydrophilic polymers are currently well-documented, and exhaustive reviews have been written (Esquena, 2016, Dickinson, 2019, Vis et al., 2015a, Hazt et al., 2020).
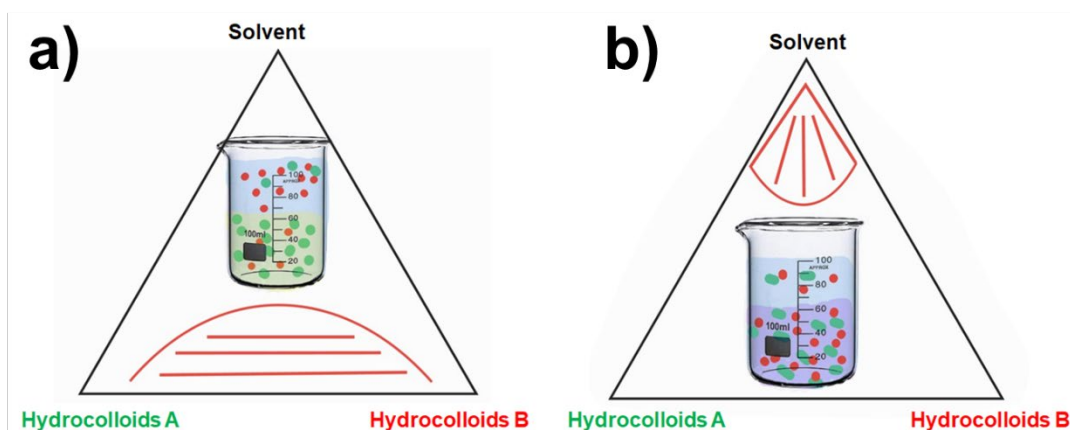
**Figure 1.2.** Schematic ternary phase diagram of a) segregative and b) associative phase separations and the corresponding partition of hydrocolloids A (green) and B (Red) in different phases.

When repulsive interactions dominate the interactions between two hydrocolloids, segregative phase separation will occur. In this sort of phase separation, the two hydrocolloids are incompatible and are separated into two distinct phases, with each phase being rich in one hydrocolloid and deficient in the other (**Fig 1.2a**). Segregative phase separation is perhaps the most frequent kind of phase separation found in hydrocolloid mixtures. This is because homotypic interactions such as those between two neutral hydrocolloids, two hydrocolloids with identical charges, or a neutral and charged hydrocolloid mixture are often more common than heterotypic ones. In addition, the entropic drive to mix between two macromolecular hydrocolloids is far less important than the enthalpic drive to segregate. **Fig. 1.2a** depicts a typical phase diagram of segregative phase separation in a common solvent, very often, water. In the lower concentration range, the two hydrocolloids are molecularly miscible, but phase separation occurs at higher concentrations. The most critical and empirically accessible characteristics that determine segregative phase separation are temperature, ionic strength, and molecular weight (Morris, 2009). As a general rule, reducing temperature facilitates segregation by shifting the phase boundary to a lower concentration range. This is because reducing the temperature reduces the proportional impact of mixing entropy (Fang, 2021). In the case of charged hydrocolloid mixtures, the counterions associated with the hydrocolloids would form a barrier to segregation since the uneven distribution of tiny counterions in various phases is entropically unfavourable (Dickinson, 2009). Additionally, increasing molecular weight promotes phase separation. This can also be attributed to an entropic factor, as blending hydrocolloids with

higher molecular weights is less favourable from an entropic standpoint than mixing those with lower molecular weights. Increasing molecular weight also leads to an increase in depletion interaction, which promotes segregation (Li et al., 2009).

When the total interactions between two hydrocolloids are attractive, associative phase separation will occur. **Fig. 1.2b** depicts a typical associative phase separation diagram. In this form of phase separation, two hydrocolloids with high affinity are condensed together in one phase, leaving the other phase depleted. Associative phase separation is also known as complex coacervation, in contrast to simple coacervation, in which a single hydrocolloid, such as gelatin, phase separates from its solvent, such as an ethanol-water combination (Schmitt et al., 1998). Typically, associative phase separation is found between hydrocolloids with mutually opposite charges, notably between proteins and charged polysaccharides (Goh et al., 2020). Although electrostatic repulsion is the most typical driving factor for associative phase separation, it should be noted that other attractive interactions, such as hydrophobic or hydrogen bonding interactions, might potentially result in the same. For example, gelatin and $\kappa$-carrageenan exhibited hydrogen-bonding-induced associative phase separation when the temperature reached the coil-to-helix transition point of gelatin following cooling (Wang et al., 2015). In addition, at larger concentrations, associative phase separation might be inhibited or completely vanish. As opposed to segregative phase separation, associative phase separation can occur at extremely diluted hydrocolloid concentrations. This is owing to a higher concentration of accompanying counterions, which inhibit electrostatic interactions between charged hydrocolloids (Fang, 2021). Schmitt et al. (1998) demonstrated that pH, ionic strength, mixing ratio, concentration, charge density, and conformations of hydrocolloids are crucial parameters governing associative phase separation. The pH range that induces associative phase separations is dependent on the categories of hydrocolloid combinations, and should generally correspond to a pH range in which the two hydrocolloids have opposite charges. Associative phase separation occurs for protein/negatively charged polysaccharide at isoelectric point of the protein. In the case of proteins and positively charged polysaccharides, pH must be greater than the isoelectric point. For hetero protein combinations such as lactoferrin and $\beta$-lactoglobulin, associative phase separation occurs at pH values between two isoelectric points (Flanagan et al., 2015).

In the absence of both oil and surfactant, W/W emulsions offer a vast array of applications that have grown substantially over the years, taking advantage of their water-only com-

position. Clarifying the molecular interactions and phase behaviour of mixed hydrocolloid systems is critical for understanding their characteristics and functions. Knowledge of the thermodynamics and kinetics of mixed hydrocolloid systems, as well as processing settings and parameters, enables the creation of sophisticated applications for microstructure design, purification, thickening, gelation, emulsification, foaming, encapsulation, film formation, *etc.*

### 1.2.3. Pickering emulsions

The accumulation of particles at the interface and their stabilising impact is well-known for O/W emulsions and is reviewed often (Sarkar and Dickinson, 2020, Sarkar et al., 2019d, Murray, 2019, Zembyla et al., 2020, Dickinson, 2020). These particles-stabilized emulsions are commonly referred to as Pickering emulsions, after one of the phenomenon's discoverers (Pickering, 1907) though it was first reported by Ramsden a few years before (Ramsden, 1904).
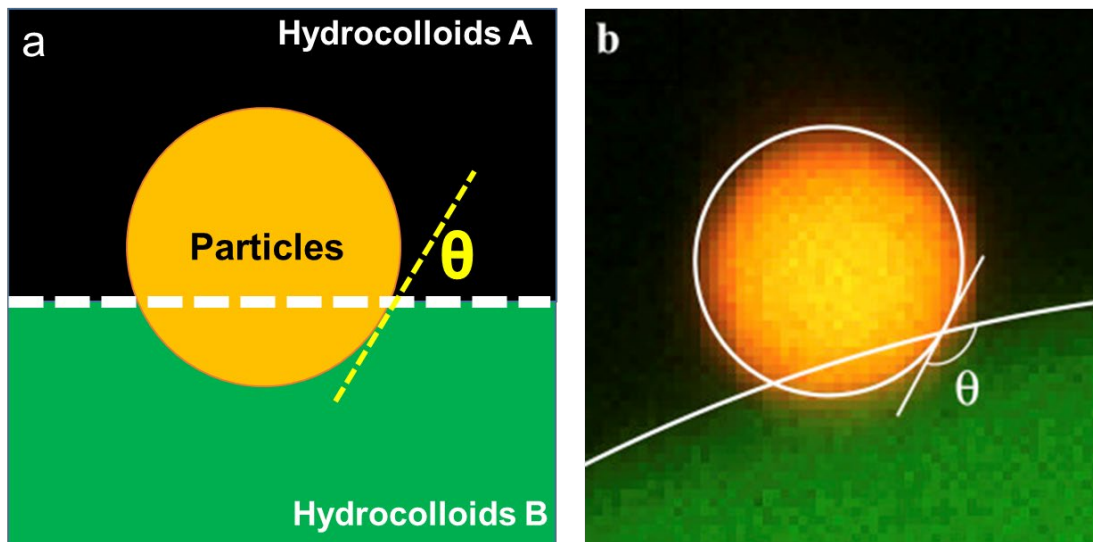


**Figure 1.3.** Schematic illustration (a) of a particle at the water-water (W-W) interface between hydrocolloids A and B. *θ* is the contact angle of the particle at the interface. (b) latex particle at the surface of large dextran droplet in polyethylene oxide (PEO) phase, adapted from Balakrishnan et al. (2012) with permission from Elsevier.

The mechanism that continues keeping the particles at the interface is the increase of the free energy ($\Delta G$) when departing particles between phases A and B increase interfacial area. Since the particle at the interface is exposed to both phases, $\Delta G$ can only be decreased if the difference between the interfacial tensions of the particles with phase A ($\gamma_{PA}$) and phase B ($\gamma_{PB}$) is less than that between the two phases ($\gamma_{AB}$). The area filled by spherical particles with a

radius R is equal to $\pi R^2 \cdot (1 - \cos(\theta))^2$, where $\theta$ is the three-phase contact angle of the particles with the interface, see **Fig.1.3**. $\Delta G$ equals the product of the decrease of the interfacial area by the interfacial tension:

$$\Delta G = -\pi R^2 \gamma_{AB} (1 - |\cos(\theta)|)^2 \qquad \textbf{(1.1)}$$

The contact angle is dictated by the difference in interfacial tension between phase A ($\gamma_{AB}$). and phase B ($\gamma_{PB}$):

$$\cos(\theta) = (\gamma_{PA} - \gamma_{PB})/\gamma_{AB} \qquad \textbf{(1.2)}$$

The assumption is that gravitational forces may be disregarded.

$\Delta G$ is orders of magnitude more than kinetic energy (kT) for nanoparticles in O/W emulsions as long as $(\gamma_{PA} - \gamma_{PB}) < \gamma_{AB}$, which is typically the case. However, the impact is much diminished for W/W emulsions, as the interfacial tension between the two aqueous macromolecule-containing solutions is orders of magnitude lower than that of the O/W interface and approaches zero at the critical point. Therefore, Firoozmand et al. (2009) hypothesised that the buildup of particles at the W/W interface was caused by the migration of particles from polymer solutions to the interface with a higher concentration of solvent. Nevertheless, assuming actual values for the parameters in **Eq 1.1**, it follows that even for W/W emulsions, $\Delta G$ can be significantly more than kT as long as the particles are not too small and the mixture does not near the critical point, as shown in the section that follows.

In the last four years, particle-stabilised W/W emulsions have garnered a growing interest, and it has become clear that their characteristics are notably distinct from those of particle-stabilised O/W emulsions. Until now, the majority of research has been conducted on non-food grade model particles, however, a handful of food grade W/W emulsions have also been studied using microgels particles such as whey protein microgel particles (Murray and Phisarnchananan, 2016, You et al., 2023, Gonzalez-Jordan et al., 2016, Khemissi et al., 2018). Following section includes an overview of the materials used in this thesis to prepare those biopolymer mixtures and W/W emulsions and rationale behind their selection.

## 1.3.     Material selection

### 1.3.1. Starch

Starch is one of the most abundant natural biopolymer followed by cellulose. The global output of cereals in 2020 is projected to reach at least 2500 million tons, with maize, rice, and wheat being the primary sources of starch from (WHO, 2020). Moreover, tubers (such as potatoes and yam), roots (such as cassava and taro), and legume seeds (such as pea) are also significant sources of starch. Starch is deposited in higher plants as an energy storage mechanism, and this has been proven to be a complex process (Zeeman et al., 2010). Starch is generated in plastids, and short-term storage may occur in chloroplasts, while long-term storage happens in amyloplasts, which are specialised plastids. Inside the amyloplasts, carbohydrates are stored in a granular form that is insoluble in cold water. In rice, for instance, several starch granules can form within the amyloplast. Depending on their botanical origin, the starch granules may have spherical, polygonal, elliptical, flat platelet-like, lenticular, *etc.* forms (Jane, 2007, Jane et al., 1994). Its size can range from 0.1 to 200 μm, and their size distribution is often bimodal. When selecting a starch for a certain purpose, the relative amounts of amylose and amylopectin are considered to be of utmost importance. Amylose content is frequently noted as a key element in cooking and processing quality, product texture, and digestibility or nutritional value (Jane et al., 1999). Depending on the evaluation methodology, terms such as apparent, total, and absolute amylose levels may be employed.

Starches are key functional materials throughout a broad range of water contents; hence, it is crucial to investigate the carbohydrate-water interactions in the majority of diets. Typically, starch gelatinization refers to the process through which native starches lose their crystallinity and eventually their granular form (Ratnayake and Jackson, 2008, Jane, 2007). Most of the amylopectin in the native starch granule is bound to the crystalline areas. For there to be sufficient mobility of the chains to permit the unravelling of the helices, the amorphous zones inside the granules must be mobile. Water can influence plasticization, transforming glassy amorphous areas into a flexible system, which aids in the melting of the granule's helical order (Schirmer et al., 2015, Donald, 2001). Not only is water essential during the first phases of native granule transformation, but it will also play a crucial role in altering the starch granule shape. When moisture levels and temperatures are high enough, the gelatinization process will

begin. Gelatinization temperature is the temperature at which the amylopectin crystallite and helical order are destroyed.

Various starches have varying gelatinization temperature ranges, *i.e.*, potato ≈ 54 ─ 60°C, wheat ≈ 44 ─ 58°C, maize ≈ 64 ─ 67°C, *etc* (Schirmer et al., 2015, Ratnayake and Jackson, 2008). When the natural starch granule's internal structures degrade, water can enter the granule remnant and induce swelling. This expansion of the starch is related to the step change in viscosity that occurs in many food items. The extremely inflated granule remains are vulnerable to shear stresses and become much more prone to polysaccharide loss to the surrounding solvent. Normally, the straighter chains of amylose are destroyed, leaving amylopectin and water in the granule remains that have swelled. It should not be assumed that all starch granules expand in a manner similar to that of a balloon; frequently, they create complicated three-dimensional forms. In general, cereal starches are believed to exhibit two stages of swelling behaviour, with the second needing a greater temperature than the first. Moreover, many starches preserve parts of their structure, notably fragments of the granules' outer surface. They are sometimes referred to as ghosts and can affect the clarity and texture of starch pastes (Carrillo-Navas et al., 2014, Debet and Gidley, 2007).

In this thesis (**Chapters 3, 4 and 5**), the gelatinized starch was used to make biopolymer mixtures or W/W emulsions with polysaccharides. The main reason for using starch in the biopolymer mixture and emulsions was that starch is responsive to salivary amylase and thus can breakdown during oral processing influencing lubricity. Numerous studies have been conducted on the thermodynamic incompatibility of starch and non-starch hydrocolloids since the 1962 work on the phase separation of aqueous polysaccharides (Alloncle and Doublier, 1991, Closs et al., 1999, Conde-Petit et al., 1997, Kulicke et al., 1996, Murray and Phisarnchananan, 2014, Tolstoguzov, 2006). These polysaccharide mixtures are utilized in a wide variety of foods where phase separation is a concern, and it has been demonstrated previously that this may occur in the absence of Pickering-like particles (Achayuthakan and Suphantharika, 2008, Ptaszek et al., 2009, Simonet et al., 2000).

### 1.3.2. Polysaccharide

Polysaccharides are carbohydrate polymers in which sugar units are connected by O-glycosidic connections created by the condensation of the hemiacetal hydroxyl group of one sugar with a hydroxyl group of another sugar unit (Stick and Williams, 2010). They are derived

from various plant components (*i.e.*, seeds, exocarp, leaves, etc.) after little processing (*i.e.*, rice or potato starch) or after extraction from food industry byproducts (*i.e.*, pectin). Algae (*i.e.*, alginates and carrageenan), arthropods (chitin), and bacteria are other sources (*i.e.*, xanthan and gellan gum). Modest structural variations, such as the kind of connections, isomeric forms, functionalization, as well as the branching and periodicity of the backbone monomers, result in a considerable degree of structural variety and functional differences in polysaccharides (Wrolstad, 2012). Very often, multiple polysaccharides coexist in the same source, such as in plant cell walls, where pectin, cellulose, and arabinoxylans with radically different physico-chemical characteristics can coexist. In this thesis, polysaccharides and amylopectin molecules (gelatinized starch) with distinct conformational shapes have trouble creating simple mixtures, even at very low concentrations, and this resulted in their phase separation which was investigated. Although a detailed literature review is included in **Chapter 2** on polysaccharides and their tribological properties, here we include rationale behind choice of polysaccharides used in the experimental part of the thesis.

## 1.3.2.1.*κ*-Carrageenan

Carrageenan is a natural ingredient that is extracted from red seaweed, specifically from a type of seaweed called Irish moss. It has been used for centuries as a thickener and stabilizer in food and other products (Rochas and Rinaudo, 1984). It is a hydrocolloid, which forms a gel when mixed with water. This property allows it to be used as a thickener and stabilizer in a wide variety of food products such as dairy products, such as ice cream, and meat products (Hotchkiss et al., 2016, de Vries, 2002), and also used in other products such as toothpaste, medicines, and other personal care items (Necas and Bartosikova, 2013, Bixler, 1996). It is often used as an emulsifier, which helps to mix ingredients that would not normally mix together, such as oil and water. And it is a complex polysaccharide, which means it is a long chain of sugar molecules. Specifically, carrageenan is made up of repeating units of a sugar called galactose, which is chemically bonded together in a specific way to form the overall structure of the molecule (Necas and Bartosikova, 2013)

In **Fig. 1.4**, there are three main types of carrageenan (*κ*- kappa, *ι*- iota, and *λ*- lambda carrageenan) based on the arrangement of the galactose units: carrageenan has a linear structure with repeating galactose units and 3.6-anhydrogalactose, both sulfated and non-sulfated (Necas and Bartosikova, 2013). Carrageenan can be classified into three types based on their structure

and chemical proper-ties; kappa-carrageenan ($\kappa$C) has one sulphate group per disaccharide, iota-carrageenan has two sulphates per disaccharide, and lambda-carrageenan has three sulphates per disaccharide. They are composed of a linear galactose backbone with a varying degree of sulfatation (between 15 % and 40 %). The different carrageenan types vary in composition and conformation, resulting in a wide range of rheological and functional properties. Carrageenan also shows temperature-induced conformational transition between a coil and helix. The helices then aggregate. This aggregation creates a physical cross-link, resulting in the formation of a macroscopic three-dimensional network (Takemasa et al., 2001). Especially. $\kappa$C forms thermo-reversible gel with high strength, though the gel shows synerisis



kappa-carrageenan

Iota-carrageenan

Lambda-carrageenan
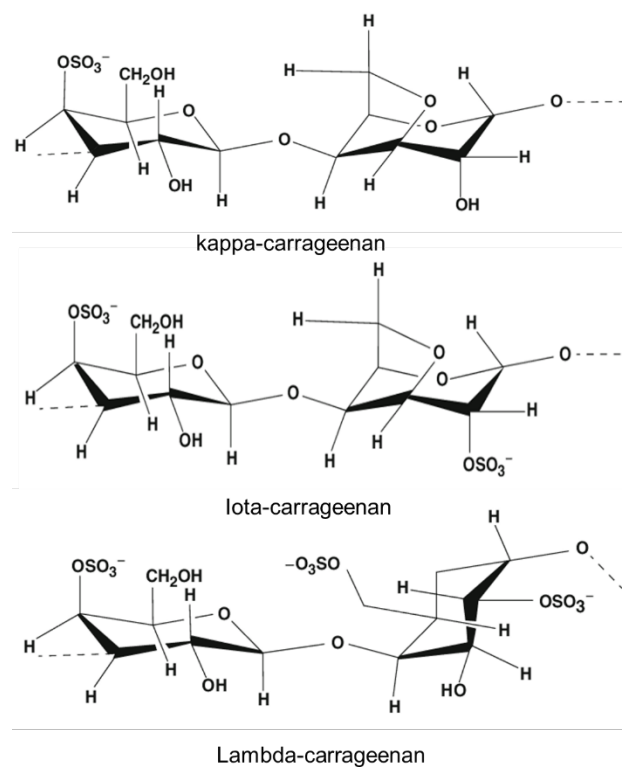
**Figure 1.4**. Chemical structure of three different types of carrageenan.

Carrageenan contains 15─40% ester-sulfate content, which makes them anionic polysaccharides, therefore they can interact with proteins at pH values above and below the isoelectric point of the proteins (Hotchkiss et al., 2016, Haug et al., 2004, Dalgleish and Morris, 1988). The capacity of anionic sulphate groups in carrageenan to create electrostatic connections with cationic patches on the hydrophilic C-terminal of kappa-casein has been ascribed to interactions above the isoelectric point of casein (Snoeren, 1976).

Interestingly, there are some investigations on phase separation between $\kappa$C and hydro-colloids (Haug et al., 2004, Lundin et al., 2000, Zhao et al., 2015, Lascombes et al., 2017). As we mentioned in **Chapter 1.2.1**, temperature, ionic strength, and molecular weight are the most important of phase separation in mixed hydrocolloids system (Morris, 2009). Interestingly, Lascombes et al. (2017) showed both compatible and incompatible phase behaviour of starch and carrageenan mixtures. Carrageenan can either preferentially adsorb on starch granules or partially penetrate into starch granules, mainly through the osmotic pressure effect or by electrostatic interactions. However, phase separation which concentrated carrageenan in the continuous water phase was also investigated when by increasing carrageenan concentration in the mixture at constant starch concentration. According to the results, one can promote an increase in the mixture interaction, which could be contributed by ionic strength. Besides, the increasing molecular weight in the mixing system could be contributed to entropic consideration, as mixing hydrocolloids of higher molecular weights is entropically more unfavourable than that of lower molecular weights, as well as leads to an enhanced depletion interaction.

The phase separation might lead to the formation of a bi-continuos structure and synergistic or antagonistic effects on various food systems. Therefore, in this thesis (**Chapters 3 and 4**), $\kappa$C was chosen to create biopolymers mixtures with gelatinized starch to understand their physicochemical and material properties including microstructure, rheology and lubricity.

### 1.3.2.2. Xanthan gum

Xanthan gum (XG) is a highly versatile ingredient due to its ability to thicken and stabilize liquids, even in small amounts, and to increase the viscosity of liquids without changing their other properties such as taste, colour or pH (Urlacher and Noble, 1997). Xanthan gum is considered to be safe for human consumption and is approved by the FDA as a food additive.
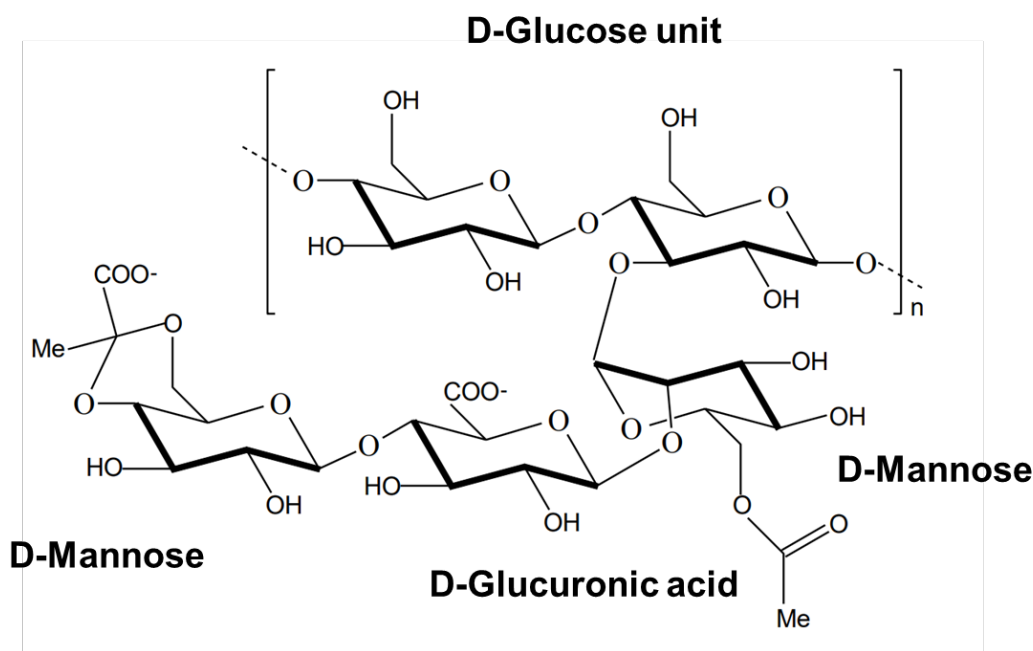
**Figure 1.5**. Chemical structure of xanthan gum.

It is also one of the complex polysaccharides, with long chain of sugar molecules (**Fig. 1.5**). The structure of XG is composed of a backbone of glucose, mannose and glucuronic acid, to which are attached side chains of mannose, glucose and glucuronic acid. The structure of xanthan gum is characterized by the presence of a trisaccharide repeat unit, composed of two glucose molecules and one mannose molecule, which are joined by glycosidic bonds (Garcıa-Ochoa et al., 2000). Xanthan gum is the negatively charged carboxyl group (COO−) on the side chains of the molecule, around pH 5 (Brunchi et al., 2016). The unique structure of xanthan gum gives it unusual properties, such as its ability to form a highly viscous solution in water, even at very low concentrations, and its ability to form a stable gel in the presence of other ingredients, such as salt or sugar (Petri, 2015). Additionally, the branched structure of xanthan gum makes it a highly effective emulsifier and thickener, allowing it to keep ingredients suspended and evenly distributed in a mixture.

Phase separation between XG and hydrocolloids has been the subject of various interesting studies (Jin et al., 2015, Hemar et al., 2001, Bryant and McClements, 2000, Moschakis et al., 2005, Sikora et al., 2008). Sikora et al. (2008) showed XG, the sole gum blended with starch pastes, was anionic due to two carboxylate groups in its side branch. Electrostatic interactions between XG and starch in their blend could anticipate a certain incompatibility. XG has

been also used as a fluid film lubricant in various studies (Andablo-Reyes et al., 2020, Torres et al., 2019, Stokes et al., 2011c, Andablo-Reyes et al., 2019), however, its properties in phase separated systems with starch remains relatively less explored. Different food systems may have either complementary or antagonistic impacts as a result of the phase separation, which may give rise to a bi-continuous structure. Hence, XG was selected to serve as a benchmark for the function of biopolymers mixtures as a natural lubricant in oral processing in this research (**Chapter 5**).

## 1.3.3. Rationale behind the selection of Pickering-like protein particles

The W/W emulsions can be stabilised by the formation of a monolayer of protein particles at the water-water interface, which is driven by the decrease in free energy caused by particle adsorption. Since native proteins were too tiny to adsorb to the interface, they are unable to stabilise water-in-water emulsions, while being good stabilisers of oil-in-water emulsions. In this thesis, water-in-water emulsions containing protein particles (Murray and Phisarnchananan, 2014, Nicolai and Murray, 2017) were used to create biocompatible emulsions which is seldom reported in literature.

### 1.3.3.1 Milk Proteins

Milk proteins are very well-characterized in literature and are mainly divided into two groups: caseins and whey proteins. The main whey proteins are β-lactoglobulin (β-lg) and α-lactalbumin (α-la) , represent about 80% and 15% respectively of the mass of industrially purified whey protein isolate (WPI) (De Wit, 1998). β-lg is a globular protein with a secondary structure mainly composed by β-sheets. It contains 162 amino acid and two disulphide bonds and a free thiol group and has a molecular weight of 18.4 kDa. In the case of α-la, it is also globular, but it exhibits a helical secondary structure. It is composed of 123 amino acids with 4 disulphide bonds and has a molecular weight of 14.2 kDa (Nicolai et al., 2011)). Both proteins possess a net negative charge at neutral pH and have an isoelectric point (pI) close to pH 5.0. Specifically, this thesis (**Chapters 4 and 5**) uses whey protein as the principal source to build microgel particles as Pickering stabilizers due to its unique ability to make Pickering emulsions for a period of weeks, whereas native proteins did not enter preferentially the interface (Li et al., 2020, Murray and Phisarnchananan, 2016, Nicolai and Murray, 2017, Sarkar et al., 2017a, Sarkar et al., 2016).

### 1.3.3.1.1.1. Whey protein isolate for designing microgel particles

Among various polymers that are available for the production of temperature-responsive microgels, food-grade proteins such as milk proteins or egg albumin have attracted significant attention since they offer the potential of creating heat-set gel structures with well-defined properties (Nicolai, 2016). Whey protein isolate (WPI) was used to design thermally cross-linked whey protein gels. When aqueous dispersions of WPI are heated above 65°C, protein gelation occurs due to heat-induced aggregation. For example, at neutral pH, heat treatment causes the unfolding of the tertiary structures as well as some secondary structures of the otherwise folded $\beta$-lg molecule. The unfolding of the globular structure causes the exposure of the free sulfhydryl group and the inner hydrophobic amino acids. Initially hydrophobic interactions followed by formation of intramolecular sulfhydryl/disulphide lead to protein aggregation and dimer formation. Further sulfhydryl-catalysed disulphide-bond interchange between the dimers create larger species, some of which are also associated with non-covalent interactions (Croguennec et al., 2004, Nicolai et al., 2011). These thermally cross-linked gels were then sheared into nano- or micro-size around 100 nm to confirm the ability to stabilise W/W emulsion (**Chapter 4).** Besides, the Pickering emulsion stabilised by whey protein particles, the microgel particles themselves was investigated to check synergy effects on lubricant behaviour, concerning rheology and tribology as microgel particls themselves are known to offer viscous lubrication (Andablo-Reyes et al., 2019, Hu et al., 2020, Torres et al., 2018, Soltanahmadi et al., 2022) or lubrication *via* a molecular ball-bearing mechanism (Sarkar et al., 2017a).

### 1.3.3.2. Plant protein (pea protein concentrate) for designing microgel particles

Protein from plants is increasingly being recognised as a viable replacement for animal-based proteins like whey protein in milk. It is now well established that the production of greenhouse gas emissions from the consumption of plant proteins is far lower than that of animal proteins (González et al., 2011, Henchion et al., 2017). Evidence of plant proteins' positive effects on a variety of health markers, including as cardiovascular and metabolic health, metabolic risk, diabetes type II, chronic illness, weight management, and mortality reduction, is mounting in the scientific literature (Ahnen et al., 2019, Hertzler et al., 2020). Historically, soy protein has been the preferred alternative plant protein (Dabija et al., 2018) due to its ability to

increase viscosity and mimic the melting properties of fat in various dairy applications (Liu, Wang, Liu, Wu, & Zhang, 2018) (Liu et al., 2018) and in meat replacement (Belloque et al., 2002). But still, it is frequently viewed adversely as an allergen and linked with off-flavors (Damodaran and Arora, 2013). Soy proteins have also demonstrated intriguing lubricating properties, with friction coefficients lowered to 0.1 when micro-particulated and reduced by an additional order of magnitude when mixed with egg white protein (Zhang et al., 2020b). Hypoallergenic pea protein has lately attracted substantial interest in product creation with soy protein.

Pea protein isolate is generated by wet processing using isoelectric precipitation or ultrafiltration, yielding a high protein content of greater than 85%. (Boye et al., 2010). It consists of two major globulins (legumin and vicilin) and one minor globulin (convicilin). Pea legumin has a molecular weight of 300-410 kDa and is composed of six polypeptides, including an acidic subunit (38-40 kDa) and a basic subunit (19-33 kDa), which are connected by a disulfide bond. According to O'Kane et al. (2004), vicilin with several smaller polypeptides spanning from 12.5 to 33 kDa constitutes one subunit. Convicilin, a 70 kDa polypeptide, has an identical amino acid profile as vicilin, with the exception of a highly charged N-terminal extension (Croy et al., 1980)Recent research by Zembyla et al. (2021)demonstrates that at low doses (1–10 mg/mL), pea protein possesses lubricating properties. Nevertheless, at greater concentrations (>100 mg/mL), pea protein tends to aggregate, and this change from dissolved polymer to aggregated particle-like behaviour leads in lubrication failure.

Pea protein gel formation has been extensively studied, with pH conditions, ionic strengths, and temperature proving to be significant contributing variables (BORA et al., 1994, Message et al., 2015, Shand et al., 2007). Due to thermal denaturation and cross-linking of two major globular proteins, Legumin 11S and Vicillin 7S, which contain free thio groups, pea protein may self-assemble to form a heat-induced gel, especially at high concentrations when heated beyond 75 °C. Legumin is denatured between 69 and 77 °C as a result of the broken disulfide bond between the acidic and basic subunits, followed by the exposure of the free active sulfhydryl groups in hydrophobic amino acids. Both hydrophobic interaction and sulfhydryl/disulfide bonds exchange process contribute to the rearrangement and aggregation of legumin when the temperature rises from 75 to 85 ° C. (J.-L. Message et al., 2015; J. L. Message, Sok, Assifaoui, & Saurel, 2013; Shand et al., 2007). In the meanwhile, vicililin denatures and

aggregates mostly via non-covalent interactions, such as hydrophobic interactions and hydrogen bonding.

Pea protein isolate has been used in literature to form a thermally cross-linked gel, which was broken to micrometre scale microgels using a high pressure homogenizer (Matsumiya and Murray, 2016). Using the same processing principle, pea protein heat-set gel was created ad hypothesized to be broken down into microgel particles by controlled shearing using a high pressure homogenizer, which was further used to stabilize W/W Pickering emulsions (**Chapter 5**). In this thesis, we focused on pea protein not only due to its great water-binding ability, as well as a high nutritional value, but also because it is recognized as a protein with limited allergenicity and thus suitable for food applications (Sandberg, 2011, Krefting, 2017, Day, 2013). Of more importance, pea protein is known to create high friction in between two hydrophobic contact surfaces (Kew et al., 2021, Liamas et al., 2023), hence it is important to understand whether microeglation of pea protein offers any benefit to reduce such high friction and also how such microgel offer lubrication (if any) when present at W-W interface.

## 1.4. Rationale behind the selection of characterization techniques
## 1.4.1. Rheology

Rheology is the study of the deformation and flow of matter under stress. It is a branch of physics and materials science that deals with the mechanical properties of materials, including liquids, solids, and complex fluids such as polymers, suspensions, and emulsions (Zhong and Daubert, 2013, Ahmed and Basu, 2016). Also, rheology is concerned with the relationship between the deformation of a material and the stress applied to it. It also deals with the properties of materials that determine how they respond to applied stress, such as viscosity, elasticity, and plasticity.

Many studies provide extensive coverage of food rheology (Ahmed and Basu, 2016). Rheology is used to build constitutive relationships between stress and strain rate, and foods are often more complicated than other materials because of their dependence on time scales of the deformation process (thixotropy, elasticity, etc.) as well as shear and thermal histories. In the context of texture perception, most studies revert to measuring viscosity over a limited set of shear rates, the apparent yield stress for soft materials, and the storage loss moduli over a limited set of frequencies as a measure of viscoelasticity. While there is a great deal of research

that seeks to link the triangle of rheology–structure–processing, most studies simply measure viscosity over a limited set of shear rates, the apparent yield stress for soft materials, and the To properly create constitutive models for intact foods and to address how foods respond under important variables present during oral processing, further research is necessary. In this thesis, we measured the rheological data of each hydrocolloid (*i.e.*, starch, $\kappa$-carrageenan, xanthan gum), as well as the mixtures including W/W emulsions.

### 1.4.1.1. Definition of terms: Shear stress, shear rate, law of viscosity, kinematic viscosity

The two-plate model is used to define the rheological parameters needed for a scientific description of flow behaviour (**Fig. 1.6**). Shear is applied to a sample sandwiched between the two plates. The lower stationary plate is mounted on a very rigid support, and the upper plate can be moved parallel to the lower plate. Before calculating the viscosity, it is necessary to first define the shear stress and the shear rate.
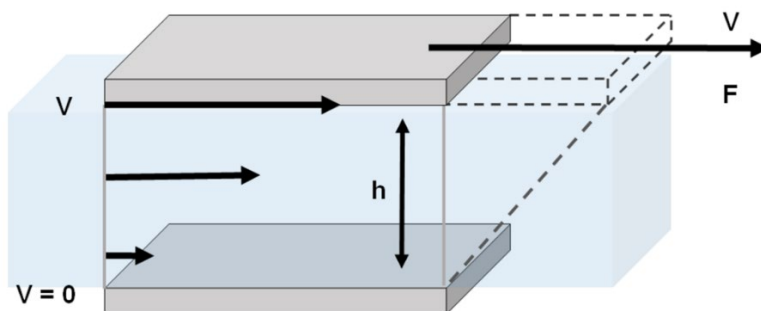


**Figure 1.6.** Calculation of shear stress and shear rate using the two-plates model with shear area *A*, gap width *h*, shear force *F*, and velocity *v*.

#### *Shear stress*

Shear stress arises when a force is applied perpendicular to the surface of an item or substance. It occurs when two forces acting in opposite directions across a surface cause the surface to deform or shear (Barnes et al., 1989). Shear stress is measured in units of force per unit shear area, such as pounds per square inch (psi) or Pascal, and is proportional to the applied force and the area over which it is applied (Pa) (Mezger, 2020). Shear stress is a crucial term in the domains of mechanics, engineering, and materials science, and it is frequently employed

to describe the behaviour of fluids and solids under various forms of stress (Zhong and Daubert, 2013, Tanner, 2000, Osswald and Rudolph, 2015).

### *Shear rate*

Shear rate is the rate at which an external force shears or deforms a fluid. It is generally stated in reciprocal seconds ($s^{-1}$). In other terms, it is the pace at which fluid layers pass one another (Barnes et al., 1989, Mezger, 2020). When we see **Figure 1.6**, as a fluid flows through a pipe, the velocity ($v$) of the fluid in the core of the pipe is greater than the velocity at the pipe wall, causing shear between the separate layers of fluid. Calculate the shear rate by dividing the velocity gradient (the rate of change of velocity with distance from the pipe wall) by the distance from the pipe wall.

### **Viscosity**

Viscosity, also known as dynamic viscosity or shear viscosity, is the resistance of a fluid to flow when a shear force is applied. It is defined as the ratio of the applied shear stress to the resultant shear rate, which reflects the fluid's velocity gradient between parallel plates (Mezger, 2020).

For a Newtonian fluid, the shear stress $\tau$ (in Pa) is exactly proportional to the shear rate $\dot{\gamma}$ (in $s^{-1}$), according to the law of viscosity. This indicates that the ratio of shear stress to shear rate is constant, and is referred to as the viscosity coefficient *($\eta$)*.

This connection is mathematically stated as:

$$\tau \ = \ \eta \ \dot{\gamma} \tag{1.3}$$

where represents shear stress ($\tau$), represents viscosity coefficient ($\eta$), and represents shear rate $\dot{\gamma}$. The connection between shear stress and shear rate may not be linear for non-Newtonian fluids (*i.e.*, hydrocolloids such as xanthan gum and carrageenan), and the viscosity coefficient may change with the applied shear rate.

## **1.4.1.2. Flow behaviour, flow curve, and viscosity curve**

Viscosity values are not constant since they depend on a variety of situations. This thesis also confirms the flow dynamics of hydrocolloids and the mixtures under shear at constant temperature. Ideally, viscous flow behaviour (or: Newtonian flow behaviour) means that the measured viscosity is independent of the shear rate (**Fig. 1.7, line 1).** Typical materials from

this group include water, mineral oil, silicone oil, salad oil, solvents such as acetone, as well as viscosity standards (e.g. calibration oils).
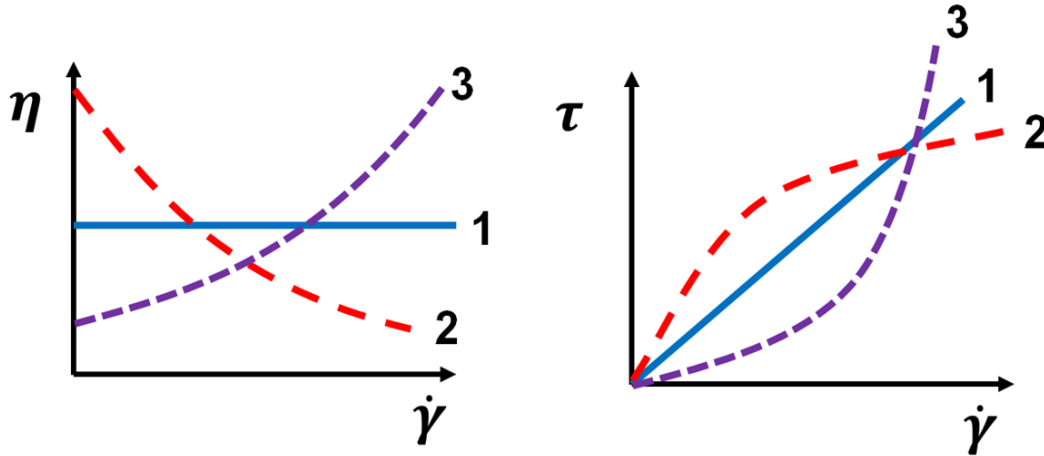


**Figure 1.7.** Viscosity curves (left) and flow curves (right) for (1) Newtonian, (2) shear-thinning, and (3) shear-thickening flow behaviour.

Shear-thinning behaviour (or: pseudoplastic flow behaviour) is characterized by decreasing viscosity with increasing shear rates (**Fig. 1.7, line 2**). Typical materials that show this behaviour are coatings, glues, shampoos, polymer solutions and polymer melts. Since viscosity is shear-dependent, it should always be given with the shear condition.

Shear-thickening (or: dilatant flow behaviour) means increasing viscosity with increasing shear rates (**Fig. 1.7, line 3**). Materials that typically display such behaviour include highly filled dispersions, such as ceramic suspensions (casting slurries), starch dispersions, plastisol pastes that lack a sufficient amount of plasticizer, dental filling masses as well as special composite materials for protective clothing. Hydrocolloids used in this thesis were all non-Newtonian and had shear-thinning properties (*i.e.,* both native and gelatinized starch, $\kappa$C, and XG).

### 1.4.1.3. Oscillation tests and viscoelasticity

In this thesis, the protein microgel particles were used to stabilise the W/W emulsions (**Chapter 5**). Oscillation test was used to investigate the viscoelastic behaviour of protein gel materials before they were sheared down into microgel particles. Viscoelasticity refers to a material's capacity to show viscous (flow-like) and elastic (solid-like) behaviour under varying circumstances of stress or deformation. In an oscillation test, the material is subjected to a modest sinusoidal stress, and the resulting deformation or strain is monitored over time. By

altering the frequency and amplitude of the applied stress, it can examine the material's response to various forms of deformation.

First, we need to understand measuring viscoelastic behaviour of samples. For example, the two-plates model can also be used for explaining oscillatory tests (**Fig. 1.8**). A sample is sheared while sandwiched between two plates, with the upper plate moving and the lower plate remaining stationary. A push rod mounted to a driving wheel moves the upper plate back and forth parallel to the lower plate, as long as the wheel is turning. At constant rotational speed, the model operates at a correspondingly constant oscillating frequency.
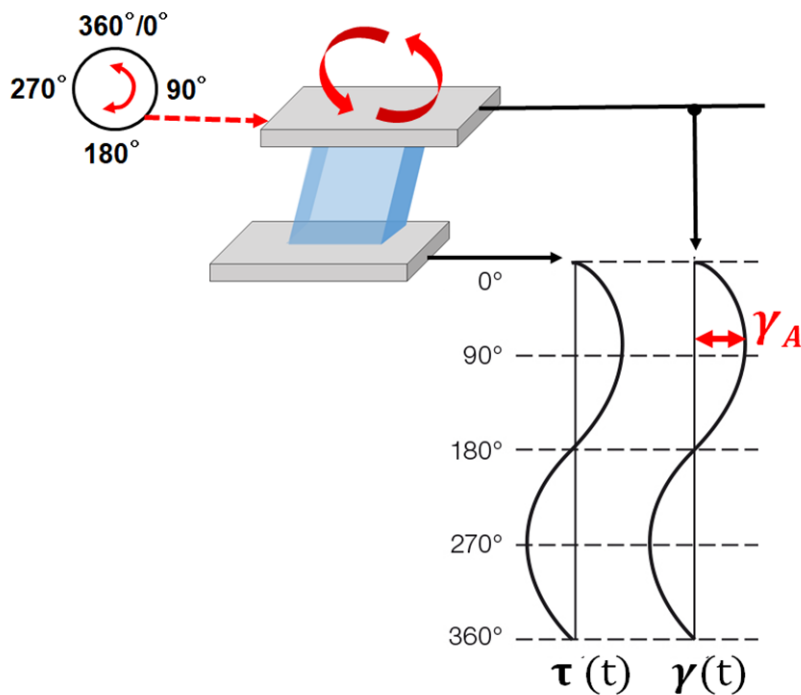


**Figure 1.8.** Oscillatory test with the two-plates model, here for ideally elastic behaviour.

The deflection path of the upper, movable plate is measured and rheologically evaluated as strain or deformation $\gamma$. When the driving wheel moves, the strain plotted versus time results in a sine curve with the strain amplitude $\gamma_A$ (**Fig. 1.8**). Parameters for oscillatory tests are usually preset in the form of a sine curve. For the two-plates model, as described above, the test is a controlled sinusoidal strain test. A sine curve is determined by its amplitude (maximum deflection) and its oscillation period. The oscillation frequency is the reciprocal of

the oscillation period. In addition, the force that acts upon the lower, stationary plate is measured. This force is required as a counter force to keep the lower plate in position. The signal is rheologically evaluated as shear stress $\tau$. If the sample is not strained by too large a deformation, the resulting diagram over time is a sinusoidal curve of the shear stress with the amplitude $\gamma_A$. The two sine curves, *i.e.* the preset as well as the response curve, oscillate with the same frequency. However, if too large a strain was to be preset, the inner structure of the sample would be destroyed, and the resulting curve would no longer be sinusoidal.
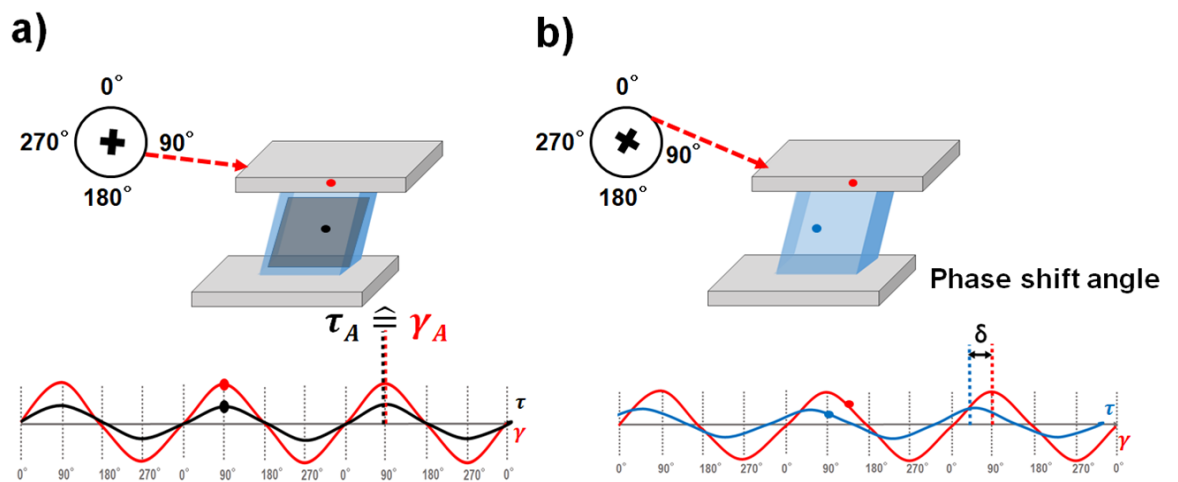


**Figure 1.9.** Comparision between a) ideally elastic behaviour, and b) viscoelastic behaviour.

For a completely rigid sample, such as one made of rubber and silicon with ideally elastic behaviour, there is no time lag between the preset and the response sine curve (**Fig. 1.8 and 1.9a**). Most samples show viscoelastic behaviour. In this case, the sine curves of the preset parameter and the measuring result show a time lag for the response signal. This lag is called the phase shift $\delta$ (**Fig. 1.9b**). It is always between 0° and 90°.

For the fluid state, the following holds: The phase shift is between 45° and 90°, thus $90° \geq \delta > 45°$. In this case, the material at rest is fluid. The following holds for the phase shift: $\delta = 0°$ for ideally elastic deformation behaviour and $\delta = 90°$ for ideally viscous flow behaviour All kinds of viscoelastic behaviour take place between these two extremes.

The shape of the viscoelasticity curve can reveal crucial information about the material's behaviour. For instance, a viscoelastic gel is characterised by a flat curve at low frequencies

(showing a viscous liquid-like behaviour) followed by a steep increase at high frequencies (saying a more elastic solid-like behaviour). Overall, oscillation testing and viscoelasticity analyses are essential for comprehending the rheological characteristics of protein particles and their behaviour under various stress or deformation circumstances. Therefore, in **Chapter 5**, we tried oscillation test to measure different viscoelastic characteristics of whey and pea protein, which could be mother-microgel particles having the same characteristic at bulk scale.

### Storage modulus G' and loss modulus G''

The storage modulus G' (G prime, in Pa) represents the elastic portion of the viscoelastic behaviour, which partly describes the solid-state behaviour of the sample. The loss modulus G'' (G double prime, in Pa) describes the viscous portion of the viscoelastic behaviour, which can be seen as the liquid-state behaviour of the sample.

Internal friction between the components of a moving fluid, thus between molecules and particles, causes viscous behaviour (White and Majdalani, 2006). This friction is always associated with the generation of frictional heat in the sample, and hence with the conversion of deformation energy into heat energy. This portion of the energy is absorbed by the sample; it is used by internal friction processes and is no longer accessible for the sample's subsequent behaviour. This energy loss is also known as energy dissipation (Wen and Huang, 2012, Pipe et al., 2008). The elastic portion of the energy, on the other hand, is stored in the deformed material; that is, by expanding and stretching the internal superstructures without overstressing the interactions or overstretching or breaking the material. When the material is subsequently released, the unused stored energy works as a driving force to rebuild the structure into its original shape.

Therefore, G' characterizes the stored deformation energy and G'' represent the deformation energy lost (dissipated) through internal friction when flowing. Viscoelastic solids have G' > G''. This is owing to internal material linkages, such as chemical bonding or physical-chemical interactions. On the other hand, viscoelastic liquids have G'' > G'. This is because there are no such strong connections between individual molecules in most of these materials (Mezger, 2020, Zhong and Daubert, 2013). In **Chapter 5**, we measured the development of viscoelastic parameters (G' and G'') during thermal processing of whey and pea protein hydrogel to check gel formation and compare the characteristics.

## 1.4.2. Oral Tribology

Oral tribology is a subfield of tribology that specifically deals with the study of friction, wear and lubrication in the oral cavity. It is a multidisciplinary field that encompasses aspects of dentistry, biomechanics, and materials science. Oral tribology is concerned with the interactions between teeth, dental restorations, and oral tissues and the effects of these interactions on the dental and periodontal (gums and supporting tissue) health. It involves the study of how oral surfaces interact with each other and how the properties of those surfaces affect the behaviour of the system. This includes the study of friction between teeth, wear of tooth enamel, and lubrication of oral tissues.

Detailed methods to measure the tribological data using Stribeck curve generated using various tribometers is discussed in the next chapter (**Chapter 2**).

The goal of this thesis was to understand the tribology of hydrocolloids, as well as mixed hydrocolloid systems, using water-in-water system with starch and polysaccharides themselves, also stabilized by protein particles and tribology was used as technique in all the experimental chapters.

## 1.4.3. Dynamic laser scattering (DLS)

Dynamic light scattering (DLS) is employed to determine the particle size of microgel particles (**Chapter 4 and 5)** that have been used to stabilize the W/W emulsions. DLS is one of the conventional techniques used to estimate the particle size in the range of 1 nm to 1 μm, including nano-scale emulsion, aggregated proteins, surfactant micelles, and other nanoparticles (Malvern, 2015). Particles in a solution undergo Brownian motion, a random movement caused by thermally induced collisions with solvent molecules (Uhlenbeck and Ornstein, 1930, Dickinson, 2009). The continuously mobile particles within dispersion cause constructive and destructive interferences and hence, the intensity of scattered light fluctuates over time (**Fig. 1.10a**) (Uemura et al., 1978). In DLS, the fluctuation of intensity in scattered light is correlated against short decay intervals ($\tau$) and the intensity autocorrelation function is obtained (Lorber et al., 2012) through the following exponential equation **(Fig. 1.10b)** for samples with mono-disperse particles (**Equation 1.5**):

$$G(\tau) = 1 + b.\, e^{-2D_t q^2 \tau} \qquad\qquad (1.5)$$

Here, b = constant dependent upon the instrument and settings of optics, $D_t$ = translational diffusion coefficient and q = scattering vector which can further be expressed as (**Equation 1.6**)

$$|q| = \frac{4\pi\eta_0}{\lambda_0 \sin\frac{\theta}{2}} \qquad\qquad (1.6)$$

where, $\eta_0$ = refractive index (RI) of the solvent, $\lambda_0$ = wavelength in vacuum and $\theta$ = scattering angle.

The intensity *ACF (G(π))* is often written as *G2(τ)* and is expressed as a function of field correlation function *G1(τ)* as mentioned in the following (**Equation 1.7**)

$$G2(\tau) = 1 + G1(\tau)^2 \qquad\qquad (1.7)$$

In DLS instruments (e.g., Malvern Zetasizer®) a correlogram is fitted with raw correlation function being plotted (**Fig. 1.8b**) against delay time ($\tau$) as shown in **Equation 1.8.**

$$RCF = G2(\tau) - 1 = G1(\tau)^2 \qquad\qquad (1.8)$$

which, shows that the raw correlation function (RCF) is dependent on the field correlation function G1($\tau$). The autocorrelation functions [G2($\tau$) or G2($\tau$) – 1] in DLS are calculated by data fitting and then the $D_t$ is calculated used in Stokes-Einstein equation (**Equation 1.9**) as follows:

$$D_t = \frac{k_B T}{3\pi\eta R_H} \qquad\qquad (1.9)$$

where, $k_B$ is the Boltzmann's constant ($1.380649 \times 10^{-23}$ $JK^{-1}$, $T$ is the absolute temperature, $\eta$ is absolute viscosity and $D_t$ is the translational diffusion coefficient. Hydrodynamic diameter is the size of a sphere that diffuses at the same rate as the particle being measured.

Through this method, we can estimate the size of particles as smaller particles exhibit a greater degree of Brownian motion, whereas larger particles diffuse at a slower rate. When particles are irradiated by a laser beam in DLS, the fluctuation of scattered waves arriving randomly in time at the detector reflects the variations in particle location (Nobbmann et al., 2007). Briefly, small particles rapidly diffuse resulting in a rapid fluctuation of the intensity signal, whereas larger particles have slower fluctuations (Dalgleish and Hallett, 1995).
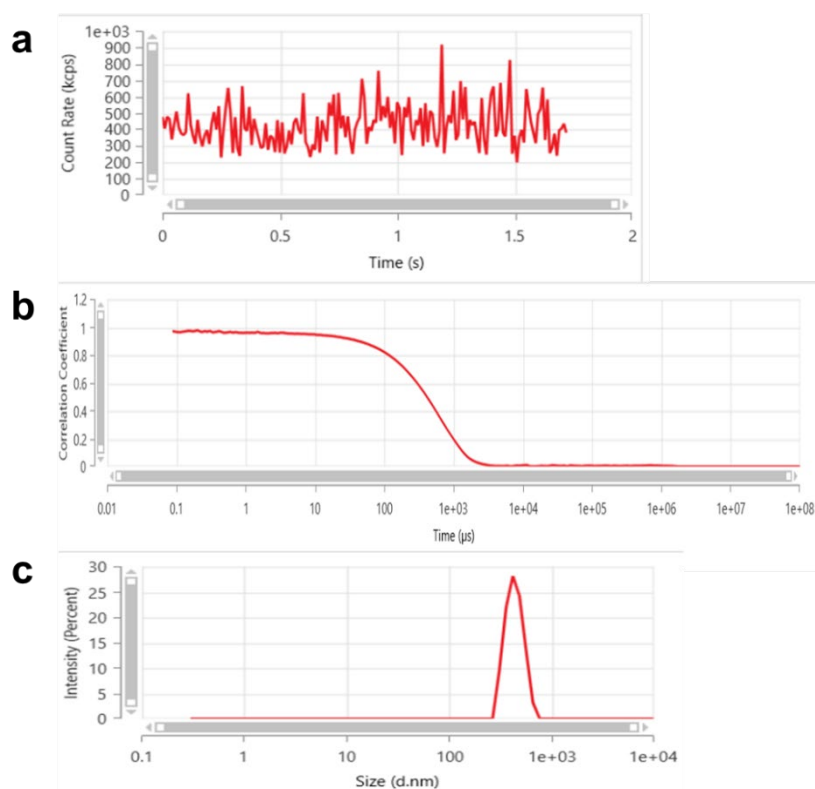


**Figure 1.10.** Fluctuation in intensity of the scattered light (a) by particles during DLS measurement due to constructive and destructive interferences. (b) The correlogram generated by and analyzed by Zetasizer® software in order to estimate the $R_H$. (c) Intensity-based DLS

On the other hand, the real size of the particles are not the only factor that affects the reported diameter; other factors such as the surface structure, *i.e.,* adsorbed polymers, and the ions around the medium also influence the size distribution (Malvern, 2015). Furthermore, the actual particle size distribution could be examined using the auto-correlation function. Measuring particle size distribution, also called the polydispersity index (PDI), is calculated using **Equation. 1.10**:

$$PdI = (\frac{\delta}{d_H})^2 \qquad\qquad (1.10)$$

where $\delta$ is the standard deviation. The value of *PDI* could change from 0 to 1.0 (Danaei et al., 2018). If the *PDI* < 0.3, the particles are generally considered as monodisperse. When the *PDI* is close to 1.0, the sample dispersion has multiple particle-sized populations and considered to be highly polydispersed.

## 1.4.4. Microscopy

Several techniques of microscopy (*i.e.*, optical, confocal, electron microscope, and atomic force microscopy) depending on various physical principles were used in this thesis to examine the morphology and surface of W/W emulsion droplets and the Pickering microgel particles.
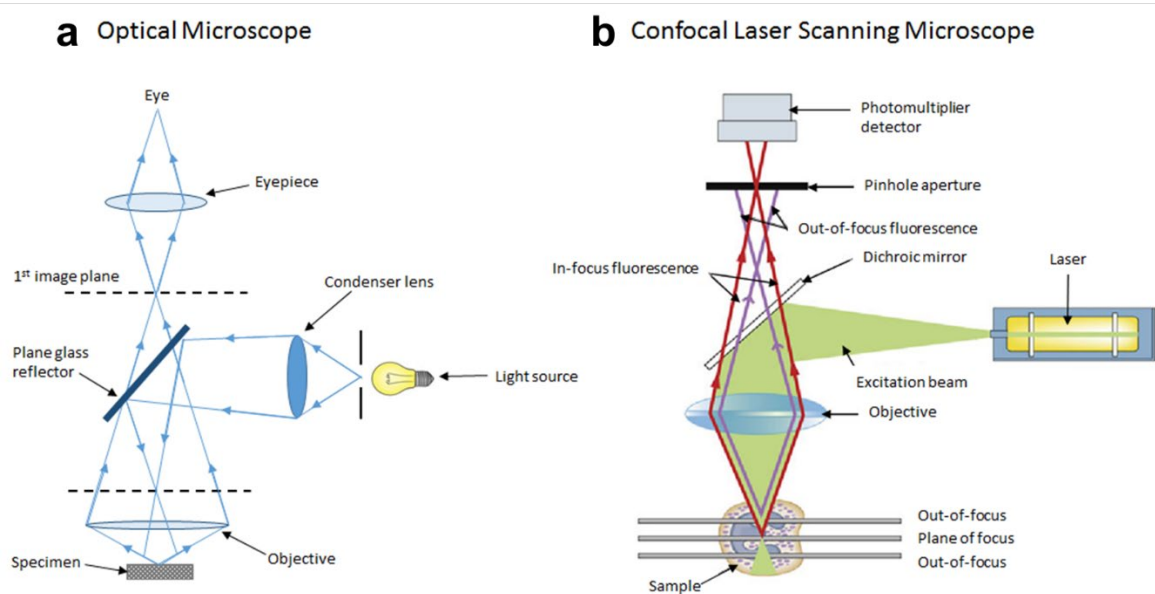
**Figure 1.11.** Diagram of the light path in optical microscope and confocal microscopy system, adapted from Microscopegenius.com and Hardham (2012)

The most basic microscopy method is the optical microscope which uses reflected light to image the surface of a sample. This microscope consists of a light source, several lenses and an eyepiece or digital camera (**Figure 1.11a**). Because the optical microscope utilises wide-field illumination, the focus plane and the plane, above or under the focus plane, are all evenly

illuminated. So, only samples that are thin and mostly transparent can be imaged (Auty et al., 2013). The wavelength of the light source, which can be as low as 200 nm, and the objective determine the resolution of an optical microscope. Unfortunately, with optical microscope, it is difficult to observe particles smaller than 1 μm because of the limitation of structures, as well as Brownian motion results in movement particularly for colloidal systems. Another limitation of the optical microscope is the limited contrast between different components in a sample due to their similar refractive indices (McClements, 2015). In order to circumvent these limitations, various types of microscopes have been created, such as the confocal laser scanning micros-copy (CLSM), which with fluorescence tool enables analysis of both two-dimensional and three-dimensional pictures.

Confocal laser scanning microscopy (CLSM), also known as confocal microscopy, is a form of optical microscopy that focuses the image of a light source and a detector on a single volume element at a well-defined depth within a sample (Auty, 2013). The principle behind CLSM is highlighted in **Figure 1.11b.** The sample's fluorophores absorb input light and then emit it at a longer wavelength. Its emitted light is redirected onto a photomultiplier detector with an emission pinhole in front of the detector by a dichroic mirror. The signal intensity accepted in the detector is further amplified and converted into pixels. Only one focal point in the sample is illuminated at a time. Therefore, 2D imaging requires regular scanning over con-secutive $x$-$y$ horizontal planes in the sample by using one or more dichroic mirrors. In addition, 3D structure is reconstructed by imaged 2D pixels at different depths. Nevertheless, the depths of the focal point are dependent on the wavelength of the used light divided by the numerical aperture of the objective lens (Pawley, 2006). The usage of fluorescent dyes to stain various components of a sample, such as proteins and lipids, further helps the analysis of a sample's morphology and microstructure. Fluorophores included into the sample can absorb input light and release light at different wavelengths. The signal is subsequently deflected by the dichroic mirror onto the photomultiplier detector. The dyes can be coupled to the sample either cova-lently or non-covalently. In this thesis, Rhodamine Blue (RB) was used to stain gelatinized starch *via* non-covalent interactions (hydrogen bonding), Acridine Orange (AO) stained WPM through hydrophobic interactions (Rawtani & Agrawal (Rawtani and Agrawal, 2013), and Fast green (FG) stained PPM via covalent interactions (Li et al., 2002)

Even though CLSM can image and distinguish the particles with different dyes, simi-larly to optical microscope the maximum resolution obtained with CLSM is around 200 nm.

Therefore, electron microscopy is a good alternative to characterize smaller samples (< 200 nm), which uses electron beams rather than light beam. In this thesis, we investigated protein microgel particles as welll as the morphology of the emulsions stabilized by the particles *via* scanning electron microscopy (SEM), a common electron microscopy technique to characterize organic and inorganic materials on a scale ranging from nanometer (3-20 nm) to micrometer (Mohammed and Abdullah, 2018, McClements, 2014)

The electron focus beam used in SEM scans surface of the particle and interacts with atoms within the particle, producing secondary electrons (SE), reflected or backs-scattered electrons (BSE), and distinctive X-rays and light. These signals include information about surface characteristics and composition of particles and are then finally collected by an electron detector. The software measures the detected signal's intensity and combines it with the beam's position to create an image. SEM resolution is not impacted by the diffraction limit or the fineness of lenses or mirrors, unlike optical microscopy. Its resolution is essentially governed by the size of the electron spot generated by the electron beam on the sample surface, which is dependent on the wavelength of the electrons, and the size of the volume that gives a detectable signal below the spot (Greiser, 2009).

In order to prevent the scatter and degradation of electron beam by gas molecules, the vast majority of electron microscopy requires imaging samples under high vacuum. In order to achieve a vacuum environment during operation, the sample must not emit gas. Unfortunately, the drying or evaporation process can typically damage the sample's inherent structure, shape, and size. Cryo-scanning electron microscopy (cryo-SEM) at low temperatures is a valuable approach in this area since it can give compatibility with the surrounding environment, limiting evaporation in the hydrated sample, and so allowing the material to keep its original structure (Greiser, 2009). To reduce the loss of structure during the imaging process, materials are treated with fast liquid nitrogen freezing. The frozen sample is transported into the preparation cryo-chamber at a low temperature and under a vacuum. In this chamber, the sample is sliced using a cold knife to investigate its internal structure. (JEOL, 2011, Greiser, 2009). In this thesis, cryo-SEM was used to observe protein particles and the distribution at the water-water interface of the emulsions (**Chapters 4 and 5).**

## 1.4.5. Atomic force microscopy (AFM)

The resolution of an optical imaging device, such as a microscope, telescope, or camera, can be restricted by issues such as flaw in the lenses or misalignment. So far, the physics of diffraction imposes a fundamental limitation on the resolution of optical systems. A diffraction-limited optical system is one whose resolution performance is at the theoretical limit of the instrument. (SAY, 1999). In contrast to competing technologies such as optical microscopy and electron microscopy, atomic force microscopy (AFM) does not utilise lenses or beam irradiation. Consequently, it is not limited in spatial resolution by diffraction and aberration, and it is not necessary to prepare a space for directing the beam (by constructing a hoover) or to stain the material. Therefore, we investigated the nano- and microscale protein particles *via* AFM in **Chapter 5**.

AFM is a very-high-resolution type of scanning probe microscopy (SPM), with demonstrated resolution on the order of fractions of a nanometer. It can image almost any type of surface, including polymers, ceramics, composites, glass, and biological samples. AFM is used to measure and localize many forces, including adhesion strength, magnetic forces, and mechanical properties (Liu and Wang, 2010, Alessandrini and Facci, 2005).
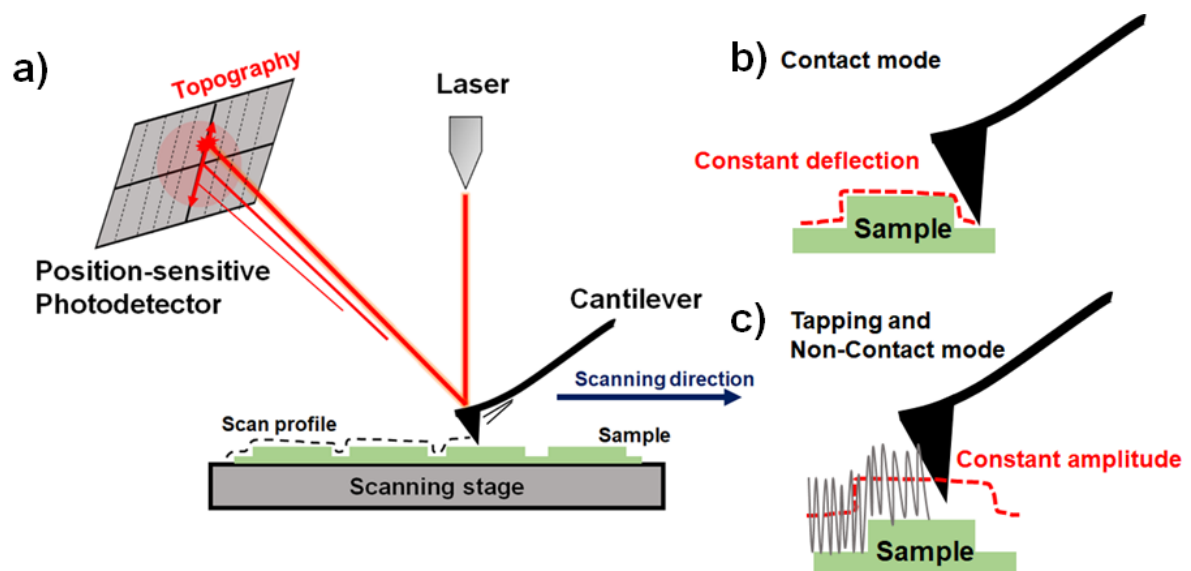


**Figure 1.12.** General working principle of AFM. The stylus of the cantilever is raster scanned across the sample to record topographic information. In the tapping mode, AFM oscillates the cantilever close to or at its resonance frequency, while maintaining a constant oscillation amplitude, and the stylus only touches the sample surface intermittently. In the contact mode,

AFM keeps the cantilever deflection constant (constant force) by adjusting the distance between stylus and sample.

The AFM operates by raster-scanning a very small tip attached to the end of a flexible microcantilever in delicate contact with the material. A piezoelectric actuator accomplishes this relative motion with sub-Angstrom precision (usually a tube, sometimes a tripod). With a laser beam impacting on the back of the cantilever, the tip–sample interaction may be observed with great resolution as the cantilever deflects upon engagement with the sample. In **Figure 1.12a**, the beam is reflected towards a split photodetector, which is configured as an optical lever that amplifies cantilever deflections. In most all operating modes, a feedback circuit attached to the cantilever deflection sensor controls the tip–sample distance by keeping the tip–sample contact constant. The quantity of feedback signal obtained at each scanning point of a 2D matrix converges to generate an image-like 3D reconstruction of the sample topography.

In general, AFM imaging modes are classified as either static (also known as contact) or dynamic (non-contact or "tapping"), in which the cantilever vibrates or oscillates at a specific frequency. The first imaging mode to be established is the contact mode, in which the tip maintains soft contact with the surface of the sample (Binnig et al., 1986). In this imaging mode, the feedback mechanism maintains a constant applied force, and consequently cantilever deflection, as the tip scans the surface (**Figure 1.12b**). By tracking the piezo-vertical position necessary to maintain a constant force, images are generated. Therefore, this mode is used for flat and somewhat rigid materials (*i.e.*, reconstituted membranes, 2D protein crystals), as it provides the maximum resolution. The existence of dragging forces related with the lateral movement of the tip in contact with the sample is a disadvantage of the contact mode. This issue is most noticeable with biological samples, which are often weakly linked to the substrate and quickly damaged. Another method of operation, the dynamic (*i.e.,* non-contact or "tapping") modes, has been designed to overcome this issue (Zhong et al., 1993). In the dynamic mode, the cantilever is oscillated at a frequency close to its resonance while the amplitude of oscillation is measured. Beginning from a free oscillation amplitude, the oscillation amplitude is dampened as the cantilever approaches the sample and begins to contact its surface (**Figure 1.12c**). By recording the feedback signal necessary to maintain constant amplitude, the surface topography of a sample can be derived. When  the tip is in touch with the sample only intermittently, the dragging forces during scanning are considerably reduced (Tamayo and Garcia,

1996). However, conventional contact mode with extremely soft cantilevers was utilised in **Chapter 5**, because soft microgel particles might be damaged by oscillation movement of tips. The contact mode of operation can be applicable in liquid conditions, reducing the contact force between the tip and the sample relative to operation in air. The interaction force reduction comes from the removal of capillary pressure due to the presence of a thin water layer on surfaces in air (Grigg et al., 1992).
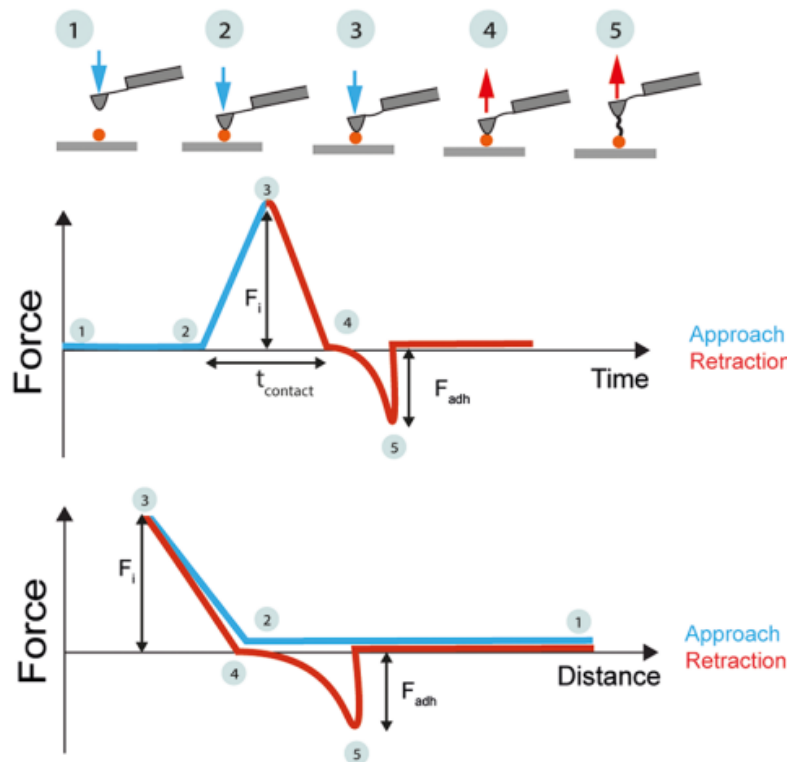


**Figure 1.13.** Examples of force-time (FT) and force−distance (FD) curves, adapted from Müller et al. (2020).

The potential of AFM is not just restricted to its imaging capabilities, but also because of its ability to examine intra- and molecular forces (Cappella & Dietler, 1999). During an approach–retract cycle between the tip and the sample, the cantilever deflection is monitored as a function of the relative motion to determine the force curve. In **Figure 1.13**, a typical force curve is shown. It can be divided into several movements. Starting from the right (#1) the AFM tip is far from the sample and no interaction is detected. Moving towards the left side of the plot (#1−2), *i.e.* the tip is approaching the sample, no interaction is detected until the cantilever deflects towards the sample due to van der Waals forces (#2−3). These forces lead the tip to snap into contact with the sample. After the contact, approaching the tip further to the surface, a positive deflection of the cantilever arises (#3−4) due to repulsive forces. This is the contact

region of the force curve, where elastic properties of the sample could be measured. Typically, the cantilever is moved towards the sample until a preset force threshold is reached (#4). After this happens, the movement direction is inverted and the cantilever starts moving away from the sample (#4−5). Initially, the behaviour of the cantilever during withdrawal equals that described for the approach, but, due to adhesion between the tip and sample, the cantilever starts to deflect negatively until the adhesion force (Fadh) is overcome by the cantilever restoring force and the contact breaks (#5). The hysteretic behaviour of curves recorded in air is mostly attributable to capillary forces caused by the thin water film that wets both the probe and the sample (Alessandrini & Facci, 2005). It is obvious that a significant adhesion restricts the amount of data that can be collected from a force curve, particularly in the extremely fascinating area of tiny tip-sample separation. Nevertheless, capillary forces may be significantly lowered by doing measurements in liquid while maintaining a physiologically relevant environment for biological material. The magnitude of the adhesion force could use to compare interaction strengths of various moleculs, including particles (Liamas, Connell, & Sarkar, 2023; Noy, Frisbie, Rozsnyai, Wrighton, & Lieber, 1995; Thomas, Houston, Crooks, Kim, & Michalske, 1995). In **Chapter 5**, we confrimed adhesion value of whey and pea protein microgel paticles by AFM, alongside capturing nanoscale topographic images of these microgel particles.

## 1.4.6. Quartz Crystal Microbalance with Dissipation Monitoring (QCM-D)

In this thesis, we used Quartz Crystal Microbalance with Dissipation monitoring (QCM-D), aiming to understand adsorption behaviour of protein particles on W-W interface. QCM-D is a label-free, surface-sensitive technique that detects mass changes at the surface with nanoscale resolution, in addition to the viscoelastic characteristics of the surface-adhering layer (Dunér et al., 2013). The basic principle of QCM-D is based on QCM; a piezoelectric sensor is excited to resonance by the application of an alternating voltage, and the resonance frequency ($f$) as a function of time is measured. The frequency of the sensor relies on its mass, or thickness. Frequency changes ($\Delta f$) will show changes of the mass linked to the sensor surface, and enables the detection and analysis of molecule-surface interactions, such as molecule adsorption and desorption, which manifest as mass absorption and mass loss, respectively. (**Figure 1.14**)
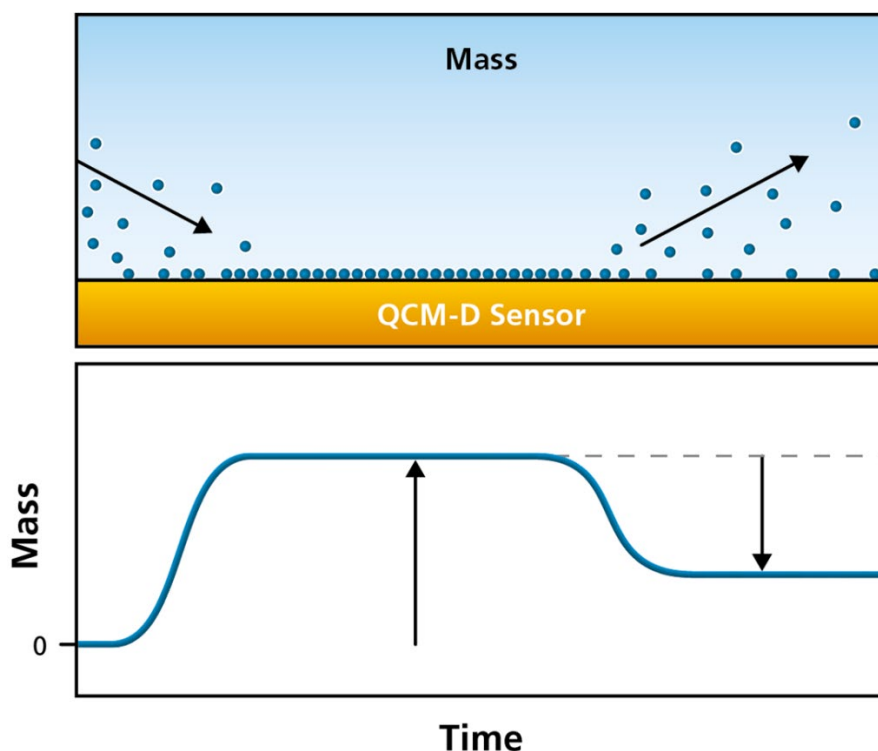
**Figure 1.14.** A schematic illustration of mass uptake and mass loss, as molecules adsorb to, and desorb from, the QCM-D sensor surface.

QCM-D not only measures $\Delta f$, but also the dissipation ($\Delta D$) of the system under investigation. In combination with $\Delta f$, the D-value, mechanical characteristics of the surface-adhering layer, could be utilised to estimate mass, thickness, and viscoelastic characteristics of soft layers; this is not achievable when only examining the $\Delta f$ response. Thus, QCM-D is well suited device for the investigation and characterization of viscoelastic hydrated systems such as microgel particles as used in this thesis because of the combined information of $\Delta f$ and $\Delta D$ it provides.

QCM-D can measure the hydrated mass, or the mass of the sensor surface molecules plus the associated solvent. This characteristic makes QCM-D a very effective instrument for analysing layer structure and for detecting structural changes of the molecular layer, such as swelling and changing structures. For example, green illustration (top) in **Figure 1.15** illustrate scenarios of molecular layer being collapsed by solution as measured with QCM-D. Initially, the molecules are extending from the surface and couple lots of solvent. The molecules then collapse, release the coupled solvent, and form a thin and rigid layer at the surface. QCM-D will detect a mass loss as the layer transitions from the highly hydrated state to the collapsed state. The detected mass loss could estimate a smaller amount of solvent linked in the collapsed state compared to the hydrated state. The QCM-D data will also reveal a transition from a soft

to a more rigid layer. The blue illustration (bottom) shows the opposite. Initially there is a thin and rigid layer at the surface, which then swells to become thick and soft. The thickness change is illustrated by the blue curve in the graph.
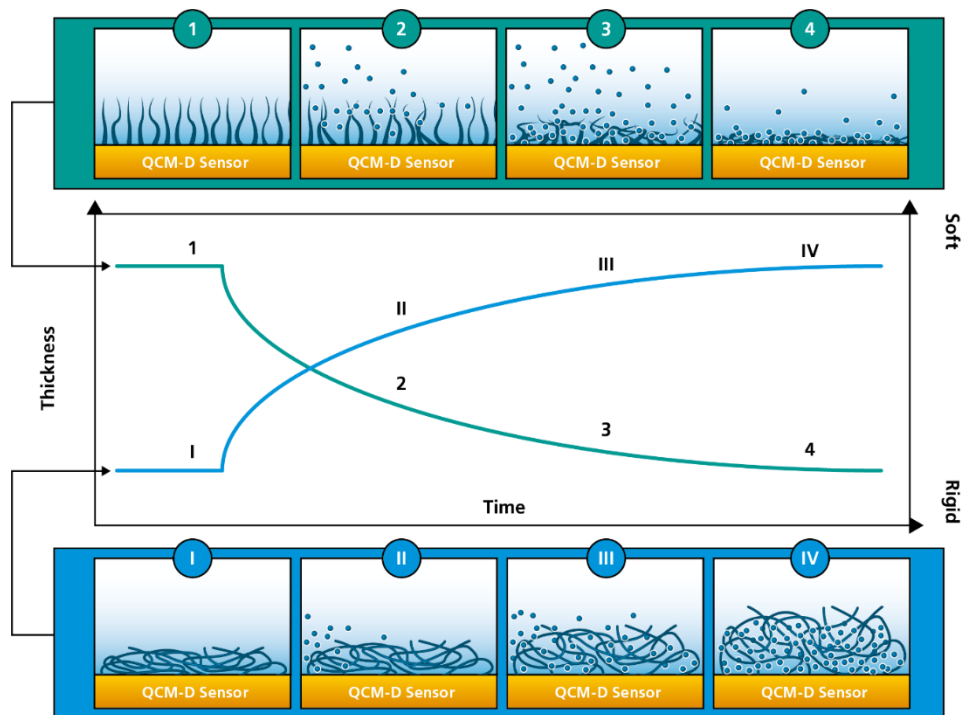


**Figure 1.15.** A schematic illustration of structural change as measured with QCM-D. The green illustration (top) shows the collapse of a highly hydrated layer. The blue illustration (bottom) shows the opposite.

In **Chapter 5**, QCM-D has been used to understand how microgels particles adsorbed at W-W interfaces by using hydrophilic gold sensor, the surface possesses an appealing quality for numerous biological and medical applications, primarily attributed to its chemical stability and compatibility with biological systems (Jachimska et al., 2018). Komorek et al. (2020) confirmed the estimation of the number of water molecules related with lysozymes film, and different adsorption on gold sensor by changing level of hydration with different pH condition. It was also confirmed that protein films were formed on the hydrophilic gold surface (Xu et al., 2020)

In summary, a range of techniques at multiple length scales have been used to understand the structure and material performance of the biopolymer mixtures and W/W emulsions.

## 1.5. Outline of the thesis

This thesis includes a combination of comprehensive literature review and a series of research studies starting from understanding oral tribology of pure hydrocolloids, including starch and non-starch polysaccharides, to the design of biopolymer mixtures and W/W emulsions and lubrication performance of these mixed systems and W/W emulsions with/ without being stabilized by animal-based and plant protein-based microgels. The outline of each chapter is highlighted in **Figure 1.16.**
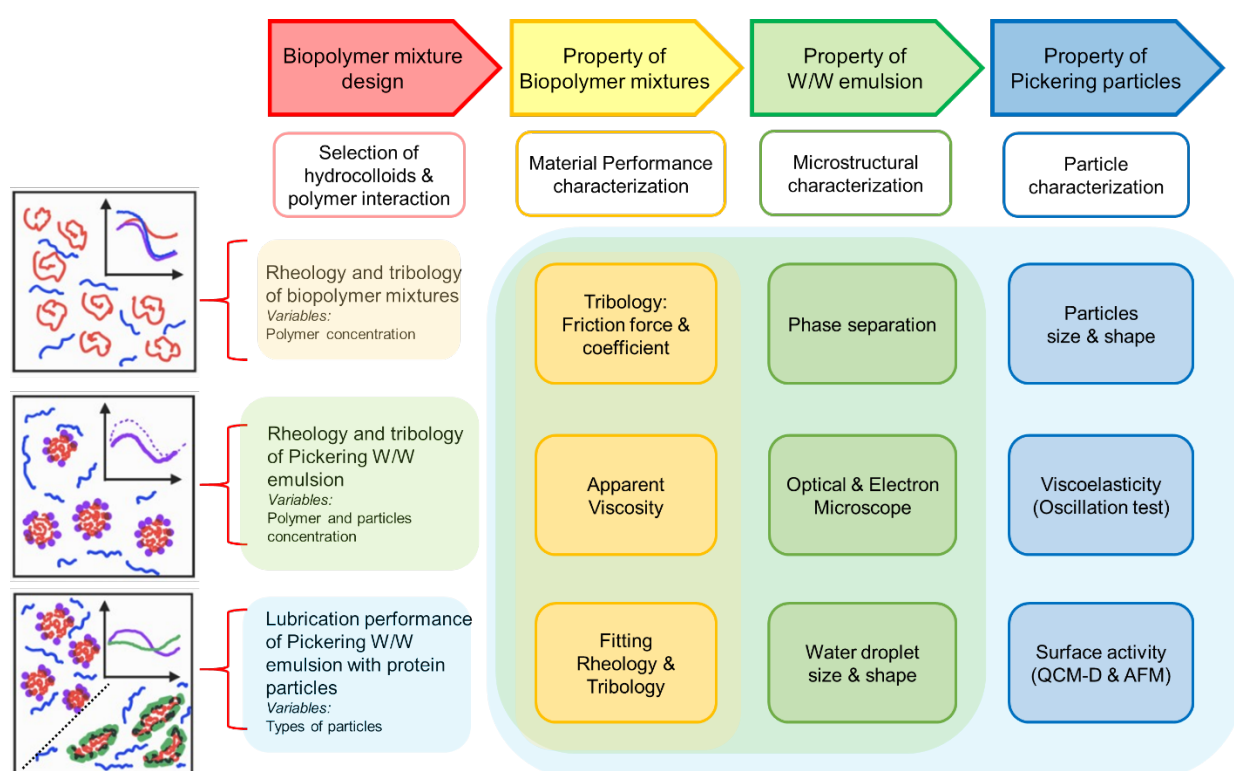


**Figure 1.16.** Schematic framework of the thesis.

This thesis includes a combination of comprehensive literature review and a series of research studies starting from understanding oral tribology of pure hydrocolloids, including starch and non-starch polysaccharides, to the design of biopolymer mixtures and W/W emulsions and lubrication performance of these mixed systems and W/W emulsions with/ without being stabilized by animal-based and plant protein-based microgels. The outline of each chapter is highlighted in **Figure 1.16.**

**Chapter 2** includes a literature review giving an overview of oral tribology including explanation of Stribeck curve. It covers a comprehensive examination of commercially available and custom-made tribometers that are used to measure the friction force in various food research laboratories. Then, it includes the oral tribology of hydrocolloids, *i.e.*, aqueous dispersions of starch and non-starch polysaccharides that are often used as fat replacers or bulking agents in food industries. Recent work on polysaccharide-based fluid gels, microgels, and mixed gels are also discussed, where tribological research is rather limited. Finally, we draw some conclusive remarks on the lubrication mechanisms of polysaccharides and highlight future prospects. The literature review forming this chapter was published in peer-reviewed book chapter, *Handbook of Hydrocolloids* (Third Edition)

**Chapter 3** investigated the tribological properties of mixtures of gelatinized corn starches and $\kappa$-carrageenan. The mixtures containing the gelatinized starch and $\kappa$-carrageenan showed lower friction coefficients in the mixed and boundary regimes compared to pure starch or $\kappa$-carrageenan solutions. These findings illustrate new opportunities for designing biopolymer mixtures with tunable lubrication performance, *via* optimizing the concentrations of the individual biopolymers and the gelatinization state of the starch. This chapter was published in a peer-reviewed journal, *Journal of Texture Studies.*

**Chapter 4** studied the rheology and tribology properties of W/W emulsion, with/ without being stabilized by whey protein microgel particles. The emulsions were made from mixtures of gelatinized corn starch and $\kappa$-carrageenan, and were found to be shear thinning liquids. The W/W emulsions stabilized by microgel particles showed higher viscosity and lower friction coefficient in the boundary and mixed regimes. It was demonstrated that microgel particles used to stabilize W/W emulsions can improve their lubrication performance validating the hypothesis in the thesis. The chapter was published in peer-reviewed journal, *Food Hydrocolloids.*

**Chapter 5** focuses on creating Pickering W/W emulsions using gelatinized starch and xanthan gum stabilized by sustainable plant protein (pea) -based microgel particles, and compare their lubrication performance with animal (whey) protein microgel particles. The results showed that pea protein microgel particles had better boundary lubrication performance and was more soft and adhesive than the animal protein counterpart, leading to lower friction in pea protein microgel particle-stabilized W/W emulsions. Overall, this chapter provides a new eco-friendly solution for designing aqueous lubricants for future nutritional and biomedical

applications. This chapter has been submitted in a peer-reviewed journal, *Advanced Material Interfaces.*

**Chapter 6** includes a general summary and discussion of the main results as well as a conclusion in relation to the principal research problem and areas for future studies.

# Reference

ACHAYUTHAKAN, P. & SUPHANTHARIKA, M. 2008. Pasting and rheological properties of waxy corn starch as affected by guar gum and xanthan gum. *Carbohydrate polymers,* 71**,** 9-17.

AGUIRRE, A., MENDOZA, B., LEVINE, M., HATTON, M. & DOUGLAS, W. 1989. In vitro characterization of human salivary lubrication. *Archives of oral biology,* 34**,** 675-677.

AHMED, J. & BASU, S. 2016. *Advances in food rheology and its applications*, Woodhead Publishing.

AHNEN, R. T., JONNALAGADDA, S. S. & SLAVIN, J. L. 2019. Role of plant protein in nutrition, wellness, and health. *Nutrition reviews,* 77**,** 735-747.

AI, Y. & JANE, J. L. 2015. Gelatinization and rheological properties of starch. *Starch-Stärke,* 67**,** 213-224.

AIREY, G. D., RAHIMZADEH, B. & COLLOP, A. C. 2002. Linear viscoelastic limits of bituminous binders. *Asphalt Paving technology,* 71**,** 89-115.

ALESSANDRINI, A. & FACCI, P. 2005. AFM: a versatile tool in biophysics. *Measurement science and technology,* 16**,** R65.

ALLONCLE, M. & DOUBLIER, J.-L. 1991. Viscoelastic properties of maize starch/hydrocolloid pastes and gels. *Food hydrocolloids,* 5**,** 455-467.

ALMDAL, K., DYRE, J., HVIDT, S. & KRAMER, O. 1993. Towards a phenomenological definition of the term 'gel'. *Polymer gels and networks,* 1**,** 5-17.

ANDABLO-REYES, E., BRYANT, M., NEVILLE, A., HYDE, P., SARKAR, R., FRANCIS, M. & SARKAR, A. 2020. 3D biomimetic tongue-emulating surfaces for tribological applications. *ACS Applied Materials & Interfaces,* 12**,** 49371-49385.

ANDABLO-REYES, E., YERANI, D., FU, M., LIAMAS, E., CONNELL, S., TORRES, O. & SARKAR, A. 2019. Microgels as viscosity modifiers influence lubrication performance of continuum. *Soft Matter,* 15**,** 9614-9624.

ARAIZA-CALAHORRA, A., MACKIE, A. R., FERRON, G. & SARKAR, A. 2022. Can tribology be a tool to help tailor food for elderly population? *Current Opinion in Food Science***,** 100968.

AUFDERHORST-ROBERTS, A., BAKER, D., FOSTER, R. J., CAYRE, O., MATTSSON, J. & CONNELL, S. D. 2018. Nanoscale mechanics of microgel particles. *Nanoscale,* 10**,** 16050-16061.

AUTY, D., GARDINER, B. A., ACHIM, A., MOORE, J. R. & CAMERON, A. D. 2013. Models for predicting microfibril angle variation in Scots pine. *Annals of Forest Science,* 70**,** 209-218.

AUTY, M. A. E. 2013. Confocal microscopy: principles and applications to food microstructures. *Food Microstructures.*

BABAULT, N., PAñZIS, C., DELEY, G., GUëRIN-DEREMAUX, L., SANIEZ, M.-H., LEFRANC-MILLOT, C. & ALLAERT, F. A. 2015. Pea proteins oral supplementation promotes muscle thickness gains during resistance training: a double-blind, randomized, Placebo-controlled clinical trial vs. Whey protein. *Journal of the International Society of Sports Nutrition,* 12**,** 3.

BAIER, S., ELMORE, D., GUTHRIE, B., LINDGREN, T., SMITH, S., STEINBACH, A., DEBON, S., VANHEMELRIJCK, J., HEYER, P. & LæUGER, J. A new tribology device for assessing mouthfeel attributes of foods.    5th International Symposium on Food Rheology and Structure, ISFRS 2009 Zurich, Switzerland.

BALAKRISHNAN, G., NICOLAI, T., BENYAHIA, L. & DURAND, D. 2012. Particles trapped at the droplet interface in water-in-water emulsions. *Langmuir,* 28**,** 5921-5926.

BARNES, H. A., HUTTON, J. F. & WALTERS, K. 1989. *An introduction to rheology*, Elsevier.

BATCHELOR, H., VENABLES, R., MARRIOTT, J. & MILLS, T. 2015. The application of tribology in assessing texture perception of oral liquid medicines. *International Journal of Pharmaceutics,* 479**,** 277-281.

BELDENGRUN, Y., ARAGON, J., PRAZERES, S. F., MONTALVO, G., MIRAS, J. & ESQUENA, J. 2018. Gelatin/maltodextrin water-in-water (w/w) emulsions for the preparation of cross-linked enzyme-loaded microgels. *Langmuir,* 34**,** 9731-9743.

BELLOQUE, J., GARCIA, M., TORRE, M. & MARINA, M. 2002. Analysis of soyabean proteins in meat products: a review. *Critical Reviews in Food Science and Nutrition,* 42**,** 507-532.

BINNIG, G., QUATE, C. F. & GERBER, C. 1986. Atomic force microscope. *Physical review letters,* 56**,** 930.

BIXLER, H. J. Recent developments in manufacturing and marketing carrageenan. Fifteenth International Seaweed Symposium: Proceedings of the Fifteenth International Seaweed Symposium held in Valdivia, Chile, in January 1995, 1996. Springer, 35-57.

BLAZEK, J. & GILBERT, E. P. 2011a. Application of small-angle X-ray and neutron scattering techniques to the characterisation of starch structure: A review. *Carbohydrate Polymers,* 85**,** 281-293.

BLAZEK, J. & GILBERT, E. P. J. C. P. 2011b. Application of small-angle X-ray and neutron scattering techniques to the characterisation of starch structure: A review. 85**,** 281-293.

BONGAERTS, J. H. H., FOURTOUNI, K. & STOKES, J. R. 2007. Soft-tribology: lubrication in a compliant PDMS–PDMS contact. *Tribology International,* 40**,** 1531-1542.

BORA, P. S., BREKKE, C. J. & POWERS, J. R. 1994. Heat induced gelation of pea (Pisum sativum) mixed globulins, vicilin and legumin. *Journal of Food Science,* 59**,** 594-596.

BROSSARD, N., CAI, H., OSORIO, F., BORDEU, E. & CHEN, J. 2016. "Oral" tribological study on the astringency sensation of red wines. *Journal of Texture Studies,* 47**,** 392-402.

BRUNCHI, C.-E., BERCEA, M., MORARIU, S. & DASCALU, M. 2016. Some properties of xanthan gum in aqueous solutions: effect of temperature and pH. *Journal of Polymer Research,* 23**,** 1-8.

BRYANT, C. & MCCLEMENTS, D. 2000. Influence of xanthan gum on physical characteristics of heat-denatured whey protein solutions and gels. *Food Hydrocolloids,* 14**,** 383-390.

BULëON, A., COLONNA, P., PLANCHOT, V. & BALL, S. 1998a. Starch granules: structure and biosynthesis. *International journal of biological macromolecules,* 23**,** 85-112.

BULëON, A., COLONNA, P., PLANCHOT, V. & BALL, S. J. I. J. O. B. M. 1998b. Starch granules: structure and biosynthesis. 23**,** 85-112.

BULGARIU, L. & BULGARIU, D. 2013. Selective extraction of Hg (II), Cd (II) and Zn (II) ions from aqueous media by a green chemistry procedure using aqueous two-phase systems. *Separation and Purification Technology,* 118**,** 209-216.

BUREY, P., BHANDARI, B., HOWES, T. & GIDLEY, M. 2008. Hydrocolloid gel particles: formation, characterization, and application. *Critical reviews in food science and nutrition,* 48**,** 361-377.

BUTLER, M. F. & HEPPENSTALL-BUTLER, M. 2003. Phase separation in gelatin/dextran and gelatin/maltodextrin mixtures. *Food Hydrocolloids,* 17**,** 815-830.

CAI, H., LI, Y. & CHEN, J. 2017. Rheology and tribology study of the sensory perception of oral care products. *Biotribology,* 10**,** 17-25.

CAPRON, I., COSTEUX, S. & DJABOUROV, M. 2001. Water in water emulsions: phase separation and rheology of biopolymer solutions. *Rheologica Acta,* 40**,** 441-456.

CARRILLO-NAVAS, H., AVILA-DE LA ROSA, G., GõMEZ-LURïA, D., MERAZ, M., ALVAREZ-RAMIREZ, J. & VERNON-CARTER, E. 2014. Impact of ghosts on the viscoelastic response of gelatinized corn starch dispersions subjected to small strain deformations. *Carbohydrate polymers,* 110**,** 156-162.

CARVALHO-DA-SILVA, A. M., VAN DAMME, I., TAYLOR, W., HORT, J. & WOLF, B. 2013. Oral processing of two milk chocolate samples. *Food & function,* 4**,** 461-469.

CASSIN, G., HEINRICH, E. & SPIKES, H. A. 2001. The influence of surface roughness on the lubrication properties of adsorbing and non-adsorbing biopolymers. *Tribology Letters,* 11**,** 95-102.

CHAUDEMANCHE, C. & BUDTOVA, T. 2008. Mixtures of pregelatinised maize starch and κ-carrageenan: Compatibility, rheology and gelation. *Carbohydrate Polymers,* 72**,** 579-589.

CHEN, J.-F., GUO, J., ZHANG, T., WAN, Z.-L., YANG, J. & YANG, X.-Q. 2018. Slowing the starch digestion by structural modification through preparing zein/pectin particle stabilized water-in-water emulsion. *Journal of agricultural and food chemistry,* 66**,** 4200-4207.

CHEN, J., LIU, Z. & PRAKASH, S. 2014. Lubrication studies of fluid food using a simple experimental set up. *Food Hydrocolloids,* 42**,** 100-105.

CHEN, J. & STOKES, J. R. 2012. Rheology and tribology: Two distinctive regimes of food texture sensation. *Trends in Food Science & Technology,* 25**,** 4-12.

CHOJNICKA-PASZUN, A., DE JONGH, H. H. J. & DE KRUIF, C. G. 2012. Sensory perception and lubrication properties of milk: Influence of fat content. *International Dairy Journal,* 26**,** 15-22.

CHOJNICKA-PASZUN, A., DOUSSINAULT, S. & DE JONGH, H. H. J. 2014. Sensorial analysis of polysaccharide–gelled protein particle dispersions in relation to lubrication and viscosity properties. *Food Research International,* 56**,** 199-210.

CLOSS, C., CONDE-PETIT, B., ROBERTS, I., TOLSTOGUZOV, V. & ESCHER, F. 1999. Phase separation and rheology of aqueous starch/galactomannan systems. *Carbohydrate Polymers,* 39**,** 67-77.

CONDE-PETIT, B., PFIRTER, A. & ESCHER, F. 1997. Influence of xanthan on the rheological properties of aqueous starch-emulsifier systems. *Food Hydrocolloids,* 11**,** 393-399.

COPELAND, L., BLAZEK, J., SALMAN, H. & TANG, M. C. 2009. Form and functionality of starch. *Food Hydrocolloids,* 23**,** 1527-1534.

CROGUENNEC, T., T O'KENNEDY, B. & MEHRA, R. 2004. Heat-induced denaturation/aggregation of β-lactoglobulin A and B: kinetics of the first intermediates formed. *International Dairy Journal,* 14**,** 399-409.

CROY, R., GATEHOUSE, J. A., TYLER, M. & BOULTER, D. 1980. The purification and characterization of a third storage protein (convicilin) from the seeds of pea (Pisum sativum L.). *Biochemical Journal,* 191**,** 509-516.

DABIJA, A., CODINĂ, G. G., GäTLAN, A.-M., SĂNDULEAC, E. T. & RUSU, L. 2018. Effects of some vegetable proteins addition on yogurt quality. *Scientific Study & Research. Chemistry & Chemical Engineering, Biotechnology, Food Industry,* 19**,** 181-192.

DALGLEISH, D. G. & HALLETT, F. R. 1995. Dynamic light scattering: applications to food systems. *Food Research International,* 28**,** 181-193.

DALGLEISH, D. G. & MORRIS, E. R. 1988. Interactions between carrageenans and casein micelles: electrophoretic and hydrodynamic properties of the particles. *Food Hydrocolloids,* 2**,** 311-320.

DAMODARAN, S. & ARORA, A. 2013. Off-flavor precursors in soy protein isolate and novel strategies for their removal. *Annual Review of Food Science and Technology,* 4**,** 327-346.

DANAEI, M., DEHGHANKHOLD, M., ATAEI, S., HASANZADEH DAVARANI, F., JAVANMARD, R., DOKHANI, A., KHORASANI, S. & MOZAFARI, M. R. 2018. Impact of Particle Size and Polydispersity Index on the Clinical Applications of Lipidic Nanocarrier Systems. *Pharmaceutics,* 10.

DAVID-BIRMAN, T., MACKIE, A. & LESMES, U. 2013. Impact of dietary fibers on the properties and proteolytic digestibility of lactoferrin nano-particles. *Food Hydrocolloids,* 31**,** 33-41.

DAY, L. 2013. Proteins from land plants – Potential resources for human nutrition and food security. *Trends in Food Science & Technology,* 32**,** 25-42.

DE FREITAS, R. A., NICOLAI, T., CHASSENIEUX, C. & BENYAHIA, L. 2016. Stabilization of water-in-water emulsions by polysaccharide-coated protein particles. *Langmuir,* 32**,** 1227-1232.

DE VICENTE, J., STOKES, J. & SPIKES, H. 2005a. The frictional properties of Newtonian fluids in rolling–sliding soft-EHL contact. *Tribology Letters,* 20**,** 273-286.

DE VICENTE, J., STOKES, J. R. & SPIKES, H. A. 2005b. Lubrication properties of non-adsorbing polymer solutions in soft elastohydrodynamic (EHD) contacts. *Tribology International,* 38**,** 515-526.

DE VICENTE, J., STOKES, J. R. & SPIKES, H. A. 2006. Soft lubrication of model hydrocolloids. *Food Hydrocolloids,* 20**,** 483-491.

DE VRIES, J. 2002. Interaction of carrageenan with other ingredients in dairy dessert gels. *Special Publication-Royal Society of Chemistry,* 278**,** 201-210.

DE VRIES, J. 2004. Hydrocolloid gelling agents and their applications. *In:* WILLIAMS, P. A. & PHILLIPS, G. O. (eds.) *Gums and Stabilisers for the Food Industry 12.* The Royal Society of Chemistry.

DE WIT, J. 1998. Nutritional and functional characteristics of whey proteins in food products. *Journal of dairy science,* 81**,** 597-608.

DEBET, M. R. & GIDLEY, M. J. 2007. Why do gelatinized starch granules not dissolve completely? Roles for amylose, protein, and lipid in granule "ghost" integrity. *Journal of Agricultural and Food Chemistry,* 55**,** 4752-4760.

DESTRIBATS, M., ROUVET, M., GEHIN-DELVAL, C., SCHMITT, C. & BINKS, B. P. 2014. Emulsions stabilised by whey protein microgel particles: towards food-grade Pickering emulsions. *Soft matter,* 10**,** 6941-6954.

DEVEZEAUX DE LAVERGNE, M., STRIJBOSCH, V. M., VAN DEN BROEK, A. W., VAN DE VELDE, F. & STIEGER, M. 2016. Uncoupling the Impact of Fracture Properties and Composition on Sensory Perception of Emulsion-Filled Gels. *Journal of Texture Studies,* 47**,** 92-111.

DIAMANTINO, V. R., COSTA, M. S., TABOGA, S. R., VILAMAIOR, P. S. L., FRANCO, C. M. L. & PENNA, A. L. B. 2019. Starch as a potential fat replacer for application in cheese: Behaviour of different starches in casein/starch mixtures and in the casein matrix. *International Dairy Journal,* 89**,** 129-138.

DICKINSON, E. 2009. Hydrocolloids and emulsion stability. *Handbook of hydrocolloids.* Elsevier.

DICKINSON, E. 2018. Hydrocolloids acting as emulsifying agents–How do they do it? *Food hydrocolloids,* 78**,** 2-14.

DICKINSON, E. 2019. Particle-based stabilization of water-in-water emulsions containing mixed biopolymers. *Trends in food science & technology,* 83**,** 31-40.

DICKINSON, E. 2020. Advances in food emulsions and foams: reflections on research in the neo-Pickering era. *Current Opinion in Food Science,* 33**,** 52-60.

DIMAKOPOULOS, Y., PAVLIDIS, M. & TSAMOPOULOS, J. 2013. Steady bubble rise in Herschel–Bulkley fluids and comparison of predictions via the augmented

Lagrangian method with those via the Papanastasiou model. *Journal of Non-Newtonian Fluid Mechanics,* 200**,** 34-51.

DING, P., WOLF, B., FRITH, W., CLARK, A., NORTON, I. & PACEK, A. 2002. Interfacial tension in phase-separated gelatin/dextran aqueous mixtures. *Journal of colloid and interface science,* 253**,** 367-376.

DONALD, A. 2001. Plasticization and self assembly in the starch granule. *Cereal chemistry,* 78**,** 307-314.

DOWSON, D. 2012. Bio-tribology. *Faraday Discussions,* 156**,** 9-30.

DOWSON, D. & WRIGHT, V. Bio-tribology.    Proceeding of the Conference on the Rheology of Lubrication, The Institute of Petroleum, The Institution of Mechanical Engineers, and the British Society of Rheology, 1973 London, UK. 81–88.

DRESSELHUIS, D. M., DE HOOG, E. H. A., STUART, M. A. C. & VAN AKEN, G. A. 2008. Application of oral tissue in tribological measurements in an emulsion perception context. *Food Hydrocolloids,* 22**,** 323-335.

DUNëR, G., THORMANN, E. & DĖDINAITĖ, A. 2013. Quartz Crystal Microbalance with Dissipation (QCM-D) studies of the viscoelastic response from a continuously growing grafted polyelectrolyte layer. *Journal of colloid and interface science,* 408**,** 229-234.

EGGLESTON, G., FINLEY, J. W. & DEMAN, J. M. 2018. Carbohydrates. *Principles of Food Chemistry.* Cham: Springer International Publishing.

ESQUENA, J. 2016. Water-in-water (W/W) emulsions. *Current Opinion in Colloid & Interface Science,* 25**,** 109-119.

EVANS, I. & LIPS, A. 1992. Viscoelasticity of gelatinized starch dispersions. *Journal of Texture Studies,* 23**,** 69-86.

FAKHARIAN, M.-H., TAMIMI, N., ABBASPOUR, H., NAFCHI, A. M. & KARIM, A. 2015. Effects of κ-carrageenan on rheological properties of dually modified sago starch: Towards finding gelatin alternative for hard capsules. *Carbohydrate polymers,* 132**,** 156-163.

FANG, Y. 2021. Mixed hydrocolloid systems. *Handbook of hydrocolloids.* Elsevier.

FARRëS, I. F., DOUAIRE, M. & NORTON, I. T. 2013. Rheology and tribological properties of Ca-alginate fluid gels produced by diffusion-controlled method. *Food Hydrocolloids,* 32**,** 115-122.

FERNãNDEZ FARRëS, I., MOAKES, R. J. A. & NORTON, I. T. 2014. Designing biopolymer fluid gels: A microstructural approach. *Food Hydrocolloids,* 42**,** 362-372.

FIROOZMAND, H., MURRAY, B. S. & DICKINSON, E. 2007. Fractal-type particle gel formed from gelatin+ starch solution. *Langmuir,* 23**,** 4646-4650.

FIROOZMAND, H., MURRAY, B. S. & DICKINSON, E. 2009. Interfacial structuring in a phase-separating mixed biopolymer solution containing colloidal particles. *Langmuir,* 25**,** 1300-1305.

FLANAGAN, S. E., MALANOWSKI, A. J., KIZILAY, E., SEEMAN, D., DUBIN, P. L., DONATO-CAPEL, L., BOVETTO, L. & SCHMITT, C. 2015. Complex equilibria, speciation, and heteroprotein coacervation of lactoferrin and β-lactoglobulin. *Langmuir,* 31**,** 1776-1783.

FOEGEDING, E. A. 2007. Rheology and sensory texture of biopolymer gels. *Current Opinion in Colloid & Interface Science,* 12**,** 242-250.

GABRIELE, A., SPYROPOULOS, F. & NORTON, I. 2009. Kinetic study of fluid gel formation and viscoelastic response with kappa-carrageenan. *Food Hydrocolloids,* 23**,** 2054-2061.

GABRIELE, A., SPYROPOULOS, F. & NORTON, I. T. 2010. A conceptual model for fluid gel lubrication. *Soft Matter,* 6**,** 4205-4213.

GAO, Z., FANG, Y., CAO, Y., LIAO, H., NISHINARI, K. & PHILLIPS, G. O. 2017. Hydrocolloid-food component interactions. *Food hydrocolloids,* 68**,** 149-156.

GARCıA-OCHOA, F., SANTOS, V., CASAS, J. & GõMEZ, E. 2000. Xanthan gum: production, recovery, and properties. *Biotechnology advances,* 18**,** 549-579.

GARREC, D. 2013. *Understanding fluid gels and hydrocolloid tribology - PhD Thesis.* University of Birmingham.

GARREC, D. A., GUTHRIE, B. & NORTON, I. T. 2013. Kappa carrageenan fluid gel material properties. Part 1: Rheology. *Food hydrocolloids,* 33**,** 151-159.

GARREC, D. A. & NORTON, I. T. 2012a. The influence of hydrocolloid hydrodynamics on lubrication. *Food Hydrocolloids,* 26**,** 389-397.

GARREC, D. A. & NORTON, I. T. 2012b. Understanding fluid gel formation and properties. *Journal of Food Engineering,* 112**,** 175-182.

GARREC, D. A. & NORTON, I. T. 2013. Kappa carrageenan fluid gel material properties. Part 2: Tribology. *Food Hydrocolloids,* 33**,** 160-167.

GISMONDI, A., D'AGOSTINO, A., CANUTI, L., DI MARCO, G., BASOLI, F. & CANINI, A. J. P. B.-A. I. J. D. W. A. A. O. P. B. 2019. Starch granules: a data collection of 40 food species. 153**,** 273-279.

GOH, K. K., TEO, A., SARKAR, A. & SINGH, H. 2020. Milk protein-polysaccharide interactions. *Milk proteins.* Elsevier.

GOH, S. M., VERSLUIS, P., APPELQVIST, I. A. M. & BIALEK, L. 2010. Tribological measurements of foods using a rheometer. *Food Research International,* 43**,** 183-186.

GONZALEZ-JORDAN, A., NICOLAI, T. & BENYAHIA, L. 2016. Influence of the protein particle morphology and partitioning on the behavior of particle-stabilized water-in-water emulsions. *Langmuir,* 32**,** 7189-7197.

GONZãLEZ, A. D., FROSTELL, B. & CARLSSON-KANYAMA, A. 2011. Protein efficiency per unit energy and per unit greenhouse gas emissions: potential contribution of diet choices to climate change mitigation. *Food policy,* 36**,** 562-570.

GRAHAM, D. & PHILLIPS, M. 1979. Proteins at liquid interfaces: II. Adsorption isotherms. *Journal of Colloid and Interface Science,* 70**,** 415-426.

GREISER, J. 2009. *Advances in Cryo-SEM: From Micrometers to Nanometers* [Online]. Available: https://www.americanlaboratory.com/914-Application-Notes/577-Advances-in-Cryo-SEM-From-Micrometers-to-Nanometers/ [Accessed].

GRIGG, D., RUSSELL, P. & GRIFFITH, J. 1992. Tip–sample forces in scanning probe microscopy in air and vacuum. *Journal of Vacuum Science & Technology A: Vacuum, Surfaces, and Films,* 10**,** 680-683.

GRINBERG, V. Y. & TOLSTOGUZOV, V. 1997. Thermodynamic incompatibility of proteins and polysaccharides in solutions. *Food Hydrocolloids,* 11**,** 145-158.

HARDHAM, A. R. 2012. Confocal microscopy in plant–pathogen interactions. *Plant fungal pathogens: methods and protocols***,** 295-309.

HAUG, I. J., DRAGET, K. I. & SMIDSRúD, O. 2004. Physical behaviour of fish gelatin-κ-carrageenan mixtures. *Carbohydrate Polymers,* 56**,** 11-19.

HAYAKAWA, F., KAZAMI, Y., ISHIHARA, S., NAKAO, S., NAKAUMA, M., FUNAMI, T., NISHINARI, K. & KOHYAMA, K. 2014. Characterization of eating difficulty by sensory evaluation of hydrocolloid gels. *Food Hydrocolloids,* 38**,** 95-103.

HAZT, B., BASSANI, H. P., ELIAS-MACHADO, J. P., BUZZO, J. L. A., SILVEIRA, J. L. & DE FREITAS, R. A. 2020. Effect of pH and protein particle shape on the stability of amylopectin–xyloglucan water-in-water emulsions. *Food Hydrocolloids,* 104**,** 105769.

HEMAR, Y., TAMEHANA, M., MUNRO, P. & SINGH, H. 2001. Viscosity, microstructure and phase behavior of aqueous mixtures of commercial milk protein products and xanthan gum. *Food Hydrocolloids,* 15**,** 565-574.

HENCHION, M., HAYES, M., MULLEN, A. M., FENELON, M. & TIWARI, B. 2017. Future protein supply and demand: strategies and factors influencing a sustainable equilibrium. *Foods,* 6**,** 53.

HERTZLER, S. R., LIEBLEIN-BOFF, J. C., WEILER, M. & ALLGEIER, C. 2020. Plant proteins: Assessing their nutritional quality and effects on health and physical function. *Nutrients,* 12**,** 3704.

HEYER, P. & LæUGER, J. A flexible platform for tribological measurements on a rheometer.   AIP Conference Proceedings, 2008. AIP, 1168-1170.

HEYER, P. & LæUGER, J. 2009. Correlation between friction and flow of lubricating greases in a new tribometer device. *Lubrication Science,* 21**,** 253-268.

HIGIRO, J., HERALD, T. J. & ALAVI, S. 2006. Rheological study of xanthan and locust bean gum interaction in dilute solution. *Food Research International,* 39**,** 165-175.

HOTCHKISS, S., BROOKS, M., CAMPBELL, R., PHILP, K. & TRIUS, A. 2016. The use of carrageenan in food. *Carrageenans: sources and extraction methods, molecular structure, bioactive properties and health effects***,** 229-243.

HU, J., ANDABLO-REYES, E., SOLTANAHMADI, S. & SARKAR, A. 2020. Synergistic microgel-reinforced hydrogels as high-performance lubricants. *ACS Macro Letters,* 9**,** 1726-1731.

HU, J., ANDABLO-REYES, E., MIGHELL, A., PAVITT, S. & SARKAR, A. 2021. Dry mouth diagnosis and saliva substitutes—A review from a textural perspective. *Journal of Texture Studies,* 52**,** 141-156.

HUC, D., MATIGNON, A., BAREY, P., DESPRAIRIES, M., MAUDUIT, S., SIEFFERMANN, J.-M. & MICHON, C. 2014. Interactions between modified starch and carrageenan during pasting. *Food hydrocolloids,* 36**,** 355-361.

HUTCHINGS, I. & SHIPWAY, P. 2017. *Tribology: friction and wear of engineering materials*, Butterworth-Heinemann.

HUTCHINGS, I. M. 2016. Leonardo da Vinci's studies of friction. *Wear,* 360-361**,** 51-66.

JANE, J.-L. 2007. Structure of starch granules. *Journal of applied glycoscience,* 54**,** 31-36.

JANE, J., CHEN, Y., LEE, L., MCPHERSON, A., WONG, K., RADOSAVLJEVIC, M. & KASEMSUWAN, T. 1999. Effects of amylopectin branch chain length and amylose content on the gelatinization and pasting properties of starch. *Cereal chemistry,* 76**,** 629-637.

JANE, J. L., KASEMSUWAN, T., LEAS, S., ZOBEL, H. & ROBYT, J. F. 1994. Anthology of starch granule morphology by scanning electron microscopy. *Starch-Stärke,* 46**,** 121-129.

JEOL, L. 2011. Introducing Cryo Scanning Electron Microscopy. *In:* JEOL APPLICATION DATA SHEET, S. (ed.). JEOL Application Data Sheet, SEM SM-B-004-00E. .

JI, Y., HAN, C., LIU, E., LI, X., MENG, X. & LIU, B. 2022. Pickering emulsions stabilized by pea protein isolate-chitosan nanoparticles: fabrication, characterization and delivery EPA for digestion in vitro and in vivo. *Food Chemistry,* 378**,** 132090.

JIAO, B., SHI, A., WANG, Q. & BINKS, B. P. 2018. High-internal-phase pickering emulsions stabilized solely by peanut-protein-isolate microgel particles with multiple potential applications. *Angewandte Chemie,* 130**,** 9418-9422.

JIN, W., SONG, R., XU, W., WANG, Y., LI, J., SHAH, B. R., LI, Y. & LI, B. 2015. Analysis of deacetylated konjac glucomannan and xanthan gum phase separation by film forming. *Food Hydrocolloids,* 48**,** 320-326.

JIN, Z., ZHENG, J., LI, W. & ZHOU, Z. 2016a. Tribology of medical devices. *Biosurface and Biotribology,* 2**,** 173-192.

JIN, Z. M., DOWSON, D. & FISHER, J. 1993. Fluid film lubrication in natural hip joints. *In:* DOWSON, D., TAYLOR, C. M., CHILDS, T. H. C., GODET, M. & DALMAZ, G. (eds.) *Tribology Series.* Elsevier.

JIN, Z. M., ZHENG, J., LI, W. & ZHOU, Z. R. 2016b. Tribology of medical devices. *Biosurface and Biotribology,* 2**,** 173-192.

JOBLING, S. 2004. Improving starch for food and industrial applications. *Current Opinion in Plant Biology,* 7**,** 210-218.

JOST, H. P. 1966. Lubrication (Tribology) – A Report on the Present Position and Industry's Needs. London, UK: Department of Education and Science, HM. Stationary Office.

JOYNER, H. S., PERNELL, C. W. & DAUBERT, C. R. 2014. Impact of parameter settings on normal force and gap height during tribological measurements. *Journal of Food Engineering,* 137**,** 51-63.

KABOORANI, A. & BLANCHET, P. 2014. Determining the linear viscoelastic region of sugar maple wood by dynamic mechanical analysis. *BioResources,* 9**,** 4392-4409.

KEATING, C. D. 2012. Aqueous phase separation as a possible route to compartmentalization of biological molecules. *Accounts of chemical research,* 45**,** 2114-2124.

KELESSIDIS, V., MAGLIONE, R., TSAMANTAKI, C. & ASPIRTAKIS, Y. 2006. Optimal determination of rheological parameters for Herschel–Bulkley drilling fluids and impact on pressure drop, velocity profiles and penetration rates during drilling. *Journal of Petroleum Science and Engineering,* 53**,** 203-224.

KEW, B., HOLMES, M., STIEGER, M. & SARKAR, A. 2021. Oral tribology, adsorption and rheology of alternative food proteins. *Food Hydrocolloids,* 116**,** 106636.

KHEMISSI, H., BASSANI, H., ASCHI, A., CAPRON, I., BENYAHIA, L. & NICOLAI, T. 2018. Exploiting complex formation between polysaccharides and protein microgels to influence particle stabilization of W/W emulsions. *Langmuir,* 34**,** 11806-11813.

KIM, C. & YOO, B. 2006. Rheological properties of rice starch–xanthan gum mixtures. *Journal of Food Engineering,* 75**,** 120-128.

KIUMARSI, M., SHAHBAZI, M., YEGANEHZAD, S., MAJCHRZAK, D., LIELEG, O. & WINKELJANN, B. 2019. Relation between structural, mechanical and sensory properties of gluten-free bread as affected by modified dietary fibers. *Food Chemistry,* 277**,** 664-673.

KOé, H., DRAKE, M., VINYARD, C. J., ESSICK, G., VAN DE VELDE, F. & FOEGEDING, E. A. 2019. Emulsion filled polysaccharide gels: Filler particle effects on material properties, oral processing, and sensory texture. *Food Hydrocolloids,* 94**,** 311-325.

KOGA, S., WILLIAMS, D. S., PERRIMAN, A. W. & MANN, S. 2011. Peptide–nucleotide microdroplets as a step towards a membrane-free protocell model. *Nature chemistry,* 3**,** 720-724.

KOKINI, J. L., KADANE, J. B. & CUSSLER, E. L. 1977. Liquid texture perceived in the mouth. *Journal of Texture Studies,* 8**,** 195-218.

KORNET, R., SHEK, C., VENEMA, P., VAN DER GOOT, A. J., MEINDERS, M. & VAN DER LINDEN, E. 2021. Substitution of whey protein by pea protein is facilitated by specific fractionation routes. *Food Hydrocolloids,* 117**,** 106691.

KREFTING, J. 2017. The Appeal of Pea Protein. *Journal of Renal Nutrition,* 27**,** e31-e33.

KROP, E. M., HETHERINGTON, M. M., HOLMES, M., MIQUEL, S. & SARKAR, A. 2019a. On relating rheology and oral tribology to sensory properties in hydrogels. *Food Hydrocolloids,* 88**,** 101-113.

KROP, E. M., HETHERINGTON, M. M., MIQUEL, S. & SARKAR, A. 2019b. The influence of oral lubrication on food intake: A proof-of-concept study. *Food Quality and Preference,* 74**,** 118-124.

KRZEMINSKI, A., WOHLHþTER, S., HEYER, P., UTZ, J. & HINRICHS, J. 2012. Measurement of lubricating properties in a tribosystem with different surface roughness. *International Dairy Journal,* 26**,** 23-30.

KULICKE, W. M., EIDAM, D., KATH, F., KIX, M. & KULL, A. H. 1996. Hydrocolloids and rheology: Regulation of visco-elastic characteristics of waxy rice starch in mixtures with galactomannans. *Starch-stärke,* 48**,** 105-114.

LAFARGUE, D., LOURDIN, D. & DOUBLIER, J.-L. 2007. Film-forming properties of a modified starch/κ-carrageenan mixture in relation to its rheological behaviour. *Carbohydrate Polymers,* 70**,** 101-111.

LAGUNA, L., FARRELL, G., BRYANT, M., MORINA, A. & SARKAR, A. 2017a. Relating rheology and tribology of commercial dairy colloids to sensory perception. *Food & function,* 8**,** 563-573.

LAGUNA, L. & SARKAR, A. 2016. Influence of mixed gel structuring with different degrees of matrix inhomogeneity on oral residence time. *Food Hydrocolloids,* 61**,** 286-299.

LAGUNA, L. & SARKAR, A. 2017a. Oral tribology: update on the relevance to study astringency in wines. *Tribology-Materials, Surfaces & Interfaces,* 11**,** 116-123.

LAGUNA, L. & SARKAR, A. 2017b. Oral tribology: update on the relevance to study astringency in wines. *Tribology - Materials, Surfaces & Interfaces,* 11**,** 116-123.

LAGUNA, L., SARKAR, A., BRYANT, M. G., BEADLING, A. R., BARTOLOMё, B. & VICTORIA MORENO-ARRIBAS, M. 2017b. Exploring mouthfeel in model wines: Sensory-to-instrumental approaches. *Food Research International,* 102**,** 478-486.

LAIHO, S., WILLIAMS, R. P. W., POELMAN, A., APPELQVIST, I. & LOGAN, A. 2017. Effect of whey protein phase volume on the tribology, rheology and sensory properties of fat-free stirred yoghurts. *Food Hydrocolloids,* 67**,** 166-177.

LAPASIN, R. 2012. *Rheology of industrial polysaccharides: theory and applications*, Springer Science & Business Media.

LAPASIN, R. & PRICL, S. 1995. Rheology of polysaccharide systems. *Rheology of Industrial Polysaccharides: Theory and Applications.* Boston, MA: Springer US.

LASCOMBES, C., AGODA-TANDJAWA, G., BOULENGUER, P., LE GARNEC, C., GILLES, M., MAUDUIT, S., BAREY, P. & LANGENDORFF, V. 2017. Starch-carrageenan interactions in aqueous media: Role of each polysaccharide chemical and macromolecular characteristics. *Food Hydrocolloids,* 66**,** 176-189.

LEE, H. J., HOLLENBECK, R. G., MORGAN, J. A., KRUGER HOWARD, A., SIDDIQUI, A., SAYEED, V. A., SELEN, A. & HOAG, S. W. 2022. A method for the tribological assessment of oral pharmaceutical liquids. *Drug Development and Industrial Pharmacy,* 48**,** 198-210.

LI, X., CHENG, Y., YI, C., HUA, Y., YANG, C. & CUI, S. 2009. Effect of ionic strength on the heat-induced soy protein aggregation and the phase separation of soy protein aggregate/dextran mixtures. *Food Hydrocolloids,* 23**,** 1015-1023.

LI, X., MURRAY, B. S., YANG, Y. & SARKAR, A. 2020. Egg white protein microgels as aqueous Pickering foam stabilizers: Bubble stability and interfacial properties. *Food Hydrocolloids,* 98**,** 105292.

LI, Y. F., HUANG, C. Z. & LI, M. 2002. A resonance light-scattering determination of proteins with fast green FCF. *Analytical sciences,* 18**,** 177-181.

LIAMAS, E., CONNELL, S. D. & SARKAR, A. 2023. Frictional behaviour of plant proteins in soft contacts: unveiling nanoscale mechanisms. *Nanoscale Advances,* 5**,** 1102-1114.

LIAMAS, E., CONNELL, S. D., ZEMBYLA, M., ETTELAIE, R. & SARKAR, A. 2021. Friction between soft contacts at nanoscale on uncoated and protein-coated surfaces. *Nanoscale,* 13**,** 2350-2367.

LIANG, H.-N. & TANG, C.-H. 2014. Pea protein exhibits a novel Pickering stabilization for oil-in-water emulsions at pH 3.0. *LWT-Food Science and Technology,* 58**,** 463-469.

LIMBERT, G., MASEN, M. A., POND, D., GRAHAM, H. K., SHERRATT, M. J., JOBANPUTRA, R. & MCBRIDE, A. 2019. Biotribology of the ageing skin—Why we should care. *Biotribology,* 17**,** 75-90.

LIU, F., OU, S.-Y. & TANG, C.-H. 2017. Ca2+-induced soy protein nanoparticles as pickering stabilizers: Fabrication and characterization. *Food Hydrocolloids,* 65**,** 175-186.

LIU, F. & TANG, C.-H. 2013. Soy protein nanoparticle aggregates as pickering stabilizers for oil-in-water emulsions. *Journal of agricultural and food chemistry,* 61**,** 8888-8898.

LIU, F. & TANG, C.-H. 2014. Emulsifying properties of soy protein nanoparticles: influence of the protein concentration and/or emulsification process. *Journal of Agricultural and Food Chemistry,* 62**,** 2644-2654.

LIU, K., STIEGER, M., VAN DER LINDEN, E. & VAN DE VELDE, F. 2016. Tribological properties of rice starch in liquid and semi-solid food model systems. *Food Hydrocolloids,* 58**,** 184-193.

LIU, R., WANG, L., LIU, Y., WU, T. & ZHANG, M. 2018. Fabricating soy protein hydrolysate/xanthan gum as fat replacer in ice cream by combined enzymatic and heat-shearing treatment. *Food Hydrocolloids,* 81**,** 39-47.

LIU, S. & WANG, Y. 2010. Application of AFM in microbiology: a review. *Scanning,* 32**,** 61-73.

LIU, S. X. & KIM, J.-T. 2009. Application of Kevin—Voigt model in quantifying whey protein adsorption on polyethersulfone using QCM-D. *JALA: Journal of the Association for Laboratory Automation,* 14**,** 213-220.

LOBATO-CALLEROS, C., RAMïREZ-SANTIAGO, C., VERNON-CARTER, E. J. & ALVAREZ-RAMIREZ, J. 2014. Impact of native and chemically modified starches addition as fat replacers in the viscoelasticity of reduced-fat stirred yogurt. *Journal of Food Engineering,* 131**,** 110-115.

LORBER, B., FISCHER, F., BAILLY, M., ROY, H. & KERN, D. 2012. Protein analysis by dynamic light scattering: Methods and techniques for students. *Biochemistry and molecular biology education,* 40**,** 372-382.

LORëN, N., HERMANSSON, A.-M., WILLIAMS, M., LUNDIN, L., FOSTER, T., HUBBARD, C., CLARK, A., NORTON, I., BERGSTRøM, E. & GOODALL, D. 2001. Phase separation induced by conformational ordering of gelatin in gelatin/maltodextrin mixtures. *Macromolecules,* 34**,** 289-297.

LUDEMA, K. C. & AJAYI, L. 2018. *Friction, wear, lubrication: a textbook in tribology*, CRC press.

LUNDIN, L., ODIC, K., FOSTER, T. & NORTON, I. 2000. Phase separation in mixed carrageenan systems. *Supramolecular and Colloidal Structures in Biomaterials and Biosubstrates.* World Scientific.

MA, L., GAISINSKAYA-KIPNIS, A., KAMPF, N. & KLEIN, J. 2015. Origins of hydration lubrication. *Nature communications,* 6**,** 1-6.

MACHADO, J. P., CAPRON, I., DE FREITAS, R. A., BENYAHIA, L. & NICOLAI, T. 2022. Stabilization of amylopectin-pullulan water in water emulsions by Interacting protein particles. *Food Hydrocolloids,* 124**,** 107320.

MALONE, M. E., APPELQVIST, I. A. M. & NORTON, I. T. 2003. Oral behaviour of food hydrocolloids and emulsions. Part 1. Lubrication and deposition considerations. *Food Hydrocolloids,* 17**,** 763-773.

MANG, T., BOBZIN, K. & BARTELS, T. 2011. *Industrial tribology: Tribosystems, friction, wear and surface engineering, lubrication*, John Wiley & Sons.

MANN, A. & TIGHE, B. 2016a. Ocular biotribology and the contact lens: surface interactions and ocular response. *Biomaterials and regenerative medicine in ophthalmology.* Elsevier.

MANN, A. & TIGHE, B. J. 2016b. 3 - Ocular biotribology and the contact lens: Surface interactions and ocular response. *In:* CHIRILA, T. V. & HARKIN, D. G. (eds.) *Biomaterials and Regenerative Medicine in Ophthalmology (Second Edition).* Woodhead Publishing.

MATSUMIYA, K. & MURRAY, B. S. 2016. Soybean protein isolate gel particles as foaming and emulsifying agents. *Food Hydrocolloids,* 60**,** 206-215.

MCCLEMENTS, D. J. 2014. *Nanoparticle-and microparticle-based delivery systems: Encapsulation, protection and release of active compounds*, CRC press.

MCCLEMENTS, D. J. 2015. *Food emulsions: principles, practices, and techniques*, CRC press.

MESHULAM, D. & LESMES, U. 2014. Responsiveness of emulsions stabilized by lactoferrin nano-particles to simulated intestinal conditions. *Food & function,* 5**,** 65-73.

MESSION, J.-L., CHIHI, M. L., SOK, N. & SAUREL, R. 2015. Effect of globular pea proteins fractionation on their heat-induced aggregation and acid cold-set gelation. *Food Hydrocolloids,* 46**,** 233-243.

MEZGER, T. 2020. *The rheology handbook: for users of rotational and oscillatory rheometers*, European Coatings.

MOHAMMED, A. & ABDULLAH, A. Scanning electron microscopy (SEM): A review.   Proceedings of the 2018 International Conference on Hydraulics and Pneumatics—HERVEX, Băile Govora, Romania, 2018. 7-9.

MORENO, H. M., DOMINGUEZ-TIMON, F., DïAZ, M. T., PEDROSA, M. M., BORDERïAS, A. J. & TOVAR, C. A. 2020. Evaluation of gels made with different commercial pea protein isolate: Rheological, structural and functional properties. *Food Hydrocolloids,* 99**,** 105375.

MORRIS, E. R. 2009. Functional interactions in gelling biopolymer mixtures. *Modern biopolymer science.* Elsevier.

MOSCHAKIS, T., MURRAY, B. S. & DICKINSON, E. 2005. Microstructural evolution of viscoelastic emulsions stabilised by sodium caseinate and xanthan gum. *Journal of Colloid and Interface Science,* 284**,** 714-728.

MULLER, D. J., DUMITRU, A. C., LO GIUDICE, C., GAUB, H. E., HINTERDORFER, P., HUMMER, G., DE YOREO, J. J., DUFRïNE, Y. F. &

ALSTEENS, D. 2020. Atomic force microscopy-based force spectroscopy and multiparametric imaging of biomolecular and cellular systems. *Chemical Reviews,* 121**,** 11701-11725.

MURRAY, B. & ETTELAIE, R. 2020. Bijel Systems Based on the Phase Separation of Biological Macromolecules. *Bijels.*

MURRAY, B. S. 2019. Pickering emulsions for food and drinks. *Current Opinion in Food Science,* 27**,** 57-63.

MURRAY, B. S. & PHISARNCHANANAN, N. 2014. The effect of nanoparticles on the phase separation of waxy corn starch+ locust bean gum or guar gum. *Food Hydrocolloids,* 42**,** 92-99.

MURRAY, B. S. & PHISARNCHANANAN, N. 2016. Whey protein microgel particles as stabilizers of waxy corn starch+ locust bean gum water-in-water emulsions. *Food Hydrocolloids,* 56**,** 161-169.

MYANT, C., SPIKES, H. A. & STOKES, J. R. 2010. Influence of load and elastic properties on the rolling and sliding friction of lubricated compliant contacts. *Tribology International,* 43**,** 55-63.

NECAS, J. & BARTOSIKOVA, L. 2013. Carrageenan: a review. *Veterinarni medicina,* 58**,** 187-205.

NGUYEN, P. T., KRAVCHUK, O., BHANDARI, B. & PRAKASH, S. 2017. Effect of different hydrocolloids on texture, rheology, tribology and sensory perception of texture and mouthfeel of low-fat pot-set yoghurt. *Food Hydrocolloids,* 72**,** 90-104.

NGUYEN, P. T. M., BHANDARI, B. & PRAKASH, S. 2016. Tribological method to measure lubricating properties of dairy products. *Journal of Food Engineering,* 168**,** 27-34.

NICOLAI, T. 2016. Formation and functionality of self-assembled whey protein microgels. *Colloids and Surfaces B: Biointerfaces,* 137**,** 32-38.

NICOLAI, T., BRITTEN, M. & SCHMITT, C. 2011. β-Lactoglobulin and WPI aggregates: Formation, structure and applications. *Food Hydrocolloids,* 25**,** 1945-1962.

NICOLAI, T. & MURRAY, B. 2017. Particle stabilized water in water emulsions. *Food Hydrocolloids,* 68**,** 157-163.

NISHINARI, K. & TAKAHASHI, R. 2003. Interaction in polysaccharide solutions and gels. *Current Opinion in Colloid & Interface Science,* 8**,** 396-400.

NOBBMANN, U., CONNAH, M., FISH, B., VARLEY, P., GEE, C., MULOT, S., CHEN, J., ZHOU, L., LU, Y. & SHENG, F. 2007. Dynamic light scattering as a relative tool for assessing the molecular integrity and stability of monoclonal antibodies. *Biotechnology and Genetic Engineering Reviews,* 24**,** 117-128.

NORTON, I. T., SPYROPOULOS, F. & COX, P. 2010. *Practical food rheology: an interpretive approach*, John Wiley & Sons.

NOSONOVSKY, M. & BHUSHAN, B. 2010. Green tribology: principles, research areas and challenges. The Royal Society Publishing.

O'KANE, F. E., HAPPE, R. P., VEREIJKEN, J. M., GRUPPEN, H. & VAN BOEKEL, M. A. 2004. Heat-induced gelation of pea legumin: Comparison with soybean glycinin. *Journal of Agricultural and Food Chemistry,* 52**,** 5071-5078.

OH, J. K., DRUMRIGHT, R., SIEGWART, D. J. & MATYJASZEWSKI, K. 2008. The development of microgels/nanogels for drug delivery applications. *Progress in polymer science,* 33**,** 448-477.

OSSWALD, T. & RUDOLPH, N. 2015. Polymer rheology. *Carl Hanser, München*.

PAWLEY, J. 2006. *Handbook of biological confocal microscopy*, Springer Science & Business Media.

PEDDIREDDY, K. R., NICOLAI, T., BENYAHIA, L. & CAPRON, I. 2016. Stabilization of water-in-water emulsions by nanorods. *ACS Macro Letters,* 5**,** 283-286.

PERRO, A., COUDON, N., CHAPEL, J.-P., MARTIN, N., BëVEN, L. & DOULIEZ, J.-P. 2022. Building micro-capsules using water-in-water emulsion droplets as templates. *Journal of Colloid and Interface Science,* 613**,** 681-696.

PETRI, D. F. 2015. Xanthan gum: A versatile biopolymer for biomedical and technological applications. *Journal of Applied Polymer Science,* 132.

PICKERING, S. U. 1907. Cxcvi.—emulsions. *Journal of the Chemical Society, Transactions,* 91**,** 2001-2021.

PICOUT, D. R. & ROSS-MURPHY, S. B. 2003. Rheology of biopolymer solutions and gels. *TheScientificWorldJournal,* 3**,** 105-121.

PIPE, C. J., MAJMUDAR, T. S. & MCKINLEY, G. H. 2008. High shear rate viscometry. *Rheologica Acta,* 47**,** 621-642.

PRADAL, C. & STOKES, J. R. 2016. Oral tribology: bridging the gap between physical measurements and sensory experience. *Current Opinion in Food Science,* 9**,** 34-41.

PRAKASH, S., TAN, D. D. Y. & CHEN, J. 2013. Applications of tribology in studying food oral processing and texture perception. *Food Research International,* 54**,** 1627-1635.

PTASZEK, A., BERSKI, W., PTASZEK, P., WITCZAK, T., REPELEWICZ, U. & GRZESIK, M. 2009. Viscoelastic properties of waxy maize starch and selected non-starch hydrocolloids gels. *Carbohydrate Polymers,* 76**,** 567-577.

PUNIA, S., SIROHA, A. K., SANDHU, K. S. & KAUR, M. 2019. Rheological and pasting behavior of OSA modified mungbean starches and its utilization in cake formulation as fat replacer. *International Journal of Biological Macromolecules,* 128**,** 230-236.

RAMASUBBU, N., THOMAS, L. M., BHANDARY, K. K. & LEVINE, M. J. 1993. Structural characteristics of human salivary statherin: a model for boundary lubrication at the enamel surface. *Critical Reviews in Oral Biology & Medicine,* 4**,** 363-370.

RAMSDEN, W. 1904. Separation of solids in the surface-layers of solutions and 'suspensions'(observations on surface-membranes, bubbles, emulsions, and mechanical coagulation).—Preliminary account. *Proceedings of the royal Society of London,* 72**,** 156-164.

RATNAYAKE, W. S. & JACKSON, D. S. 2008. Starch gelatinization. *Advances in food and nutrition research,* 55**,** 221-268.

RAWTANI, D. & AGRAWAL, Y. 2013. A study of the behavior of HNT with DNA intercalator acridine orange. *BioNanoScience,* 3**,** 52-57.

RENAUD, M., BELGACEM, M. N. & RINAUDO, M. 2005. Rheological behaviour of polysaccharide aqueous solutions. *Polymer,* 46**,** 12348-12358.

RMAILE, A., CARUGO, D., CAPRETTO, L., ZHANG, X., WHARTON, J. A., THURNER, P. J., ASPIRAS, M., WARD, M. & STOODLEY, P. 2013. Microbial tribology and disruption of dental plaque bacterial biofilms. *Wear,* 306**,** 276-284.

ROBINSON, G., ROSS-MURPHY, S. B. & MORRIS, E. R. 1982. Viscosity-molecular weight relationships, intrinsic chain flexibility, and dynamic solution properties of guar galactomannan. *Carbohydrate Research,* 107**,** 17-32.

ROCHAS, C. & LANDRY, S. 1987. Molecular organization of kappa carrageenan in aqueous solution. *Carbohydrate polymers,* 7**,** 435-447.

ROCHAS, C. & RINAUDO, M. 1982. Calorimetric determination of the conformational transition of kappa carrageenan. *Carbohydrate Research,* 105**,** 227-236.

ROCHAS, C. & RINAUDO, M. 1984. Mechanism of gel formation in κ-carrageenan. *Biopolymers: Original Research on Biomolecules,* 23**,** 735-745.

ROFES, L., ARREOLA, V., MUKHERJEE, R., SWANSON, J. & CLAVë, P. 2014. The effects of a xanthan gum-based thickener on the swallowing function of patients with dysphagia. *Alimentary Pharmacology & Therapeutics,* 39**,** 1169-1179.

SANDBERG, A. S. 2011. 15 - Developing functional ingredients: a case study of pea protein. *In:* SAARELA, M. (ed.) *Functional Foods (Second Edition).* Woodhead Publishing.

SANTAGIULIANA, M., CHRISTAKI, M., PIQUERAS-FISZMAN, B., SCHOLTEN, E. & STIEGER, M. 2018. Effect of mechanical contrast on sensory perception of heterogeneous liquid and semi-solid foods. *Food Hydrocolloids,* 83**,** 202-212.

SARKAR, A., ADEMUYIWA, V., STUBLEY, S., ESA, N. H., GOYCOOLEA, F. M., QIN, X., GONZALEZ, F. & OLVERA, C. 2018. Pickering emulsions co-stabilized by composite protein/polysaccharide particle-particle interfaces: Impact on in vitro gastric stability. *Food Hydrocolloids,* 84**,** 282-291.

SARKAR, A., ANDABLO-REYES, E., BRYANT, M., DOWSON, D. & NEVILLE, A. 2019a. Lubrication of soft oral surfaces. *Current Opinion in Colloid & Interface Science,* 39**,** 61-75.

SARKAR, A., ANDABLO-REYES, E., BRYANT, M., DOWSON, D. & NEVILLE, A. 2019b. Lubrication of soft oral surfaces. *Current opinion in colloid & interface science.*

SARKAR, A. & DICKINSON, E. 2020. Sustainable food-grade Pickering emulsions stabilized by plant-based particles. *Current Opinion in Colloid & Interface Science,* 49**,** 69-81.

SARKAR, A., KANTI, F., GULOTTA, A., MURRAY, B. S. & ZHANG, S. 2017a. Aqueous lubrication, structure and rheological properties of whey protein microgel particles. *Langmuir,* 33**,** 14699-14708.

SARKAR, A. & KROP, E. M. 2019a. Marrying oral tribology to sensory perception: A systematic review. *Current Opinion in Food Science,* 27**,** 64-73.

SARKAR, A. & KROP, E. M. 2019b. Marrying oral tribology to sensory perception: a systematic review. *Current Opinion in Food Science.*

SARKAR, A., MURRAY, B., HOLMES, M., ETTELAIE, R., ABDALLA, A. & YANG, X. 2016. In vitro digestion of Pickering emulsions stabilized by soft whey protein microgel particles: influence of thermal treatment. *Soft Matter,* 12**,** 3558-3569.

SARKAR, A. & SINGH, H. 2012. Oral Behaviour of Food Emulsions. *In:* CHEN, J. & ENGELEN, L. (eds.) *Food Oral Processing: : Fundamentals of Eating and Sensory Perception.* Chicester, West Sussex, UK: Blackwell Publishing Ltd.

SARKAR, A., SOLTANAHMADI, S., CHEN, J. & STOKES, J. R. 2021. Oral tribology: Providing insight into oral processing of food colloids. *Food Hydrocolloids,* 117**,** 106635.

SARKAR, A., XU, F. & LEE, S. 2019c. Human saliva and model saliva at bulk to adsorbed phases–similarities and differences. *Advances in Colloid and Interface Science,* 273**,** 102034.

SARKAR, A., YE, A. & SINGH, H. 2017b. Oral processing of emulsion systems from a colloidal perspective. *Food & Function,* 8**,** 511-521.

SARKAR, A., ZHANG, S., HOLMES, M. & ETTELAIE, R. 2019d. Colloidal aspects of digestion of Pickering emulsions: Experiments and theoretical models of lipid digestion kinetics. *Advances in colloid and interface science,* 263**,** 195-211.

SAXENA, S., HANSEN, C. E. & LYON, L. A. 2014. Microgel mechanics in biomaterial design. *Accounts of chemical research,* 47**,** 2426-2434.

SAY, G. A. J. M. M. 1999. Principles of optics.

SCHIPPER, R. G., SILLETTI, E. & VINGERHOEDS, M. H. 2007. Saliva as research material: biochemical, physicochemical and practical aspects. *Archives of oral biology,* 52**,** 1114-1135.

SCHIRMER, M., JEKLE, M. & BECKER, T. 2015. Starch gelatinization and its complexity for analysis. *Starch-Stärke,* 67**,** 30-41.

SCHMITT, C., SANCHEZ, C., DESOBRY-BANON, S. & HARDY, J. 1998. Structure and technofunctional properties of protein-polysaccharide complexes: a review. *Critical reviews in food science and nutrition,* 38**,** 689-753.

SCHOLTEN, E., VISSER, J. E., SAGIS, L. M. & VAN DER LINDEN, E. 2004. Ultralow interfacial tensions in an aqueous phase-separated gelatin/dextran and gelatin/gum arabic system: A comparison. *Langmuir,* 20**,** 2292-2297.

SELWAY, N. & STOKES, J. R. 2013. Insights into the dynamics of oral lubrication and mouthfeel using soft tribology: Differentiating semi-fluid foods with similar rheology. *Food Research International,* 54**,** 423-431.

SEMENOVA, M. G. & DICKINSON, E. 2010. *Biopolymers in food colloids: Thermodynamics and molecular interactions*, CRC Press.

SHAHRIVAR, K., ORTIGOSA-MOYA, E. M., HIDALGO-ALVAREZ, R. & DE VICENTE, J. 2019. Isoviscous elastohydrodynamic lubrication of inelastic Non-Newtonian fluids. *Tribology International*.

SHAND, P., YA, H., PIETRASIK, Z. & WANASUNDARA, P. 2007. Physicochemical and textural properties of heat-induced pea protein isolate gels. *Food Chemistry,* 102**,** 1119-1130.

SHAO, Y. & TANG, C.-H. 2016. Gel-like pea protein Pickering emulsions at pH 3.0 as a potential intestine-targeted and sustained-release delivery system for β-carotene. *Food research international,* 79**,** 64-72.

SHERMAN 1969. A texture profile of foodstuffs based upon well-defined rheological properties. *Journal of Food Science,* 34**,** 458-462.

SHEWAN, H. M., PRADAL, C. & STOKES, J. R. 2019. Tribology and its growing use toward the study of food oral processing and sensory perception. *Journal of Texture Studies*.

SHEWAN, H. M. & STOKES, J. R. 2013. Review of techniques to manufacture micro-hydrogel particles for the food industry and their applications. *Journal of Food Engineering,* 119**,** 781-792.

SHIMIZU, Y. & SPIKES, H. A. 2016. The influence of slide–roll ratio on ZDDP tribofilm formation. *Tribology Letters,* 64**,** 19.

SHUM, H. C., ABATE, A. R., LEE, D., STUDART, A. R., WANG, B., CHEN, C. H., THIELE, J., SHAH, R. K., KRUMMEL, A. & WEITZ, D. A. 2010. Droplet

microfluidics for fabrication of non-spherical particles. *Macromolecular rapid communications,* 31**,** 108-118.

SIKORA, M., KOWALSKI, S. & TOMASIK, P. 2008. Binary hydrocolloids from starches and xanthan gum. *Food Hydrocolloids,* 22**,** 943-952.

SILVĕRIO, S. C., RODRïGUEZ, O., TAVARES, A. P., TEIXEIRA, J. & MACEDO, E. 2013. Laccase recovery with aqueous two-phase systems: enzyme partitioning and stability. *Journal of Molecular Catalysis B: Enzymatic,* 87**,** 37-43.

SIMONET, F., GARNIER, C. & DOUBLIER, J.-L. 2000. Partition of proteins in the aqueous guar/dextran two-phase system. *Food hydrocolloids,* 14**,** 591-600.

SNOEREN, T. H. M. 1976. *Kappa-Carrageenan: a study on its physico-chemical properties, sol-gel transition and interaction with milk proteins*, Wageningen University and Research.

SOLTANAHMADI, S., MURRAY, B. S. & SARKAR, A. 2022. Comparison of oral tribological performance of proteinaceous microgel systems with protein-polysaccharide combinations. *Food Hydrocolloids,* 129**,** 107660.

STICK, R. V. & WILLIAMS, S. 2010. *Carbohydrates: the essential molecules of life*, Elsevier.

STOKES, J. R., BOEHM, M. W. & BAIER, S. K. 2013. Oral processing, texture and mouthfeel: From rheology to tribology and beyond. *Current Opinion in Colloid & Interface Science,* 18**,** 349-359.

STOKES, J. R., MACAKOVA, L., CHOJNICKA-PASZUN, A., DE KRUIF, C. G. & DE JONGH, H. H. 2011a. Lubrication, adsorption, and rheology of aqueous polysaccharide solutions. *Langmuir,* 27**,** 3474-3484.

STOKES, J. R., MACAKOVA, L., CHOJNICKA-PASZUN, A., DE KRUIF, C. G., DE JONGH, H. H. J. & INSTITUTET, Y. K. I. Y. 2011b. Lubrication, adsorption, and rheology of aqueous polysaccharide solutions. *Langmuir* 27**,** 3474-3484.

STOKES, J. R., MACAKOVA, L., CHOJNICKA-PASZUN, A., DE KRUIF, C. G., DE JONGH, H. H. J. & INSTITUTET, Y. K. I. Y. 2011c. Lubrication, adsorption, and rheology of aqueous polysaccharide solutions. *Langmuir : the ACS journal of surfaces and colloids,* 27**,** 3474-3484.

STOKES, J. R., WOLF, B. & FRITH, W. 2001. Phase-separated biopolymer mixture rheology: Prediction using a viscoelastic emulsion model. *Journal of Rheology,* 45**,** 1173-1191.

STRIBIȚCAIA, E., GIBBONS, C., SIER, J., BOESCH, C., BLUNDELL, J., FINLAYSON, G. & SARKAR, A. 2021. Effects of oral lubrication on satiety, satiation and salivary biomarkers in model foods: A pilot study. *Appetite,* 165**,** 105427.

STRIBIȚCAIA, E., KROP, E. M., LEWIN, R., HOLMES, M. & SARKAR, A. 2020. Tribology and rheology of bead-layered hydrogels: Influence of bead size on sensory perception. *Food Hydrocolloids,* 104**,** 105692.

SUJKA, M. & JAMROZ, J. 2013. Ultrasound-treated starch: SEM and TEM imaging, and functional behaviour. *Food Hydrocolloids,* 31**,** 413-419.

TAKEMASA, M., CHIBA, A. & DATE, M. 2001. Gelation mechanism of κ-and ι-carrageenan investigated by correlation between the strain− optical coefficient and the dynamic shear modulus. Macromolecules, 34, 7427-7434.

TAMAYO, J. & GARCIA, R. 1996. Deformation, contact time, and phase contrast in tapping mode scanning force microscopy. *Langmuir,* 12**,** 4430-4435.

TANG, T.-Y. D., VAN SWAAY, D., DEMELLO, A., ANDERSON, J. R. & MANN, S. 2015. In vitro gene expression within membrane-free coacervate protocells. *Chemical Communications,* 51**,** 11429-11432.

TANNER, R. I. 2000. *Engineering rheology*, OUP Oxford.

TECANTE, A. & DOUBLIER, J. 1999. Steady flow and viscoelastic behavior of crosslinked waxy corn starch-κ-carrageenan pastes and gels. *Carbohydrate Polymers,* 40**,** 221-231.

TECANTE, A. & DOUBLIER, J. 2002. Rheological investigation of the interaction between amylose and κ-carrageenan. *Carbohydrate Polymers,* 49**,** 177-183.

TOLSTOGUZOV, V. 2006. 17 Phase Behavior in Mixed Polysaccharide Systems. *Food polysaccharides and their applications***,** 589.

TORRES, M. D., MOREIRA, R., CHENLO, F. & VãZQUEZ, M. J. 2012. Water adsorption isotherms of carboxymethyl cellulose, guar, locust bean, tragacanth and xanthan gums. *Carbohydrate Polymers,* 89**,** 592-598.

TORRES, O., ANDABLO-REYES, E., MURRAY, B. S. & SARKAR, A. 2018. Emulsion microgel particles as high-performance bio-lubricants. *ACS Applied Materials & Interfaces,* 10**,** 26893-26905.

TORRES, O., MURRAY, B. & SARKAR, A. 2016. Emulsion microgel particles: Novel encapsulation strategy for lipophilic molecules. *Trends in Food Science & Technology,* 55**,** 98-108.

TORRES, O., MURRAY, B. & SARKAR, A. 2017a. Design of novel emulsion microgel particles of tuneable size. *Food Hydrocolloids,* 71**,** 47-59.

TORRES, O., TENA, N. M., MURRAY, B. & SARKAR, A. 2017b. Novel starch based emulsion gels and emulsion microgel particles: Design, structure and rheology. *Carbohydrate Polymers,* 178**,** 86-94.

TORRES, O., TENA, N. M., MURRAY, B. & SARKAR, A. 2017c. Novel starch based emulsion gels and emulsion microgel particles: Design, structure and rheology. *Carbohydrate Polymers*, Dec 15.

TORRES, O., YAMADA, A., RIGBY, N. M., HANAWA, T., KAWANO, Y. & SARKAR, A. 2019. Gellan gum: A new member in the dysphagia thickener family. *Biotribology,* 17**,** 8-18.

TUNICK, M. H. 2000. Rheology of dairy foods that gel, stretch, and fracture. *Journal of Dairy Science,* 83**,** 1892-1898.

TURGEON, S., BEAULIEU, M., SCHMITT, C. & SANCHEZ, C. 2003. Protein–polysaccharide interactions: phase-ordering kinetics, thermodynamic and structural aspects. *Current opinion in colloid & interface science,* 8**,** 401-414.

TURGEON, S., SCHMITT, C. & SANCHEZ, C. 2007. Protein–polysaccharide complexes and coacervates. *Current Opinion in Colloid & Interface Science,* 12**,** 166-178.

UEMURA, Y., FUJIMURA, M., HASHIMOTO, T. & KAWAI, H. 1978. Application of Light Scattering from Dielectric Cylinder Based upon Mie and Rayleigh—Gans—Born Theories to Polymer Systems. I. Scattering from a Glass Fiber. *Polymer Journal,* 10**,** 341-351.

UHLENBECK, G. E. & ORNSTEIN, L. S. 1930. On the theory of the Brownian motion. *Physical review,* 36**,** 823.

UPADHYAY, R. & CHEN, J. 2019. Smoothness as a tactile percept: Correlating 'oral'tribology with sensory measurements. *Food Hydrocolloids,* 87**,** 38-47.

URLACHER, B. & NOBLE, O. 1997. Xanthan gum. *Thickening and gelling agents for food***,** 284-311.

VINKE, J., KAPER, H. J., VISSINK, A. & SHARMA, P. K. 2018. An ex vivo salivary lubrication system to mimic xerostomic conditions and to predict the lubricating properties of xerostomia relieving agents. *Scientific reports,* 8**,** 9087.

VIS, M., OPDAM, J., VAN'T OOR, I. S., SOLIGNO, G., VAN ROIJ, R., TROMP, R. H. & ERNë, B. H. 2015a. Water-in-water emulsions stabilized by nanoplates. *ACS Macro Letters,* 4**,** 965-968.

VIS, M., PETERS, V. F., BLOKHUIS, E. M., LEKKERKERKER, H. N., ERNÉ, B. H. & TROMP, R. H. 2015b. Effects of electric charge on the interfacial tension between coexisting aqueous mixtures of polyelectrolyte and neutral polymer. *Macromolecules,* 48**,** 7335-7345.

VIS, M., PETERS, V. F., BLOKHUIS, E. M., LEKKERKERKER, H. N., ERNë, B. H. & TROMP, R. H. 2015c. Decreased interfacial tension of demixed aqueous polymer solutions due to charge. *Physical review letters,* 115**,** 078303.

WANG, L., CAO, Y., ZHANG, K., FANG, Y., NISHINARI, K. & PHILLIPS, G. O. 2015. Hydrogen bonding enhances the electrostatic complex coacervation between κ-carrageenan and gelatin. *Colloids and Surfaces A: Physicochemical and Engineering Aspects,* 482**,** 604-610.

WANG, M. L. & PENG, Z. X. 2015. Wear in human knees. *Biosurface and Biotribology,* 1**,** 98-112.

WANG, Q., ZHU, Y. & CHEN, J. 2021. Development of a simulated tongue substrate for in vitro soft "oral" tribology study. *Food Hydrocolloids,* 120**,** 106991.

WANG, X. & CHEN, J. 2017. Food oral processing: Recent developments and challenges. *Current Opinion in Colloid & Interface Science,* 28**,** 22-30.

WANG, Y., YUAN, J., ZHAO, Y., WANG, L., GUO, L., FENG, L., CUI, J., DONG, S., WAN, S. & LIU, W. 2022. Water-in-water emulsions, ultralow interfacial tension, and biolubrication. *CCS Chemistry,* 4**,** 2102-2114.

WELLERT, S., RICHTER, M., HELLWEG, T., VON KLITZING, R. & HERTLE, Y. 2015. Responsive microgels at surfaces and interfaces. *Zeitschrift für physikalische Chemie,* 229**,** 1225-1250.

WEN, S. & HUANG, P. 2012. *Principles of tribology*, John Wiley & Sons.

WHITE, F. M. & MAJDALANI, J. 2006. *Viscous fluid flow*, McGraw-Hill New York.

WHO 2020. *The state of food security and nutrition in the world 2020: transforming food systems for affordable healthy diets*, Food & Agriculture Org.

WILLIAMS, P. A., ANNABLE, P., PHILLIPS, G. O. & NISHINARI, K. 1993. Mixed polysaccharide gels formed between xanthan gum and glucomannan. *In:* NISHINARI, K. & DOI, E. (eds.) *Food hydrocolloids: Structures, properties, and functions.* Boston, USA: Springer.

WILLIAMS, P. A. & PHILLIPS, G. O. 2021. Introduction to food hydrocolloids. *Handbook of hydrocolloids.* Elsevier.

WOLF, B., SCIROCCO, R., FRITH, W. & NORTON, I. 2000. Shear-induced anisotropic microstructure in phase-separated biopolymer mixtures. *Food Hydrocolloids,* 14**,** 217-225.

WROLSTAD, R. E. 2012. *Food carbohydrate chemistry*, John Wiley & Sons.

WU, K., GUNARATNE, A., COLLADO, L. S., CORKE, H. & LUCAS, P. W. 2015. Adhesion, cohesion, and friction estimated from combining cutting and peeling test results for thin noodle sheets. *Journal of food science,* 80**,** E370-E376.

XU, F., LIAMAS, E., BRYANT, M., ADEDEJI, A. F., ANDABLO-REYES, E., CASTRONOVO, M., ETTELAIE, R., CHARPENTIER, T. V. & SARKAR, A. 2020. A self-assembled binary protein model explains high-performance salivary lubrication from macro to nanoscale. *Advanced Materials Interfaces,* 7**,** 1901549.

XU, Q., QI, B., HAN, L., WANG, D., ZHANG, S., JIANG, L., XIE, F. & LI, Y. 2021a. Study on the gel properties, interactions, and pH stability of pea protein isolate emulsion gels as influenced by inulin. *Lwt,* 137**,** 110421.

XU, X., SHARMA, P., SHU, S., LIN, T.-S., CIAIS, P., TUBIELLO, F. N., SMITH, P., CAMPBELL, N. & JAIN, A. K. 2021b. Global greenhouse gas emissions from animal-based foods are twice those of plant-based foods. *Nature Food,* 2**,** 724-732.

XUE, L.-H., XIE, C.-Y., MENG, S.-X., BAI, R.-X., YANG, X., WANG, Y., WANG, S., BINKS, B. P., GUO, T. & MENG, T. 2017. Polymer–protein conjugate particles

with biocatalytic activity for stabilization of water-in-water emulsions. *ACS Macro Letters,* 6**,** 679-683.

YAKUBOV, G. E., BRANFIELD, T. E., BONGAERTS, J. H. H. & STOKES, J. R. 2015. Tribology of particle suspensions in rolling-sliding soft contacts. *Biotribology,* 3**,** 1-10.

YOU, K., MURRAY, B. S. & SARKAR, A. 2021a. Rheology and tribology of starch+ κ-carrageenan mixtures. *Journal of texture studies,* 52**,** 16-24.

YOU, K. & SARKAR, A. 2021. Oral tribology of polysaccharides. *Handbook of Hydrocolloids.* Elsevier.

YOU, K. M., MURRAY, B. S. & SARKAR, A. 2021b. Rheology and tribology of starch+ κ-carrageenan mixtures. *Journal of texture studies,* 52**,** 16-24.

YOU, K. M., MURRAY, B. S. & SARKAR, A. 2023. Tribology and rheology of water-in-water emulsions stabilized by whey protein microgels. *Food Hydrocolloids,* 134**,** 108009.

ZEEMAN, S. C., KOSSMANN, J. & SMITH, A. M. 2010. Starch: its metabolism, evolution, and biotechnological modification in plants. *Annual review of plant biology,* 61**,** 209-234.

ZEMBYLA, M., LIAMAS, E., ANDABLO-REYES, E., GU, K., KROP, E. M., KEW, B. & SARKAR, A. 2021. Surface adsorption and lubrication properties of plant and dairy proteins: A comparative study. *Food Hydrocolloids,* 111**,** 106364.

ZEMBYLA, M., MURRAY, B. S. & SARKAR, A. 2020. Water-in-oil emulsions stabilized by surfactants, biopolymers and/or particles: A review. *Trends in Food Science & Technology,* 104**,** 49-59.

ZHANG, B., SELWAY, N., SHELAT, K. J., DHITAL, S., STOKES, J. R. & GIDLEY, M. J. 2017. Tribology of swollen starch granule suspensions from maize and potato. *Carbohydrate polymers,* 155**,** 128-135.

ZHANG, J., MEI, L., MA, P., LI, Y., YUAN, Y., ZENG, Q.-Z. & WANG, Q. 2021a. Microgel-Stabilized Hydroxypropyl Methylcellulose and Dextran Water-in-Water Emulsion: Influence of pH, Ionic Strength, and Temperature. *Langmuir,* 37**,** 5617-5626.

ZHANG, S., HOLMES, M., ETTELAIE, R. & SARKAR, A. 2020a. Pea protein microgel particles as Pickering stabilisers of oil-in-water emulsions: Responsiveness to pH and ionic strength. *Food Hydrocolloids,* 102**,** 105583.

ZHANG, S., MURRAY, B. S., SURIYACHAY, N., HOLMES, M., ETTELAIE, R. & SARKAR, A. 2021b. Synergistic interactions of plant protein microgels and cellulose nanocrystals at the interface and their inhibition of the gastric digestion of Pickering emulsions. *Langmuir,* 37**,** 827-840.

ZHANG, T., GUO, J., CHEN, J.-F., WANG, J.-M., WAN, Z.-L. & YANG, X.-Q. 2020b. Heat stability and rheological properties of concentrated soy protein/egg white protein composite microparticle dispersions. *Food Hydrocolloids,* 100**,** 105449.

ZHAO, H., ZHOU, F., PENG, W., ZHENG, J., DZIUGAN, P. & ZHANG, B. 2015. The effects of carrageenan on stability of arachin and the interactions between them. *Food Hydrocolloids,* 43**,** 763-768.

ZHONG, Q. & DAUBERT, C. R. 2013. Food rheology. *Handbook of farm, dairy and food machinery engineering.* Elsevier.

ZHONG, Q., INNISS, D., KJOLLER, K. & ELINGS, V. 1993. Fractured polymer/silica fiber surface studied by tapping mode atomic force microscopy. *Surface Science Letters,* 290**,** L688-L692.

ZHOU, Z. R. & JIN, Z. M. 2015. Biotribology: Recent progresses and future perspectives. *Biosurface and Biotribology,* 1**,** 3-24.

ZHU, Y., BHANDARI, B. & PRAKASH, S. 2019. Tribo-rheology characteristics and microstructure of a protein solution with varying casein to whey protein ratios and addition of hydrocolloids. *Food Hydrocolloids,* 89**,** 874-884.

ZOBEL, H. F. 1988. Molecules to granules: A comprehensive starch review. *Starch - Stärke,* 40**,** 44-50.

# Chapter 2ᵃ

# Tribology of polysaccharides

**Abstract**

Oral tribology deals with the study of friction, wear and lubrication between oral surfaces that are in relative motion, such as tongue-oral palate, food-tongue, teeth-food, teeth-teeth *etc.* Although food material scientists have extensively studied bulk rheology of food, tribology has attracted research attention relatively recently in order to understand the surface interactions between the food, saliva or food-saliva mixtures and oral surfaces during oral processing. In this chapter, we focus on oral tribology of hydrocolloids *i.e.* aqueous dispersions of starch and non-starch polysaccharides that are often used as fat replacers or bulking agents in food industries. We examine the commercially available and custom-made tribometers that are used to measure the friction force in various food research laboratories. Recent work on polysaccharide-based fluid gels, microgels and mixed gels are presented, where tribological research is rather limited. Finally, we draw some conclusive remarks on lubrication mechanisms of polysaccharides and highlight future prospects.

## 2.1.	Introduction

Tribology is the science and engineering of friction, wear and lubrication between two interacting surfaces that are in relative motion. The term 'tribology' is derived from the Greek word *tribos*, which means 'rubbing'. Although the laws of friction were already existing since the 15th century (Hutchings, 2016), the term 'tribology' was first coined about 53 years ago by the British commission report guided by Jost (1966), which identified that improper lubrication, friction issues and associated wear were the key reasons behind the failure of most mechanical systems leading to huge economic losses. Classical tribology within the context of mechanical engineering covers such applications as ball bearings, gear drives, clutches, spindle, cams, and couplings, which involves interactions and friction between moving parts in contacts. Besides typical industrial applications, tribology seems to be ubiquitous in our daily lives for maintenance and wear of equipment ranging from household appliances, personal and healthcare devices (*e.g.* shavers, contact lenses, catheters) to automobiles.

In addition, tribology is highly relevant to the optimal functioning of the human body that also consists of a plethora of interacting biological surfaces in sliding motions (Dowson, 2012). For example, the natural joints, such as knee and hip (Jin et al., 1993, Wang and Peng, 2015) are highly sophisticated nature-engineered bearings, where synovial fluid, a bio-lubricant reduces the friction and prevents wear between the articular cartilage and other tissues allowing human beings to move freely. 'Biotribology', which was first defined by Dowson and Wright (1973) is as an active field within tribology that embraces practically all "aspects of tribology concerned with biological systems". Although biotribological research in synovial joints, eyes, skin surfaces and biomedical implants (Limbert et al., 2019, Zhou and Jin, 2015, Mann and Tighe, 2016b, Jin et al., 2016b) is well-established over several decades, oral tribology involving gnashing teeth, tongue-hard palate, tongue-soft palate, tongue-teeth, teeth-food, tongue-food, lips, food-lips surfaces is a rather emerging area (Chen and Stokes, 2012).

Oral tribology has garnered significant research momentum relatively recently by food scientists where the research community focusses on understanding the underlying lubrication mechanisms during oral processing of foods and beverages (Sarkar et al., 2019b, Stokes et al., 2013, Sarkar and Krop, 2019b, Shewan et al., 2019, Pradal and Stokes, 2016, Prakash et al., 2013, Laguna and Sarkar, 2017a). Tribology of model oral surfaces in the presence of food is a new yet rapidly evolving area within the food community. This is mainly because food sci-

entists have traditionally attempted to characterise textural properties of foods in terms of hardness, fracturability, adhesiveness, springiness, chewiness, gumminess *etc.* (Sherman, 1969, Tunick, 2000). These types of textural characteristics are important in the initial stage of oral processing involving first-bite and largely encompass bulk rheology-dominated phenomena *i.e.* the material properties of the food (Sarkar et al., 2019b, Chen and Stokes, 2012, Stokes et al., 2013). On the other hand, tribology becomes increasingly important in the later stages of oral processing as the food is mixed with saliva and forms a thin film between the tongue and palate. Therefore, not only the food material properties, but also how the food interacts with the oral surfaces play a dominant role in the frictional dissipation.

As schematically shown in **Figure 2.1**, oral processing involves both rheological and tribological phenomena (Sarkar et al., 2019b). During the early stages of oral processing, bulk rheological phenomena are dominant where the food is considered to be in the continuum, which is measured at a fixed gap, equivalent to the size of the food material. However, with dynamic mechanical deformations of food that span several length and time scales, such gaps between tongue and oral palate diminishes to the size of the food constituents, eventually resulting in asperity contacts and friction between the oral tissue-food as well as tissue-tissue interfaces   (Stokes et al., 2013, Sarkar et al., 2019b). Therefore, the tribological properties become dominant in the later stages with surface interactions of the food with the oral mucosa overshadowing the bulk material properties of the food itself.
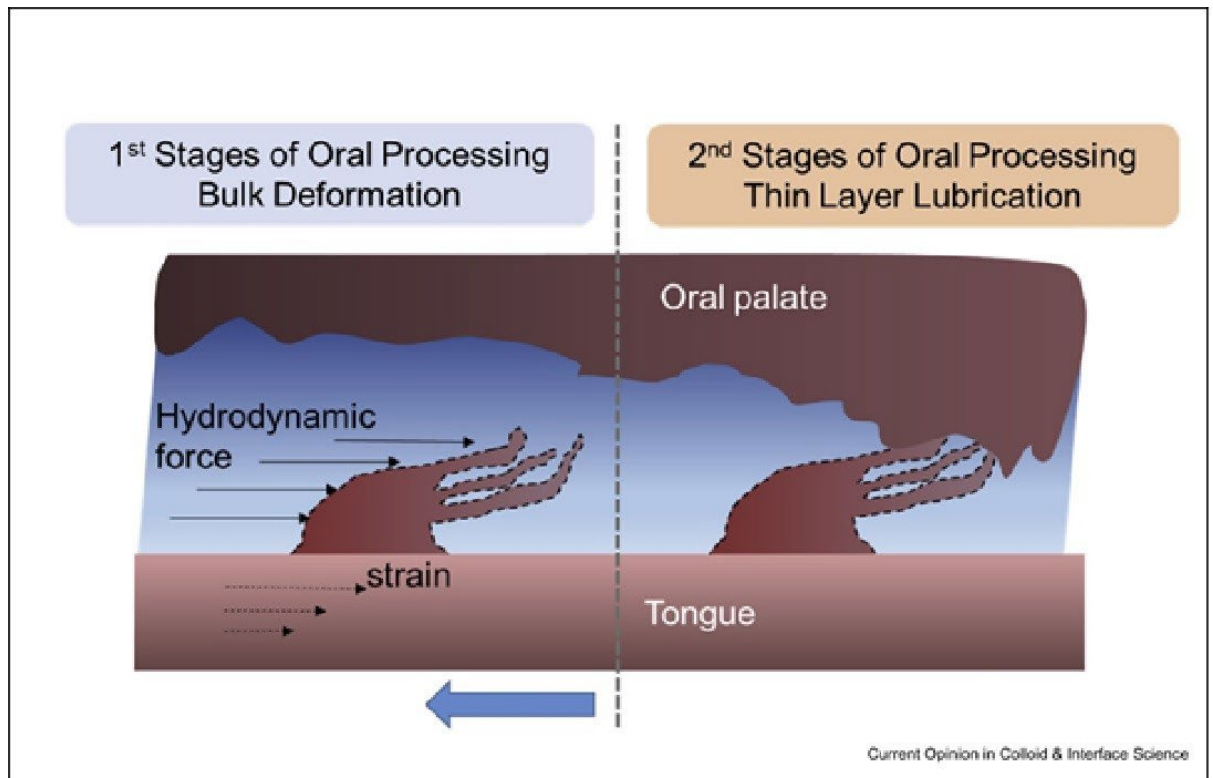
**Figure 2.1.** Schematic illustration of the rheological (early stages) and tribological (later stages) phenomena during oral processing showing the soft tongue tissue (lower surface) and hard palate (upper surface) with the flow of food and/ or saliva is showed in blue. On the tongue surface, only crown-shaped filiform papillae are shown. Reproduced from Sarkar et al. (2019b) with permission.

Application of oral tribology in food science is attributed to the original research of Kokini et al. (1977), where "smoothness" was demonstrated to be inversely proportional to the frictional force and "slipperiness" was shown to be inversely proportional to a known average of viscous and frictional forces. However, the growing interests in studying oral tribology particularly in the last two decades can be attributed to the availability of various commercial as well as custom-made tribometers to measure friction. Also, such upsurge in interests in tribological research can be partly related to the latest evidences of friction coefficients being correlated with various fat- or non-fat-related mouthfeel perception, such as smoothness, astringency, pastiness and so on (Krop et al., 2019a, Brossard et al., 2016, Upadhyay and Chen, 2019, Nguyen et al., 2017, Laguna et al., 2017a, Laiho et al., 2017, Chojnicka-Paszun et al., 2012). Thus, it has been lately realized, food material scientists recognize now that tribology provides information that is not covered by any other complementary techniques, such as rheology, scattering or microscopy.

Hydrocolloids, such as starch and non-starch polysaccharides have been often used in food industries as fat replacers or bulking agents in the case of low calorie products. Although there are several textbooks on the rheology of hydrocolloids, a detailed review on oral tribology of polysaccharides in aqueous dispersion or in complex gels is missing from the literature to date. Knowledge of lubrication mechanisms of polysaccharides is crucial to food scientists in order to rationally design sensorially acceptable low-calorie foods in future. Hence, this chapter aims to cover the oral tribology of polysaccharides that have been studied so far. We cover the frictional laws and Stribeck curve to understand the key parameters in tribological analysis. We then examine the tribometers used in various food research laboratories highlighting their pros and cons. Then, we discuss the work carried out on tribological analysis of various food polysaccharides, such as starch of various sources and non-starch polysaccharides (*e.g.* agarose, xanthan gum, gellan gum, carrageenan, guar gum, pectin, agarose and alginate). Insights from this chapter on oral tribology of polysaccharide is not only relevant for food science applications, but also the fundamental knowledge complied in this chapter can be useful for designing medicines with optimized lubrication properties (Batchelor et al., 2015), therapies for dry mouth (Vinke et al., 2018), studying biofilms (Rmaile et al., 2013), designing oral care products with appropriate lubrication (Cai et al., 2017), and so on. Finally, we discuss the future prospects of tribology in food science and gaps that need to be bridged to decode the underlying physical mechanisms during oral processing of polysaccharides and eventually predict accurately mouthfeel perception based on quantitative frictional force, size, microstructural analysis and rheology measurements.

## 2.2.    Stribeck curve

The two fundamental macroscopic 'laws of friction' were first given by Leonardo da Vinci (1452–1519), before they were finally articulated by Amontons in 1699 (Hutchings, 2016). The first law states that when two surfaces are in relative motion at a sliding velocity of V (m/s), the frictional force ($F_R$) (N) can be expressed by **Equation 2.1**:

$$F_R = \mu \ \times \ F_L \qquad\qquad\qquad (2.1)$$

where, μ is the friction coefficient (dimensionless constant) and $F_L$ (N) is the normal load *i.e.* the load pressing the two surfaces together. The second law states that $F_R$ is independent of the apparent area of contact between these two sliding surfaces. In tribology, μ is an important parameter because the geometry of the surface *i.e.* the surface roughness can affect the magnitude of μ irrespective of the type of lubricant present within the contact surfaces. In the case of oral tribology, when a lubricant, such as saliva or food material is entrained within the moving tongue and steady oral palate surfaces, μ between these oral surfaces can vary
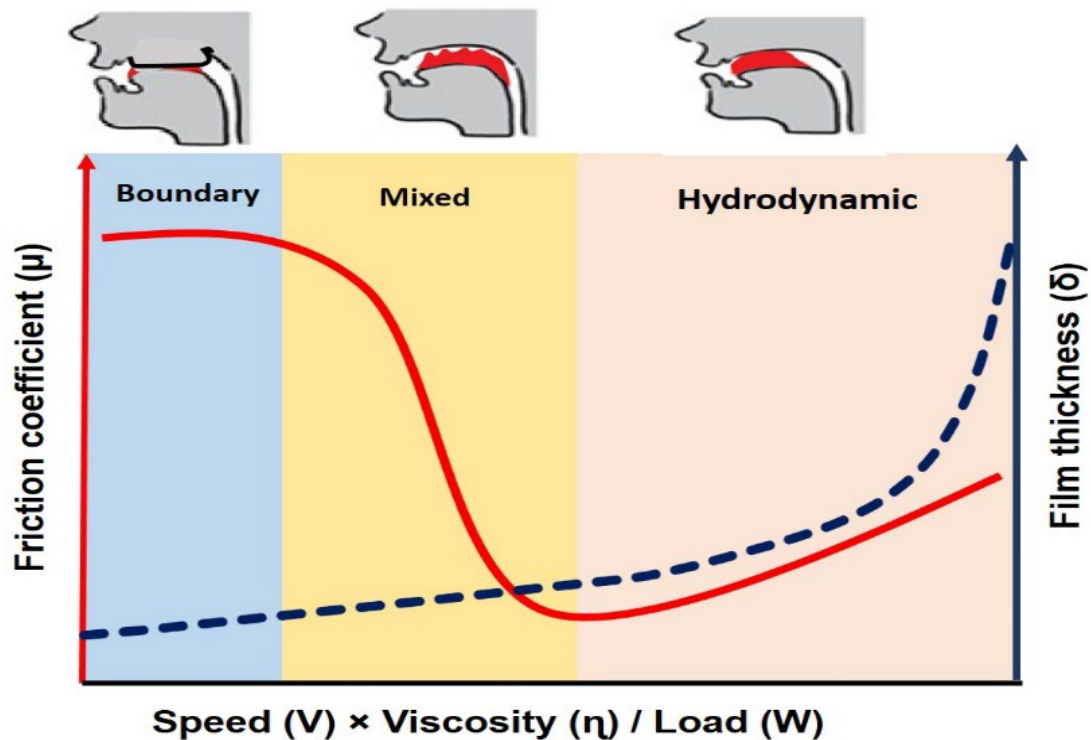


**Figure 2.2.** Stribeck curve (red thick line) showing friction coefficients between contact surfaces in relative motion as a function of the product of parameters of entrainment speed, viscosity and load that is equivalent to the film thickness (δ), latter shown by navy blue dashed line. For coloured image, see the online version.

depending upon $F_L$, the moving speed (V) as well as the properties of the lubricant.

The Stribeck curve (**Figure 2.2**) is the curve that plots μ as a function of the main working conditions ($F_L$, viscosity *i.e.* η, V) that is essentially representative of the film thickness between the two contact surfaces (δ) (Sarkar et al., 2019b, Chen and Stokes, 2012). Focusing on oral tribology, the Stribeck curve may include three regimes that represent three different scenarios of entrainment of lubricant *i.e.* food, food-saliva mixture or saliva between the oral palate and tongue surfaces during oral processing. In contrast to the mechanical engineering

discipline where speeds increase in a bearing from low to high, in oral processing the tongue shear forces in mouth might alter from high to low *i.e.* from first bite to swallowing. Hence, from an oral tribology perspective, it is beneficial to read the curve from high entrainment speed to low entrainment speed *i.e.* from the hydrodynamic regime to the boundary regime (**Figure 2.2**), contrary to the mechanical engineering discipline.

In oral processing, starting from the first biting until swallowing and clearing, food (lubricants) is coming into the mouth where the gap between the rubbing tongue and oral palate surfaces is relatively wide due to thick food film size and hydrodynamic force keeping the food film in the continnum. Therefore, in hydrodynamic regimes *i.e.* at highest entrainment speeds and wider separation (highest $\delta$) between the two oral contact surfaces, $F_L$ is fully supported by the lubricant's rheological characteristics. As the food processing continues, the food structure becomes comminuted into smaller food particles and food particle-saliva mixture *i.e.* bolus through mastication. The hydrodynamic flow of the bulk food is no longer enough to allow sufficient entrainment of the food or bolus. Eventually, the food lubricant film is not sufficient to fully sustain $F_L$. In such a case, $F_L$ is partly borne by the lubricant's fluid pressure and partly by the surfaces themselves, which is referred to as 'mixed lubrication regime' (**Figure 2.2**). In many, if not most cases, food tribology results have shown correlations with sensory perceptions in the mixed lubrication regime, where both viscosity and surface interactions of food are relevant (Sarkar and Krop, 2019b). Finally, when the food is swallowed, and there are only remnants of food's constituents that may form discontinuous boundary films, ranging from a few nanometers to molecular scale thickness *via* surface adsorption of species, a 'boundary lubrication regime' results. In this regime, there is almost no lubricant and $F_L$ is fully supported by the asperity contact pressure of the material surface. Hence, in the boundary regime, only surface properties dominate that may include elastic modulus, wettability and roughness of the oral surfaces as well as the interaction of the lubricant with the contact surfaces.

## 2.3.    Devices for measuring oral tribology

A range of devices *i.e.* tribometers have been used for studying tribology of model and real foods. The design of a tribometer should consider many factors in order to measure friction forces; 1) controlling the type and degree of motion between the two interacting surfaces, 2) ability to support surfaces of different chemistries and roughness to closely mimic the human

oral cavity, 3) ability to adjust to lower loads to have pressures equivalent to oral pressures, 4) temperature control, and 5) low sample volume requirement. The tribometers used until now can be categorized into commercially available off-the-shelf tribometers, tribo-rheo cell *i.e.* a tribological set up attached to an existing benchtop rheometer and custom-made tribometers that have been developed in a specific University workshop. In this chapter, we discuss the pros and cons of these devices for measuring tribological properties as well as examine whether the above-mentioned factors are applied to the tribometer by giving examples of research work carried out using these tribometers. **Figures 2.3, 2.4** and **2.5** show the schematic representations of the various types of tribometers that have been used for food applications to date.

### *2.3.1.      Mini Traction Machine (MTM)*

Mini Traction Machine (PCS Instrument, UK) is the most commonly used tribometer in this field offering a greater range of flexibility on changing $F_L$ (from 1 to 8 N), velocity (1 to 2400 mm/s), slide-to-roll ratio (1 to 200 %) and also supports surface materials that can range from steel, glass, stainless, silicon rubber, elastic rubber to polydimethylsiloxane (PDMS) (Myant et al., 2010, Cassin et al., 2001, Chojnicka-Paszun et al., 2014, Sarkar et al., 2017a, Torres et al., 2018, Gabriele et al., 2010). This device consists of a ball and disc in an insulated chamber where the sample is loaded, where the ball represents the upper palate and the disc represents the tongue in case of oral tribology measurements (**Figure 2.3**). The ball makes a contact with the disc at a defined $F_L$ and the $F_R$ is measured from the instrument's force transducers using **Equation 2.1** and the software represents the data in the form of μ versus entrainment speed (*U*).
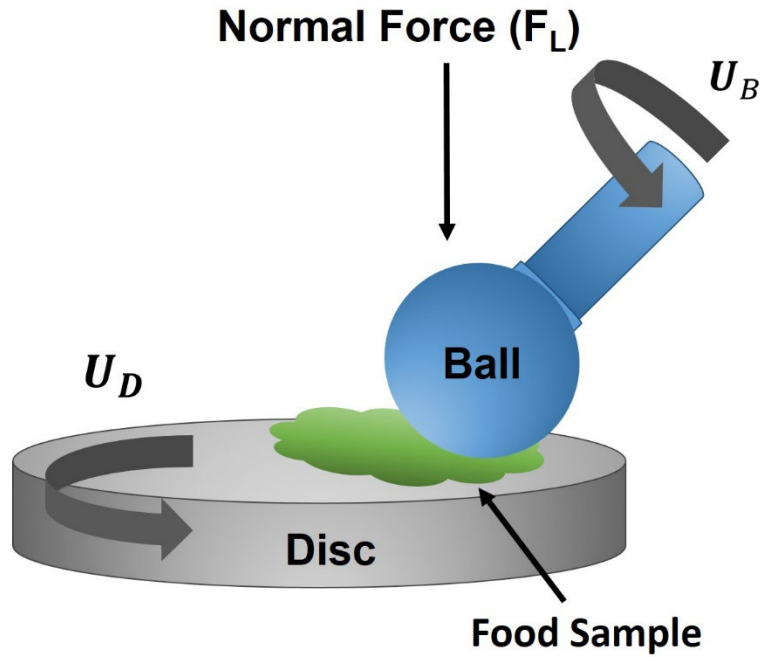
**Figure 2.3.** Schematic representation of a mini-traction ball-on-disc machine (Myant et al., 2010, Laguna et al., 2017a), where $U_B$ and $U_D$ are the speeds of ball and disc speed, respectively.

The procedure of using this machine is very simple, the conditions are set first *i.e.*, the range of sliding velocity, temperature, slide-to-roll ratio, and interval to measure each entrainment speed *etc.*, and then the ball is brought close to the disc in the chamber and the lubricant to be measured is added in sufficient amount into the chamber avoiding any fluid starvation. The ball and disc can be rotated at different speeds to create a relative sliding/rolling motion, which creates the entrainment speed or the mean speed ($U$), the latter can be calculated using **Equation 2.2**, with $U_B$ and $U_D$ being the velocities of the ball and disc, respectively:

$$U = \frac{1}{2} \ (U_B + U_D) \tag{2.2}$$

A wide range of slide-to-roll ratio (SRR) can be obtained using the following equation:

$$SRR \ (\%) = \frac{|U_D - U_B|}{U} \ \times 100 \tag{2.3}$$

When the ball and disc rotate at the same surface speed in the same direction, the contact conditions are "pure rolling" (Shimizu and Spikes, 2016). However, if the SRR is adjusted to 200%, that means one of the surfaces is stationary and this situation is referred to as "pure sliding".

Yakubov et al. (2015) showed that the μ remains constant when SRR is under 100% for a 10 wt% suspension of hollow glass microspheres (size of 9 µm) in water. Interestingly, in this study pure water also displayed similar μ to those of 10 wt% suspensions at rolling conditions (SRR < 10%), which suggests the importance of the adjustment of appropriate SRR when doing the experiments. de Vicente et al. (2006) suggested that the measurement at low SRR is the same as those at SRR = 50 %, indicating that friction was not dependent on the SRR in the boundary regime *i.e.* at low $U\eta$. (**Figure 2.2**). Moreover, errors for each test depending on different surfaces (elastomer-steel and PDMS-PDMS), $F_L$ and SRR were measured by Garrec (2013). The lowest errors were obtained when the SRR was set at 50%. Many, if not most, tribological studies of model and real foods have been conducted using SRR adjusted to 50% (Laguna et al., 2017a, Laguna et al., 2017b, Selway and Stokes, 2013).

Numerous tribological studies have been performed using MTM in various laboratories in order to understand the underlying physical mechanisms behind mouthfeel perception. For example, in our laboratory, Laguna et al. (2017a) used the MTM machine with hydrophobic surfaces (PDMS) and these experiments have allowed differentiation of commercially available iso-rheological fat-free/ low-fat and high-fat yoghurts or cream cheese that were sensorially different in terms of creaminess, latter validated by untrained panellists (n=63). An order of magnitude lower μ was obtained for the full-fat yoghurt (μ ~ 0.05), when compared to fat-free (μ ~ 0.4-0.6) counterparts at lower entertainment velocities (<10 mm$s^{-1}$), whereas no differences were shown in their apparent viscosities. Similarly, Selway and Stokes (2013) demonstrated that MTM with PDMS surfaces was capable of differentiating custards and yoghurts of low and high fat contents that had similar apparent viscosities. Garrec and Norton (2013) compared the tribopairs, elastomer disc & stainless steel ball as well as PDMS disc & PDMS ball, in order to identify the most appropriate tribopairs for accurate measurement for tribology measurements of $\kappa$-carrageenan fluid gels. The authors reported PDMS to be the closest approximation to the human mouth in terms of surface elasticity. However, it is noteworthy that PDMS has at least a two orders of magnitude higher modulus than that of the human tongue (Sarkar et al., 2019b). In addition, a separate study showed that tribology measurements using

elastomer-steel tribopairs correlated with sensory attributes (slipperiness) when measuring guar gum solutions (Malone et al., 2003).

With MTM, experiments have been conducted with PDMS where surfaces of different chemistry or roughness have been utilized to measure friction forces. For example, in our laboratory, we have used $O_2$-plasma treatment followed by physisorption by salivary mucins to change the wettability of PDMS surfaces (static water contact angle 108° to 47°) (Sarkar et al., 2017a). Such change in wettability of the tribopairs had a remarkable effect on µ of whey protein microgels (WPM) measured using MTM. In particular, 65 vol% of WPM was necessary in hydrophobic PDMS substrates (static water contact angle 108°) whereas at the same volume fraction of WPM, the friction was increased to a maxima in the boundary regime in the case of hydrophilic mucin-coated PDMS substrates (static water contact angle 108°) due to jamming of the contact zone in the latter. In another study, Bongaerts et al. (2007) measured the effect of surface roughness (varying from 8.6 nm to 3.6 µm) in PDMS using MTM and it was suggested that increasing surface roughness might cause a shift in the transition point between the lubrication regimes. Particularly, in the boundary regimes, increasing surface roughness may lower friction in PDMS substrates but extend this regime to larger values of $U\eta$.

Besides fat-rich emulsions or emulsion-based foods, MTM has also shown the ability to distinguish the tribological characteristics of aqueous polysaccharides (Stokes et al., 2011b, Torres et al., 2019). For example, Stokes et al. (2011b) compared µ of aqueous polysaccharides, *i.e.* pectin, xanthan gum, locust bean gum (LBG), gellan gum, and κ/ι-carrageenan at 25°C using a compliant PDMS ball and PDMS disc. The friction was determined as a function of U in the range of 1 and 750 mm/s, while $F_L$ was set at 1 N with SRR equal to 50%. The results showed different minimum µ of polysaccharides (pectin: $9 \times 10^{-4}$, xanthan: $2.4 \times 10^{-3}$, LBG: $2.9 \times 10^{-3}$, gellan gum: $9.4 \times 10^{-3}$, and carrageenan: $2.1 \times 10^{-3}$) at the transition between the mixed and hydrodynamic regimes. These results point out that MTM has been used in various laboratories using a wide range of surfaces of different chemistry, roughness and modulus and has generated powerful insights in understanding the tribological properties of food-based lubricants.

*Advantage*s. The MTM device allows the ball or the disc to be made up of practically any surface chemistry, as well as allowing a whole range of sliding speeds, from 1 to 2400 mm/s, higher speeds help to understand the hydrodynamic regime. It allows measurement of the rolling friction behaviour and enables reciprocating motion with an additional rig. Most

studies in food tribology have been done so far using MTM in various laboratories, this has generated fundamental insights for Newtonian, Non-Newtonian fluids as well as model and real food products.

*Disadvantages.* Errors in experiments with pure sliding conditions (SRR 200%) are relatively large as compared to that using SRR 50%. It does not allow going to lower speeds than 1 mm/s and lower $F_L$ than 1 N in most of the types of MTM tribometers available currently in food science laboratories. It requires relatively large quantities of samples (approximately 10-25 mL) for a single experiment, which can be a challenge particularly when dealing with biological samples, such as human saliva.

### 2.3.2.     *Tribo-rheo cell attachments*

A mounted tribological device (MTD) is an example of a tribo-rheo cell attachment that can be fitted to a benchtop rheometer, that is available in most food material science laboratories (Heyer and Läuger, 2009). The configuration includes a ball loaded onto three plates arranged in the form of an inverted pyramid (**Figure 2.4a**). The $F_L$ is applied onto three plates by pressing down the balls, and the $F_R$ is measured by sliding the ball against the immobile plates within the rheometer (Anton Paar, Austria). This machine offers a greater range of flexibility on changing the $F_L$ (from 0.01 to 50 N), velocity (rotational speed $10^{-6}$ to 3000 rpm; torque, $10^{-7}$) and also surface materials *i.e.*, styrene butadiene rubber, natural rubber, foamed rubber, glass, stainless, PDMS etc (Baier et al., 2009, Heyer and Läuger, 2008, Krzeminski et al., 2012).
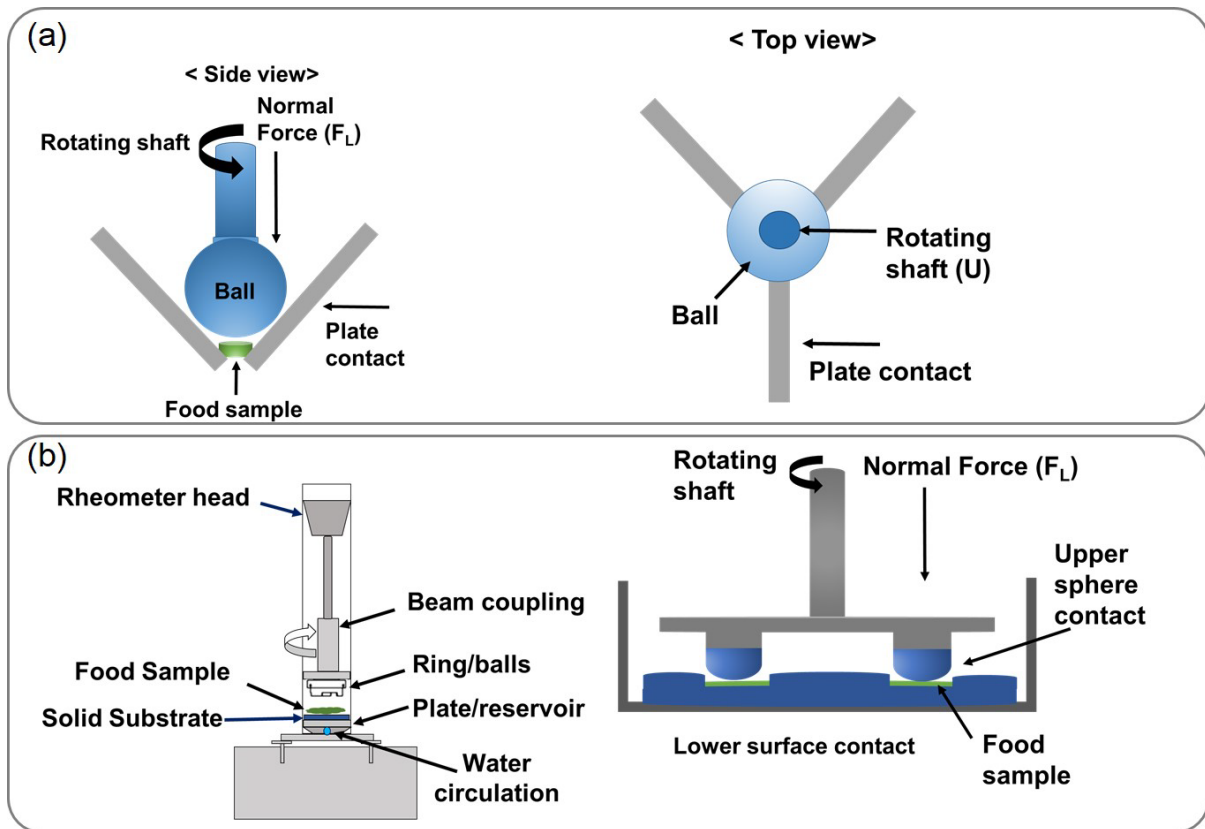
**Figure 2.4.** Schematic representations of two varieties of tribo-rheo cells, (a) mounted tribological device (MTD) of ball-on-three-plates in a controlled-stress rheometer (Anton Paar, Austria) (Heyer and Läuger, 2008) and (b) tribo-rheometry measuring friction under numerous loading conditions with ring on plate set up (left) in a controlled-stress rheometer (TA Instrument, USA) (Nguyen et al., 2016) or hemispheres-on-plate set up in a controlled-stress rheometer (Anton Paar, Austria) (Goh et al., 2010, Kavehpour and McKinley, 2004) (right).

Krzeminski et al. (2012) investigated the influence of stiffness and surface roughness characteristics of elastic pads, styrene butadiene rubber, natural rubber, and foamed rubber in this device. This research used water, full-fat yoghurt (3.5 wt%, fat) and low-fat yoghurt (<0.1 wt%, fat) having the same protein performed with a speed ranging from 0.1 to 3000 $min^{-1}$, $F_L$ from 3 to 9 N under the same temperature 20°C. This study showed that surface roughness of each rubber pad was more crucial for lubricating properties of the yoghurts in this tribo-cell system rather than the stiffness parameters.

The capability of MTD has been evaluated with fluid milk depending on oil volume fraction (2% reduced fat milk, whole milk, and heavy cream) by Baier et al. (2009). This study showed the Stribeck curves were clearly divided into three distinct regimes (boundary, mixed, and hydrodynamic regime as discussed in **Figure 2.2**) when measuring different dairy products

in accordance with different sliding speeds. Also, the dairy products with fat contents have very distinctive frictional behaviour at several sliding speeds. These types of tribo-rheo cell attachments have also been used by few laboratories for doing tribology measurements in chocolate (Carvalho-da-Silva et al., 2013) or bread (Kiumarsi et al., 2019) samples.

**Figure 2.4b** presents another set-up of a tribo-rheo cell. The ring (left) or balls (right) are connected to the rheometer head through a coupling adapter and a load beam coupling to perform the rotation movement. The load beam connected is self-aligning to measure exactly a uniform solid-solid contact and axial force distribution between the contact surfaces. The lower plate, which is the counter surface has a Peltier plate in which water circulation is used to control the temperature. Nguyen et al. (2017) used the ring-on-plate set up (**Figure 2.4b,** left, TA Instruments, USA) to measure the effect of addition of hydrocolloids, *i.e.* gelatin (0.5-1.5%), xanthan gum (0.05-0.015%), carrageenan (0.01-0.08%) and modified starch (0.5-15%) on tribology of yoghurt formulations. The plate was modified to use a rough plastic surface of 3M Transpore Surgical Tape 1527-2 with 100 µm surface roughness (3M Health Care, USA) (Nguyen et al., 2016). The friction forces were recorded for rotational speed from 0.01 to 100 $s^{-1}$ with 20 points per decade under the normal force of 2 N and room temperature (22-25 °C). The study demonstrated the ability of this set up to distinguish hydrocolloids investigated, especially in mixed and hydrodynamic regimes. In particular, gelatin appeared to be the best hydrocolloid because skim milk-yoghurt with added gelatin had similar lubrication properties with full-fat yoghurt when comparing the results of adding other hydrocolloids to the yoghurt formulation. This is because of the melting properties of gelatin at 35°C enhanced the thin film lubrication of the skim milk yoghurt sample in the mixed lubrication regime. It is also interesting to note that both xanthan and carrageenan had no significant effect on µ, except in the hydrodynamic regime, where it is rheology-dominant phenomena. Hence, the results indicate that tribo-rheometry can measure the difference of lubrication properties in terms of three regimes (boundary, mixed and hydrodynamic) and distinguish the lubrication properties with different biopolymers.

Tribo-rheometry also has been customized to different set-ups, such as hemispheres on a plate in a particular lab (Goh et al., 2010) (**Figure 2.4b,** right, Anton Paar, Austria). The upper contact probe consists of two balanced hemispheres equidistant from the central rheometer shaft, giving two contact points for measurement. The cell can measure tribological properties under various loading conditions, such as speed, load or gap ramp. In an attempt to identify the

effect of parameters such as normal force and gap height by using the customized cell, Joyner et al. (2014) studied the effect of controlling normal force and gap height by using polypropylene (PP) balls and steel and whey protein isolate (WPI) gel plates under the conditions (normal force; 1-5 N, rotational speed; 1-10 RPM). This study showed μ was not affected by $F_L$ for Newtonian lubricants, however, variation in $F_L$ can increase measurement variation in elastomeric plates because they affect the modulus and contact area. On the other hand, this cell can measure tribological properties depending on the extent of normal force and gap height variation, which affect the rheometer base, tribological plate material, tribological tool orientation, dynamic force control and sliding speeds. Thus, these results should indicate that the tribo-rheometer can offer a high degree of modularity to allow mimicking oral processing.

*Advantages*. The instrument enables precise measurement due to the control of the much wider range of speed and force than the MTM machine, associated with the abilities of a rheometer for a wide range of measurements with sensitive oscillatory control. Besides, there are many options to choose upper and lower tribopairs, *i.e.* ring on the plate, ball on three plates, ball on three balls, and three balls on a plate. In addition, the sample volume required is low (< 5 mL).

*Disadvantages*. The principle of operation allows only studying pure sliding friction and restricts any other kind of motion like rolling, as the ball is fixed with a stationary shaft. This type of set-up is yet to validate the characteristics of non-Newtonian lubricants and fundamental studies on model systems are limited. In general, there are limited papers using this set-up to date to measure tribological parameters in food samples and correlating with sensory perception.
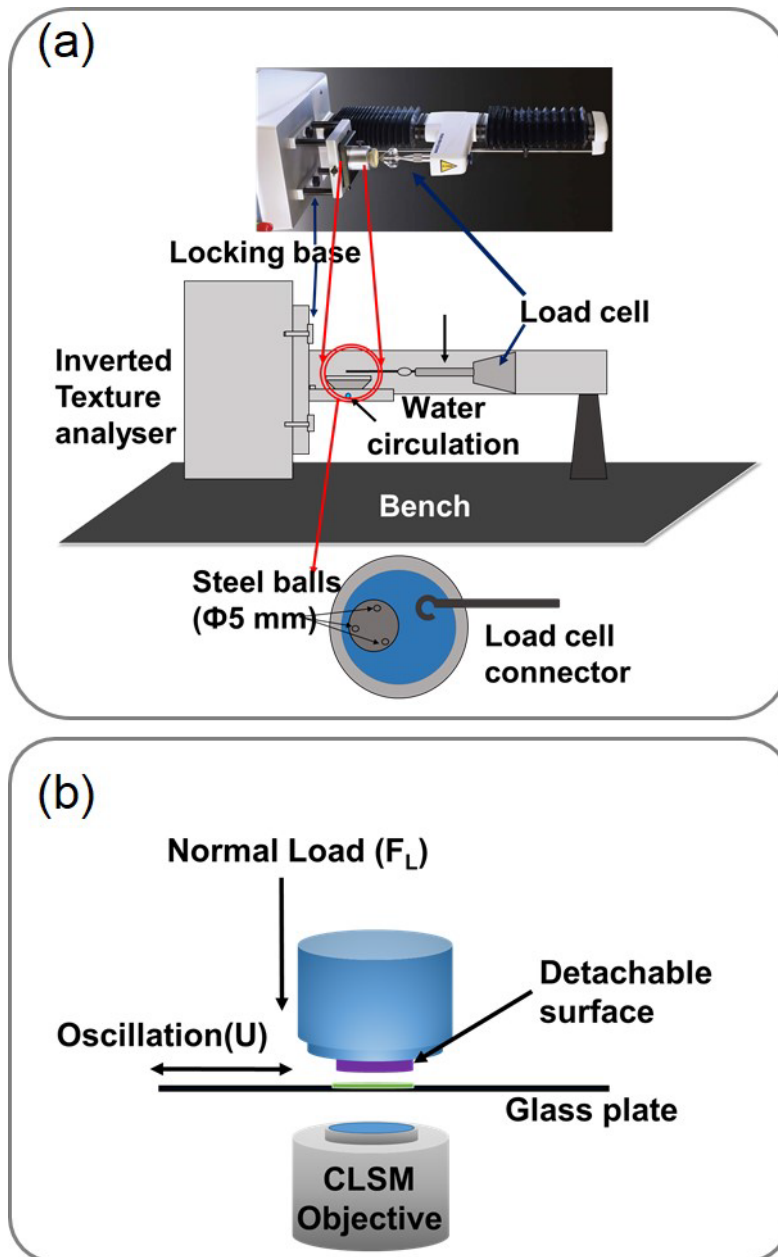
**Figure 2.5.** Custom-made tribometers in food research laboratories, (a) inverted texture analyser modified into three steel balls-on-disc set up (Chen et al., 2014) and (b) bespoke optical tribological configuration (OTC) including an confocal objective lens (Dresselhuis et al., 2008).

### 2.3.3. *Custom-made tribometers*

Some bespoke tribometers have been also designed in food research laboratories. In this chapter, we explain two types of them: 1) Inverted texture analyser set-up (Chen et al., 2014) and 2) Optical tribological configuration (OTC) (Dresselhuis et al., 2008).

***Inverted texture analyser set-up.*** This machine has been devised using a commercial texture analyser (Stable Microsystems, Surrey, UK) with a few additional settings and attachments (Chen et al., 2014). **Figure 2.5a** shows the illustration, where a moving probe with three stainless steel balls in a triangle arrangement, and an adapting connector to connect the moving ball probe to the load cell of a texture analyser. The texture analyser is laid to its side on a levelled workbench. The stainless steel base is screw-secured to the working-platform of the texture analyser. Once the disc is dragged, the balls are in sliding movement against the substrate surface. The disc is connected to the load cell of the texture analyser *via* a metal connector with a hook at the end. The movement of the disc is controlled by the step-motor of the texture analyser. The sliding speed of the ball against the static lower surface can be set from as low as 0.01 mm/s to as high as 40 mm/s, *i.e.* the maximum speed range of the texture analyser. The friction force acting on the load cell can be recorded automatically by exponent software pre-loaded on the texture analyser. Brossard et al. (2016) studied the astringency sensation of red wine using this machine with sliding speeds ranging in from 0.025 and 10 mm/s under a controlled temperature by using steel balls-PDMS surfaces. The result showed that using a sliding speed of 0.075 mm/s, the set-up was able to appropriately measure the differences in μ in different red wines, which were also different in their oral astringency perception.

*Advantages.* The set-up can be conveniently designed and has easy to control parameters, *i.e.* sliding speed, normal force, and temperature.

*Disadvantages.* First of all, this tribometer only measures sliding friction and has no ability to measure rolling friction. Secondly, the sliding speed is limited between 0.01 mm/s and 40 mm/s compared to MTM (1-2400 mm/s). Until now, the choice of substrate has been shown to be limited to steel balls as compared to use of PDMS or other elastomeric balls in MTM or borosilicate glass balls in case of tribo-rheo cells. Since it is a bespoke machine designed in a particular laboratory, it is hard to compare the results with other laboratories.

***Optical tribological configuration (OTC).*** The configuration consists of a lower plate glass surface that oscillates from side to side against a stationary upper probe to which a second surface is attached, such as a pig's tongue section, rubber surface and PDMS (**Figure 2.5b**). The use of a glass lower plate allows the use of a confocal laser scanning microscope (CLSM) to observe the sample while undergoing testing. The friction force ($F_R$) is measured when the force ($F_L$) is applied downward from the upper surface by oscillating the lower glass platform.

The use of CLSM gives an understanding of how the lubricants structurally behave in the contact zone within the microscale. Liu et al. (2016) applied this experimental set up to identify the tribological properties of liquid and semi-solid food model systems containing rice starch using PDMS probe and glass plate (0.5 N normal force, oscillation speed form 10 to 80 mm/s, and 20°C) and this set-up enabled microstructural imaging to understand the lubrication mechanism.

*Advantage.* The main advantage of this device over any of the afore-mentioned tribometers is that it allows visualizing *in situ* microstructural changes of samples while shearing the sample. Hence, this set-up can provide powerful information on the physical or chemical interactions as well as the degree of instability, such as coalescence encountered in an emulsion system under tribological stress (Devezeaux de Lavergne et al., 2016).

*Disadvantages.* The $F_L$ is generally fixed at 0.5 N and a much lower sliding speed ranging from 10 to 80 mm/s is allowed, while most tribometers allow higher load and speed ranges to probe the hydrodynamic regime. The counter surface is always restricted to glass, which limits the modularity of the surfaces that can be used. Similar to the texture analyser set-up, it is difficult to compare the results generated by OTC with other laboratories.

## 2.4.    Oral tribology of polysaccharides

Polysaccharides are complex macromolecular carbohydrates consisting of long chains of monosaccharide units bound together *via* glycosidic linkages. Polysaccharides are derived from vegetable, microbial or synthetic sources, and have a range of functional properties. Polysaccharides are used in the Food industry to improve the processability of foods (Lapasin, 2012) as well as for their thickening, gelling and water binding properties (Torres et al., 2012). Polysaccharides help in emulsion stabilization by virtue of their proteinaceous impurities that have interfacial properties (Dickinson, 2018). In addition to aqueous dispersions, polysaccharides are widely used to create hydrogels, emulsion gels for studying their textural (rheological as well as tribological), mouthfeel and satiating properties (Laguna and Sarkar, 2016, Krop et al., 2019a, Krop et al., 2019b, Santagiuliana et al., 2018, Foegeding, 2007, Koç et al., 2019, Torres et al., 2016, Hayakawa et al., 2014).

One of the most important characteristics of polysaccharides that can be relevant to tribology is the number of hydroxyl groups, or acetal functional groups in their structure, which can influence the interactions of the polysaccharides with the tribological surfaces as well as

with other food components. While the rheological properties of polysaccharides have been extensively investigated (Lapasin and Pricl, 1995, Renaud et al., 2005, Picout and Ross-Murphy, 2003, Foegeding, 2007, Nishinari and Takahashi, 2003), there are relatively few studies to date that have probed their effectiveness as lubricants in tribological contacts, the latter includes evaluation of both of their surface adsorption properties and their rheological behaviours in the high shear limits. Considering that biological speeds during real oral processing are not likely to exceed 100 mm/s (Sarkar et al., 2019b), we have focused only on boundary and mixed lubrication regime results of starch and non-starch polysaccharides that have been studied either as aqueous solutions, dispersions or as hydrogels.
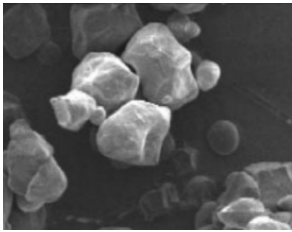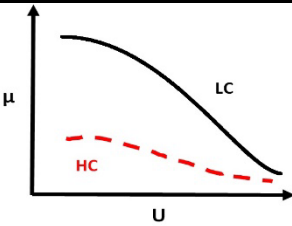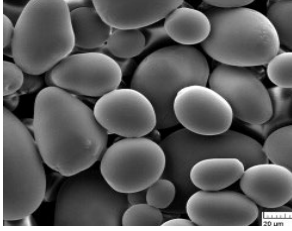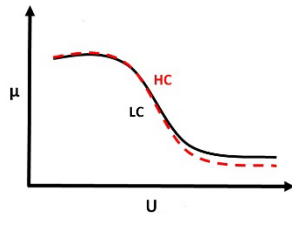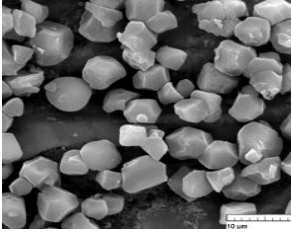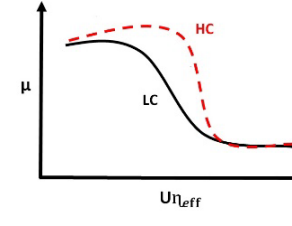
### 2.4.1.    *Tribology of starch*

Starch is the second-most abundant hydrocolloid to cellulose, and is composed of a large number of glucose units linked by glycosidic bonds (Buléon et al., 1998b, Blazek and Gilbert, 2011b, Gismondi et al., 2019). Starch is found as granules and is composed of D-glucose units connected *via* α-1,4-glycosidic linkages, and, extensively branched amylopectin composed of glucose units linked primarily by α-1,4-glycosidic bonds with occasional α-1,6-linkages creating the branched structure (Zobel, 1988). The main sources of starch investigated in literature are derived from corn (maize), wheat, potato, tapioca, and rice starches are also been. The forms and functionalities of starch may vary depending upon the botanical species (Copeland et al., 2009). For example, the granules   are micron-sized but may vary based on the origin (maize ~2-30 μm, wheat ~1-45 μm and potato ~5-100 μm) (Jobling, 2004). Starch is a highly versatile and inexpensive natural ingredient, which is widely used as thickener, water binder, emulsion stabilizer when starch is hydrophobically modified, and/or gelling agent.

Of the two components of starch, amylose has the most useful functions as a hydro-colloid. The extended conformation of amylose generates high viscosity in aqueous dispersions that varies very little with temperature. Increasing amylose concentration may decrease the stickiness of hydrogels but might increase the modulus of the resultant gels (Eggleston et al., 2018). Starches have been widely used as natural fat replacers in food products, such as ice cream, dressing, sausages as they have been empirically shown to provide a smooth mouthfeel with sufficient body emulating fat-related creaminess perception (Diamantino et al., 2019, Punia et al., 2019, Lobato-Calleros et al., 2014). Hence, this section discusses the tribological properties of different types of starches either as an aqueous dispersion or as gels or microgels

so that the mechanisms behind such mouthfeel perception can be better understood. In **Table 2.1**, we have schematically illustrated the tribological behaviours based on the experimental graphs of the studies to understand the difference (if any) on increasing concentration of starches.

**Table 2.1.** Tribology and micrographs of starches, respectively. The SEM images of the starches* are reproduced with permission (Sujka and Jamroz, 2013).

| Starch types | Scanning electron micrographs (SEM) | Concentration (wt%) | Schematic representation of tribology graphs (friction coefficients ($\mu$) versus entrainment speeds ($U$) or product of U and effective viscosity ($\eta_{eff}$) | References |
|---|---|---|---|---|
| **Maize*** (Cooked swollen granules suspension/ ghost suspension) |  | 0.01-1.0 |  | (Zhang et al., 2017), |
| **Potato*** (Cooked swollen granules suspension/ ghost suspension) |  | 0.01-0.87 |  | (Zhang et al., 2017) |
| **Rice*** (Native, Gelatinized) |  | 0.5-10.0 |  | (Liu et al., 2016) |

| Wheat (Microgels, *i.e.* gelatinized and sheared) |  | 15.0-20.0 |  | (Torres et al., 2018, Torres et al., 2017c) |
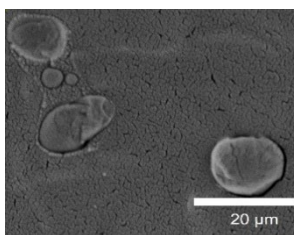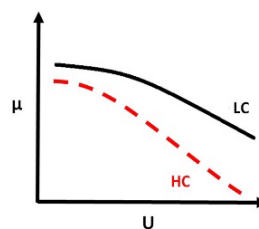
Note: LC and HC represent the lowest and highest concentrations of starch or starch microgels tested, respectively, that show the schematically illustrated tribological curves.

It is clear from **Table 2.1** that limited studies have been performed on the tribological properties of starch and all these studies have been carried out within the last three years. Zhang et al. (2017) demonstrated the tribological properties of suspensions of cooked swollen starch (ghost suspensions) from maize or potato across a wide range of concentration. Using MTM tribometer with PDMS ball and disc, temperature of 35 °C, 50% SRR, and sliding velocity ranging from 1 to 1000 mm/s, the frictional behaviour was compared to water. The $\mu$ was shown to decrease in the boundary and mixed regimes with increasing concentration (0.01-1.0 wt%) of maize ghost suspensions (**Table 2.1**) because the ghost particles were entrained in the contact zone at a speed of 40 mm/s as compared to that of water, which was squeezed out of the hydrophobic PDMS contact surfaces. However, there was no further reduction in $\mu$ in the case of higher concentrations of maize ghost systems (*i.e.*, >1.0 to ≤ 3.0 wt%). This is because once a threshold concentration is reached, where a layer of particles provides a complete surface separation (Sarkar et al., 2017a), further increasing the number of particles does not have a marked influence on $\mu$.

Interestingly, potato starch behaved very differently from maize starch (Zhang et al., 2017). Potato ghost particles did not reduce $\mu$ in comparison to water even on increasing the concentration up to 0.87 wt% as they were most likely excluded from or degraded within the confinement. This difference in tribological behaviour between starches of different origin can be explained on the basis of their size and shape *i.e.* maize ghost particles have a nearly spherical appearance with relatively small size (around 20-35 μm), whereas potato ghosts are ellipsoidal and have larger particle sizes (50-150 μm) (**Table 2.1**). According to Liu et al. (2016), the boundary regime extends with increasing concentration (0.5-10.0 wt %) for rice starches irrespective of being in the native or gelatinized state. Presence of native rice starch extends

the boundary regime because of its irregular shape, not spherical, and particle agglomeration at high concentration, which induces increasing surface roughness and asperity contacts (**Table 2.1**). Gelatinized rice starch also increases μ due to potential "stickiness of the leached starch polymers" as described by the authors, which needs further investigation.

Besides native and gelatinized starch, Torres et al. (2018) investigated the tribological effects of wheat starch-based microgels in our laboratory (**Table 2.1**), which were prepared by high pressure homogenization of starch gels (Torres et al., 2017c). The magnitude of $\mu$ was decreased in these microgels upon increasing starch content (15.0 wt% wheat starch, $\mu = 0.48$ at $U = 3$ mm/s and $\mu = 0.09$ at $U = 50$ mm/s, whereas at 20.0 wt% wheat starch, $\mu = 0.16$ at $U = 3$ mm/s and $\mu = 0.01$ at $U = 50$ mm/s). Although the microgels with 15.0 wt% starch (elastic modulus, $G' = 640$ Pa) might enter the contact zone at low entrainment speed ($U < 10$ mm/s), they might flatten out as they are too soft to support the load (Torres et al., 2018). However, the microgels with 20.0 wt% starch (elastic modulus, $G' = 1600$ Pa) were harder and less deformable and thus they were able to act as surface separators by carrying some part of the load when they enter the contact zone between the ball and disc, accelerating the onset of the mixed regime.
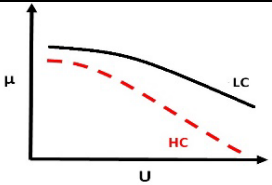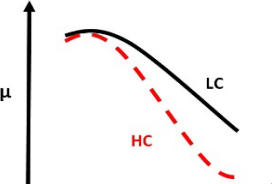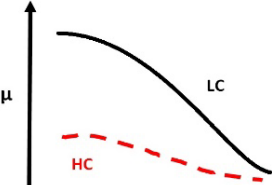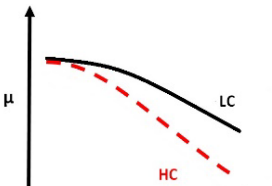
To sum up, tribological properties of starch are influenced by many factors, such as granule structure, particle size and shape of starch granules, state (native, gelatinization etc.). In the case of starch-based microgels, the modulus and particle size are the key parameters affecting their lubrication behaviour. On the other hand, the rheological properties of starch may affect the hydrodynamic lubrication regime where a decrease in the friction coefficient can be achieved at higher $U\eta$ by increasing the high shear viscosity (Torres et al., 2019).

### 2.4.2. Tribology of non-starch polysaccharides

Non-starch polysaccharides (NSPs) such as locust bean gum (LBG), carrageenan, gellan, guar, pectin, xanthan gums *etc.* have been used for stabilizing, thickening, gelling purposes in the Food Industry. They are often used for fat replacement purposes. Hence, investigations of the tribological properties of NSPs have attracted recent research attention (Stokes et al., 2011b, Krop et al., 2019a, Torres et al., 2019, Garrec and Norton, 2013, Farrés et al., 2013), which demands a systematic review. Here, we discuss the lubrication behaviour of NSPs based on the state of matter *i.e.* aqueous solutions, fluid gels or gel particles and mixed gel particles.

*Aqueous solutions.* The influence of different hydrocolloids on lubrication of tribolog-ical contact surfaces have been investigated by few researchers (**Table 2.2**).

**Table 2.2.** Tribological properties of polysaccharides as aqueous solutions or fluid gels or gel particles.

| Polysaccharides | Concentration (wt%) | Schematic representation of tribology graphs (friction coefficients ($\mu$) versus entrainment speeds ($U$), mm/s) | References |
|---|---|---|---|
| **Aqueous solutions** | | | |
| **Kappa-carrageenan (*$\kappa$C*)** | 0.5-2.0 |  | (Garrec and Norton, 2013, Stokes et al., 2011b) |
| **Locust bean gum (LBG)** | 0.8-1.7 |  | (Chojnicka-Paszun et al., 2014, Stokes et al., 2011b) |
| **Gellan gum (GG)** | 0.075-0.3 |  | (Stokes et al., 2011b, Torres et al., 2019) |
| **Guar gum** | 0.02-1.5 |  | (Cassin et al., 2001, de Vicente et al., 2006, Garrec and Norton, 2012a) |

| Pectin | 1.27-3.0 | | (Chojnicka-Paszun et al., 2014, Stokes et al., 2011b) |
|---|---|---|---|
| Xanthan gum (XG) | 0.2-1 | | (Stokes et al., 2011b, Torres et al., 2019, Shahrivar et al., 2019, Chojnicka-Paszun et al., 2014, de Vicente et al., 2005b) |
| **Fluid gels/ Gel particles** | | | |
| Agarose | 0.5-2.0 | | (Gabriele et al., 2010) |
| Calcium alginate (CaA) | 1.0-4.0 | | (Farrés et al., 2013, Fernández Farrés et al., 2014) |
| Kappa-carrageenan (κC) | 0.5-2.0 | | (Garrec and Norton, 2013, Krop et al., 2019a) |
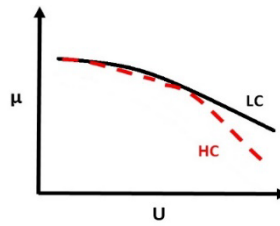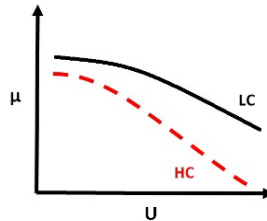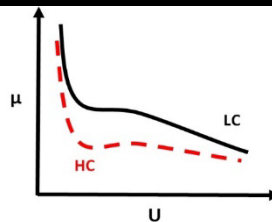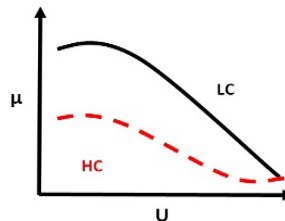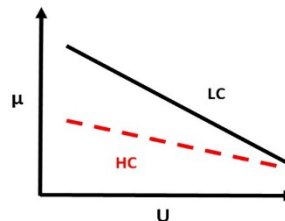
Note: LC and HC represent the lowest and highest concentrations of aqueous solutions of polysaccharides or polysaccharide fluid gels/ gel fragments tested, respectively, that show the schematically illustrated tribological curves.

Most of these studies have been conducted using the MTM tribometer with PDMS-PDMS or steel-PDMS substrates with loads ranging from 1 to 5 N, respectively. There are

essentially two key factors that affect lubrication properties of NSPs in the boundary and mixed regime: 1) the conformation of the NSPs in solution, such as disordered random coil, ordered rigid rod, extended ribbon like structure which dictates the entrainment in the contact zone and 2) the ability of the hydrocolloids to form an adsorbed film at the surface. The first factor is explained using a simple schematic illustration in **Figure 2.6** (Garrec and Norton, 2012a, Garrec and Norton, 2013). The hydrocolloids with expanded chain-like conformations are most likely to slide into the contact region, resulting in low boundary friction. Whilst, biopolymers with disordered random coil structure might not align in the direction of the flow and will be excluded from entrainment providing poor lubrication.

The effect of conformation of aqueous solution of NSPs on friction properties was elegantly shown using $\kappa$-carrageenan ($\kappa$C) (**Table 2.2**), which has an extended chain-like con-formation (Garrec and Norton, 2013, Stokes et al., 2011b). Either of the tribopairs used *i.e.* elastomer-steel or PDMS-PDMS were seemingly lubricated with 0.5- 2 wt% $\kappa$-C in boundary conditions ($U$ = 3mm/s and fixed $F_L$ = 2 N). As the concentration of $\kappa$C increased (Garrec and Norton, 2013), the polymer was entrained in the contact zone and μ decreased at the site of the converging geometry formed between the tribopairs in both the boundary and mixed regimes. Interestingly, the lubrication behaviour by $\kappa$C was consistent across smooth to rough PDMS substrates (10 to 400 nm, respectively), highlighting their ability to entrain and prevent PDMS-PDMS asperity contact (Stokes et al., 2011b).
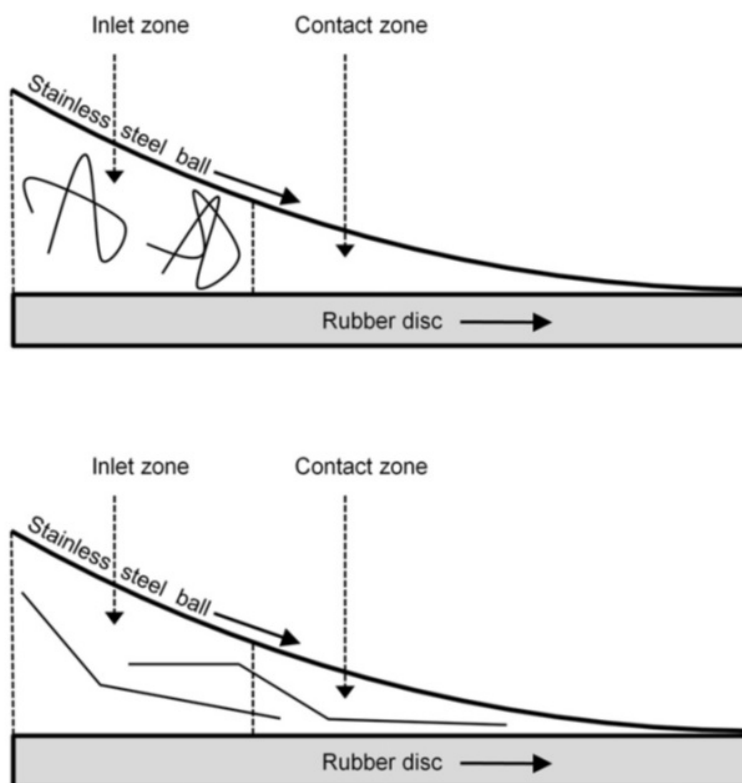
**Figure 2.6.** Schematic of the hypothesis of the behaviour of hydrocolloids at the ball-and-disc contact. Reproduced with permission from Garrec and Norton (2012a). Solid arrows indicate the direction of ball-and disk movement. Due to the alignment of an extended coil and rigid-rod polymer chains to flow, the hydrodynamic volume at the inlet zone to the ball and disk is lower for extended-coil and rigid-rod polysaccharides (bottom) than random coils (top).

In contrast to the extended conformation of $\kappa$-C, LBG has a random-coil configuration (Robinson et al., 1982, Higiro et al., 2006) and was found to behave similar to water in the boundary regime. Regardless of the LBG concentration (**Table 2.2**), LBG did not influence boundary lubrication (Chojnicka-Paszun et al., 2014). Focusing on the second factor *i.e.* surface adsorption, LBG has been shown to have limited adsorption on PDMS surface with adsorption capacity (*i.e.* hydrated mass) of 4.8 mg/m$^2$ as estimated by Quartz crystal microbalance-dissipation (QCM-D) and dry mass of 1.0 mg/ m$^2$ as obtained using surface plasmon resonance (SPR) and forms a very rigid film with limited dissipation (Stokes et al., 2011b). This suggests that neither the conformation nor the surface adsorption can support LBG to behave as boundary lubricant.

Tribological studies of xanthan gum (XG) has been studied by various groups not only because of their wide usage as a thickening agent in food products but also because of their

recent acceptance as a dysphagia thickener for vulnerable people suffering from swallowing disorders (Torres et al., 2019, Rofes et al., 2014). Unlike afore-mentioned NSPs, XG has a stiff rigid-rod like conformation in dilute solutions (Williams et al., 1993, de Vries, 2004). It was observed that XG did not behave as a boundary lubricant at low concentrations (0.2 wt%) and the frictional response was similar to water (de Vicente et al., 2005b). However, Chojnicka-Paszun et al. (2014) investigated the lubrication properties of XG (**Table 2.2**) as a function of concentration. The friction of XG was lowered by over 30% when the XG concentration was doubled (3 wt%) and by nearly 60% when the concentration was increased up to 4 wt%. Similar concentration-dependent reduction in μ for XG was also observed in our laboratory (Torres et al., 2019). Gellan gum (GG) also shows concentration-dependent boundary lubrication behaviour (Torres et al., 2019). Interestingly, both XG and GG showed adsorption of a significant amount of hydrated mass as estimated by QCM-D, however the film was considerably more dilute in GG as compared to GG as quantified using SPR (Stokes et al., 2011b).

Pectin in aqueous solution (**Table 2.2**) has been demonstrated to be an effective lubricant. Pectin has been shown to promote full film lubrication at 1.27 wt% concentration on PDMS surfaces. Interestingly, pectin shows boundary lubrication behaviour largely dictated by its strong surface adsorption to PDMS in terms of both hydrated mass ($38.7$ mg/m$^2$) and dry mass ($3.1$ mg/m$^2$), latter is two times higher than that of XG and three times higher than that of LBG or GG (Stokes et al., 2011b). However, Chojnicka-Paszun et al. (2014) did not report any boundary lubrication behaviour of pectin and did not show any concentration effect on boundary lubrication behaviour even when the concentration was raised from 1.5 to 3.0 wt%. In summary, polysaccharides have shown the ability to decrease μ between hydrophobic surfaces in the boundary and/or mixed regimes if they get entrained in the contact region, largely dictated by their macromolecular conformation and/or get adsorbed to the surface of the tribopairs. In addition, increasing lubricant viscosity upon increasing the concentration of hydrocolloids has a prominent effect on reducing μ between PDMS-PDMS contacts in the hydrodynamic regime, irrespective of the type of hydrocolloids used due to the dominance of the rheological phenomena (Torres et al., 2019).

*Fluid gels/ gel particles.* Besides thickening agents, many of NSPs are known to form gels. Researchers have investigated the tribological behaviour of NSP-gels using gel particles suspended in a continuum and the motivation is largely to examine their lubrication potential

for fat replacement purposes. Such gel particles can be created by a top-down approach *i.e.* creating a gel and breaking them down into smaller micron- to millimetre-sized gel particles, which most likely happens during oral processing (Krop et al., 2019a) or creating well-defined microgels of optimum size using a homogenization process (Torres et al., 2017a, Sarkar et al., 2017a), as discussed previously for starch-based gels (Torres et al., 2018, Torres et al., 2017c). Another approach of studying tribological properties of gels involves designing fluid gels that are formed by applying an appropriate flow field to a biopolymer solution while that is under-going a gelatinization process; which results in a highly concentrated suspension of gelled particles (Norton et al., 2010).

Farrés et al. (2013) investigated the lubricating abilities of Ca-alginate (CaA) fluid gels as a function of hydrocolloid concentration. **Table 2.2** shows the curves of μ versus U as a function of the concentration of CaA fluid gels. A clear shift in tribological behvaiour can be identified when comparing these fluid gels at low concentration of alginate (1.0 wt%) versus high concentration (3.0 wt%). According to the study, polysaccharides like alginate enhance the viscosity and particle elasticity as a function of increasing centration, which results in re-duction in friction between the tribopairs. Because of classical hydrodynamic theory, this be-haviour is expected simply due to the high alginate viscosity in the inlet zone, where the shear rates are still relatively moderate (Stokes et al., 2013), which plays a role in dragging these gel particles into the contact zone. On the other hand, the higher modulus of the particles allows them to not get destroyed by the PDMS-PDMS contact pressure (Sarkar et al., 2019b, Torres et al., 2018).

Similar to CaA, agarose- (Gabriele et al., 2010) or *κ*-C-fluid gels (Garrec and Norton, 2013) as well as *κ*-C gel particles (Krop et al., 2019a) showed similar behaviour *i.e.* reduction in μ in the boundary regime and early onset of the mixed regime with increasing volume frac-tion of particles as well as the biopolymer concentration. Hence, in case of gel particles and fluid gels, the elasticity of the particles, viscosity of the continuum and size of the particles might be the key drivers for reducing μ between hydrophobic contact surfaces.

***Mixed gel particles.*** Recently, there has been increasing research efforts to design mixed hydrogels with structural complexity, such as beads inside gels or multi-layered gels for various oral processing related studies (Laguna and Sarkar, 2016, Santagiuliana et al., 2018, Krop et al., 2019a). Although most studies focus on rheology, in our laboratory we conducted

the first tribological study with the MTM tribometer using mixed hydrogels. In this work (Krop et al., 2019a), the hydrogels were prepared using $\kappa$C-LBG, $\kappa$C-sodium alginate (NaA) as well as $\kappa$C-CaA beads, where CaA beads of 300-1000 μm within a $\kappa$C gel matrix. The hydrogels were broken down using simulated oral processing at 37 °C in the presence of artificial saliva containing mucin. In the case of gel bolus fragments containing CaA beads of either 300 or 1000 μm, the μ (μ = 0.05-0.15 at U = 3 mm/s) was an order of magnitude lower than that of artificial saliva and showed rapid onset of the mixed regime. Theoretical considerations using Hertz theory suggested that the CaA microgels were not capable of showing any 'ball-bearing effect' but they were capable of being entrained between the PDMS surfaces. Since most of our food systems are more complex than hydrogels made up of single polysaccharides, tribological properties of mixed hydrogel particles require systematic investigation in future to understand the interactions between NSP-NSP and NSP-surface.

## 2.5. Conclusions and future recommendations

Oral tribology has shown remarkable progress over the last 15 years showing some interesting empirical relationships with sensory properties that were not achievable by using apparent viscosity measurements alone (Sarkar and Krop, 2019b). Considering the current need of the obesogenic society for fat replacers and low calorie bulking agents, understanding the oral lubrication mechanism of starch and non-starch polysaccharides as thickeners and/or as hydrogel particles have become more important than ever before. With the limited work carried out so far on tribology of food polysaccharides either in aqueous solution or as fluid gels, microgels or mixed gel fragments, few conclusive remarks can be drawn. Tribology of polysaccharides are mainly dictated by their molecular conformation (*e.g.* extended linear chain, random coil, rigid rod), size (nanometres (nms) to hundreds of microns), shape (*e.g.* irregular, spherical, ellipsoidal) and the degree of surface adsorption. One might then speculate that for a polysaccharide to be an ideal lubricant, it should have an extended chain like to allow it to enter into the contact and should have sufficient proteinaceous impurities that are capable of allowing interfacial adsorption. Although increasing polymer concentration has a prominent effect on increasing viscosity and subsequently reduce friction coefficients in the hydrodynamic regime, such viscosity effects might not always be realized in lower speeds *i.e.* boundary and mixed regimes, both these regimes are crucial from oral processing perspectives. For polysaccharide-based fluid gels or microgels, the gel particles should be sufficiently small to enter

into the contact zone, have enough viscosity in the continuum to drag the gel particle into the contact zone as well as the elasticity of the particles should be high enough to avoid complete deformation by the pressures within the tribological shear region.

In future, more studies are needed to understand the surface adsorption behaviour of polysaccharides using QCM-D and SPR (Stokes et al., 2011b). Saliva is an important aspect of oral processing (Sarkar et al., 2017b, Sarkar and Singh, 2012), which has been largely under-estimated in the tribological studies of polysaccharides, except a few studies (Torres et al., 2018, Torres et al., 2019, Krop et al., 2019a). It is crucial to understand the interactions with saliva not only from viewpoint of the role of α-amylase in case of starch but also from the reference to interactions of non-starch polysaccharides to mucins, other small molecular proteins and ionic species.

The tribology data should be always integrated with other complementary approaches such as size distribution, microscopy and rheology to generate robust hypothesis about the mechanism behind particular mouthfeel and instrumental-sensory correlations. It is also important to microstructurally evaluate the polysaccharide gel particles in the contact region after tribological shear, which can provide meaningful insights about the potential deformation of these systems due to the high pressures in the contact zone (Sarkar et al., 2017a). The observed tribological data should be fitted using theoretical approximations (Bongaerts et al., 2007, Krop et al., 2019a) and calculation of drag forces of the polysaccharides in the continuum and defor-mation of polysaccharide-based particles due to the pressures within the contact region can help to accurately predict the sensory behaviour (Sarkar et al., 2019b, Torres et al., 2018). Alt-hough a range of tribometers has been developed, standardization in test procedures across laboratories is necessary. Finally, designing more appropriate surfaces (roughness, modulus, wettability) for mimicking human mucosa is crucial (Sarkar et al., 2019b) to allow bottom-up design of food structure with appropriate polysaccharides and develop tribologically-informed low-calorie foods with 'just-right' mouthfeel and high consumer acceptance.

As limited efforts have been made on understanding of tribological performance of mixed hydrocolloids system, tribological properties of hydrocolloid mixtures, *i.e.* starch and non-starch polysaccharides (κ-carrageenan) were monitored in the following **Chapter 3** using a combination of rheology, tribology and microstructural techniques/.

# References

BAIER, S., ELMORE, D., GUTHRIE, B., LINDGREN, T., SMITH, S., STEINBACH, A., DEBON, S., VANHEMELRIJCK, J., HEYER, P. & LæUGER, J. A new tribology device for assessing mouthfeel attributes of foods. 5th International Symposium on Food Rheology and Structure, ISFRS 2009 Zurich, Switzerland.

BATCHELOR, H., VENABLES, R., MARRIOTT, J. & MILLS, T. 2015. The application of tribology in assessing texture perception of oral liquid medicines. *International Journal of Pharmaceutics,* 479**,** 277-281.

BLAZEK, J. & GILBERT, E. P. J. C. P. 2011. Application of small-angle X-ray and neutron scattering techniques to the characterisation of starch structure: A review. 85**,** 281-293.

BONGAERTS, J. H. H., FOURTOUNI, K. & STOKES, J. R. 2007. Soft-tribology: lubrication in a compliant PDMS–PDMS contact. *Tribology International,* 40**,** 1531-1542.

BROSSARD, N., CAI, H., OSORIO, F., BORDEU, E. & CHEN, J. 2016. "Oral" tribological study on the astringency sensation of red wines. *Journal of Texture Studies,* 47**,** 392-402.

BULëON, A., COLONNA, P., PLANCHOT, V. & BALL, S. J. I. J. O. B. M. 1998. Starch granules: structure and biosynthesis. 23**,** 85-112.

CAI, H., LI, Y. & CHEN, J. 2017. Rheology and tribology study of the sensory perception of oral care products. *Biotribology,* 10**,** 17-25.

CARVALHO-DA-SILVA, A. M., VAN DAMME, I., TAYLOR, W., HORT, J. & WOLF, B. 2013. Oral processing of two milk chocolate samples. *Food & function,* 4**,** 461-469.

CASSIN, G., HEINRICH, E. & SPIKES, H. A. 2001. The influence of surface roughness on the lubrication properties of adsorbing and non-adsorbing biopolymers. *Tribology Letters,* 11**,** 95-102.

CHEN, J., LIU, Z. & PRAKASH, S. 2014. Lubrication studies of fluid food using a simple experimental set up. *Food Hydrocolloids,* 42**,** 100-105.

CHEN, J. & STOKES, J. R. 2012. Rheology and tribology: Two distinctive regimes of food texture sensation. *Trends in Food Science & Technology,* 25**,** 4-12.

CHOJNICKA-PASZUN, A., DE JONGH, H. H. J. & DE KRUIF, C. G. 2012. Sensory perception and lubrication properties of milk: Influence of fat content. *International Dairy Journal,* 26**,** 15-22.

CHOJNICKA-PASZUN, A., DOUSSINAULT, S. & DE JONGH, H. H. J. 2014. Sensorial analysis of polysaccharide–gelled protein particle dispersions in relation to lubrication and viscosity properties. *Food Research International,* 56**,** 199-210.

COPELAND, L., BLAZEK, J., SALMAN, H. & TANG, M. C. 2009. Form and functionality of starch. *Food Hydrocolloids,* 23**,** 1527-1534.

DE VICENTE, J., STOKES, J. R. & SPIKES, H. A. 2005. Lubrication properties of non-adsorbing polymer solutions in soft elastohydrodynamic (EHD) contacts. *Tribology International,* 38**,** 515-526.

DE VICENTE, J., STOKES, J. R. & SPIKES, H. A. 2006. Soft lubrication of model hydrocolloids. *Food Hydrocolloids,* 20**,** 483-491.

DE VRIES, J. 2004. Hydrocolloid gelling agents and their applications. *In:* WILLIAMS, P. A. & PHILLIPS, G. O. (eds.) *Gums and Stabilisers for the Food Industry 12.* The Royal Society of Chemistry.

DEVEZEAUX DE LAVERGNE, M., STRIJBOSCH, V. M., VAN DEN BROEK, A. W., VAN DE VELDE, F. & STIEGER, M. 2016. Uncoupling the Impact of Fracture Properties and Composition on Sensory Perception of Emulsion-Filled Gels. *Journal of Texture Studies,* 47**,** 92-111.

DIAMANTINO, V. R., COSTA, M. S., TABOGA, S. R., VILAMAIOR, P. S. L., FRANCO, C. M. L. & PENNA, A. L. B. 2019. Starch as a potential fat replacer for application in cheese: Behaviour of different starches in casein/starch mixtures and in the casein matrix. *International Dairy Journal,* 89**,** 129-138.

DICKINSON, E. 2018. Hydrocolloids acting as emulsifying agents–How do they do it? *Food hydrocolloids,* 78**,** 2-14.

DOWSON, D. 2012. Bio-tribology. *Faraday Discussions,* 156**,** 9-30.

DOWSON, D. & WRIGHT, V. Bio-tribology.   Proceeding of the Conference on the Rheology of Lubrication, The Institute of Petroleum, The Institution of Mechanical Engineers, and the British Society of Rheology, 1973 London, UK. 81–88.

DRESSELHUIS, D. M., DE HOOG, E. H. A., STUART, M. A. C. & VAN AKEN, G. A. 2008. Application of oral tissue in tribological measurements in an emulsion perception context. *Food Hydrocolloids,* 22**,** 323-335.

EGGLESTON, G., FINLEY, J. W. & DEMAN, J. M. 2018. Carbohydrates. *Principles of Food Chemistry.* Cham: Springer International Publishing.

FARRëS, I. F., DOUAIRE, M. & NORTON, I. T. 2013. Rheology and tribological properties of Ca-alginate fluid gels produced by diffusion-controlled method. *Food Hydrocolloids,* 32**,** 115-122.

FERNãNDEZ FARRëS, I., MOAKES, R. J. A. & NORTON, I. T. 2014. Designing biopolymer fluid gels: A microstructural approach. *Food Hydrocolloids,* 42**,** 362-372.

FOEGEDING, E. A. 2007. Rheology and sensory texture of biopolymer gels. *Current Opinion in Colloid & Interface Science,* 12**,** 242-250.

GABRIELE, A., SPYROPOULOS, F. & NORTON, I. T. 2010. A conceptual model for fluid gel lubrication. *Soft Matter,* 6**,** 4205-4213.

GARREC, D. 2013. *Understanding fluid gels and hydrocolloid tribology - PhD Thesis.* University of Birmingham.

GARREC, D. A. & NORTON, I. T. 2012. The influence of hydrocolloid hydrodynamics on lubrication. *Food Hydrocolloids,* 26**,** 389-397.

GARREC, D. A. & NORTON, I. T. 2013. Kappa carrageenan fluid gel material properties. Part 2: Tribology. *Food Hydrocolloids,* 33**,** 160-167.

GISMONDI, A., D'AGOSTINO, A., CANUTI, L., DI MARCO, G., BASOLI, F. & CANINI, A. J. P. B.-A. I. J. D. W. A. A. O. P. B. 2019. Starch granules: a data collection of 40 food species. 153**,** 273-279.

GOH, S. M., VERSLUIS, P., APPELQVIST, I. A. M. & BIALEK, L. 2010. Tribological measurements of foods using a rheometer. *Food Research International,* 43**,** 183-186.

HAYAKAWA, F., KAZAMI, Y., ISHIHARA, S., NAKAO, S., NAKAUMA, M., FUNAMI, T., NISHINARI, K. & KOHYAMA, K. 2014. Characterization of eating difficulty by sensory evaluation of hydrocolloid gels. *Food Hydrocolloids,* 38**,** 95-103.

HEYER, P. & LæUGER, J. A flexible platform for tribological measurements on a rheometer.   AIP Conference Proceedings, 2008. AIP, 1168-1170.

HEYER, P. & LæUGER, J. 2009. Correlation between friction and flow of lubricating greases in a new tribometer device. *Lubrication Science,* 21**,** 253-268.

HIGIRO, J., HERALD, T. J. & ALAVI, S. 2006. Rheological study of xanthan and locust bean gum interaction in dilute solution. *Food Research International,* 39**,** 165-175.

HUTCHINGS, I. M. 2016. Leonardo da Vinci′s studies of friction. *Wear,* 360-361**,** 51-66.

JIN, Z. M., DOWSON, D. & FISHER, J. 1993. Fluid film lubrication in natural hip joints. *In:* DOWSON, D., TAYLOR, C. M., CHILDS, T. H. C., GODET, M. & DALMAZ, G. (eds.) *Tribology Series.* Elsevier.

JIN, Z. M., ZHENG, J., LI, W. & ZHOU, Z. R. 2016. Tribology of medical devices. *Biosurface and Biotribology,* 2**,** 173-192.

JOBLING, S. 2004. Improving starch for food and industrial applications. *Current Opinion in Plant Biology,* 7**,** 210-218.

JOST, H. P. 1966. Lubrication (Tribology) – A Report on the Present Position and Industry's Needs. London, UK: Department of Education and Science, HM. Stationary Office.

JOYNER, H. S., PERNELL, C. W. & DAUBERT, C. R. 2014. Impact of parameter settings on normal force and gap height during tribological measurements. *Journal of Food Engineering,* 137**,** 51-63.

KAVEHPOUR, H. P. & MCKINLEY, G. H. 2004. Tribo-rheometry: from gap-dependent rheology to tribology. *Tribology Letters,* 17**,** 327-335.

KIUMARSI, M., SHAHBAZI, M., YEGANEHZAD, S., MAJCHRZAK, D., LIELEG, O. & WINKELJANN, B. 2019. Relation between structural, mechanical and sensory properties of gluten-free bread as affected by modified dietary fibers. *Food Chemistry,* 277**,** 664-673.

KOé, H., DRAKE, M., VINYARD, C. J., ESSICK, G., VAN DE VELDE, F. & FOEGEDING, E. A. 2019. Emulsion filled polysaccharide gels: Filler particle effects on material properties, oral processing, and sensory texture. *Food Hydrocolloids,* 94**,** 311-325.

KOKINI, J. L., KADANE, J. B. & CUSSLER, E. L. 1977. Liquid texture perceived in the mouth. *Journal of Texture Studies,* 8**,** 195-218.

KROP, E. M., HETHERINGTON, M. M., HOLMES, M., MIQUEL, S. & SARKAR, A. 2019a. On relating rheology and oral tribology to sensory properties in hydrogels. *Food Hydrocolloids,* 88**,** 101-113.

KROP, E. M., HETHERINGTON, M. M., MIQUEL, S. & SARKAR, A. 2019b. The influence of oral lubrication on food intake: A proof-of-concept study. *Food Quality and Preference,* 74**,** 118-124.

KRZEMINSKI, A., WOHLHþTER, S., HEYER, P., UTZ, J. & HINRICHS, J. 2012. Measurement of lubricating properties in a tribosystem with different surface roughness. *International Dairy Journal,* 26**,** 23-30.

LAGUNA, L., FARRELL, G., BRYANT, M., MORINA, A. & SARKAR, A. 2017a. Relating rheology and tribology of commercial dairy colloids to sensory perception. *Food & Function,* 8**,** 563-573.

LAGUNA, L. & SARKAR, A. 2016. Influence of mixed gel structuring with different degrees of matrix inhomogeneity on oral residence time. *Food Hydrocolloids,* 61**,** 286-299.

LAGUNA, L. & SARKAR, A. 2017. Oral tribology: update on the relevance to study astringency in wines. *Tribology - Materials, Surfaces & Interfaces,* 11**,** 116-123.

LAGUNA, L., SARKAR, A., BRYANT, M. G., BEADLING, A. R., BARTOLOMë, B. & VICTORIA MORENO-ARRIBAS, M. 2017b. Exploring mouthfeel in model wines: Sensory-to-instrumental approaches. *Food Research International,* 102**,** 478-486.

LAIHO, S., WILLIAMS, R. P. W., POELMAN, A., APPELQVIST, I. & LOGAN, A. 2017. Effect of whey protein phase volume on the tribology, rheology and sensory properties of fat-free stirred yoghurts. *Food Hydrocolloids,* 67**,** 166-177.

LAPASIN, R. 2012. *Rheology of industrial polysaccharides: theory and applications,* Springer Science & Business Media.

LAPASIN, R. & PRICL, S. 1995. Rheology of polysaccharide systems. *Rheology of Industrial Polysaccharides: Theory and Applications.* Boston, MA: Springer US.

LIMBERT, G., MASEN, M. A., POND, D., GRAHAM, H. K., SHERRATT, M. J., JOBANPUTRA, R. & MCBRIDE, A. 2019. Biotribology of the ageing skin—Why we should care. *Biotribology,* 17**,** 75-90.

LIU, K., STIEGER, M., VAN DER LINDEN, E. & VAN DE VELDE, F. 2016. Tribological properties of rice starch in liquid and semi-solid food model systems. *Food Hydrocolloids,* 58**,** 184-193.

LOBATO-CALLEROS, C., RAMïREZ-SANTIAGO, C., VERNON-CARTER, E. J. & ALVAREZ-RAMIREZ, J. 2014. Impact of native and chemically modified starches addition as fat replacers in the viscoelasticity of reduced-fat stirred yogurt. *Journal of Food Engineering,* 131**,** 110-115.

MALONE, M. E., APPELQVIST, I. A. M. & NORTON, I. T. 2003. Oral behaviour of food hydrocolloids and emulsions. Part 1. Lubrication and deposition considerations. *Food Hydrocolloids,* 17**,** 763-773.

MANN, A. & TIGHE, B. J. 2016. 3 - Ocular biotribology and the contact lens: Surface interactions and ocular response. *In:* CHIRILA, T. V. & HARKIN, D. G. (eds.) *Biomaterials and Regenerative Medicine in Ophthalmology (Second Edition).* Woodhead Publishing.

MYANT, C., SPIKES, H. A. & STOKES, J. R. 2010. Influence of load and elastic properties on the rolling and sliding friction of lubricated compliant contacts. *Tribology International,* 43**,** 55-63.

NGUYEN, P. T., KRAVCHUK, O., BHANDARI, B. & PRAKASH, S. 2017. Effect of different hydrocolloids on texture, rheology, tribology and sensory perception of texture and mouthfeel of low-fat pot-set yoghurt. *Food Hydrocolloids,* 72**,** 90-104.

NGUYEN, P. T. M., BHANDARI, B. & PRAKASH, S. 2016. Tribological method to measure lubricating properties of dairy products. *Journal of Food Engineering,* 168**,** 27-34.

NISHINARI, K. & TAKAHASHI, R. 2003. Interaction in polysaccharide solutions and gels. *Current Opinion in Colloid & Interface Science,* 8**,** 396-400.

NORTON, I. T., SPYROPOULOS, F. & COX, P. 2010. *Practical food rheology: an interpretive approach*, John Wiley & Sons.

PICOUT, D. R. & ROSS-MURPHY, S. B. 2003. Rheology of biopolymer solutions and gels. *TheScientificWorldJournal,* 3**,** 105-121.

PRADAL, C. & STOKES, J. R. 2016. Oral tribology: bridging the gap between physical measurements and sensory experience. *Current Opinion in Food Science,* 9**,** 34-41.

PRAKASH, S., TAN, D. D. Y. & CHEN, J. 2013. Applications of tribology in studying food oral processing and texture perception. *Food Research International,* 54**,** 1627-1635.

PUNIA, S., SIROHA, A. K., SANDHU, K. S. & KAUR, M. 2019. Rheological and pasting behavior of OSA modified mungbean starches and its utilization in cake formulation as fat replacer. *International Journal of Biological Macromolecules,* 128**,** 230-236.

RENAUD, M., BELGACEM, M. N. & RINAUDO, M. 2005. Rheological behaviour of polysaccharide aqueous solutions. *Polymer,* 46**,** 12348-12358.

RMAILE, A., CARUGO, D., CAPRETTO, L., ZHANG, X., WHARTON, J. A., THURNER, P. J., ASPIRAS, M., WARD, M. & STOODLEY, P. 2013. Microbial tribology and disruption of dental plaque bacterial biofilms. *Wear,* 306**,** 276-284.

ROBINSON, G., ROSS-MURPHY, S. B. & MORRIS, E. R. 1982. Viscosity-molecular weight relationships, intrinsic chain flexibility, and dynamic solution properties of guar galactomannan. *Carbohydrate Research,* 107**,** 17-32.

ROFES, L., ARREOLA, V., MUKHERJEE, R., SWANSON, J. & CLAVë, P. 2014. The effects of a xanthan gum-based thickener on the swallowing function of patients with dysphagia. *Alimentary Pharmacology & Therapeutics,* 39**,** 1169-1179.

SANTAGIULIANA, M., CHRISTAKI, M., PIQUERAS-FISZMAN, B., SCHOLTEN, E. & STIEGER, M. 2018. Effect of mechanical contrast on sensory perception of heterogeneous liquid and semi-solid foods. *Food Hydrocolloids,* 83**,** 202-212.

SARKAR, A., ANDABLO-REYES, E., BRYANT, M., DOWSON, D. & NEVILLE, A. 2019. Lubrication of soft oral surfaces. *Current Opinion in Colloid & Interface Science,* 39**,** 61-75.

SARKAR, A., KANTI, F., GULOTTA, A., MURRAY, B. S. & ZHANG, S. 2017a. Aqueous lubrication, structure and rheological properties of whey protein microgel particles. *Langmuir,* 33**,** 14699-14708.

SARKAR, A. & KROP, E. M. 2019. Marrying oral tribology to sensory perception: a systematic review. *Current Opinion in Food Science.*

SARKAR, A. & SINGH, H. 2012. Oral Behaviour of Food Emulsions. *In:* CHEN, J. & ENGELEN, L. (eds.) *Food Oral Processing: : Fundamentals of Eating and Sensory Perception.* Chicester, West Sussex, UK: Blackwell Publishing Ltd.

SARKAR, A., YE, A. & SINGH, H. 2017b. Oral processing of emulsion systems from a colloidal perspective. *Food & Function,* 8**,** 511-521.

SELWAY, N. & STOKES, J. R. 2013. Insights into the dynamics of oral lubrication and mouthfeel using soft tribology: Differentiating semi-fluid foods with similar rheology. *Food Research International,* 54**,** 423-431.

SHAHRIVAR, K., ORTIGOSA-MOYA, E. M., HIDALGO-ALVAREZ, R. & DE VICENTE, J. 2019. Isoviscous elastohydrodynamic lubrication of inelastic Non-Newtonian fluids. *Tribology International*.

SHERMAN 1969. A texture profile of foodstuffs based upon well-defined rheological properties. *Journal of Food Science,* 34**,** 458-462.

SHEWAN, H. M., PRADAL, C. & STOKES, J. R. 2019. Tribology and its growing use toward the study of food oral processing and sensory perception. *Journal of Texture Studies*.

SHIMIZU, Y. & SPIKES, H. A. 2016. The influence of slide–roll ratio on ZDDP tribofilm formation. *Tribology Letters,* 64**,** 19.

STOKES, J. R., BOEHM, M. W. & BAIER, S. K. 2013. Oral processing, texture and mouthfeel: From rheology to tribology and beyond. *Current Opinion in Colloid & Interface Science,* 18**,** 349-359.

STOKES, J. R., MACAKOVA, L., CHOJNICKA-PASZUN, A., DE KRUIF, C. G., DE JONGH, H. H. J. & INSTITUTET, Y. K. I. Y. 2011. Lubrication, adsorption, and rheology of aqueous polysaccharide solutions. *Langmuir* 27**,** 3474-3484.

SUJKA, M. & JAMROZ, J. 2013. Ultrasound-treated starch: SEM and TEM imaging, and functional behaviour. *Food Hydrocolloids,* 31**,** 413-419.

TORRES, M. D., MOREIRA, R., CHENLO, F. & VãZQUEZ, M. J. 2012. Water adsorption isotherms of carboxymethyl cellulose, guar, locust bean, tragacanth and xanthan gums. *Carbohydrate Polymers,* 89**,** 592-598.

TORRES, O., ANDABLO-REYES, E., MURRAY, B. S. & SARKAR, A. 2018. Emulsion microgel particles as high-performance bio-lubricants. *ACS Applied Materials & Interfaces,* 10**,** 26893-26905.

TORRES, O., MURRAY, B. & SARKAR, A. 2016. Emulsion microgel particles: Novel encapsulation strategy for lipophilic molecules. *Trends in Food Science & Technology,* 55**,** 98-108.

TORRES, O., MURRAY, B. & SARKAR, A. 2017a. Design of novel emulsion microgel particles of tuneable size. *Food Hydrocolloids,* 71**,** 47-59.

TORRES, O., TENA, N. M., MURRAY, B. & SARKAR, A. 2017b. Novel starch based emulsion gels and emulsion microgel particles: Design, structure and rheology. *Carbohydrate Polymers,* 178**,** 86-94.

TORRES, O., YAMADA, A., RIGBY, N. M., HANAWA, T., KAWANO, Y. & SARKAR, A. 2019. Gellan gum: A new member in the dysphagia thickener family. *Biotribology,* 17**,** 8-18.

TUNICK, M. H. 2000. Rheology of dairy foods that gel, stretch, and fracture. *Journal of Dairy Science,* 83**,** 1892-1898.

UPADHYAY, R. & CHEN, J. 2019. Smoothness as a tactile percept: Correlating 'oral'tribology with sensory measurements. *Food Hydrocolloids,* 87**,** 38-47.

VINKE, J., KAPER, H. J., VISSINK, A. & SHARMA, P. K. 2018. An ex vivo salivary lubrication system to mimic xerostomic conditions and to predict the lubricating properties of xerostomia relieving agents. *Scientific reports,* 8**,** 9087.

WANG, M. L. & PENG, Z. X. 2015. Wear in human knees. *Biosurface and Biotribology,* 1**,** 98-112.

WILLIAMS, P. A., ANNABLE, P., PHILLIPS, G. O. & NISHINARI, K. 1993. Mixed polysaccharide gels formed between xanthan gum and glucomannan. *In:* NISHINARI, K. & DOI, E. (eds.) *Food hydrocolloids: Structures, properties, and functions.* Boston, USA: Springer.

YAKUBOV, G. E., BRANFIELD, T. E., BONGAERTS, J. H. H. & STOKES, J. R. 2015. Tribology of particle suspensions in rolling-sliding soft contacts. *Biotribology,* 3**,** 1-10.

ZHANG, B., SELWAY, N., SHELAT, K. J., DHITAL, S., STOKES, J. R. & GIDLEY, M. J. 2017. Tribology of swollen starch granule suspensions from maize and potato. *Carbohydrate Polymers,* 155**,** 128-135.

ZHOU, Z. R. & JIN, Z. M. 2015. Biotribology: Recent progresses and future perspectives. *Biosurface and Biotribology,* 1**,** 3-24.

ZOBEL, H. F. 1988. Molecules to granules: A comprehensive starch review. *Starch - Stärke,* 40**,** 44-50.

# Chapter 3ᵇ

# Rheology and tribology of starch + *κ*-carrageenan mixtures
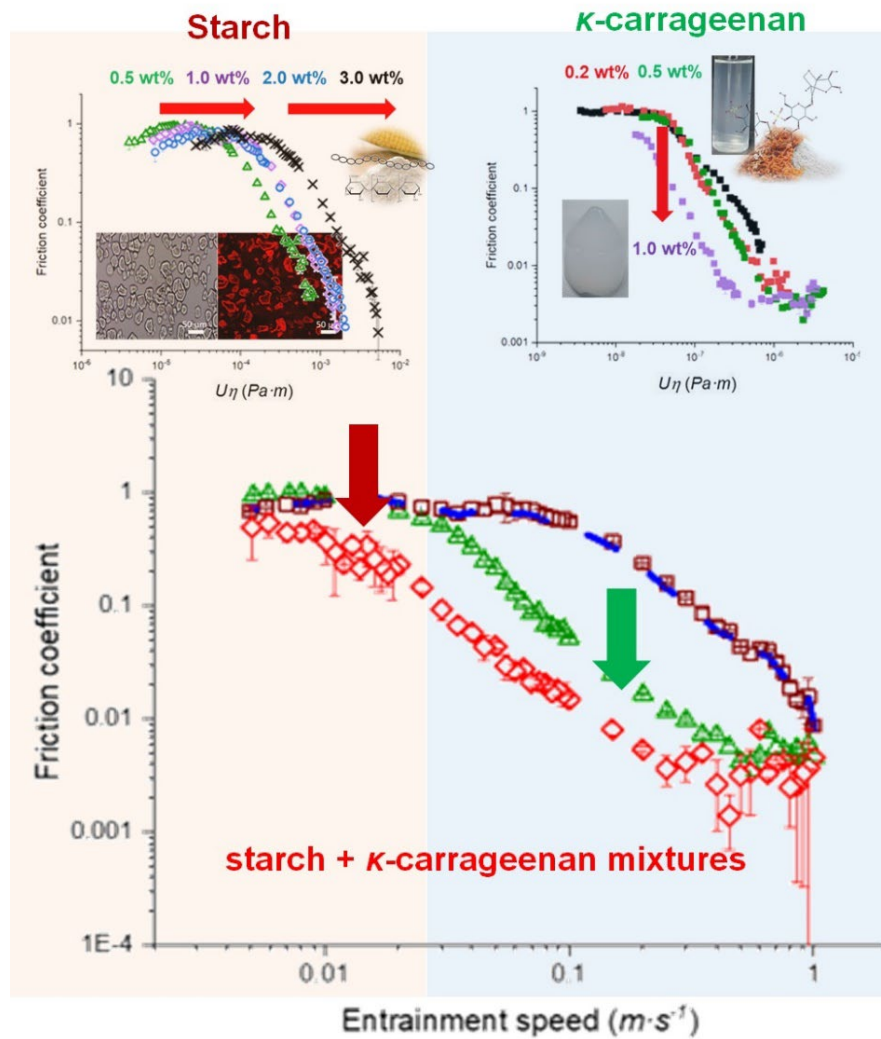


## Abstract

In this study, we investigated the rheological and tribological properties of biopolymer mixtures of gelatinized corn starches (0.5–10.0 wt%) and *κ*-carrageenan (*κ*C) (0.05–1.0 wt%). Two different starch samples were used. The first starch (CS1), despite extensive heating and shearing contained 'ghost' granules, while the second starch (CS2) had no visible ghost gran-

ules after the same gelatinization process as CS1. Apparent viscosity measurements demonstrated that $\kappa$C + CS1 mixtures were shear thinning liquids, with viscosity values being lower than the corresponding weight average of the values of the individual equilibrium phases at shear rates < 50 s$^{-1}$. Tribological results revealed that $\kappa$C $\geq$ 0.5 wt% was required to observe any decrease in friction coefficients in the mixed lubrication regime. Starch (CS1) showed an unusual behaviour at $\geq$ 5 wt%, where the friction coefficient decreased not only in the mixed regime but also in the boundary regime, probably due to the presence of the 'ghost' granules, latter became entrained in the contact region. The CS1 + $\kappa$C mixtures showed significantly lower friction coefficients than that of pure CS1 and $\kappa$C in the mixed regime. However, the CS2 + $\kappa$C mixture (*i.e.*, containing no ghost granules) showed similar behaviour to pure $\kappa$C in the mixed regime, while lower friction coefficients than that of the pure CS2 and $\kappa$C in the boundary regime. These findings illustrate new opportunities for designing biopolymer mixtures with tunable lubrication performance, via optimizing the concentrations of the individual biopolymers and the gelatinization state of the starch.

## 3.1.    Introduction

Tribology is the science of friction, wear, and lubrication of surfaces in relative motion (Ludema and Ajayi, 2018). Such surface interactions can control the function of practically every macroscopic systems with interacting moving parts and are of the utmost importance to various engineering applications, such as gears, bearings, seals, clutches, couplings, and cams (Hutchings and Shipway, 2017, Mang et al., 2011). In the food community, the importance of 'interacting surfaces in relative motion' has been increasingly recognized with respect to oral processing, *i.e.* the processing of food in the mouth, such as tooth-tooth, tongue-palate, tongue-tooth, tooth-food, tongue-food, lip-lip, lip-food interactions, and so on. More importantly, many of these surface interactions often tend to explain mouthfeel attributes, such as smoothness, pastiness, astringency, which are not solely driven by the bulk rheological properties of the food and cannot be fully explained by measuring apparent viscosity (Prakash et al., 2013, Sarkar and Krop, 2019b, Pradal and Stokes, 2016, Laguna and Sarkar, 2017b). Therefore, oral tribology has become an increasingly important part of oral processing studies of model and real foods (Sarkar et al., 2019a, Stokes et al., 2013, Laguna et al., 2017a, Stribiţcaia et al., 2020).

There has also been a gradual increase in interest in understanding specifically the tribological properties of polysaccharides, since they can play an essential role in adjusting the mouthfeel of foods and beverages (Stokes et al., 2011a, Torres et al., 2019, Zhang et al., 2017, Garrec and Norton, 2012b, Garrec and Norton, 2013). Starch is the most widespread polysaccharide in foods that affects food structure and texture and absenc eand starch textural properties tend to vary widely depending on their origin, *e.g.*, corn (maize), wheat, potato, tapioca, and rice. In addition, the textural properties of starches of one origin depend on the starch granule size, shape, degree of swelling, dispruption, *i.e.*, gelatinization. (Blazek and Gilbert, 2011a, Buléon et al., 1998a). The degree of gelatinization may determine the tribological properties, *e.g.*, stickness, slipperiness, *etc.* (Evans and Lips, 1992, Ai and Jane, 2015), though there have been relatively few systematic studies on the lubrication properties of starch (Zhang et al., 2017, Torres et al., 2017b, Torres et al., 2018).

Zhang et al. (2017) studied the tribological properties of suspensions of cooked swollen starch granules (ghost suspensions) from maize or potato across a wide range of concentration. The coefficient of friction ($\mu$) was shown to decrease in the boundary and mixed regimes with increasing concentration (0.01-1.0 wt%) because the ghost particles became entrained in the contact zone at low entrainment speed ($U$, 40 mm s$^{-1}$) as compared to that of water, latter was squeezed out of the hydrophobic tribological surfaces used in their study. Torres et al. (2018) on the other hand investigated the tribological effects of wheat starch-based microgel particles. The magnitude of $\mu$ decreased on increasing starch content of the microgels from 15 to 20 wt%, the latter particles having been formed from a bulk gel with a higher shear modulus. It was postulated that these higher starch content microgels might therefore be slightly stiffer and better at keeping the hydrophobic tribological surfaces apart and enable lowering the $\mu$ values.

The lubricating behaviour of non-starch polysaccharides, such as locust bean gum, carrageenan, gellan, guar, pectin, xanthan gums, *etc,* in the boundary and mixed lubrication regimes has also attracted recent research attention. In particular, the tribological properties of $\kappa$-carrageenan ($\kappa$C) have been investigated (Garrec and Norton, 2013, Stokes et al., 2011a). Garrec et al. (2013) showed that as the concentration of $\kappa$C increased, the polymer was entrained in the contact zone, and $\mu$ values decreased at the site of the converging geometry formed between the tribopairs. Interestingly, the lubrication behaviour by $\kappa$C was consistent across smooth to rough PDMS substrates (mean asperity radius 10 nm to 400 nm), highlighting

their ability to entrain and prevent direct PDMS-PDMS asperity contact, irrespective of the degree of surface roughness (Stokes et al., 2011a).

Although some information on the tribological properties of biopolymer solutions is available in the literature, studies of combinations of biopolymers are very rare. On the other hand, there is extensive literature on the phase separation of biopolymer mixtures. Biopolymers phase separate due to thermodynamic incompatibility (Semenova and Dickinson, 2010, Capron et al., 2001, Lorén et al., 2001, Vis et al., 2015a, Firoozmand et al., 2007, Murray and Phisarnchananan, 2016), giving rise to two-phase systems. Previous studies have shown that such phase separation leads to modification in the bulk rheology of the mixtures, related to excluded volume effects between two biopolymers, such as starch and $\kappa$C, which mutually concentrate each other in solution (Lafargue et al., 2007, Tecante and Doublier, 1999, Huc et al., 2014, Fakharian et al., 2015). Thus, both the storage modulus ($G'$) and loss modulus ($G''$) can be much higher in mixtures than with $\kappa$C alone (Lafargue et al., 2007, Fakharian et al., 2015). Also, a slight increase in apparent viscosity of the mixtures compared to $\kappa$C alone has been observed (Huc et al., 2014). Thermodynamic incompatibility between starch and other polysaccharides has been extensively described previously (Murray and Phisarnchananan, 2016, Firoozmand et al., 2007, Tecante and Doublier, 2002, Chen et al., 2018).

In this study, we used corn starch (CS) and $\kappa$C as model biopolymers to investigate the rheological and tribological properties of the biopolymer mixture. We measured the shear viscosity, load-bearing properties and Stribeck curves of $\kappa$C and CS individually and then the properties of mixtures of the two. In particular two types of corn starches were employed, one containing ghost granules and other containing no ghost granules post gelatinization to understand the effect (if any) of these intact starch granules on the tribological properties of the biopolymer mixtures. To our knowledge, this is the first study that reports the frictional properties of biopolymer mixtures of CS and $\kappa$C and the findings can bring new knowledge to design biopolymer mixtures with tailored lubrication performance.

## 3.2.    Material and Methods

### 3.2.1. Materials

$\kappa$-carrageenan ($\kappa$C), product code 22048 (CAS number 11114-20-8), corn starch (CS1), product code S9679 (CAS number 9005-25-8) and the second corn starch sample (CS2) 10120 (CAS number 9037-22-3), both derived from maize, were all purchased from Sigma-Aldrich,

Dorset, UK. Polysaccharide solutions were prepared in 20 mM phosphate buffer at pH 7.0. Smooth polydimethylsiloxane (PDMS, Sylgard 184, Dow Corning, USA) tribo-couples, *i.e.,* ball (Ø 47 mm) and disc (Ø 19 mm, 4 mm thickness), with the surface roughness of 50 nm, were purchased from PCS Instruments, London, UK. Rhodamine B (product code R-6626) was purchased from Sigma Aldrich, Dorset, UK. Water purified by a Milli-Q apparatus (Millipore, Bedford, UK), with a resistivity not less than 18.2 M□ .cm, was used for the preparation of the buffer and any other solutions.

## 3.2.2. Preparation of starch + *κ*C mixtures

Gelatinized waxy corn starch (CS1 or CS2) (0.5-5 wt%) was prepared by dispersing the starch powder in phosphate buffer at pH 7.0, followed by heating in a water bath at 90 °C for 20 min with constant shearing using a magnetic stirrer, to gelatinize the starch. *κ-carrageenan (κC)* was similarly dispersed in phosphate buffer at pH 7.0 (0.05-1.0 wt%) for at least 24 h at room temperature and then heated dispersed κC solution at 90°C for 20 min before mixing starch. To prepare the biopolymer mixtures, both solutions were prepared separately as above before mixing. Equal volumes of starch solution and κC solution of different concentrations were blended and homogenized at 21,000 rpm for 30 min using an Ultra Turrax T25 homogenizer (IKA-Werke GmbH &Co., Staufen Germany).

## 3.2.3. Apparent viscosity

Rheological characterization of the pure biopolymers and their mixtures was performed using a modular compact rheometer, model MCR 302 (Anton Paar, Austria) at shear rates ranging from 0.1 to 1000 $s^{-1}$ at 37 °C. The biopolymer mixtures did not phase separate within the first 2 h of preparation but started to separate after 7 days of storage at ambient conditions (see **Figure A1**) and all the rheological experiments were carried out within 2 h of preparation of the biopolymer mixtures. A cone-and-plate geometry system (CP50-2, cone diameter 50 mm, cone angle: 2 °) with a gap of 1 mm was used for all measurements. For each measurement, 2 mL of sample were pipetted onto the plate, excluding any air bubbles. A temperature-controlled cover prevented evaporation during the measurements and helped to maintain the temperature at 37 °C (*i.e.*, representing oral processing temperature). Samples were left on the plate for approximately 2 min to achieve a steady state, following which the apparent viscosities were

measured. High shear rate limiting viscosity ($\eta_\infty$) was determined to scale the tribological data in the Stribeck curves (see later in the results and discussion section).

### 3.2.4. Tribology

Tribological measurements on the pure biopolymers and their mixtures samples were performed using a Mini Traction Machine 2 (MTM2, PCS Instruments, London, UK) with hydrophobic polydimethylsiloxane (PDMS) ball and disc as tribopairs. All the tribological experiments were carried out within 2 h of preparation of the biopolymer mixtures where the mixtures were in a single phase (**Figure A1**). A normal load ($W$) of 2 N and a slide-to-roll ratio (*SRR*) of 50% were set for all Stribeck measurements. The sliding speeds were varied from 1 to 0.001 m s$^{-1}$. The coefficient of friction was measured for all samples as a function of entrainment speed. The entrainment speed $U$ is defined as in **Equation 2.2**:

$$U = \frac{1}{2} \; (U_B + U_D) \tag{2.2}$$

where, $U_B$ is the rolling speed of the ball and $U_D$ is the sliding speed of the disc. The temperature in the tribological experiment was set at $37 \pm 1°C$, matching that of the rheological measurements. In addition, the load-bearing ability of the biopolymers was also measured at load ($W$) ranging from 1 to 5 N, at $U = 0.005$ m s$^{-1}$. The friction coefficients are reported as the mean and standard deviation of 3 measurements carried out on at least triplicate samples prepared on different days.

### 3.2.5. Microscopy

Optical microscopy (Nikon, SMZ-2T, Japan) was used to observe the microstructure of the heated starch samples to identify any residual granule structures. Samples were diluted with buffer (1:10 w/w). A confocal laser scanning microscope (Model LSM 880, Carl Zeiss Micro Imaging GmbH, Jena, Germany) was also used for microstructural characterization of some samples, after mixing with 0.5 wt% Rhodamine Blue (RB), excited at 514 nm, to fluorescently label the starch. Samples were excited with a He/Ne (543, 633 nm) laser source. A 20× objective with numerical aperture 0.5 was used to obtain all images, at 1024 × 1024-pixel resolution.

### 3.2.6. Statistics

All experimental results were reported as mean and standard deviations of three measurements on triplicate samples (n = 3 × 3). The statistical analyses were conducted for the rheological data at 50 s$^{-1}$ simulating oral processing shear and tribological data at boundary regime (0.005 m s$^{-1}$) and mixed regimes (0.05 m s$^{-1}$, 0.1 m s$^{-1}$) using one-way ANOVA and multiple comparison test using SPSS software (IBM, SPSS statistics, version 24) and the significant difference between samples were considered when $p < 0.05$ using Tukey's test. Statistical results can be observed in **Tables A1a-d** and **A2a-c**.

## 3.3.     Results and Discussion

### 3.3.1. Tribological and rheological properties of pure biopolymers

**Figures 3.1ai** and **3.1bi** illustrate the friction coefficients ($\mu$) as a function of entrainment speed ($U$) of $\kappa$C (0.05–1.0 wt%) and CS1 (0.5–5.0 wt%), respectively. The phosphate buffer on its own (**Figure 3.1ai**) shows a prolonged boundary regime with $\mu \approx 1.0$ until $U \approx 0.1$ m s$^{-1}$ followed by a decrease in $\mu$ as the mixed lubrication regime commences, where the pressure in the contact region between the PDMS tribopairs is sustained partly by the fluid and partly by the surfaces. Such a prolonged boundary regime with phosphate buffer has been seen previously (Sarkar et al., 2017a), where phosphate buffer was proposed to be squeezed out of the hydrophobic PDMS-PDMS contact zone.

The $\kappa$C solutions (**Figure 3.1ai**) showed interesting concentration-dependent tribological properties, where the extents of the boundary regime were shortened, *i.e.*, the onset of mixed regime occurred at lower speeds, upon increasing the concentration of $\kappa$C from 0.05 to 1.0 wt% with no changes in boundary friction observed from 0.05 to 0.5 wt% concentration ($p > 0.05$) (see **Table A1a** for statistical analyses). Also, the $\mu$ values in the mixed lubrication regime decreased sharply as the concentration was increased from 0.05 wt% to 0.1 wt% ($p < 0.05$) but no significant decline was observed when the concentration increased from 0.5 wt% to 1.0 wt% ($p > 0.05$) (see **Table A1a** for statistical analyses). For instance, the $\mu$ values decreased by an order of magnitude at $U = 0.1$ m s$^{-1}$, when the concentration of $\kappa$C was increased by order of magnitude, *i.e.*, from 0.1 to 1.0 wt%. Stokes et al. (2011a) have already indicated that $\kappa$C is a useful potential lubricant because it decreases friction coefficients efficiently in the mixed regime, compared to numerous other aqueous polysaccharides (locust bean, gellan, and

xanthan gums). Because $\kappa$C mainly helps the results for the smooth surface by surface wetting effect. It is noteworthy that $\kappa$C solutions $\geq 0.5$ wt% also demonstrated a characteristic hydro-dynamic lubrication regime behaviour, where the $\mu$ values started to increase at the highest $U$.
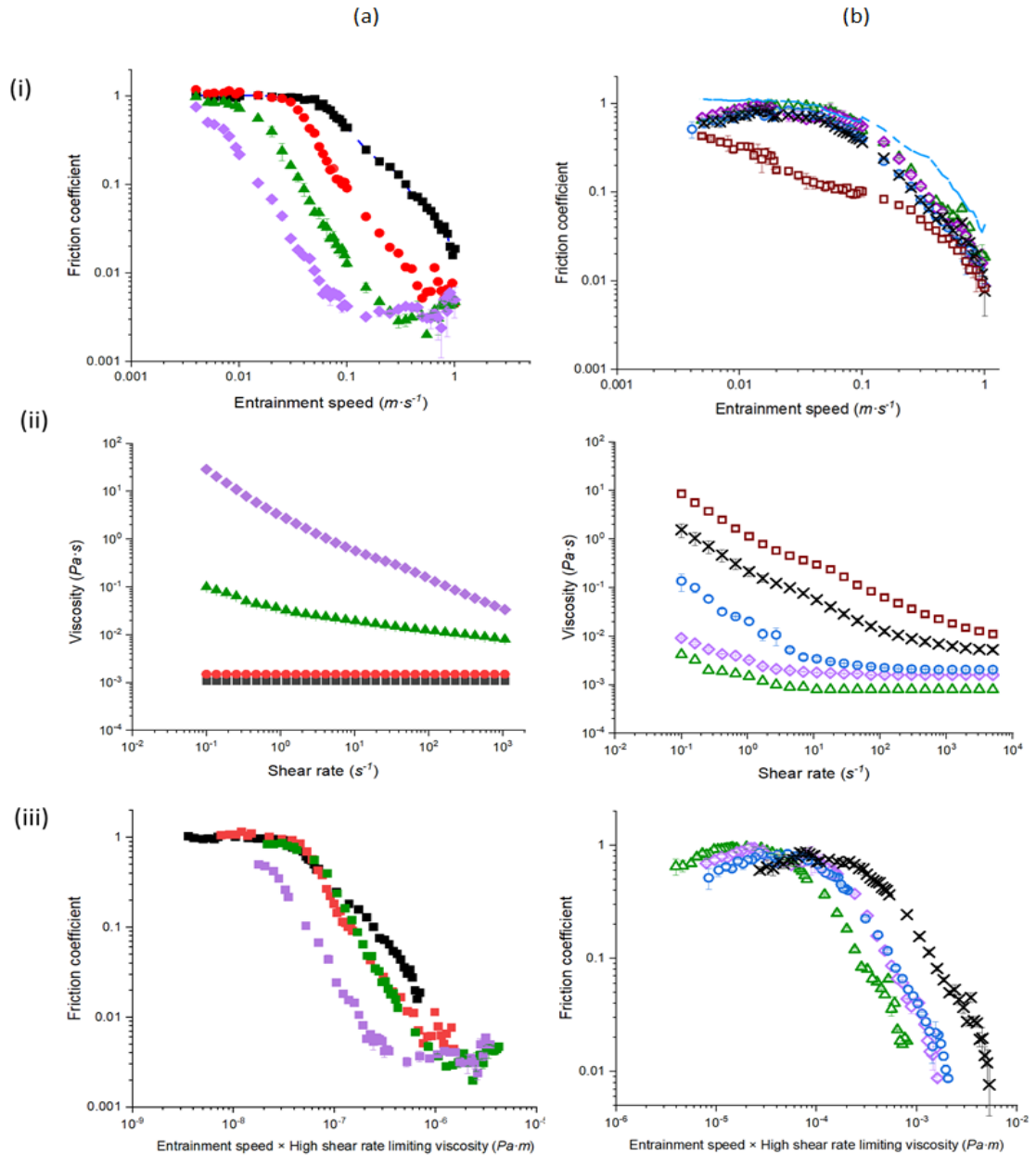


**Figure 3.1.** (i) Friction coefficient ($\mu$) versus entrainment speed ($U$), (ii) apparent viscosity ($\eta$) versus shear rate ($\dot{\gamma}$), and (iii) friction coefficient ($\mu$) as a function of product of entrainment speed and effective viscosity ($U\eta$) of (a) $\kappa$C, and (b) CS1 at various concentrations ($\kappa$C: 0.05 wt% (■), 0.1 wt% (●), 0.5 wt% (▲), and 1.0 wt% (◆); CS1: 0.5 wt% (△), 1.0 wt% (◇), 2.0 wt% (○), 3.0 wt% (✕) and 5.0 wt% (□). Phosphate buffer is used as a control (--). Values represent means and error bars represent the standard deviations for at least three measurements on triplicate samples (n = 3 × 3).

Shifting our focus to starch, 0.5–2.0 wt% CS1 (**Figure 3.1bi**) showed similar boundary behaviour to that of the phosphate buffer (up to $U = 0.1$ m s$^{-1}$), but slightly lower $\mu$ values in the mixed lubrication regime as compared to that of the buffer. Interestingly, $\mu$ was more or less the same for all CS1 concentrations between 0.5 to 2.0 wt% irrespective of the regimes (*p > 0.05*) (see **Table A1b** for statistical analyses), unlike the behaviour with $\kappa$C (**Figure 3.1ai**), Latter showed a strong concentration-dependence on frictional behaviour. However, $\mu$ values at 5.0 wt% CS1 (**Figure 3.1bi**) were significantly lower than for the other starch concentrations in the mixed regime at $U = 1$ m s$^{-1}$ (*p > 0.05*) (see **Table A1b** for statistical analyses), but converged on the same values as $U$ approached the maximum applied ($U = 1$ m s$^{-1}$). Particularly CS1 at 5.0 wt% did not show any visible boundary regime. This behaviour might be due to the presence of higher concentrations of 'ghost' granules at the higher CS1 concentration, which potentially might have granule-granule inter-molecular friction, flattened and providing sufficient hydrodynamic lift to separate the PDMS surfaces leading to immediate onset of mixed lubrication regime even at low speeds ($U \leq 0.005$ m s$^{-1}$).
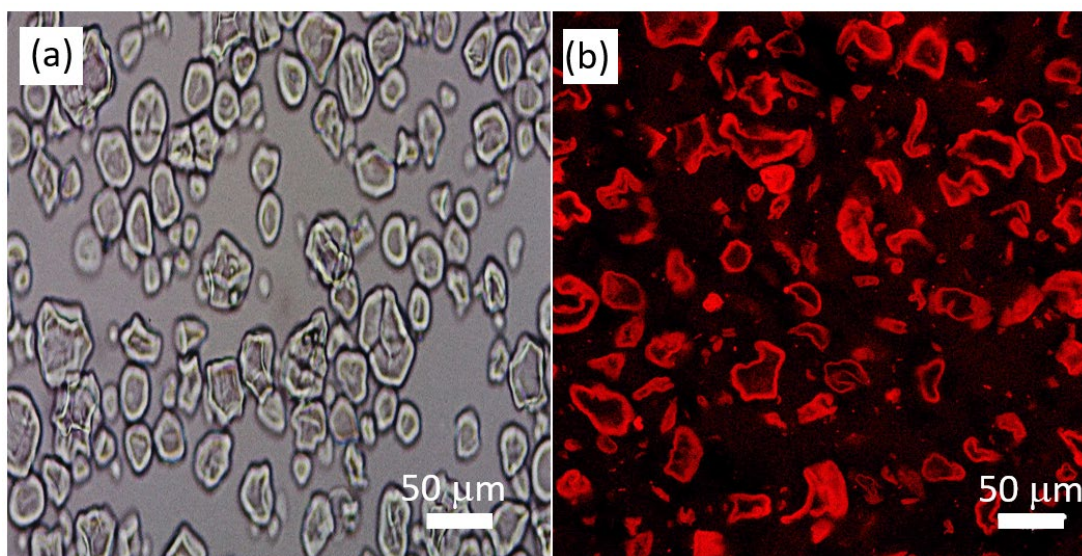


**Figure 3.2.** Optical (a) and confocal (b) micrographs of 1 wt% CS1 after gelatinization. The bright regions in (b) are due to CS1 labelled with Rhodamine Blue. Scale bar is 50 μm.

The presence of ghost granules in the CS1 sample was evidenced *via* optical and confocal laser scanning microscopy, as shown in **Figures 3.2a** and **3.2b**, respectively. It is clear from both these images that ghost granules remained in the CS1 sample even though the starch was subjected to high temperature ($\approx 90°C$) and shearing. Liu et al. (2016) have reported that

the tribological properties of rice starch in liquid and semi-solid model food systems are often associated with the soft and deformable nature of the gelatinized starch granules - that can flatten and fill the asperities between the PDMS-PDMS contact region in the boundary regime. This creates a smoother surface contact zone. In addition, the gelatinized rice starch granules in the afore-mentioned study formed a thicker continuous tribological film that separated the tribo-pair surfaces due to the increased viscosity. Therefore, the deformability of ghost granules, which are tens of microns in size, plus their potential ability to form a more continuous film, could explain the absence of the boundary regime and rapid onset of mixed lubrication regime seen (**Figure 3.1bi**) for 5.0 wt% *CS1*.

**Figures 3.1aii** and **3.1bii** show the flow curves of different concentrations of $\kappa$C and CS1 solutions, respectively. As one might expect, higher viscosity values occurred at higher concentrations of the biopolymers (see **Tables A2a and A2b** for statistical analyses) and both $\kappa$C and CS1 showed shear thinning behaviour. However, marked shear thinning only occurred for CS1 at higher concentrations ($\geq$ 3.0 wt%) and the viscosity was significantly lower than those of 0.5-2.5 wt% CS1 at the typical oral processing shear rate of 50 s$^{-1}$ (see **Table A2b** for statistical analyses).   In order to estimate the viscous contribution in the tribological data, the high shear rate limiting viscosity ($\eta_\infty$) was obtained. The Reynolds equation for soft-elastohydrodynamic lubrication (EHL) was applied when the sample showed a clear hydrodynamic regime (iso-viscous-elastic lubrication regime), as observed for $\kappa$C in **Figure 3.1ai** at $\geq$ 0.5 wt%.   This model (De Vicente et al., 2005a) gives an arithmetic expression of the Reynold's equation for the soft EHL lubrication regime between sliding-rolling ball and plate contact under fully flooded conditions.   The friction coefficient in contact can be expressed in terms of the characteristic parameters: *W*, *η* and *U*, as follows (**Equation 3.1**):

$$\mu = 1.46 \ \frac{(\eta U)^{0.65} W^{-0.76}}{E^{*1.35} R^{*2.05}} + SRR \left( 3.8 \frac{(\eta U)^{0.71} W^{-0.76}}{E^{*1.47} R^{*2.23}} + 0.96 \frac{(\eta U)^{0.36} W^{-0.11}}{E^{*0.47} R^{*0.58}} \right) \qquad \textbf{(3.1)}$$

where $E^* = \left( \dfrac{1 - v_1{}^2}{E'} + \dfrac{1 - v_2{}^2}{E''} \right)^{-1}$ and $R^* = \left( \dfrac{1}{R'} + \dfrac{1}{R''} \right)^{-1}$ are the reduced Young's modulus and reduced radius of the contact, respectively. Here $E'$ and $E''$ are the elastic moduli of the surface material and $R'$ and $R''$ are the radius of the surfaces.

The first term in **Equation 3.1**. is the Poiseuille contribution to the friction, while the second corresponds to the Couette friction. Stokes et al. (2011a), Andablo-Reyes et al. (2019)

showed that **Equation 3.1** can be successfully fitted to the experimental data in **Figure 3.1aii**, and consequently, the value of $\eta$ obtained. In our study, $SRR = 0.5$, $E'$ of the PDMS ball and disk $\approx 2.4$ MPa and $R'$ $(= R'') = 9.5 \times 10^{-3}$ m.

The calculated values of $\eta$ for 0.5 wt% and 1.0 wt% $\kappa$C, showing EHL lubrication regimes for the Reynolds equation, were 0.00267, and 0.004 Pa s, respectively. Using these estimated values of $\eta$ ($\eta_\infty$) from **Equation 3.1** and **Figures 3.1aii** and **3.1bii**, we plotted the corresponding Stribeck curves (**Figure 3.1aiii**) to identify the concentrations of $\kappa$C where the tribology was dominated by the bulk rheological properties. **Figure 3.1aiii** shows that 0.1 to 0.5 wt% $\kappa$C gave similar shaped curves with overlapping characteristics, which means that the tribological properties of these solutions were dominated by their $\eta_\infty$ (**Figure 3.1aiii**). However, at concentrations $\geq 0.5$ wt% $\kappa$C, there was a lower $\mu$ in the mixed lubrication regime, which might be attributed to the coil-helix transition of $\kappa$C as it transforms from a solution to a gel (Rochas and Landry, 1987, Garrec and Norton, 2013, Rochas and Rinaudo, 1982, Gabriele et al., 2009), allowing $\kappa$C to entrain into the contact zone fully.

For CS1 (**Figure 3.1biii)**, the fitted Stribeck curve obtained using **Equation 3.1** did not show good agreement with increasing concentration of CS1, the Stribeck curves being significantly shifted to the right of the data points. These results support the idea that the stickiness of starch granules in the dispersions might resist the relative motion of the tribo-pairs due to molecular adhesion as reported by previous studies (Wu et al., 2015, Zhang et al., 2017, Liu et al., 2016), although this needs further investigation.

## 3.3.2. Load-bearing abilities of the biopolymers
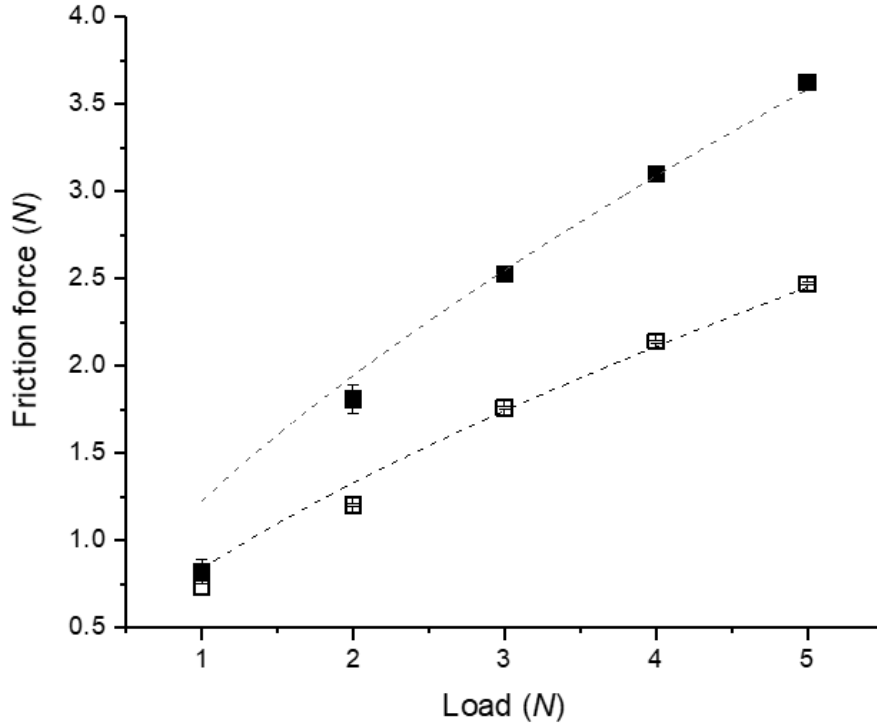


**Figure 3.3.** Friction force versus applied load for $\kappa$C (■) and CS1 (□) when sheared between polydimethylsiloxane (PDMS) ball and disc at a constant speed of 0.005 m s$^{-1}$. Values represent means and error bars represent the standard deviations for at least three measurements on triplicate samples (n = 3 × 3).

The load-bearing capacity of the lubricating film is important parameter to help understand the lubrication performance of biopolymers. The $\mu$ values of $\kappa$C and CS1 as a function of $U$ at different $W$ are shown in **FigureA2**. The friction force ($F$) of $\kappa$C and CS1 as a function of $W$ at low $U$ (0.005 m s$^{-1}$) is shown in **Figure 3.3**, aiming to test the load-bearing abilities of the biopolymers. According to Stokes et al. (2011a), $\mu$ for an adsorbed polysaccharide scales with W as $\mu \sim W^{\frac{2}{3}}$. This dependency originates from **Equation 3.2**:

$$F = \tau_i \times A \tag{3.2}$$

where $A$ = the contact area for a circular contact $= \pi \left( \frac{3}{4E^*} \frac{WR^*}{} \right)^{\frac{2}{3}}$ ; $\tau_i$ is the interfacial shear stress between the surfaces. The $F$ versus $W$ data in **Figure 3.3** were thus fitted using **Equation 3.3**:

$$F = 8.5 \cdot 10^{-6} \cdot \tau_i \times W^{\frac{2}{3}} \qquad\qquad \textbf{(3.3)}$$

The dashed lines in **Figure 3.3** show the best fits and the slope of these lines gives $\tau_i$, which for $\kappa$C and CS1 were 0.144 and 0.099 MPa, respectively, *i.e.*, lower than the value for PDMS/water/PDMS ($\tau_i = 0.23$ MPa). Thus CS1 lowers the interfacial shear stress between the surfaces even more than $\kappa$C suggesting that CS1 is more likely to remain bound to the PDMS surfaces. This further explains the larger decrease in friction coefficient with CS1 and the almost non-existent boundary lubrication regime illustrated in **Figure 3.1bi**.

### 3.3.3. Rheological versus tribological behaviour of starch + κC mixtures

Both **Figures 3.4ai** and **3.4bi** demonstrate that the CS1 + $\kappa$C mixtures, irrespective of the total biopolymer concentration (1.65 wt% or 2.75 wt%) have non-Newtonian behaviour and the viscosity values at orally relevant shear rate of 50 s$^{-1}$ were significantly different in comparison to either CS1 or $\kappa$C (see **Table B2c** for statistical analyses). As can be seen for both biopolymer concentrations, the viscosity values of the mixture containing the weighted average of the individual equilibrium phases ($\kappa$C and CS1) were similar to that of the starch alone (see dashed line in both **Figures 3.4ai and 3.4bi**). Interestingly, the measured viscosity values at either biopolymer concentration (1.65 or 2.75 wt%) were lower than the mixture containing weighted average of the individual equilibrium phases ($\kappa$C and CS1) at corresponding shear rates, except in case of 1.65 wt% mixtures at $\geq$ around 50 s$^{-1}$ (**Figures 3.4ai**). In other words, the viscosity behaviour appeared to be inordinately affected by the $\kappa$C in the mixture. This is in line with the rheological properties of the biopolymer mixtures studied previously, where the viscosity value of the mixtures tends to higher than the value of $\kappa$C alone (Fakharian et al., 2015; Lafargue et al., 2007; Huc et al., 2014).
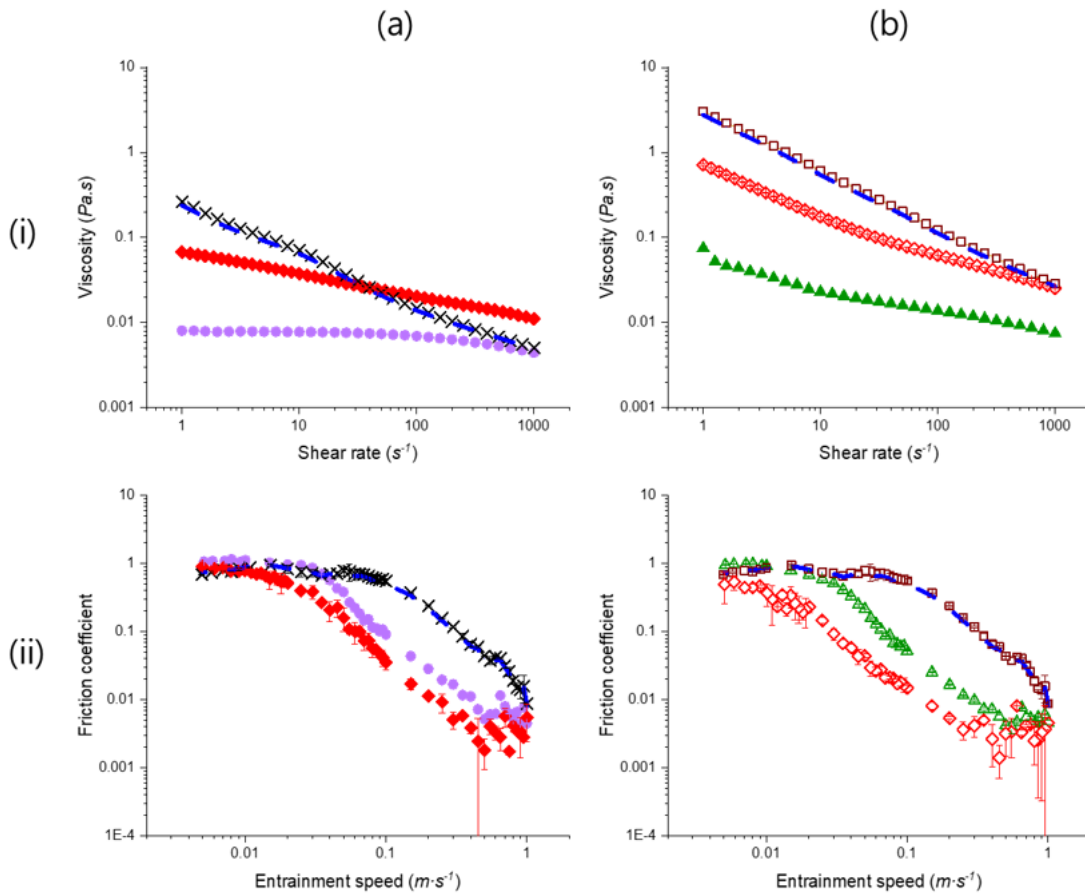
**Figure 3.4.** (i) Apparent viscosity ($\eta$) as a function of shear rate ($\dot{\gamma}$) and (ii) friction coefficients ($\mu$) versus entrainment speed ($U$) of biopolymer mixtures at (a) lower biopolymer concentrations: (1.5 wt% CS1 + 0.15 wt% $\kappa$C, ◆) and (b) high biopolymer concentrations (2.5 wt% CS1 + 0.25 wt% $\kappa$C, ◇) plus the controls of 0.15 wt% $\kappa$C (●), 0.25 wt% $\kappa$C (▲), 1.5 wt% CS1 (✕) and 2.5 wt% CS1 (□) alone. The weight average values of the corresponding individual controls for the mixtures are also shown (— —). Values represent means and error bars represent the standard deviations for at least three measurements on triplicate samples (n = 3 × 3).

Looking at the tribological data, the $\mu$ of the mixtures (**Figures 3.4aii** and **Figure 3.4bii** at 1.65 wt% and 2.75 wt%, respectively) were considerably lower than that of pure CS1 across the whole range of mixed regime (see **Tables A1c** and **A1d** for statistical analyses). Most surprisingly, unlike the bulk rheology results (**Figure 3.4ai** and **Figure 3.4bi**), the $\mu$ values of the mixtures were statistically similar to those of pure $\kappa$C ($p > 0.05$) except for the 2.75 wt% mixture ($p < 0.05$) (see **Tables B1c** and **B1d** for statistical analyses). Nevertheless, the $\mu$ values were always lower than the values of mixture containing weighted average of the individual phases (**Figure 3.4aii** and **Figure 3.4bii**), irrespective of the total biopolymer concentration. Possibly this is related to local potential phase separation within the mixtures at the time of

measurement, although the measurements were made immediately after mixing and phase separation is normally quite slow to evolve (see **Figure A1**). No phase separation was visible by eye at the time of measurement so this requires further investigation. The other possibility is that the behaviour is driven by the presence of the starch ghost 'granules' observed in the mixture. Tecante and Doublier (1999), Chaudemanche and Budtova (2008) have proposed that non-penetration between $\kappa$C and swollen starch granules induces a "excluded volume effect", in other words swollen starch granules produce an effective increase in the local concentration of $\kappa$C, which might have caused the reduction in friction irrespective of the total biopolymer concentration ((1.65 wt% or 2.75 wt%) (**Figure 3.4aii** and **Figure 3.4bii**). In addition, the swollen, more deformable gelatinized granules could entrain in the gap to support the load (Torres et al., 2018).

To understand further the role of these 'ghost' starch granules, **Figure 3.5** shows the $\mu$ values versus $U$ of mixture of 2.5 wt% CS2 + 0.25 wt% $\kappa$C, *i.e.*, the starch which contained no starch granules. Similar to the mixtures containing CS1 (**Figure 3.4aii** and **3.4bii**), the 2.5 wt% CS2 + 0.25 wt% $\kappa$C mixture did not show a reduction in friction in comparison to pure $\kappa$C in the mixed lubrication regime ($p > 0.05$) (see **Table A1d** for statistical analyses). Comparing the data of the mixture containing CS2 in **Figure 3.5** with the behaviour of CS1 in **Figure 3.4bii,** the $\mu$ values of the CS2 + $\kappa C$ mixture appeared to be comparatively higher than those of the CS1+ $\kappa C$ mixture at higher entrainment speeds, though statistically this was not significant ($p > 0.05$) (see **Table A1d** for statistical analyses). Nevertheless, it was interesting to observe that the 2.5 wt% CS2 + 0.25 wt% $\kappa$C mixture (**Figure 3.5**) reduced the boundary friction significantly as compared to pure $\kappa$C and friction in the mixed regime with respect to CS2 ($p < 0.05$) (**Figure 3.4bii and Table A1d** for statistical analyses).
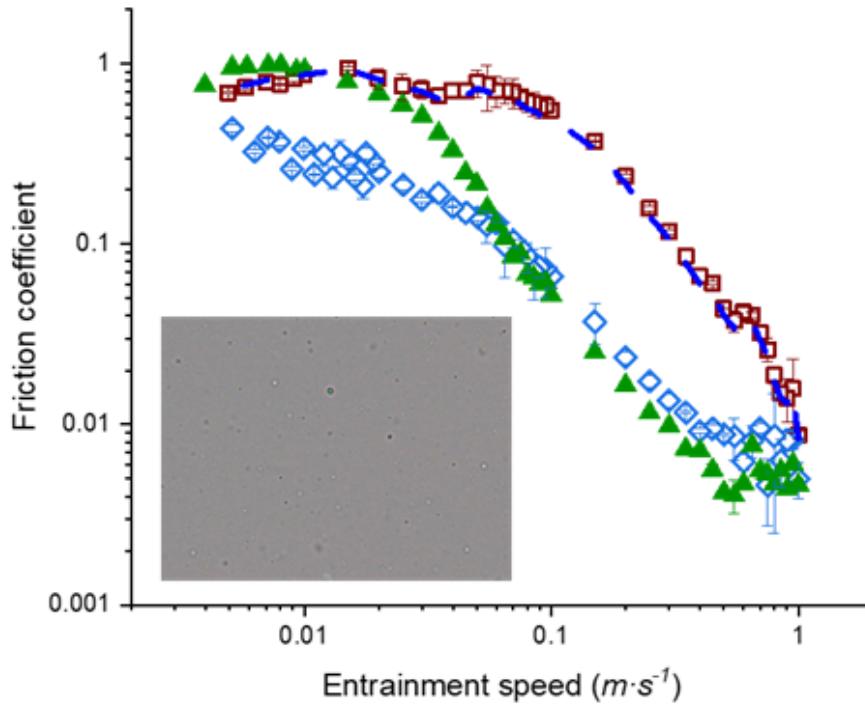
**Figure 3.5.** Friction coefficient ($\mu$) versus entrainment speed entrainment speed ($U$) of biopolymer mixtures using CS2 without the 'ghost' granules, *i.e.*, 2.5 wt% CS2 + 0.25 wt% $\kappa$C, ($\diamondsuit$) and controls of 2.5 wt% CS2 ($\square$) and 0.25 wt% $\kappa$C ($\blacktriangle$). Values represent means and error bars represent the standard deviations for at least three measurements on triplicate samples (n = 3 × 3). The inset is an optical micrograph of CS2 starch after gelatinization, illustrating the lack of 'ghost' granules. The weight average values of the corresponding individual controls for the mixtures are also shown (━ ━). Error bars represent standard deviations.

The inset to **Figure 3.5** is a corresponding optical micrograph of the CS2 starch after gelatinization, clearly illustrating the lack of 'ghost' granules, which would therefore appear to be the explanation of this stark difference in behaviour compared to CS1. This suggest that although the micron-sized 'ghost' starch granules present in the CS1 + $\kappa$C mixtures were efficient in reducing the friction in the mixed lubrication regime, they were not able to get entrained in the contact in the boundary region, *i.e.*, at low $U$. On the other hand, the CS2 + $\kappa$C mixture containing no 'ghost' granules were beneficial in creating potentially nanometric sized boundary films creating smoother tribo-contact surfaces. It is worth highlighting that CS2 apparently formed such boundary lubrication films only in presence of $\kappa$C - such behaviour is not seen in pure CS2 (**Figure 3.5**). This suggests some local interaction is occurring between CS2 and $\kappa$C in the boundary region, which requires further investigation in the future.

## 3.4.    Conclusions

In this study, we investigated the rheological and tribological properties of $\kappa$-carragee-nan and gelatinized corn starch and their mixtures. Both $\kappa$C solutions and gelatinized starch dispersions were shear-thinning liquids, and one starch (CS1) still contained ghost granules whilst the other (CS2) did not. In tribological measurements, $\kappa$C showed good lubrication per-formance by efficiently reducing the friction coefficient in the mixed lubrication regime, espe-cially when the concentration was $\geq$ 0.5 wt% and also showed hydrodynamic behaviour at higher entrainment speeds ($U$). On the other hand, the CS1 at $\geq$ 5 wt% immediately showed onset of a mixed lubrication regime at $U < 0.01$ m s$^{-1}$ without any observed boundary regime. This was attributed to the presence of 'ghost' starch granules that flattened in the confinement and enabled accelerated onset on mixed lubrication regime, which also provided better load-bearing ability than $\kappa$C. Mixtures of CS1 + $\kappa$C (at 1:10 w/w ratio) showed that the viscosity values were lower than the weight average of the individual equilibrium phases (CS1 + $\kappa$C) and the $\mu$ values of the mixtures containing the ghost starch granules (from CS1) were much lower than in the mixed lubrication regime. The mixture CS2 + $\kappa$C, lacking ghost starch gran-ules, did not offer such lubrication benefits in the mixed lubrication regime. However, CS2 + $\kappa$C did offer effective boundary lubrication with respect to $\kappa$C, owing to the gelatinized starch + $\kappa$C somehow forming a lubricating film. This highlights the crucial nature of the state of gelatinization of the starch in understanding the friction and lubrication properties of such mix-tures.

Although biopolymer mixture was studied for their tribological performance, it was intriguing to understand whether such mixtures form water-in-water emulsion droplets in cer-tain concentrations. Next chapter (**Chapter 4**) focuses on identifying the mechanisms of the tribological behaviour *i.e.* creation of water droplets in W/W emulsion systems with gelatinized starch and $\kappa$C and how such droplets may deform and increase lubrication performance.

# References

AI, Y. & JANE, J. L. 2015. Gelatinization and rheological properties of starch. *Starch-Stärke,* 67**,** 213-224.

ANDABLO-REYES, E., YERANI, D., FU, M., LIAMAS, E., CONNELL, S., TORRES, O. & SARKAR, A. 2019. Microgels as viscosity modifiers influence lubrication performance of continuum. *Soft Matter,* 15**,** 9614-9624.

BLAZEK, J. & GILBERT, E. P. 2011. Application of small-angle X-ray and neutron scattering techniques to the characterisation of starch structure: A review. *Carbohydrate Polymers,* 85**,** 281-293.

BULёON, A., COLONNA, P., PLANCHOT, V. & BALL, S. 1998. Starch granules: structure and biosynthesis. *International journal of biological macromolecules,* 23**,** 85-112.

CAPRON, I., COSTEUX, S. & DJABOUROV, M. 2001. Water in water emulsions: phase separation and rheology of biopolymer solutions. *Rheologica Acta,* 40**,** 441-456.

CHAUDEMANCHE, C. & BUDTOVA, T. 2008. Mixtures of pregelatinised maize starch and κ-carrageenan: Compatibility, rheology and gelation. *Carbohydrate Polymers,* 72**,** 579-589.

CHEN, J.-F., GUO, J., ZHANG, T., WAN, Z.-L., YANG, J. & YANG, X.-Q. 2018. Slowing the starch digestion by structural modification through preparing zein/pectin particle stabilized water-in-water emulsion. *Journal of agricultural and food chemistry,* 66**,** 4200-4207.

DE VICENTE, J., STOKES, J. & SPIKES, H. 2005. The frictional properties of Newtonian fluids in rolling–sliding soft-EHL contact. *Tribology Letters,* 20**,** 273-286.

EVANS, I. & LIPS, A. 1992. Viscoelasticity of gelatinized starch dispersions. *Journal of Texture Studies,* 23**,** 69-86.

FAKHARIAN, M.-H., TAMIMI, N., ABBASPOUR, H., NAFCHI, A. M. & KARIM, A. 2015. Effects of κ-carrageenan on rheological properties of dually modified sago starch: Towards finding gelatin alternative for hard capsules. *Carbohydrate polymers,* 132**,** 156-163.

FIROOZMAND, H., MURRAY, B. S. & DICKINSON, E. 2007. Fractal-type particle gel formed from gelatin+ starch solution. *Langmuir,* 23**,** 4646-4650.

GABRIELE, A., SPYROPOULOS, F. & NORTON, I. 2009. Kinetic study of fluid gel formation and viscoelastic response with kappa-carrageenan. *Food Hydrocolloids,* 23**,** 2054-2061.

GARREC, D. A., GUTHRIE, B. & NORTON, I. T. 2013. Kappa carrageenan fluid gel material properties. Part 1: Rheology. *Food hydrocolloids,* 33**,** 151-159.

GARREC, D. A. & NORTON, I. T. 2012. Understanding fluid gel formation and properties. *Journal of Food Engineering,* 112**,** 175-182.

GARREC, D. A. & NORTON, I. T. 2013. Kappa carrageenan fluid gel material properties. Part 2: Tribology. *Food Hydrocolloids,* 33**,** 160-167.

HUC, D., MATIGNON, A., BAREY, P., DESPRAIRIES, M., MAUDUIT, S., SIEFFERMANN, J.-M. & MICHON, C. 2014. Interactions between modified starch and carrageenan during pasting. *Food hydrocolloids,* 36**,** 355-361.

HUTCHINGS, I. & SHIPWAY, P. 2017. *Tribology: friction and wear of engineering materials*, Butterworth-Heinemann.

LAFARGUE, D., LOURDIN, D. & DOUBLIER, J.-L. 2007. Film-forming properties of a modified starch/κ-carrageenan mixture in relation to its rheological behaviour. *Carbohydrate Polymers,* 70**,** 101-111.

LAGUNA, L., FARRELL, G., BRYANT, M., MORINA, A. & SARKAR, A. 2017. Relating rheology and tribology of commercial dairy colloids to sensory perception. *Food & Function,* 8**,** 563-573.

LAGUNA, L. & SARKAR, A. 2017. Oral tribology: update on the relevance to study astringency in wines. *Tribology-Materials, Surfaces & Interfaces,* 11**,** 116-123.

LIU, K., STIEGER, M., VAN DER LINDEN, E. & VAN DE VELDE, F. 2016. Tribological properties of rice starch in liquid and semi-solid food model systems. *Food Hydrocolloids,* 58**,** 184-193.

LORëN, N., HERMANSSON, A.-M., WILLIAMS, M., LUNDIN, L., FOSTER, T., HUBBARD, C., CLARK, A., NORTON, I., BERGSTRøM, E. & GOODALL, D. 2001. Phase separation induced by conformational ordering of gelatin in gelatin/maltodextrin mixtures. *Macromolecules,* 34**,** 289-297.

LUDEMA, K. C. & AJAYI, L. 2018. *Friction, wear, lubrication: a textbook in tribology*, CRC press.

MANG, T., BOBZIN, K. & BARTELS, T. 2011. *Industrial tribology: Tribosystems, friction, wear and surface engineering, lubrication*, John Wiley & Sons.

MURRAY, B. S. & PHISARNCHANANAN, N. 2016. Whey protein microgel particles as stabilizers of waxy corn starch+ locust bean gum water-in-water emulsions. *Food Hydrocolloids,* 56**,** 161-169.

PRADAL, C. & STOKES, J. R. 2016. Oral tribology: bridging the gap between physical measurements and sensory experience. *Current Opinion in Food Science,* 9**,** 34-41.

PRAKASH, S., TAN, D. D. Y. & CHEN, J. 2013. Applications of tribology in studying food oral processing and texture perception. *Food Research International,* 54**,** 1627-1635.

ROCHAS, C. & LANDRY, S. 1987. Molecular organization of kappa carrageenan in aqueous solution. *Carbohydrate polymers,* 7**,** 435-447.

ROCHAS, C. & RINAUDO, M. 1982. Calorimetric determination of the conformational transition of kappa carrageenan. *Carbohydrate Research,* 105**,** 227-236.

SARKAR, A., ANDABLO-REYES, E., BRYANT, M., DOWSON, D. & NEVILLE, A. 2019. Lubrication of soft oral surfaces. *Current opinion in colloid & interface science.*

SARKAR, A., KANTI, F., GULOTTA, A., MURRAY, B. S. & ZHANG, S. 2017. Aqueous lubrication, structure and rheological properties of whey protein microgel particles. *Langmuir,* 33**,** 14699-14708.

SARKAR, A. & KROP, E. M. 2019. Marrying oral tribology to sensory perception: a systematic review. *Current opinion in food science.*

SEMENOVA, M. G. & DICKINSON, E. 2010. *Biopolymers in food colloids: Thermodynamics and molecular interactions*, CRC Press.

STOKES, J. R., BOEHM, M. W. & BAIER, S. K. 2013. Oral processing, texture and mouthfeel: From rheology to tribology and beyond. *Current Opinion in Colloid & Interface Science,* 18**,** 349-359.

STOKES, J. R., MACAKOVA, L., CHOJNICKA-PASZUN, A., DE KRUIF, C. G. & DE JONGH, H. H. 2011. Lubrication, adsorption, and rheology of aqueous polysaccharide solutions. *Langmuir,* 27**,** 3474-3484.

STRIBIŢCAIA, E., KROP, E. M., LEWIN, R., HOLMES, M. & SARKAR, A. 2020. Tribology and rheology of bead-layered hydrogels: Influence of bead size on sensory perception. *Food Hydrocolloids,* 104**,** 105692.

TECANTE, A. & DOUBLIER, J. 1999. Steady flow and viscoelastic behavior of crosslinked waxy corn starch-κ-carrageenan pastes and gels. *Carbohydrate Polymers,* 40**,** 221-231.

TECANTE, A. & DOUBLIER, J. 2002. Rheological investigation of the interaction between amylose and κ-carrageenan. *Carbohydrate Polymers,* 49**,** 177-183.

TORRES, O., ANDABLO-REYES, E., MURRAY, B. S. & SARKAR, A. 2018. Emulsion microgel particles as high-performance bio-lubricants. *ACS applied materials & interfaces,* 10**,** 26893-26905.

TORRES, O., TENA, N. M., MURRAY, B. & SARKAR, A. 2017. Novel starch based emulsion gels and emulsion microgel particles: Design, structure and rheology. *Carbohydrate Polymers*, Dec 15.

TORRES, O., YAMADA, A., RIGBY, N. M., HANAWA, T., KAWANO, Y. & SARKAR, A. 2019. Gellan gum: A new member in the dysphagia thickener family. *Biotribology,* 17**,** 8-18.

VIS, M., OPDAM, J., VAN'T OOR, I. S., SOLIGNO, G., VAN ROIJ, R., TROMP, R. H. & ERNë, B. H. 2015. Water-in-water emulsions stabilized by nanoplates. *ACS Macro Letters,* 4**,** 965-968.

WU, K., GUNARATNE, A., COLLADO, L. S., CORKE, H. & LUCAS, P. W. 2015. Adhesion, cohesion, and friction estimated from combining cutting and peeling test results for thin noodle sheets. *Journal of food science,* 80**,** E370-E376.

ZHANG, B., SELWAY, N., SHELAT, K. J., DHITAL, S., STOKES, J. R. & GIDLEY, M. J. 2017. Tribology of swollen starch granule suspensions from maize and potato. *Carbohydrate polymers,* 155**,** 128-135.

# Chapter 4[c]

# Tribology and rheology of water-in-water emulsions stabilized by whey protein microgels
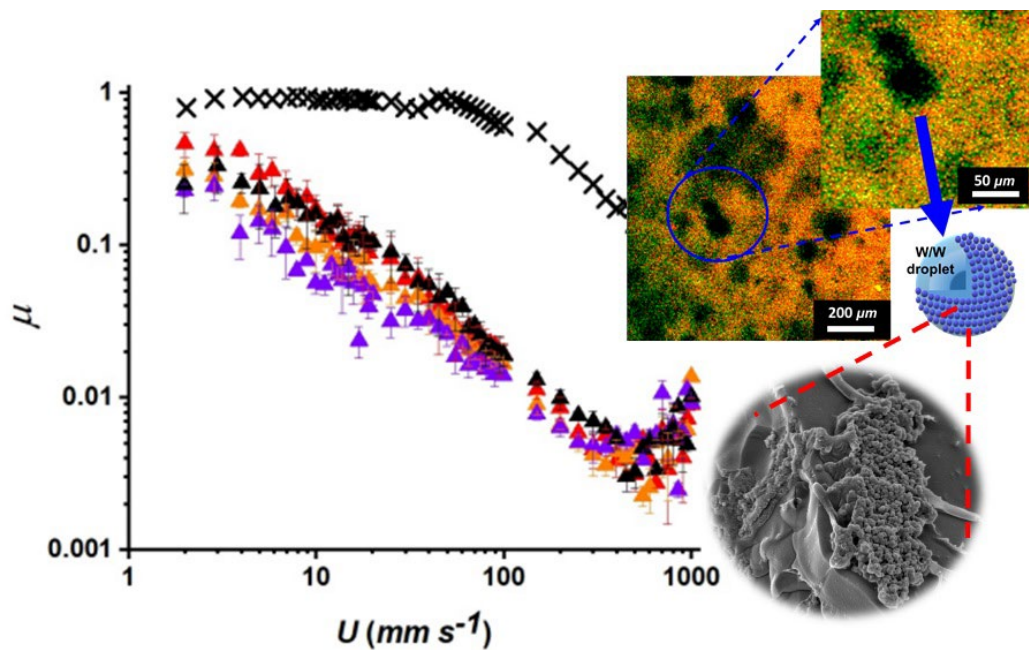


## Abstract

The aim of this study was to investigate the tribological performance of water-in-water (W/W) emulsion droplets with or without stabilization by proteinaceous microgel particles. The W/W emulsions were prepared from mixtures of gelatinized corn starch (GS) and $\kappa$-carrageenan ($\kappa$C) in the two-phase regime and when particle-stabilized whey protein microgel particles (WPM) were used. The W/W emulsions were shear thinning liquids, with

viscosity values being higher than the corresponding weight average values of the individual equilibrium phases at all shear rates. Tribological results revealed that the frictional properties of W/W emulsions formed from 1.0 wt% GS + 0.1 w% $\kappa$C were dominated by the $\kappa$C properties alone in the mixed and hydrodynamic regimes, even though the starch played an essential role in decreasing friction coefficient ($\mu$) in the boundary regime. Unlike the corresponding solutions of GS and $\kappa$C, W/W emulsions containing higher concentrations of the biopolymers (3.0 wt% starch + 0.3 wt% $\kappa$C) decreased $\mu$ in the mixed and boundary regimes, probably due to water droplets becoming entrained and forming a hydration film in the contact region. In the case of W/W emulsions containing WPM, confocal and cryo-scanning electron microscopy confirmed the presence of WPM at the interface and hence a Pickering-like stabilization. The WPM-stabilized W/W emulsions showed much higher apparent viscosity (than those without WPM) and lower $\mu$ in the boundary and mixed regimes. Stabilization of W/W emulsions via microgel particles therefore seems to be a useful tool to improve the lubrication performance of such systems.

## 4.1. Introduction

Water-in-water (W/W) emulsions are thermodynamically incompatible dispersions of two biopolymers (Esquena, 2016, Hazt et al., 2020, Vis et al., 2015a, Nicolai and Murray, 2017). Such emulsions demonstrate phase separation, producing water droplets much richer in one biopolymer dispersed in a continuous phase much richer in the other biopolymer. The degree and rate of phase separation are associated with the molecular weight of the biopolymers and any charge interaction between the polymer segments. (Grinberg and Tolstoguzov, 1997, Nicolai and Murray, 2017). Since W/W emulsions evolve from a 'mixed' solution, they start off, at least in the early stages of their formation, with a much larger interfacial area compared to that of oil-in-water (O/W) or water-in-oil (W/O) emulsion systems formed by mechanical dispersion of one immiscible phase into the other. Furthermore, the interfacial tensions of W/W emulsions (*e.g.*, $< 10^{-2}$ mM m$^{-1}$) are orders of magnitude smaller than those of O/W emulsions (*e.g.*, 30 mM m$^{-1}$) (Ding et al., 2002, Scholten et al., 2004, Vis et al., 2015c, Vis et al., 2015b). Recently, there has been increasing interest in using surface active particles to stabilize W/W emulsions (Esquena, 2016). A wide range of proteinaceous microgel particles, for example, using $\beta$-lactoglobulin, whey protein isolate (WPI), bovine serum albumin (BSA) and gelatin,

have been used (Hazt et al., 2020, Murray and Phisarnchananan, 2014, Murray and Phisarnchananan, 2016, Beldengrun et al., 2018, Zhang et al., 2021a, Machado et al., 2022)

Although the design principles and formulation strategies of W/W emulsions have been well-researched (Murray and Ettelaie, 2020, Esquena, 2016), the interaction of W/W emulsions with bodily fluids has attracted little attention to date. In particular, very little is known about the oral behaviour of W/W emulsions, which is crucial if such emulsions are to be used in food applications. Oral processing involves a dynamic range of deformation in a relatively short span of time that can be assessed using rheological and tribological analysis to understand the bulk and surface effects, respectively (Chen and Stokes, 2012, Sarkar et al., 2019b). There is now a consensus that the bulk effects dominate oral processing in the early stages - affecting sensory perception such as thickness - whereas surface-driven tribological effects dominate the oral processing in the later stages – affecting smoothness, slipperiness *etc* (Stokes et al., 2013, Sarkar and Krop, 2019b). Many previous studies have shown the difference in the bulk rheological behaviour of W/W emulsions compared with that of the individual constituent biopolymer solutions (Firoozmand et al., 2007, Semenova and Dickinson, 2010, Vis et al., 2015a).

In terms of tribology, there has been significant progress in the frictional analysis of emulsions, microgels, emulsion microgels in the last decade (Sarkar et al., 2021, Upadhyay and Chen, 2019, Torres et al., 2018). Upadhyay and Chen (2019) demonstrated that oil volume fraction and droplet size in an O/W emulsion could affect smoothness perception via decreasing the friction coefficient ($\mu$). According to Torres et al. (2018), the lubrication performance of O/W emulsions is strongly dependent on the coalescence stability of the droplets and they also highlighted that emulsions stabilized by modified starch can help to reduce $\mu$ further by being responsive to α-amylase in mouth. Although there is some understanding of the tribological performance of mixtures of starch and non-starch polysaccharides (You and Sarkar, 2021, You et al., 2021a), no study has yet investigated the tribological performance of W/W emulsions that can evolve from such mixtures. Interestingly, stability of W/W emulsions can be modified by incorporating proteinaceous microgel particles, which pin to the interface via the Pickering mechanism despite the low interfacial tension, whilst at the same time is already known that such microgels can impact the lubrication performance themselves (Sarkar et al., 2017a, Andablo-Reyes et al., 2019). It remains to be seen if the rheological and tribological properties of such W/W emulsions are dominated by the presence of stable droplets, the microgels or the induvial biopolymer solutions.

Consequently, the aim of this study was to form W/W emulsion droplets by combining solutions of gelatinized starch (GS) and $\kappa$-carrageenan ($\kappa$C) with or without whey protein microgel particles (WPM) as droplet stabilizer and to assess their rheological and tribological properties. We mapped the phase diagram and measured the shear viscosity and tribology of $\kappa$C and GS individually and also when present together as W/W emulsions with and without WPM. We hypothesize that W/W emulsions should reduce $\mu$ mostly via accretion of water droplets under the tribological stress into a hydration layer between the tribological contact surface. To our knowledge, this is the first report that investigates the frictional properties of W/W emulsion systems with and without the addition of Pickering-like microgel particles. The findings should bring new knowledge to aid the design of low calorie products without compromising their mouthfeel.

## 4.2. Material and Methods

### 4.2.1. Materials

$\kappa$-carrageenan ($\kappa$C), product code 22048 (CAS number 11114-20-8), and waxy corn starch, product code 10120 (CAS number 9037-22-3) were purchased from Sigma-Aldrich, Dorset, UK. Biopolymer solutions were made in 20 mM phosphate buffer at pH 7.0. Smooth polydimethylsiloxane materials with a surface roughness of 50 nm (PDMS, Sylgard 184, Dow Corning, USA) tribo-set (ball; $\varnothing$ 47 mm, disk; $\varnothing$ 19 mm and 4 mm thickness) were purchased from PCS Instruments, London, UK. Rhodamine B (product code R-6626) and Acridine Orange (Product code 15855) was purchased from Sigma Aldrich, Dorset, UK. Phosphate buffer was made up with water purified by a Milli-Q apparatus (Millipore, Bedford, UK), with an electrical resistivity not less than 18.2 M$\Omega$.cm.

### 4.2.2. Preparation of W/W emulsions

Gelatinised starch (GS) (0.2-6.0 wt%) was prepared by dispersing the starch powder in phosphate buffer at pH 7.0 followed by thermal treatment in an oil bath at 90 °C for 15 min with constant shearing using an Ultra Turrax T25 homogenizer (IKA-Werke GmbH &Co., Staufen Germany) to gelatinize the starch. $\kappa$-carrageenan ($\kappa$C) (0.02 to 0.6 wt%) was dispersed in phosphate buffer at pH 7.0 for at least 24 h at room temperature and then similarly dispersed

and heated at 90 °C for 15 min. Equal volumes of GS and $\kappa$C dispersions of different concentrations were mixed at 90 °C and homogenized at 21,000 rpm for 10 min via the Ultra Turrax T25 homogenizer. For Pickering W/W emulsions stabilized by microgel particles, the microgel particles (0.1-1.5 vol% in the final mixture) were added to either the GS or $\kappa$C dispersion before blending the two phases together.

## 4.2.3. Preparation of whey protein isolate microgel particles (WPM)

The WPM were prepared using the procedure described in previous reports (Andablo-Reyes et al. (2019), Sarkar et al. (2017a)). Briefly, whey protein isolate (WPI) solution was prepared by dissolving 12.0 g WPI in 88.0 g of 20 mM phosphate buffer at pH 7.0 and stirred for 2 h at room temperature to ensure complete dissolution. Crosslinking to form a WPI gel was achieved by heating the WPI solution at 90 °C for 30 minutes. After cooling to room temperature the gel was stored at 4 °C for 12 h, followed by blending for 2 minutes with 20 mM phosphate buffer, at a 1:5 w/w ratio of gel to buffer, via a hand blender (HB711M, Kenwood, UK). The subsequent dispersion of 'coarse' WPI gel fragments was degassed via a THINKY mixet (ARE-250, Kidlington, UK) using a mixing cycle of 2 min at 2,000 rpm, followed by 1 min degassing at 2,200 rpm. Finally, the dispersion was formed into a dispersion of WPM via two passes through a bespoke Jet Homogenizer (University of Leeds, UK) at $300 \pm 20$ bar. The final concentration of WPM particles in the dispersion added to the GS or $\kappa$C dispersions to form the W/W emulsions (see above) was 20.0 vol% (equivalent to 2.4 wt% protein).

## 4.2.4. Dynamic light scattering

The particle size of the WPM was measured via dynamic light scattering (DLS) using a Zetasizer (Nano ZS series, Malvern Instruments, Worcestershire, UK). A sample of the WPM dispersion was diluted with 20 mM phosphate buffer solution at a 1 : 50 v/v ratio of WPM to buffer and placed in a disposable plastic cuvette (ZEN 0040). Measurements were performed by time-dependent correlation functions, using a detection angle of 173°, and refractive indices of 1.54 and 1.33 for WPM and buffer, respectively. The absorbance of the WPM particles was assumed to be 0.001.

### 4.2.5. Apparent viscosity

Rheological characterization of the biopolymer solutions and W/W emulsions was performed via a model MCR 302 (Anton Paar, Austria) shear rheometer, using cone-and-plate geometry (CP50-2, cone diameter 50 mm, cone angle 2 °, 1 mm gap) at shear rates ranging from 0.1 to 1000 s$^{-1}$ All the experiments were carried out within 2 h of W/W emulsion formation, during which time no visible phase separation of the emulsions occurred. For each measurement, 2 mL of sample were pipetted onto the plate and a temperature-controlled cover was used to prevent evaporation and maintain the temperature at 37 ± 0.1 °C, in order to mimic oral processing conditions. Samples were left on the plate for 2 min to achieve thermal equilibrium before rheological measurements commenced

.

### 4.2.6. Tribology

A Mini Traction Machine 2 (MTM2, PCS Instruments, London, UK) with hydrophobic polydimethylsiloxane (PDMS) ball and disc as tribopairs, was using to measure the tribological performance of the samples. All the experiments were carried out within 2 h of W/W emulsion formation. A normal load (*W*) of 2 N and a slide-to-roll ratio (*SRR*) of 50% were used for all frictional measurements. The friction coefficients were measured for all samples as a function of entrainment speed (*U*); sliding speeds were varied from 1 to 1000 mm s$^{-1}$. The temperature was controlled at 37 ± 1 °C. The friction coefficients are reported below as the mean and standard deviation of at least three measurements carried out on triplicate samples prepared on different days.

### 4.2.7. Phase diagram via imaging of the W/W emulsions

Freshly prepared W/W emulsions were stored at 25 °C in flat bottom test tubes sealed with a plastic cap and photographed periodically to establish the 1 or 2 phase regions of the phase diagram as a function of composition.

### 4.2.8. Microscopy

Optical microscopy (Nikon, SMZ-2T, Japan) was used to observe the microstructure of the W/W emulsions with different concentrations of GS and $\kappa$C with 40x magnification lens. A confocal laser scanning microscope (CLSM, Model LSM 880, Carl Zeiss MicroImaging GmbH, Jena, Germany) was also used to observe the W/W emulsions, after mixing with 0.5

w% Acridine Orange (AO) and 0.5 wt% Rhodamine Blue (RB), excited at 502 nm and 546 nm, respectively to fluorescently label WPM and GS. Samples were excited using a He/Ne (543, 633 nm) laser source. A 20× objective with numeral aperture of 0.5 was used to capture all images at 1024 × 1024 pixel resolution.

Cryogenic scanning electron microscopy (cryo-SEM) of the W/W emulsions was also conducted. The samples were mounted on rivets attached to the sample stub. The samples were plunge-frozen in liquid nitrogen "slush" at −180 °C, then transferred to the cryo-preparation chamber on the SEM. The samples were then cleaved and etched at −95 °C for 4 min, followed by coating with 5 nm of platinum (Pt). Finally, the Pt-coated samples were transferred to the SEM chamber for imaging at −135 °C.

## 4.2.9. Statistical analysis

All experimental results are presented the mean and standard deviation of at least three measurements on triplicate samples (n = 3 × 3). Statistical analyses were carried out for tribological data at boundary regimes (5-10 m s$^{-1}$), mixed regimes (100-150m s$^{-1}$) and hydrodynamic regimes (700-900 m s$^{-1}$) using one-way ANOVA and multiple comparison test via SPSS software and differences between samples were deemed acceptable when $p < 0.05$ via Tukey's test.

## 4.3. Results and Discussion

## 4.3.1. Phase diagram

Published phase diagrams in literature appear to vary, even using the same biopolymers, due to the wide range of conformation of macromolecules from different sources, batches, *etc.* (Capron et al., 2001). The phase diagram for our samples of GS and $\kappa$C is shown in **Figure 4.1**. After three months of quiescent storage under normal gravity, phase separation was confirmed with the formation of an opaque lower (GS-rich) phase and a more clear upper ($\kappa$C-rich) phase, similar to that determined previously by Murray and Phisarnchananan (2014) for GS-locust bean gum and GS-guar gum systems. Further measurements (not shown) for longer times showed that phase separation was still not entirely complete for those systems where two phases were already visible after storage for three months. The rate of phase separation was

slower at higher concentrations of $\kappa$C and/or GS, as expected due to the increased viscosity of the $\kappa$C and GS phases, which is discussed later.
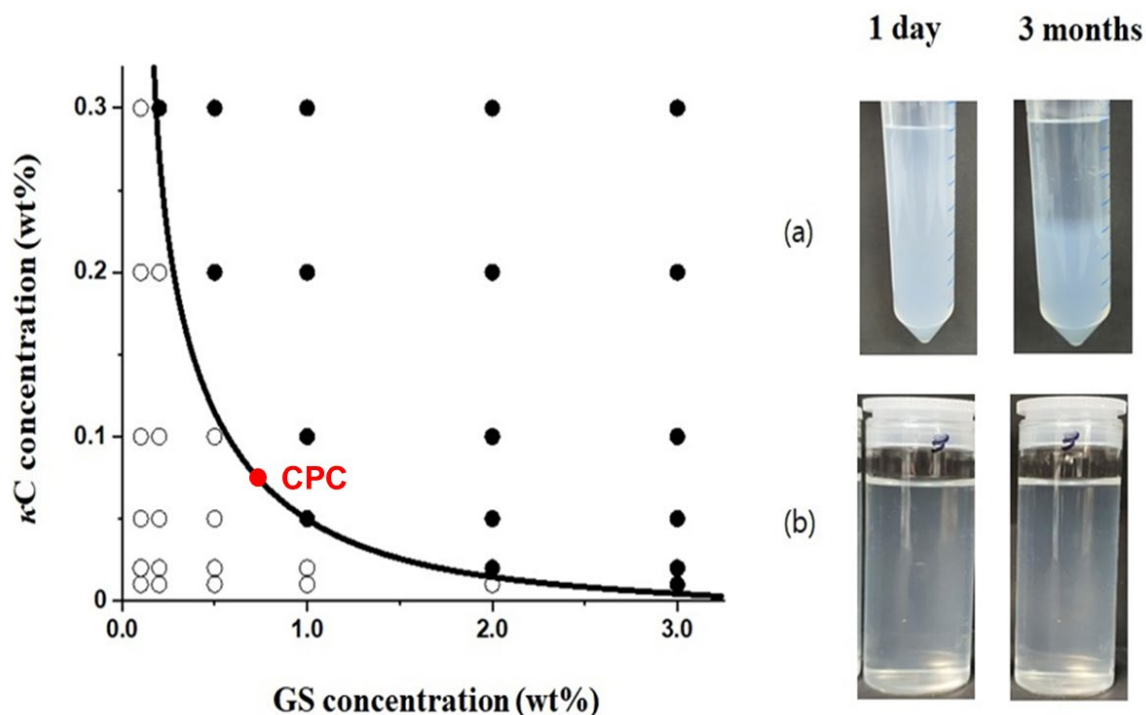


**Figure 4.1.** Phase diagram showing the estimated binodal (—) single-phase (○) and biphasic (●) mixtures of gelatinized waxy corn starch (S) and κ-carrageenan ($\kappa$C) with visual images of (a) 2.0 wt% GS + 0.2 wt% $\kappa$C, and (b); 0.25 wt% GS + 0.5 wt% $\kappa$C immediately and after a storage period of 3 months.

It can be seen that the binodal line lies close to GS concentration axis and very close to the $\kappa$C concentration axis at low GS but higher $\kappa$C (**Figure 4.1**). At higher concentrations of GS (1.0, 2.0 and 3.0 wt.%), the mixtures were all biphasic at $\kappa$C concentrations up to the lowest concentration studied (0.05 wt %). The critical polymer concentration (CPC) in which phase separation could be observed at the 50:50 wt% line was 0.75:0.075 (GS: $\kappa$C). Below this value, there was no visible macroscopic difference in turbidity of the mixtures in the tubes, and so it was assumed that no phase separation occurred (*i.e.*, one phase, no W/W emulsions formed). Note that, immediately (< 15 min) after their formation, all the mixtures appeared homogeneous by visual observation.
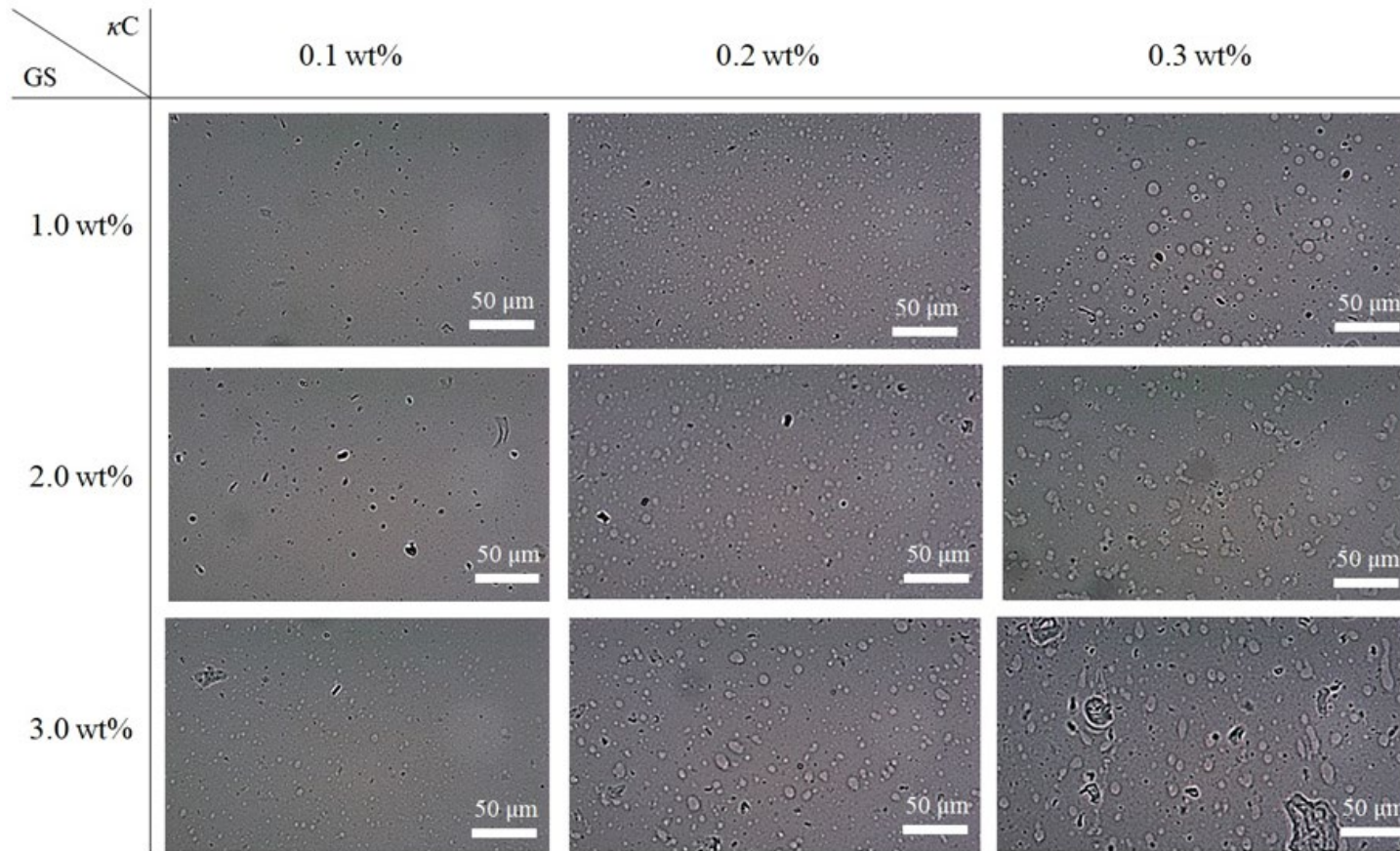
**Figure 4.2.** Optical micrographs of water droplets inside GS + κC phase separating W/W emulsions prepared with different concentrations of GS (1.0 to 3.0 wt%) and κC (0.1 to 0.3 wt%).

## 4.3.2. W/W emulsion microstructure without and with WPM

Above the CPC after 15 min, W/W droplets could be observed via optical microscopy in the 1.0 wt% GS + 0.1 wt% $\kappa$C system, with different sizes and shapes of water droplets (**Figure 4.2**). The concentration of GS appeared to affect the size of the droplets, with the smallest droplets visible in the 1.0 wt% GS + 0.1 wt% $\kappa$C system and the droplets becoming larger with increasing concentration of GS. Interestingly, $\kappa$C seemed to affect the shape of the W/W droplets. At lower $\kappa$C concentrations (0.1 wt%), the water droplets were more spherical, whilst they appeared to be oval-shaped at higher concentrations (e.g., 0.3 wt% $\kappa$C + 3.0 wt% GS). It is possible to control W/W droplet size by modulating the shear rate (Stokes et al., 2001) during phase separation. For example, Stokes et al. (2001) showed 7 μm droplets at a shear rate between two parallel plates of 100 s$^{-1}$ but 30 μm at shear rates of 10 s$^{-1}$ . Differences in shape affect the W/W interfacial area and, therefore the overall free energy of the system, spheres minimizing this, of course. The final morphology is dependent on temperature, molecular ordering and the relative phase volume of the equilibrium phases (Shewan and Stokes, 2013, Esquena, 2016) and consequently, many different W/W droplet structures are inherently unstable. Butler and Heppenstall-Butler (2003) demonstrated bicontinuous structures in biopolymer mixtures whilst decreasing the temperature accelerated spinodal decomposition. Non-spherical structures can also be kinetically trapped by crosslinking the dispersed phase (Shewan and Stokes, 2013). In summary, a wide range of shapes can be expected (spheres, ellipsoids, rods, and fibrils), depending on the exact combination of polymer samples, conditions of phase separation and whether or not there is any material that can preferentially adsorb at the W–W interface (Wolf et al., 2000, Turgeon et al., 2007, Murray and Phisarnchananan, 2016).

**(a)**

**(b)**



**(d)**

**(c)**
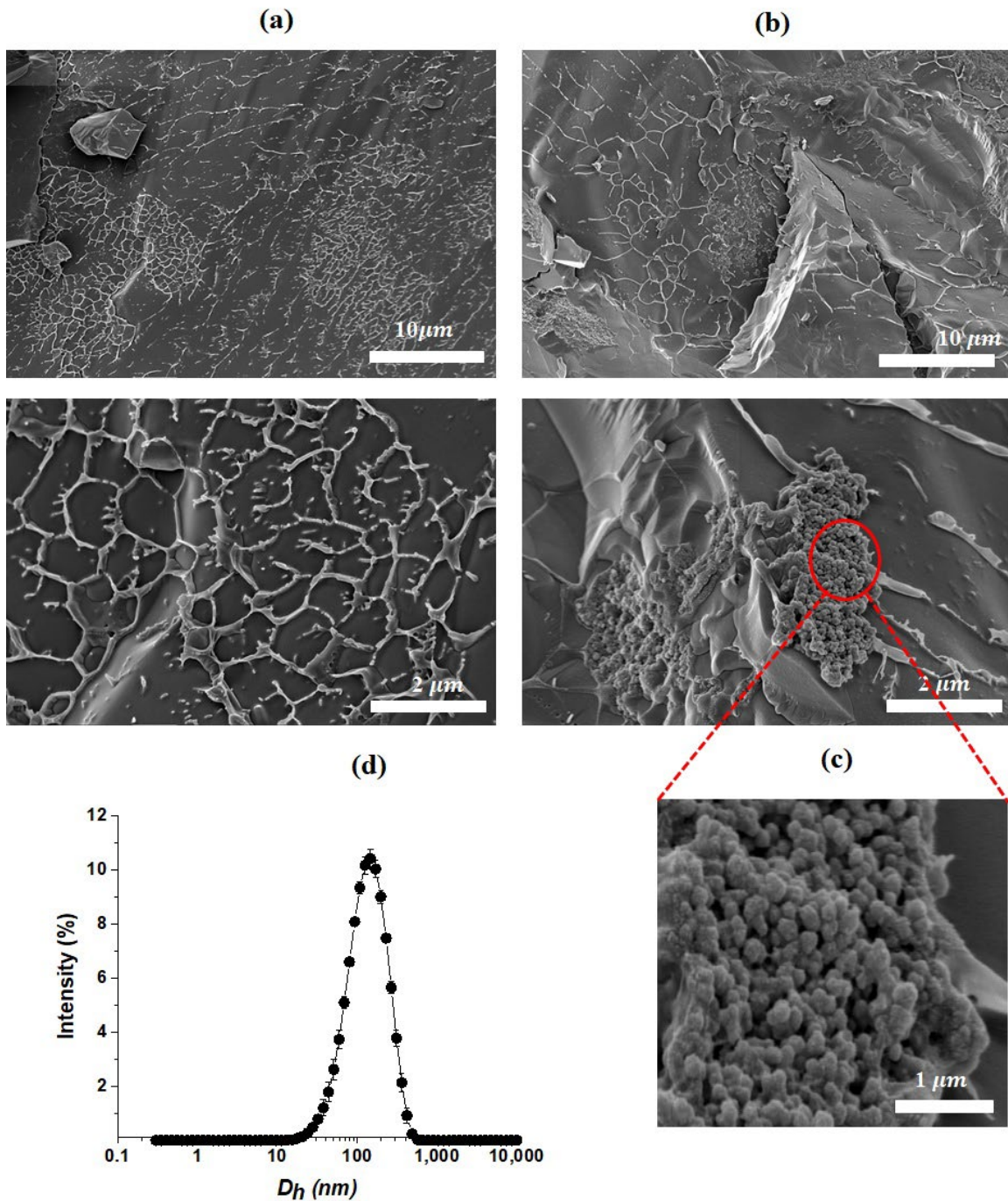


**Figure 4.3.** Cryo-SEM images of 3.0 wt% GS + 0.3 wt% κC W/W emulsions (a) in the absence of whey protein microgel particles (WPM) and (b) in the presence of WPM, with top image showing 20,000× magnification (scale bar = 10 μm) and bottom image showing 50,000× magnification (scale bar = 2 μm). Zoomed image of the interface containing WPM (c), and hydrodynamic size (d) of WPM particles measured using dynamic light scattering.

Cryogenic scanning electron microscopy (Cryo-SEM) observations at lower length scales (**Figure 4.3**) show separation of the samples into polyhedral aqueous regions, which may therefore be the water droplets that have become distorted during the preparation.    In the presence of WPM (**Figures 4.3b** and **c**), and in particular in the zoomed in region of **Figure 4.3c**, there appear to be particles at the interstices of the polyhedral regions. **Figure 4.3d** shows the particle size distribution of the WPM particles alone, measured via DLS, that shows a strong peak at a hydrodynamic diameter ($d_H$) = 115 ± 3 nm.    This size seems to correspond well to the interstitial particles, although clearly they might be quite aggregated (**Figure 4.3c**), but suggests that a major fraction of the WPM do collect at the W−W interface.    To our knowledge, limited study has shown cryo-SEM evidence of WPM at the interface of W/W emulsion droplets, although, many cryo-SEM studies have shown WPM at the oil-water interface of oil-in-water (O/W) emulsions (Sarkar et al., 2017a, Destribats et al., 2014).    In these studies, similar kind of interfacial aggregation of WPM is observed as in **Figure 4.3c**.

**(a)**                                                    **(b)**
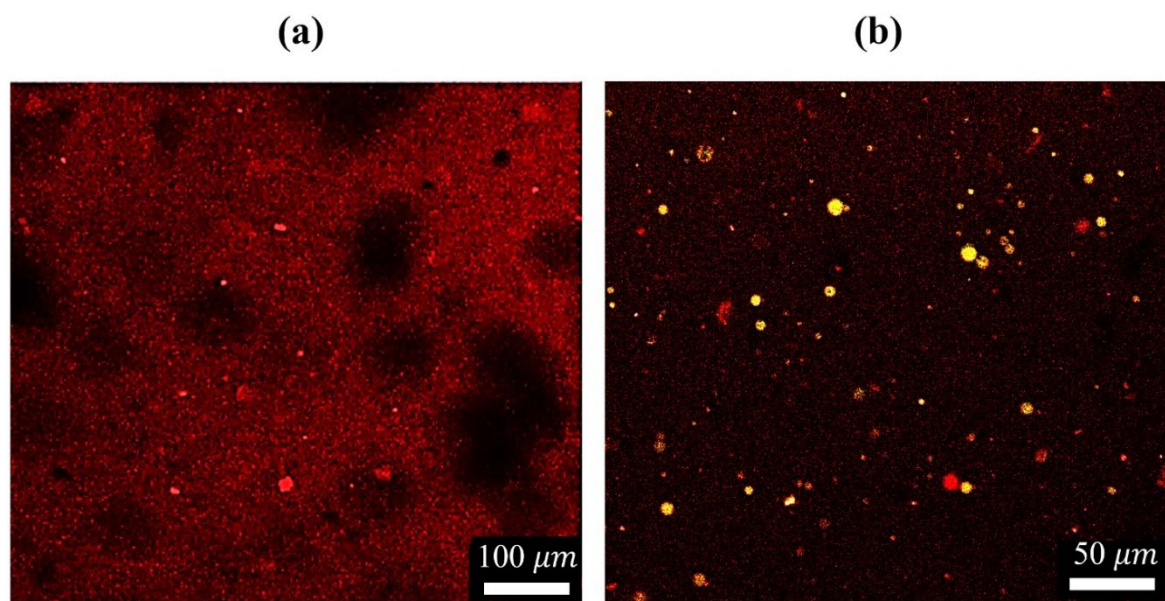


**Figure 4.4.** Confocal micrographs of the 3 wt% GS + 0.3 wt% κC W/W emulsion (a) in the absence and (b) in the presence of whey protein microgel (WPM). GS and WPM are fluorescently labelled by Rhodamine B ($\lambda \approx 546$ nm) and Acridine Orange ($\lambda \approx 502$ nm), respectively.

CLSM micrographs of the W/W emulsions are shown in **Figures 4,4a** and **4,4b**. In **Figure 4.4a**, in the absence of the WPM, coalescence of droplets (the darker, unstained regions) is suggested. In **Figure 4.4b**, in the presence of WPM, stained with Acridine Orange (AO), numerous spherical objects can be observed, much smaller than the dark aqueous regions in

**Figure 4.4a** (where no WPM is present). These spherical regions in **Figure 4.4b** are uniformly stained with AO, suggesting that they are W/W droplets coated in WPM, again demonstrating the ability of WPM to act as the Pickering-like particles necessary for stabilizing W/W emulsion systems (Esquena, 2016, Beldengrun et al., 2018, Vis et al., 2015a, Hazt et al., 2020). There are many studies that have discussed how the pH can be tuned to induce protein microgel particles to adsorb at the W–W interface more effectively and reduce the size of the discontinuous phase regions in W/W systems (Hazt et al., 2020, de Freitas et al., 2016). However, the objective of our study was to understand the behaviour under oral processing conditions, hence the pH was kept at 7.0 and pH variations were not pursued further.

### 4.3.3. Rheological and tribological characteristics

### 4.3.3.1.        W/W emulsions without WPM

  **Figures 4a** and **4b** show apparent viscosity ($\eta$) of the W/W emulsions prepared using lower (1.0 wt% GS + 0.1 wt% $\kappa$C) and higher (3.0 wt% GS + 0.3 wt% $\kappa$C) biopolymer concentrations, respectively, alongside controls of same concentrations of GS and $\kappa$C alone. These emulsions were prepared without WPM. Rheologically speaking, the W/W emulsions, regardless of concentration, were different to either $\kappa$C or GS, and have non-Newtonian behaviour, with shear-thinning properties. The dashed lines in **Figures 4a** and **4b** are the calculated weighted averages of the individual equilibrium phases (GS and $\kappa$C) and are dominated by the GS, since the concentration of GS is 10 x higher than that of $\kappa$C. Particularly for the lower biopolymer concentrations, $\eta$ for the emulsions was significantly higher than these average values at the corresponding shear rates. At the higher biopolymer concentrations (3.0 wt% GS + 0.3 wt% $\kappa$C), there was some convergence at the lowest shear rate measured (1 s$^{-1}$). Apart from the $\kappa$C solutions alone (0.1 or 0.3 wt%), all systems were also significantly shear thinning. There are many studies that show that the viscosity of biopolymer mixtures including $\kappa$C tends to be higher than that of $\kappa$C alone (Fakharian et al., 2015; Lafargue et al., 2007; Huc et al., 2014) as in our case. This is usually explained by some sort of attractive interaction between GS and $\kappa$C (for example via hydrogen bonding between the hydroxyl groups on the polysaccharides). In the case of the emulsions without WPM, as seen in **Figure 4a**, there appeared to be coalescence of the droplets (presumably preceded by aggregation), which might also contribute to enhanced viscosity of the emulsions compared to the individual biopolymers. In addition, any increasing

volume fraction of dispersed phase will increase the viscosity of the continuous phase. In these systems it is hard to estimate what this volume fraction might be at any instant, since it evolves with time as the phase separation proceeds.
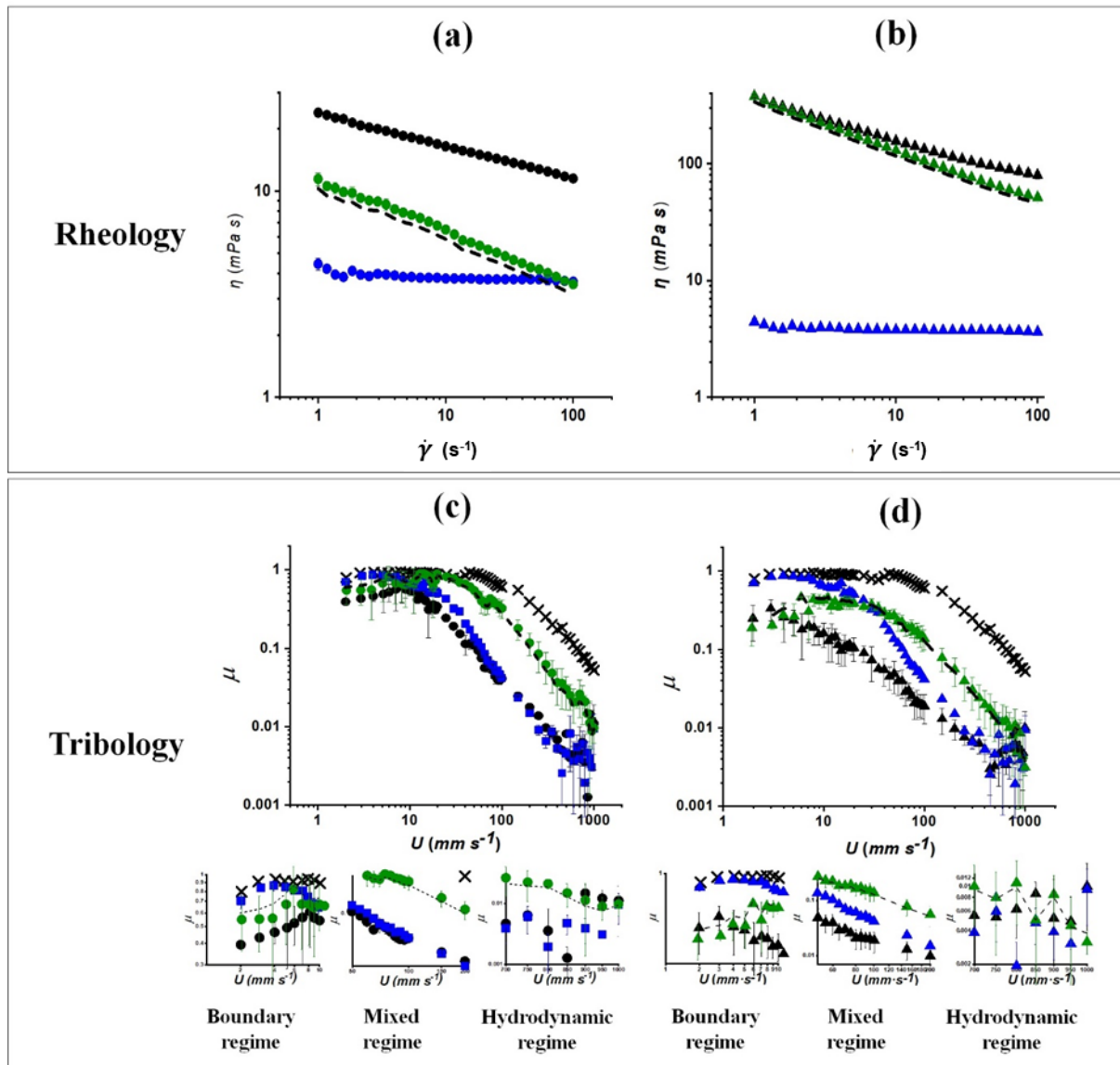


**Figure 4.5.** Mean apparent viscosity ($\eta$) as a function of shear rate ($\dot{\gamma}$) (a, b) and mean friction coefficient ($\mu$) versus entrainment speed ($U$) (c, d) of W/W emulsions without the addition of WPM; (a and c) 1.0 wt% GS (●), 0.1 wt% $\kappa$C (●), and (b and d) 3.0 wt% S (▲), 0.3 wt% $\kappa$C (▲), and W/W emulsions (●; 1.0 wt% GS + 0.1 wt% $\kappa$C, ▲; 3.0 wt% GS + 0.3 wt% $\kappa$C). The weight average values of the corresponding individual controls for the mixtures are also shown (--), and phosphate buffer is used as a control (×). Error bars represent standard deviations. The images in the bottom show the zoomed version of (c) and (d) each lubrication regime.

In the case of tribology data, **Figures 4.5c** and **4.5d** illustrate the friction coefficient ($\mu$) as a function of entrainment speed ($U$) of the W/W emulsions with lower and higher biopolymer concentrations, respectively, whilst the corresponding controls for the GC and $\kappa$C alone are also shown, along with that of the phosphate buffer.

The buffer shows boundary and mixed lubrication regimes but no hydrodynamic regime until $U \approx 1000$ mm s$^{-1}$. The boundary regime is maintained at $\mu \approx 1.0$, and then a decrease in $\mu$ is observed as a function of increasing $U$. Such a prolonged boundary regime with phosphate buffer has been observed previously as phosphate buffer is squeezed out of the hydrophobic PDMS-PDMS contact zone (Sarkar et al., 2017a, You et al., 2021a).

The tribological behaviour of the W/W emulsion at the lower biopolymer concentrations (1.0 wt% GS + 0.1 wt% $\kappa$C) was similar to that reported previously by You et al. (2021a), where either $\kappa$C or GS dominates in the different regimes. In boundary regime, GS dominates whilst in the mixed and hydrodynamic regimes, the W/W emulsion behaviour increasingly seems to follow the signature of the $\kappa$C alone. At the higher concentrations (3.0 wt% GS + 0.3 wt% $\kappa$C) in boundary and mixed regimes the W/W emulsion had a lower $\mu$ than the corresponding GS and $\kappa$C solutions alone (**Figure 4.5d**). We explain this as due to the water droplets becoming entrained and forming a hydration film in the contact region. As noted earlier (**Figure 4.2**), the water droplets appear to have different sizes, morphologies and also volume fractions, depending on the biopolymer concentrations. The higher concentrations seem to give more droplets, larger droplets and droplets with more non-spherical shapes, whereas the lower concentrations seem to give fewer droplets, smaller droplets but droplets with more spherical shapes.
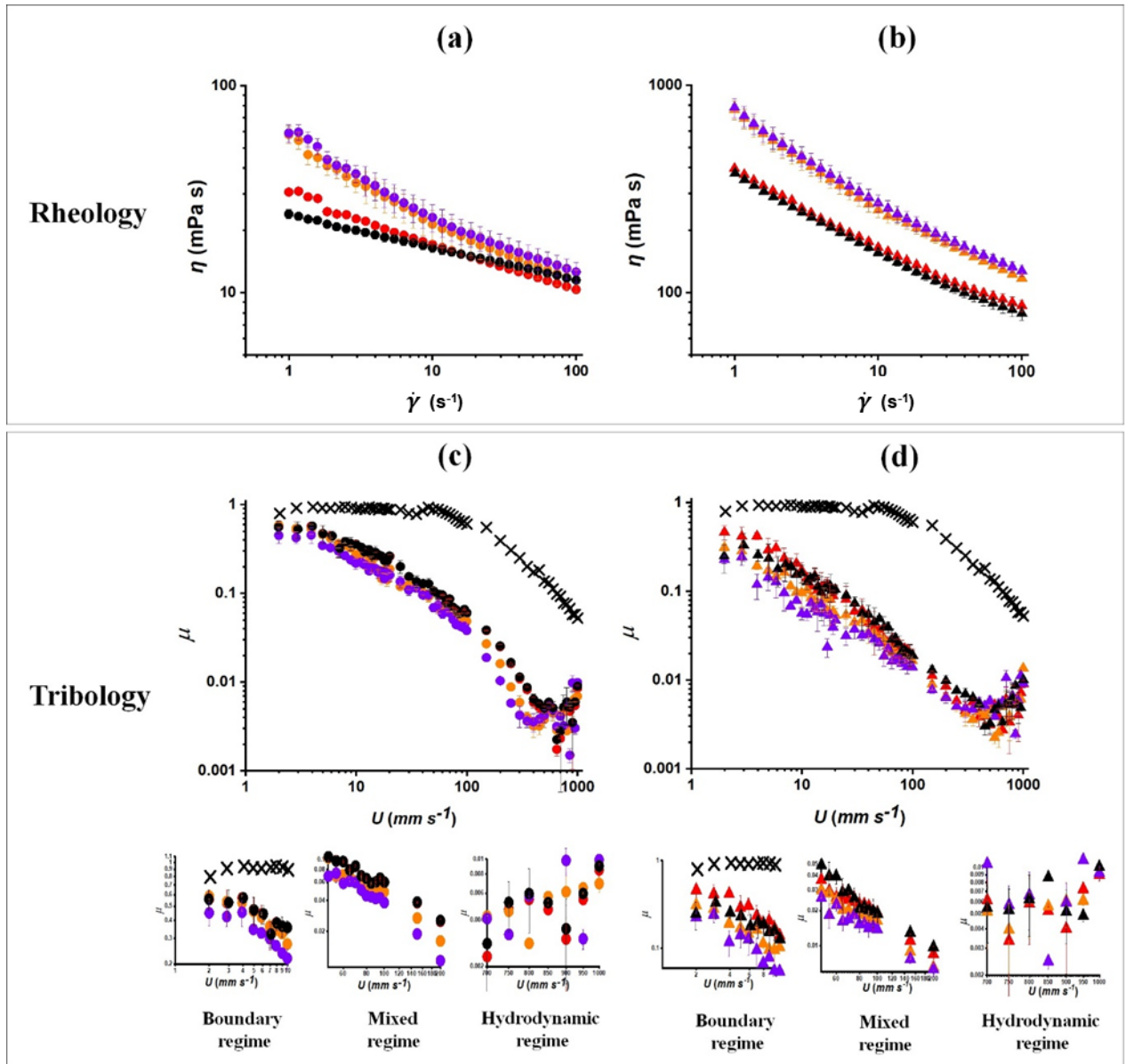
**Figure 4.6.** Apparent viscosity ($\eta$) as a function of shear rate ($\dot{\gamma}$) (a, b) and friction coefficient ($\mu$) versus entrainment speed ($U$) (c, d) of W/W emulsions with the addition of WPM; at (a and c) lower biopolymer concentrations (1.0 wt% GS and 0.1 wt% $\kappa$C, ●) and (b and d) higher biopolymer concentrations (3.0 wt% GS and 0.3 wt% $\kappa$C, ▲) with different concentration of WPM; 0.5 vol% (●, ▲), 1.5 vol% (●, ▲), and 3.0 vol% (●, ▲). Phosphate buffer is used as a control (×). Error bars represent standard deviations. The images in the bottom show the zoomed version of (c) and (d) each lubrication regime.

## 4.3.3.2.　　　W/W emulsions with WPM

WPM was observed using cryo-SEM and confocal microscopy at the interface of the two phases (**Figures 4.3b** and **4,4b**). The WPM adsorbed the interface could affect the structure of emulsion system, by increasing the viscosity (Sarkar et al., 2017a, Destribats et al., 2014, Zhu et al., 2019).

In the case of Pickering W/W emulsions, *i.e.*, those W/W systems with added WPM, **Figures 4.6a** and **4.6b** show their bulk rheological behaviour. A significant increase in $\eta$ was observed on addition of WPM at 1.5 and 3.0 vol%, the increases being rather similar, whereas addition at 0.5 vol% WPM did not have a significant effect on $\eta$. Similar effects were observed at both the higher and lower biopolymer concentrations, although all the viscosities were much higher in the latter.

The presence of WPM affected the tribological results significantly (See **Figures.4.6c, 4.6d** and **Table 4.1**). At the lower biopolymer concentrations (**Figure 4.6c**), by increasing WPM from 0.5 to 3.0 vol%, $\mu$ decreased in the mixed and hydrodynamic regimes ($p < 0.05$) whilst at the higher biopolymer concentrations (**Figure 4.6d**) the emulsions showed a similar trend. Irrespective of the biopolymer concentrations, $\mu < 0.05$ in the mixed regimes in presence of W/W emulsions containing 1.5-3.0 vol% WPM (**Table 4.1**). This might be expected, given the increase in bulk viscosity on addition of WPM (see above), so improving the fluid film lubrication behaviour (Andablo-Reyes et al., 2019). However, another possibility is that the WPM-coated W/W emulsion droplets were stable and rolled into the contact zone effectively as compared to the droplets without WPM (**Table 4.1**). Interestingly, $\mu$ increased in the boundary regime on adding 0.5 vol% WPM (**Table 4.1**). Sarkar et al. (2017a) also showed that low volume fractions of WPM give relatively poor lubrication properties because the WPM particles could not sufficiently replenish the contact region with particles and overcome the adhesion of PDMS-PDMS surfaces. Thus, the presence of WPM improved the stability of droplets but did not show a decrease in boundary lubrication property at low volume fractions. We suppose that: (i) there was not a high enough volume fraction of WPM particles to lower $\mu$ in the boundary regime, and (ii) the pressure in the contact region between the PDMS tribopairs was high enough to exclude such low volume fraction of WPM as well as WPM-coated droplets from the interface.

**Table 4.1**. Means and standard deviations (SDs) of friction coefficient the W/W emulsions in the absence of WPM; 1.0 wt% GS + 0.1 wt% κC and 3.0 wt% GS and 0.3 wt% κC, and presence of 0.5 to 3.0 vol% WPM in each boundary, mixed, and hydrodynamic regimes. Different lower case letters in the same column indicate a statistically significant difference ($p < 0.05$).

| (a) | Friction coefficient of 1.0 wt% GS + 0.1 wt% *κ*C emulsions without or with WPM | | | | | |
|---|---|---|---|---|---|---|
| | Boundary lubrication regime (5-10 mm s$^{-1}$) | | Mixed lubrication regime (100-150 mm s$^{-1}$) | | Hydrodynamic lubrication regime (700-900 mm s$^{-1}$) | |
| | Mean | SD | Mean | SD | Mean | SD |
| no added WPM | 0.550[a] | 0.0373 | 0.049[a] | 0.0083 | 0.0085[a] | 0.0018 |
| 0.5 vol% WPM | 0.390[a] | 0.0513 | 0.048[b] | 0.0109 | 0.0059[b] | 0.0018 |
| 1.5 vol% WPM | 0.365[ab] | 0.0617 | 0.038[c] | 0.0108 | 0.0056[c] | 0.0015 |
| 3.0 vol% WPM | 0.283[ac] | 0.0459 | 0.029[d] | 0.0096 | 0.0060[d] | 0.0034 |
| (b) | Friction coefficient of 3.0 wt% GS + 0.3 wt% *κ*C emulsions without or with WPM | | | | | |
| | Boundary lubrication regime (5-10 mm s$^{-1}$) | | Mixed lubrication regime (100-150 mm s$^{-1}$) | | Hydrodynamic lubrication regime (700-900 mm s$^{-1}$) | |
| | Mean | SD | Mean | SD | Mean | SD |
| no added WPM | 0.178[a] | 0.0320 | 0.016[a] | 0.0029 | 0.0070[a] | 0.0020 |
| 0.5 vol% WPM | 0.235[b] | 0.0493 | 0.015[b] | 0.0041 | 0.0063[b] | 0.0017 |
| 1.5 vol% WPM | 0.132[c] | 0.0306 | 0.013[c] | 0.0037 | 0.0075[c] | 0.0031 |
| 3.0 vol% WPM | 0.095[d] | 0.0313 | 0.011[d] | 0.0031 | 0.0071[d] | 0.0030 |

## 4.4. Conclusions

In this study, we demonstrated for the first time the tribological properties of W/W emulsions formed from mixtures of GS and $\kappa$C with or without WPM. Different sizes and shapes of the droplet were observed in different parts of the two-phase region of the phase diagram, using microscopy across various length scales. The W/W emulsions were shear thinning liquids, with viscosity values being much higher than the corresponding weight average of the values of the individual components. The morphology of water droplets appeared to affect the rheological and tribological performance. In the case of Pickering-like W/W emulsion droplets, with WPM acting as the stabilizing particles, the apparent bulk viscosity of was significantly higher than that of the corresponding mixtures in the absence of WPM. Interestingly, although there was no dramatic change in boundary lubrication performance with WPM, they appeared to produce a lowering friction coefficient in the mixed regimes at higher volume fractions of WPM.

Although particles may provide ultra-stability to water-in-water (W/W) emulsion formed in phase-separating polymer systems, we still need to understand how the microgel particles at W-W interface influence lubrication behaviour. Therefore, **Chapter-5** investigated parallel systems of W/W emulsions prepared using starch and xanthan gum stabilised by WPM as well as plant-based pea protein microgel particles (PPM), with different physico-chemical and material characteristics which could affect the lubrication performance of water droplets.

## References

ANDABLO-REYES, E., YERANI, D., FU, M., LIAMAS, E., CONNELL, S., TORRES, O. & SARKAR, A. 2019. Microgels as viscosity modifiers influence lubrication performance of continuum. *Soft Matter,* 15**,** 9614-9624.

BELDENGRUN, Y., ARAGON, J., PRAZERES, S. F., MONTALVO, G., MIRAS, J. & ESQUENA, J. 2018. Gelatin/maltodextrin water-in-water (w/w) emulsions for the preparation of cross-linked enzyme-loaded microgels. *Langmuir,* 34**,** 9731-9743.

BUTLER, M. F. & HEPPENSTALL-BUTLER, M. 2003. Phase separation in gelatin/dextran and gelatin/maltodextrin mixtures. *Food Hydrocolloids,* 17**,** 815-830.

CAPRON, I., COSTEUX, S. & DJABOUROV, M. 2001. Water in water emulsions: phase separation and rheology of biopolymer solutions. *Rheologica Acta,* 40**,** 441-456.

CHEN, J. & STOKES, J. R. 2012. Rheology and tribology: Two distinctive regimes of food texture sensation. *Trends in Food Science & Technology,* 25**,** 4-12.

DE FREITAS, R. A., NICOLAI, T., CHASSENIEUX, C. & BENYAHIA, L. 2016. Stabilization of water-in-water emulsions by polysaccharide-coated protein particles. *Langmuir,* 32**,** 1227-1232.

DESTRIBATS, M., ROUVET, M., GEHIN-DELVAL, C., SCHMITT, C. & BINKS, B. P. 2014. Emulsions stabilised by whey protein microgel particles: towards food-grade Pickering emulsions. *Soft matter,* 10**,** 6941-6954.

DING, P., WOLF, B., FRITH, W., CLARK, A., NORTON, I. & PACEK, A. 2002. Interfacial tension in phase-separated gelatin/dextran aqueous mixtures. *Journal of colloid and interface science,* 253**,** 367-376.

ESQUENA, J. 2016. Water-in-water (W/W) emulsions. *Current Opinion in Colloid & Interface Science,* 25**,** 109-119.

FIROOZMAND, H., MURRAY, B. S. & DICKINSON, E. 2007. Fractal-type particle gel formed from gelatin+ starch solution. *Langmuir,* 23**,** 4646-4650.

GRINBERG, V. Y. & TOLSTOGUZOV, V. 1997. Thermodynamic incompatibility of proteins and polysaccharides in solutions. *Food Hydrocolloids,* 11**,** 145-158.

HAZT, B., BASSANI, H. P., ELIAS-MACHADO, J. P., BUZZO, J. L. A., SILVEIRA, J. L. & DE FREITAS, R. A. 2020. Effect of pH and protein particle shape on the stability of amylopectin–xyloglucan water-in-water emulsions. *Food Hydrocolloids,* 104**,** 105769.

MACHADO, J. P., CAPRON, I., DE FREITAS, R. A., BENYAHIA, L. & NICOLAI, T. 2022. Stabilization of amylopectin-pullulan water in water emulsions by Interacting protein particles. *Food Hydrocolloids,* 124**,** 107320.

MURRAY, B. & ETTELAIE, R. 2020. Bijel Systems Based on the Phase Separation of Biological Macromolecules. *Bijels.*

MURRAY, B. S. & PHISARNCHANANAN, N. 2014. The effect of nanoparticles on the phase separation of waxy corn starch+ locust bean gum or guar gum. *Food Hydrocolloids,* 42**,** 92-99.

MURRAY, B. S. & PHISARNCHANANAN, N. 2016. Whey protein microgel particles as stabilizers of waxy corn starch+ locust bean gum water-in-water emulsions. *Food Hydrocolloids,* 56**,** 161-169.

NICOLAI, T. & MURRAY, B. 2017. Particle stabilized water in water emulsions. *Food Hydrocolloids,* 68**,** 157-163.

SARKAR, A., ANDABLO-REYES, E., BRYANT, M., DOWSON, D. & NEVILLE, A. 2019. Lubrication of soft oral surfaces. *Current Opinion in Colloid & Interface Science,* 39**,** 61-75.

SARKAR, A., KANTI, F., GULOTTA, A., MURRAY, B. S. & ZHANG, S. 2017. Aqueous lubrication, structure and rheological properties of whey protein microgel particles. *Langmuir,* 33**,** 14699-14708.

SARKAR, A. & KROP, E. M. 2019. Marrying oral tribology to sensory perception: a systematic review. *Current opinion in food science.*

SARKAR, A., SOLTANAHMADI, S., CHEN, J. & STOKES, J. R. 2021. Oral tribology: Providing insight into oral processing of food colloids. *Food Hydrocolloids,* 117**,** 106635.

SCHOLTEN, E., VISSER, J. E., SAGIS, L. M. & VAN DER LINDEN, E. 2004. Ultralow interfacial tensions in an aqueous phase-separated gelatin/dextran and gelatin/gum arabic system: A comparison. *Langmuir,* 20**,** 2292-2297.

SEMENOVA, M. G. & DICKINSON, E. 2010. *Biopolymers in food colloids: Thermodynamics and molecular interactions*, CRC Press.

SHEWAN, H. M. & STOKES, J. R. 2013. Review of techniques to manufacture micro-hydrogel particles for the food industry and their applications. *Journal of Food Engineering,* 119**,** 781-792.

STOKES, J. R., BOEHM, M. W. & BAIER, S. K. 2013. Oral processing, texture and mouthfeel: From rheology to tribology and beyond. *Current Opinion in Colloid & Interface Science,* 18**,** 349-359.

STOKES, J. R., WOLF, B. & FRITH, W. 2001. Phase-separated biopolymer mixture rheology: Prediction using a viscoelastic emulsion model. *Journal of Rheology,* 45**,** 1173-1191.

TORRES, O., ANDABLO-REYES, E., MURRAY, B. S. & SARKAR, A. 2018. Emulsion microgel particles as high-performance bio-lubricants. *ACS applied materials & interfaces,* 10**,** 26893-26905.

TURGEON, S., SCHMITT, C. & SANCHEZ, C. 2007. Protein–polysaccharide complexes and coacervates. *Current Opinion in Colloid & Interface Science,* 12**,** 166-178.

UPADHYAY, R. & CHEN, J. 2019. Smoothness as a tactile percept: Correlating 'oral'tribology with sensory measurements. *Food Hydrocolloids,* 87**,** 38-47.

VIS, M., OPDAM, J., VAN'T OOR, I. S., SOLIGNO, G., VAN ROIJ, R., TROMP, R. H. & ERNë, B. H. 2015a. Water-in-water emulsions stabilized by nanoplates. *ACS Macro Letters,* 4**,** 965-968.

VIS, M., PETERS, V. F., BLOKHUIS, E. M., LEKKERKERKER, H. N., ERNÉ, B. H. & TROMP, R. H. 2015b. Effects of electric charge on the interfacial tension between coexisting aqueous mixtures of polyelectrolyte and neutral polymer. *Macromolecules,* 48**,** 7335-7345.

VIS, M., PETERS, V. F., BLOKHUIS, E. M., LEKKERKERKER, H. N., ERNë, B. H. & TROMP, R. H. 2015c. Decreased interfacial tension of demixed aqueous polymer solutions due to charge. *Physical review letters,* 115**,** 078303.

WOLF, B., SCIROCCO, R., FRITH, W. & NORTON, I. 2000. Shear-induced anisotropic microstructure in phase-separated biopolymer mixtures. *Food Hydrocolloids,* 14**,** 217-225.

YOU, K., MURRAY, B. S. & SARKAR, A. 2021. Rheology and tribology of starch+ κ-carrageenan mixtures. *Journal of texture studies,* 52**,** 16-24.

YOU, K. & SARKAR, A. 2021. Oral tribology of polysaccharides. *Handbook of Hydrocolloids.* Elsevier.

ZHANG, J., MEI, L., MA, P., LI, Y., YUAN, Y., ZENG, Q.-Z. & WANG, Q. 2021. Microgel-Stabilized Hydroxypropyl Methylcellulose and Dextran Water-in-Water Emulsion: Influence of pH, Ionic Strength, and Temperature. *Langmuir,* 37**,** 5617-5626.

ZHU, Y., BHANDARI, B. & PRAKASH, S. 2019. Tribo-rheology characteristics and microstructure of a protein solution with varying casein to whey protein ratios and addition of hydrocolloids. *Food Hydrocolloids,* 89**,** 874-884.

# Chapter 5[d]

# Fabrication and Lubrication Performance of Sustainable Pickering-like Water-In-Water Emulsions Using Plant Protein Microgels
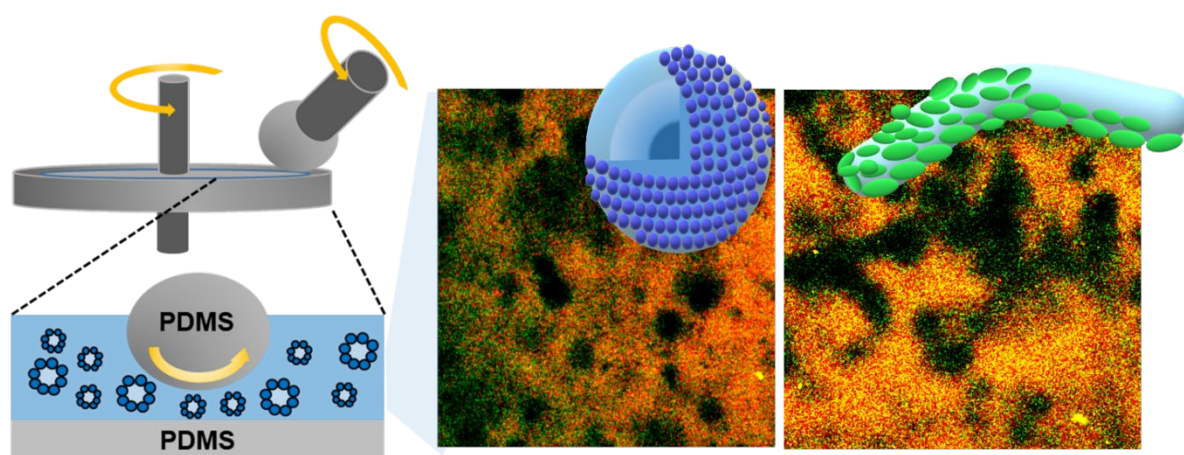


## Abstract

Aqueous multiphasic systems have attracted a great deal of interest recently owing to the growing demands of environmental sustainability for the development of stable 'oil-free' emulsions, often complicated by their limited stability against droplet coarsening. Although particles may provide ultrastability to water-in-water (W/W) emulsions formed in phase-separating polymer systems, the need for lubrication in such oil-free W/W emulsions presents an important challenge for their use in diverse applications. In this work, W/W Pickering emulsions were stabilized by sustainable plant protein (pea)-based microgels (PPM) using starch and xanthan gum as the biopolymers generating the W/W phase separating droplet structures. The lubricity of these systems was compared with that of parallel systems stabilised by animal

---

(whey) protein microgels (WPM). Unprecedented results reveal that PPM are more soft and adhesive than WPM and outperform the latter in boundary lubrication performance in striking contrast to the behaviour of the non-microgelled proteins. Furthermore, the PPM tend to stabilize a different, less spherical type of W/W droplet that may contribute to the lower friction observed in PPM-stabilized W/W emulsions. The novel approach of fabricating lubricious W/W emulsions utilizing sustainable microgels opens up new eco-friendly solutions in designing aqueous lubricants for future nutritional and biomedical applications.

## 5.1. Introduction

In recent times, there has been a burgeoning interest in designing eco-friendly multi-compartmental water-based systems (Esquena, 2016, Nicolai and Murray, 2017) using thermodynamically incompatible hydrophilic polymers for diverse applications such as food (You et al., 2023, Hazt et al., 2020), cell biology (Koga et al., 2011, Perro et al., 2022, Tang et al., 2015), encapsulation of biologics (Keating, 2012), biocatalysis (Xue et al., 2017, Silvério et al., 2013), biomedical (Wang et al., 2022). However, often these 'oil-free' water-in-water (W/W) emulsions suffer from poor stability. Low molecular weight surfactants are not able to offer any additional stabilization because the interfacial tension is orders of magnitude smaller compared with that of a typical oil-water (O–W) interface (Nicolai and Murray, 2017, Peddireddy et al., 2016). Therefore, Pickering stabilization, *i.e.*, using particles as stabilizers, including microgel particles fabricated using animal proteins such as $\beta$-lactoglobulin and whey protein (Beldengrun et al., 2018, You et al., 2023, Murray and Phisarnchananan, 2016) have been used as a promising strategy to improve their stability (Khemissi et al., 2018). By such particles adsorbing to and possibly cross-linking at the water-water (W–W) interface, spinodal decomposition and macroscopic phase separation can be deterred and water droplets of discrete length scales are maintained (Dickinson, 2019).

At the same time, apart from instability problems, a key challenge to address in these 'oil-free' W/W emulsion systems is a lack of lubrication performance compared to 'oily' systems, including oil-in-water emulsions. Lubrication from oil droplets is often translated into sensory perception described by creaminess and smoothness (Sarkar and Krop, 2019a, Torres

et al., 2018, Stokes et al., 2013). It is important to characterize both bulk rheological and tribological performance in order to control oral processing (Chen and Stokes, 2012, Sarkar and Krop, 2019a), which is particularly relevant for food (Carvalho-da-Silva et al., 2013, Selway and Stokes, 2013) but also oral pharmaceuticals (Lee et al., 2022, Batchelor et al., 2015) and oral care products (Cai et al., 2017). Replacing oil droplets with aqueous solutions can result in diminished lubrication performance unless the water is structured with biopolymers, as widely evidenced in nature-engineered lubricants, such as in tear, synovial fluids, saliva *etc.* (Ma et al., 2015, Xu et al., 2020). Recent years have witnessed a growing interest in "green tribology" (Nosonovsky and Bhushan, 2010), which strives to find alternatives to environmentally harmful lubricants. Hence, understanding the lubrication behaviour of W/W Pickering emulsions is highly topical and could contribute to a new era of green tribology. Currently, this is limited to just one study (You et al., 2023), where it was shown that adsorbing animal (whey) protein-based microgels at W–W interface improved the lubrication performance of a starch-carrageenan biphasic W/W system, as compared to their absence.

Interestingly, soft, proteinaceous microgels in the size range of hundreds of nanometers have been shown to have an influence on lubrication between interacting biological surfaces in sliding motion, *i.e.*, as in natural joints, such as the knee and hip (Jin et al., 2016a, Limbert et al., 2019, Mann and Tighe, 2016a) as well as in food applications (Sarkar et al., 2017a). Various microgels from animal or plant-based proteins have been used to design Pickering emulsions. Aggregation of the microgels in the bulk and at interfaces can vary, from a network of aggregated or fused particles that can be packing densely at interfaces to discrete monolayers at liquid-liquid interfaces (Oh et al., 2008). For animal-based protein microgels, whey(Sarkar et al., 2017a, Destribats et al., 2014), lactoferrin(David-Birman et al., 2013, Meshulam and Lesmes, 2014, Sarkar et al., 2018), and egg white (Li et al., 2020) have been investigated for their ability to stabilize Pickering emulsions.

Particles derived from plant proteins have recently attracted much interest in the design of Pickering emulsions owing to growing sustainability demands in technological applications. For example, it is now established that plant-based foods generate half the greenhouse gases as compared to animal-based foods (Xu et al., 2021b). While studies have focused on the lubrication performance of animal-derived microgels and as Pickering stabilizers, the design of

W/W emulsions that are stabilized by sustainable plant particles remains principally unexplored. Although soy protein aggregates (Liu and Tang, 2013, Liu and Tang, 2014, Liu et al., 2017), peanut protein microgels (Jiao et al., 2018) and pea protein microgels (Liang and Tang, 2014, Shao and Tang, 2016, Zhang et al., 2020a) have shown abilities to stabilize O/W emulsions, to our knowledge, no study has shown the fabrication of W/W emulsions using plant-based particles to date. More importantly, it has been shown experimentally that aqueous dispersions of plant proteins tend to increase friction compared to their animal protein counterparts (Kew et al., 2021, Zembyla et al., 2021). Thus, the question remains to what extent can such undesirable frictional behaviour be modulated by converting plant proteins to plant protein *microgels* and what happens when such microgels are present alongside with a W–W interface.

In this work, firstly, we fabricate plant protein (pea protein)-based microgels (PPM) to design Pickering W/W emulsions for the first time. Secondly, we show the unique ability of pea protein microgels to offer higher boundary lubrication properties compared to whey protein microgels (WPM) by virtue of their larger size and more importantly softer and more adhesive properties. In addition, the PPM tend to stabilize less spherical W/W droplets than with WPM, which may also contribute to the enhanced lubrication properties of the W/W systems with PPM. This knowledge was achieved *via* the use of a comprehensive suite of multiscale characterization techniques such as rheology, tribology, quartz crystal microbalance with dissipation monitoring, light scattering, confocal laser scanning microscopy, cryogenic scanning electron microscopy and atomic force microscopy. The findings present a novel route to the design of green, stable aqueous lubricants for the future.

## 5.2. Material and Methods

### 5.2.1. Materials.

Xanthan gum (XG, product code G1253, CAS number 11138-66-2), and waxy corn starch (CS, product code 10120, CAS number 9037-22-3) were purchased from Sigma-Aldrich, Dorset, UK. Whey protein isolate (WPI) powder containing 96.3 wt% protein was kindly donated by Fonterra Limited (Auckland, New-Zealand) and commercial pea protein concentrate (PPC) (Nutralys S85XF) with 85% protein content was kindly gifted by Roquette (Lestrem, France). All other chemicals used in the experiments were purchased from Sigma-Aldrich, Dorset, UK unless otherwise specified. MilliQ water purified by a Milli-Q apparatus (Millipore,

Bedford, UK), with an electrical resistivity not less than 18.2 MΩ.cm was used as the solvent throughout the experiments.

## 5.2.2. Preparation of hydrogel and microgel particles.

Protein hydrogels and microgel particles were prepared using the methods described elsewhere (You et al., 2023, Zhang et al., 2020a, Sarkar et al., 2017a). Briefly, WPI and PPC solutions were prepared by dissolving 12.0 wt% protein (WPI or PPC) in MIlliQ water and stirred for 2 h at room temperature to ensure complete dissolution. Crosslinking to form hydrogels was achieved by heating the whey or pea protein solutions at 90 °C for 30 minutes. After cooling to room temperature (22 °C), the gel was stored at 4 °C for 12 h. This was followed by blending for 2 min with MilliQ water at a 1:5 w/w ratio of gel to buffer using a hand blender (HB711M, Kenwood, UK). The subsequent dispersion of 'coarse' gel fragments was degassed *via* a THINKY mixer (ARE-250, Kidlington, UK) using a mixing cycle of 2 min at 2,000 rpm, followed by 1 min degassing at 2,200 rpm. Finally, the dispersion of the gel fragments was homogenised using a two-stage valve homogeniser (Panda Plus 2000; GEA Niro Soavi Homogeneizador Parma, Italy) for two passes, operating at two stages of 250 and 50 bar pressures to form whey protein microgel particles (WPM) and pea protein microgel particles (PPM).

## *5.2.3.* Rheology.

Samples were studied *via* a cone-and-plate geometry (CP50-2, cone diameter 50 mm, cone angle 2 °, 1 mm gap) in an MCR 302 (Anton Paar, Austria) controlled-stress rheometer. Protein solutions were gelled *in situ* by performing a temperature ramp (25-90 °C at a rate of 0.08 °C/s and held at 90 °C for 10 min), then cooling to 25 °C, after which a frequency sweep of 0.1-100 rad/s at a strain of 0.1% was initialised. Due to the long experimental time, the edge of the sample was sealed with a high-viscosity silicone oil (350 cSt) to provide additional protection against sample drying. Strain ($\gamma$) sweeps with eight data points per decade of $\gamma$, with $\gamma$ = 0.01–100 % were employed. In separate experiments, frequency sweeps were performed after gelation. Frequency sweeps with six data points per decade of frequency ($\omega$) = 100 – 0.01 rad/s were employed. Rheological characterisation of the biopolymer solutions and water-in-water (W/W) emulsions was performed at shear rates ($\dot{\gamma}$) ranging from 0.1 to 1000 s$^{-1}$ at 37 ± 0.1 °C, in order to mimic oral processing conditions. The viscosities of the microgels (WPM

and PPM), were also measured at shear rates ($\dot{\gamma}$) ranging from 0.1 to 100 s$^{-1}$ at room temperature. All the experiments were carried out within 2 h of W/W emulsion formation, during which no visible phase separation of the emulsions had occurred.

### 5.2.4.  **Atomic Force Microscopy (AFM**).

All nanoscale experiments including topographic imaging, nanoscale roughness, and adhesive force measurements of WPM and PPM were carried out with a Multimode 8 AFM on a Nanoscope V controller (Bruker) equipped with a liquid cell. Microgel suspensions were diluted by a factor of 100 using Milli-Q water and 100 µL aliquots were pipetted on to a fresh but untreated silicon wafer substrate. The samples were incubated in a hydrated state for 30 min at room temperature and rinsed five times with 100 µL of Milli-Q water using a micropipette to remove non-adsorbed particles that could otherwise adhere to the AFM cantilever tip. Samples were then transferred to the AFM for imaging and kept hydrated at all times. Oscillatory AFM modes such as Peak Force Tapping (at a range of frequencies) and standard liquid Tapping Mode (8-10kHz) result in highly unstable imaging, presumably due to the soft microgels oscillating in sympathy. Therefore, standard contact mode with very soft cantilevers was used. The probes, MLCT-DC-BIO (Bruker) are also thermal drift compensated which helps to maintain imaging force at the lowest possible force, with Cantilever C being selected, having a spring constant in the range 0.007-0.011 Nm$^{-1}$.

### 5.2.5. **Dynamic light scattering (DLS).**

Dynamic light scattering to determine the hydrodynamic microgel particle size was performed using a Zetasizer (Nano ZS series, Malvern Instruments, Worcestershire, UK) A sample of the WPM or PPM dispersion was diluted with MiliQ water solution at a 1 : 50 v/v ratio of microgel particles to water and placed in standard folded capillary electrophoresis cells (DTS1070). Measurements were performed by time-dependent correlation functions, using a detection angle of 173°, and the refractive index of WPM and PPM were set at 1.52 and 1.54, respectively, versus water (1.33). The absorbance of the microgel particles was assumed to be 0.001.

## 5.2.6. **Quartz Crystal Microbalance with Dissipation Monitoring (QCM-D).**

The adsorption behaviour of the microgel particles was measured using Quartz Crystal Microbalance with Dissipation Monitoring (QCM-D, E4 system, Q-Sense, Sweden). In attempting to mimic the adsorption properties of the protein microgel particles (WPM or PPM) at water-water (W−W) interface, hydrophilic gold-covered sensor (QSX-301, Q-Sense) was used. Frequency ($f$) as well as dissipation (D) were monitored in real time. All the solutions were supplied into QCM-D chamber by a peristaltic pump at a flow rate of 100 µL min$^{-1}$ at 25 °C. The first step was to inject Milli-Q water until a stable baseline was observed. The aqueous dispersions of the microgel particles were then injected into the system and left to adsorb under the flow conditions. Each gold sensor was used only once for each experiment. The data were fitted using Voigt model for viscoelastic solids (namely "Smartfit Model") by D find (Q-Sense, Sweden) software to calculate the hydrated mass of the hydrated layers of microgel particles.

## 5.2.7. **Preparation of W/W emulsions**

Gelatinized starch (GS) (0.2–4.0 wt%) was prepared by dispersing the starch powder in Milli-Q water, followed by heating in an oil bath at 90 °C for 15 min with constant shearing using an Ultra Turrax T25 homogeniser (IKA-Werke GmbH &Co., Staufen Germany). Xanthan gum (XG) (0.02–0.4 wt%) was dispersed in Milli-Q at pH 7.0 for at least 24 h at room temperature and then similarly dispersed and heated at 90 °C for 15 min. Equal volumes of GS and XG dispersions of different concentrations were mixed at 90 °C and homogenised at 21,000 rpm for 10 min via the Ultra Turrax T25 homogeniser. For designing Pickering-like W/W emulsions stabilised by microgel particles, WPM or PPM (2.0 vol% in the final mixture, here density of microgels were considered to be 1 g/ mL) were added to the XG dispersion before blending the two phases together. Noteworthy, adding microgel particles to either phases (XG or GS resulted in W/W emulsions with similar rheological properties. The W/W emulsions stabilized by microgels showed no signs of phase separation after 4 weeks of storage but the W/W emulsions without microgels showed phase separation after 2 weeks of storage at room temperature (see **Supplementary Figure S6**). Hence, all W/W emulsions were measured rheologically and tribologically within a week within which all the emulsions were stable, which was also in line with previous study where W/W emulsions were stabilized by using whey protein microgels.

### 5.2.8. Determination of phase separation and phase diagram.

The GS + XG mixtures stored in 75 × 25 mm flat bottom test tubes sealed with plastic cap were visually monitored at room temperature for two months. To confirm the phase separation accurately, also a few mixtures of arbitrarily chosen concentrations were centrifuged at high speed (20,000 × g) for 30 min, at 4 °C in Avanti J-30I centrifuge (Beckman Coulter, USA) and the supernatant was collected very carefully. Then, apparent viscosity measurements were performed *via* a model MCR 302 (Anton Paar, Austria) shear rheometer, using cone-and-plate geometry (CP50-2, cone diameter 50 mm, cone angle 2 °, 1 mm gap) at shear rates ranging from 1 to 100 $s^{-1}$. For each measurement, 2 mL of sample were pipetted onto the plate and a temperature-controlled cover was used to prevent evaporation and maintain the temperature at 22 °C. Samples were left on the plate for 2 min to achieve thermal equilibrium before rheological measurements commenced.

### 5.2.9. Confocal laser scanning microscope (CLSM).

Samples were visualised using a confocal laser scanning microscope (CLSM, Model LSM 880, Carl Zeiss MicroImaging GmbH, Jena, Germany). Ar/ArKr (488, 514 nm) and He/Ne (543, 633 nm) laser wavelengths were used. 0.5 wt% of Rhodamine B, Acridine orange, and Fast green were dissolved with MilliQ water and the solutions were stored in the dark when not being used. Rhodamine B showed preferential staining of GS whilst Acridine Orange and Fast green preferred attaching to WPM and PPM, respectively. Unlabelled areas were therefore assumed to be the XG-rich regions. For systems containing microgel particles, it was necessary to wait for 20 min to allow any air bubbles to rise out of the samples before they could be poured into the welled slide and the cover slip was then added before imaging.

### 5.2.10. Cryo-scanning electron microscopy (cryo-SEM).

A cryo-scanning electron microscopy (FEI Quanta 200F FEG ESEM, Japan) was used to study the structural features of microgel-loaded W/W emulsion systems following previous methods (You et al., 2023, Xu et al., 2020). All the samples were first loaded onto the rivet sample holders and frozen in liquid nitrogen. The frozen samples were transferred to the cryo-preparation chamber on the SEM, cleaved and etched at −95 °C for 4 min. Finally, the Pt-coated samples were transferred to the SEM chamber for imaging at −135 °C.

### 5.2.11. Tribology of microgel particles and emulsion systems.

The lubricating properties of microgels and W/W emulsion samples were measured using a Mini Traction Machine (MTM2, PCS Instruments, London, UK) with PDMS (Sylgard 184, Dow Corning, Midland, MI, USA, base fluid and cross-linker (10:1 w/w)) ball (Ø 19 mm)-on-disk (Ø 46 mm) configuration, with surface roughness, $R_a$ of 50 nm. All the tribological experiments were carried out within 2 h of preparation of the microgel particles and W/W emulsions, *i.e.*, when no visible phase separation had occurred. A normal load ($W$) of 2 N and a slide-to-roll ratio (*SRR*) of 50% were set for all measurements. The sliding speeds were varied from 1 to 1000 mm s$^{-1}$. The coefficient of friction was measured for all samples as a function of entrainment speed. The entrainment speed $U$ is defined as in **Equation 2.2**:

$$U = \frac{1}{2} \ (U_B + U_D) \tag{2.2}$$

where, $U_B$ is the rolling speed of the ball and $U_D$ is the sliding speed of the disc.

### 5.2.12. Statistical analyses.

All values are reported as the mean and standard deviation of three measurements carried out on at least triplicate samples (n = 3 × 3) prepared on different days. Statistical analyses were carried out using one-way ANOVA and multiple comparison test via SPSS software and differences between samples were deemed significantly different with $p < 0.05$ via Tukey's test.

## 5.3. Results and Discussion

Microgels fabricated using proteins, polysaccharides, lipids and synthetic polymers have attracted significant research attention recently due to their outstanding aqueous lubrication performance in various food, biomedical and pharmaceutical applications. Recent studies have shown that microgels can be fabricated from various food proteins, from both animal and more sustainable plant sources, using just physical crosslinking variables such as heat and pH, *i.e.*, with the commercial advantage of not using additional chemical crosslinking agents. However, the lubrication performance of microgels, especially those fabricated from plant proteins at water-water interface remains largely unexplored.
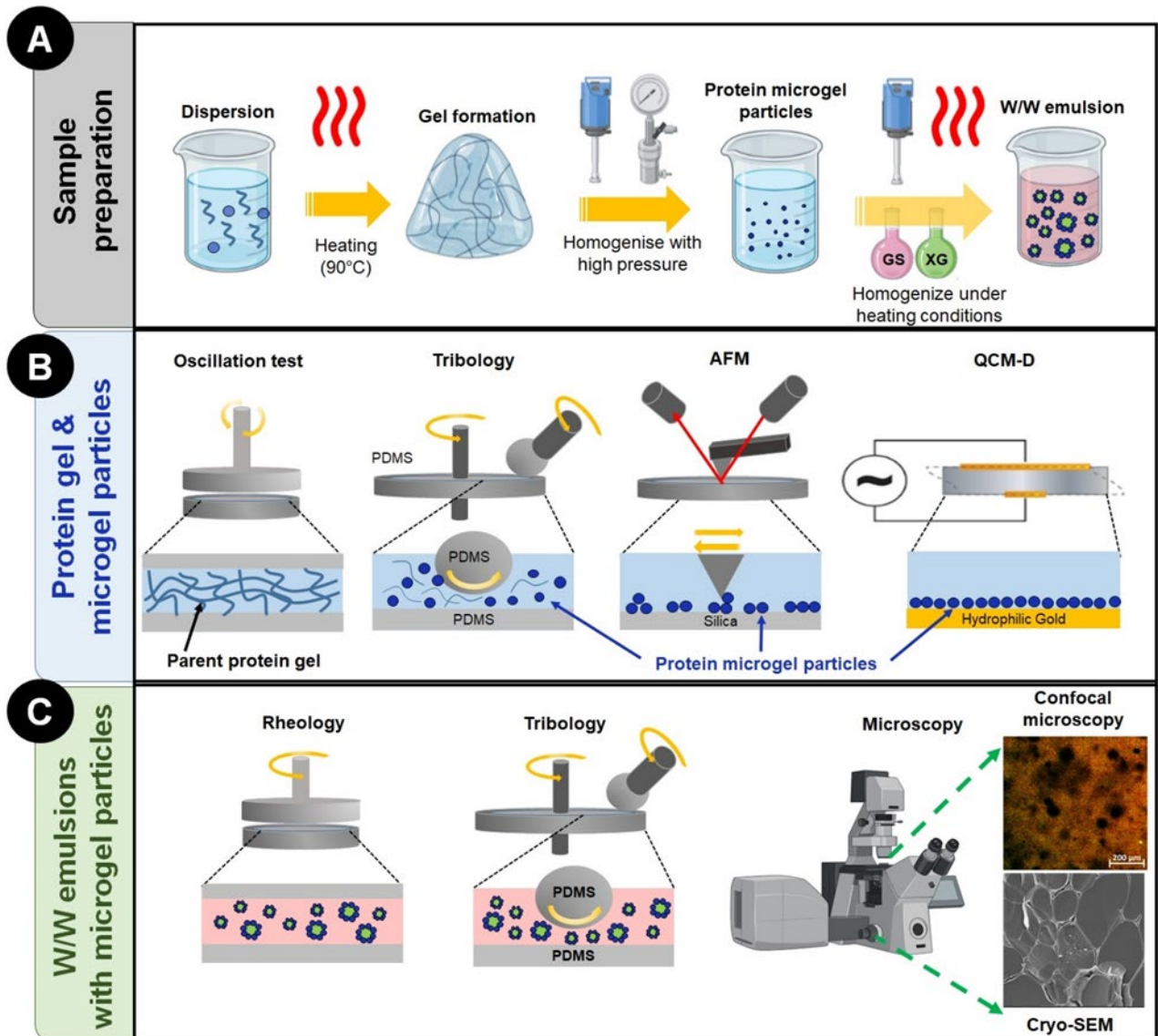
**Figure 5.1. Multiscale methodology.** (A) Sample preparation of whey and pea protein microgel particles (WPM and PPM, respectively) and water-in-water (W/W) emulsions fabricated using the microgel particles. (B) Characterization of protein hydrogels and microgel particles; dynamic viscoelasticity during and after gel formation; tribology with polydimethylsiloxane (PDMS) ball-and-disk tribometer; imaging of microgels using atomic force microscopy (AFM); quantification of film formation on gold surface using quartz crystal microbalance with dissipation monitoring (QCM-D). (C) Characterization of W/W emulsions from xanthan gum (XG) + gelatinized corn starch (GS) mixtures stabilized by microgel particles *via* bulk viscosity; tribology; confocal scanning laser microscopy (CLSM) and cryogenic scanning electron microscopy (Cryo-SEM).

Firstly, we investigated whether microgels of the two different types of protein, *i.e.* whey protein microgel (WPM) or pea protein microgel (PPM) could be used to fabricate Pickering-like water-in-water (W/W) emulsions formed from gelatinized starch (GS) and xanthan gum (XG) mixtures at various concentrations (**Figure 5.1A**). Although WPM has been used previously to design W/W emulsions (You et al., 2021b, You et al., 2023), to our knowledge this is the first study on use of plant-based PPM microgels for designing such W/W emulsions. It was also important to understand how PPM compares to WPM in terms of tribological performance, as it is known that non-microgelled pea protein jams the tribo-contacts and tends to increase friction significantly as compared to its whey protein counterpart (Kew et al., 2021).

To set the scene for understanding the properties of the Pickering W/W emulsions, we first characterized the rheological, tribological, and surface properties of the microgels on their own. This was done via a quartz crystal microbalance with dissipation monitoring (QCM-D) on hydrophilic gold substrates, combined with measurement of surface adhesion *via* an atomic force microscope (AFM), as illustrated schematically in **Figure 5.1B**. Having characterized the microgels alone, we explored their behaviour in the W/W emulsion systems. We also tried to answer questions about how the microstructure of the droplets may affect frictional properties using cryogenic scanning electron microscopy (cryo-SEM) and confocal laser scanning microscopy of the water droplets **(Figure 5.1C)**.

## 5.3.1. Rheological features of the parent protein gels

The dynamic shear rheological properties of the parent gels from which the microgels were formed were measured, in order to gain insights into the viscoelasticity of the individual microgel particles themselves, with the assumption that the two are directly related and not too disparate as a result of the process of mechanical breakdown from bulk gel to microgel (Andablo-Reyes et al., 2019). **Figures 5.2A** and **5.2B** show the results of oscillatory shear rheometry experiments performed on whey and pea protein hydrogels where *in situ* gel formation (*via* heating and cooling) was performed between the parallel plates of the rheometer, as illustrated in **Figure 5.1B**. Interestingly, there were marked differences in the kinetics of development of the storage ($G'$) and loss ($G''$) between the whey and pea proteins (see **Figures B1A** and **B1B**, respectively). Gelation (taken as where $G' > G''$) occurred at a much higher temperature (90 °C) for whey protein (**Figure B1B**). Gelation in pea protein appeared to be a two-step process, most likely involving a solubilizing step at around 60 °C, followed by the onset of the

most significant thermal crosslinking at around 70 °C (**Supplementary Figure S1B)**, the end result being a weak gel for the pea protein.
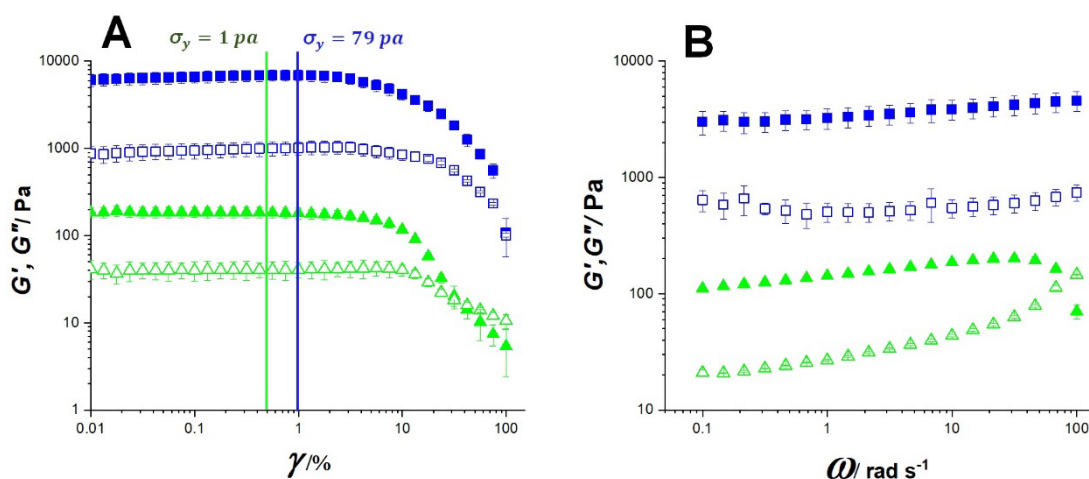


**Figure 5.2. Bulk viscoelasticity of parent hydrogels.** Oscillatory shear rheometry performed on 12.0 wt% whey (■) and pea protein hydrogels (▲). Closed symbols = $G'$, open symbols = $G''$. (A) Strain ($\gamma$) amplitude sweeps at $\omega$ = 6.28 rad $s^{-1}$. The vertical colored lines (green and blue) indicate the apparent yield points where $G'$ deviates from linearity by > 5%. The corresponding apparent yield stresses ($\sigma_y$) for pea and whey protein gels are given based on apparent yield strain in the LVER region, which is 1% for whey protein gel and 0.5% for pea protein gel, respectively. (B) Oscillatory frequency sweeps at $\gamma$ = 1 %. Means and standard deviations are reported for at least three measurements on experiments performed in triplicates (n = 3 × 3).

In terms of the strain dependence of $G'$ at $\omega$ = 6.28 rad $s^{-1}$, both the protein gels showed a plateau in $G'$ at low strain amplitudes. The apparent yield strain ($\gamma_y$), was taken as the point of deviation from this linear viscoelastic region (LVER) (Figure 2A), as defined by where $G'$ falls to 95% (Kaboorani and Blanchet, 2014, Airey et al., 2002) of its value at $\gamma$ = 0.01 %. This gave $\gamma_y$ values of 1% and 0.5 % for whey and pea protein, respectively. However, it should be noted that the corresponding apparent yield stress ($\sigma_y$) (Kelessidis et al., 2006, Dimakopoulos et al., 2013) values were 79 × higher for the whey than the pea protein gels. The pea protein gels also showed an increase in $G''$ over $G'$ beyond $\gamma_y$ unlike whey protein, although the data from different samples was quite scattered beyond this cross-over region. **Figure 5.2B** shows the result for frequency sweeps within the LVER (*i.e.*, strain amplitude between 0.5 and 1 %). Strong gel behaviour may be defined as a frequency-independent plateau in $G'$ where $G' \gg G''$ (Almdal et al., 1993, Burey et al., 2008). Both $G'$ and $G''$ were

independent (within experimental error) of $\omega$ for whey protein, whilst the pea protein gels showed inversion with G" > G' at $\omega$ = 70 rad $s^{-1}$.

Overall, the whey protein gels can be considered as much stronger and stiffer than the pea protein gels. The higher values of $\sigma_y$ and $G'$ as well as the relative frequency independence of the whey protein gels is not surprising given that there is widespread evidence that covalent disulphide bonding is a major contributor to the gelation of whey protein, whereas it has not been shown to play a major role for pea protein gelation (Kornet et al., 2021). Cystine, a sulfur-containing amino acid obtained by the oxidation of two cysteine molecules, is found at twice the concentration in whey protein than in pea protein (Babault et al., 2015), thus contributing to increased disulfide bonding in the former and hence the higher gel strength in whey protein gels

.

### 5.3.2. Microstructural, bulk and surface properties of microgels

Having understood the deformability of the gels, we have focused on the interactions of microgels with surfaces in order to explain the tribological features in the boundary regime, where surface interactions are particularly important to the mechanism behind frictional dissipation (Sarkar et al., 2019b).
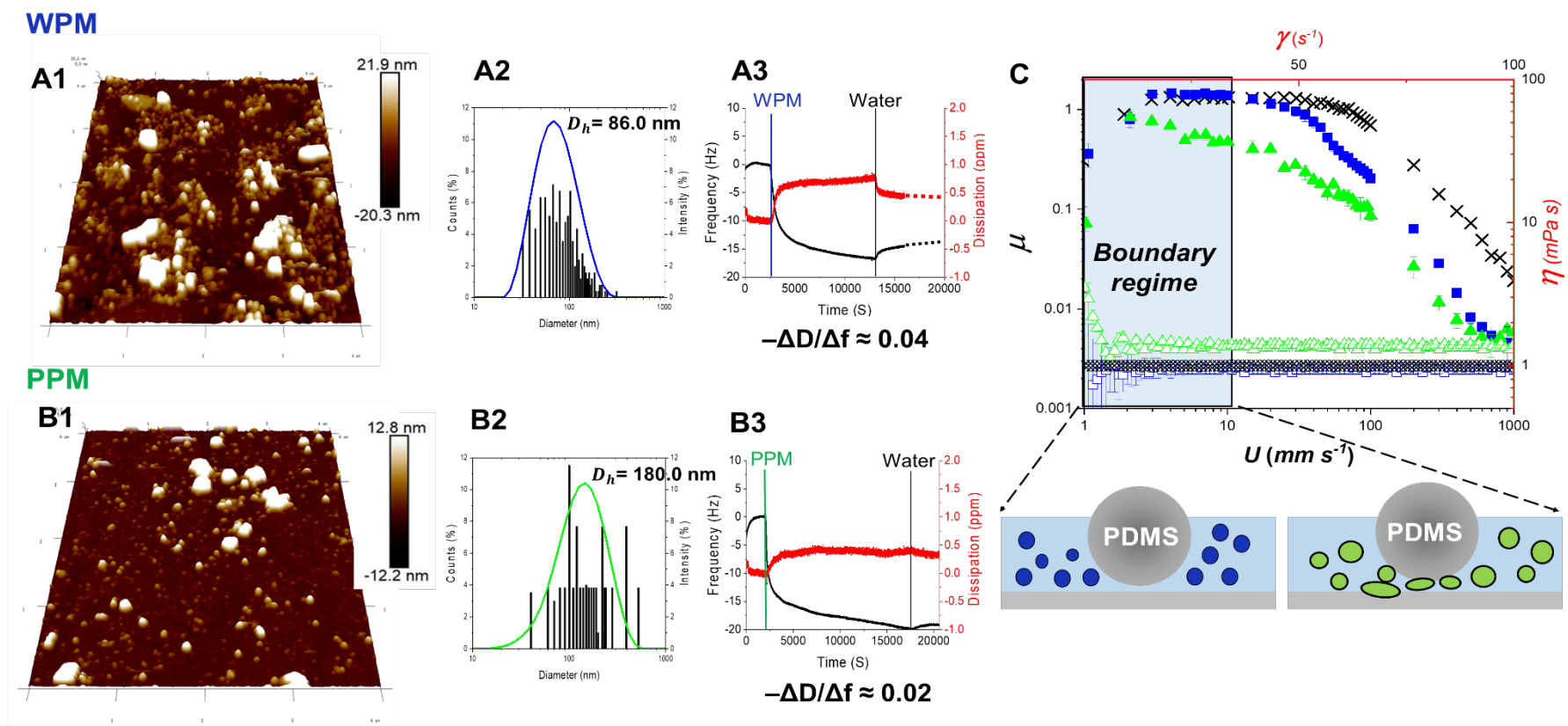
**Figure 5.3. Structure and performance of microgels in the bulk phase**. Three-dimensional topographic images of microgels deposited on a silicon substrate, as obtained by contact mode AFM for WPM (A1) and PPM (B1). Histogram plots showing the particle size distributions obtained from the AFM images for WPM (A2) and PPM (B2). Superimposed on figures A2 and B2 are the corresponding particle size distributions obtained via DLS. Mean frequency shift ($\Delta f$, —) and dissipation change ($\Delta D$, —) are obtained using QCM-D for 0.05 vol% WPM (A3) and PPM (B3) on gold sensors. The final values of $-\Delta D/\Delta f$ (before rinsing) are also given. The vertical line indicates the time at which the system was rinsed with MilliQ water. Mean apparent visosities ($\eta$) versus shear rate ($\dot{\gamma}$) of WPM ($\square$) and PPM ($\triangle$) are shown in (C). Mean

friction coefficient ($\mu$) versus entrainment speed ($U$) of WPM (■), PPM (▲) and water (X) between PDMS surfaces are also shown in (C) with statistical differences in $\mu$ reported in Supplementary Table S1A.   Also shown are schematic illustrations of the proposed state of the WPM (blue) and PPM (green) during these measurements where size and shape of the microgel particles are informed by AFM, DLS and rheology results. Error bars represent standard deviations for at least three measurements on experiments performed in triplicates (n = 3 × 3).

AFM allowed structural characterisation of the submicron-sized WPM and PPM, shown in **Figures 5.3A1** and **5.3B1**, respectively. Both WPM and PPM led to large instabilities when using peak force tapping mode, therefore contact mode was employed. Topographical images of the microgels (**Figures 5.3A1** and **5.3B1**) deposited on a silicon surface revealed a range of sizes of spherical shaped particles as well as small clusters that appeared to contain 2 to 6 individual particles. The surfaces of both WPM and PPM appeared to be relatively smooth, in agreement with measurements elsewhere on proteinaceous (Andablo-Reyes et al., 2019) and non-proteinaceous microgels (Aufderhorst-Roberts et al., 2018). Using dynamic light scattering, microgels made from 12.0 wt% WPM and PPM showed a narrow size distribution with a single peak in the size range of 100-1000 nm and the average hydrodynamic diameters ($D_h$) were 86 ± 4 and 180 ± 6 nm, respectively with polydispersity index < 0.25 (**Figures 5.3A2** and **5.3B2**). The particle size distribution was also quantified in the topographic images using the particle analysis function (WPM; 90.0 ± 2, and PPM; 178.4 ± 4 nm) with Nanoscope Analysis v1.9, also shown on **Figures 5.3A2** and **5.3B2**. All these size values were similar to those reported previously for these types of microgels (You et al., 2023, Zhang et al., 2020a).

QCM-D was used to understand the adsorption kinetics of the microgels at water-water interface using hydrophilic gold surfaces and also the mechanical properties of the microgel films at the surface. When either of the WPM or PPM was added at 0.01 vol%, a substantial decrease in frequency ($f$), $|\Delta f|$ =15 to 20 Hz occurred over 3 h, with an increase in dissipation (D) (**Figures 5.3A3** and **5.3B3**), this signifies protein adsorption. The changes in $|\Delta f|$ and D and consequently the structural changes of the microgelled films appeared to occur slower for PPM than WPM and both the adsorption appeared to be somewhat slower as compared to those observed in non-microgelled protein counterparts (Zembyla et al., 2021, Kew et al., 2021). After nearly 12,500 s for WPM and 17,500 s for PPM, the $|\Delta f|$ and D values were changing very slowly and so the aqueous phase was exchanged for water to check for reversibility of adsorption. Only a small proportion of the change in $|\Delta f|$ and D values on adsorption were reversed, particularly for PPM, suggesting that most of the microgel material remained adsorbed. The adsorbed hydrated mass was calculated using Voigt's model, since D also increased rapidly as a function of time, rendering the Sauerbrey model invalid (Liu and Kim, 2009, Dunér et al., 2013)**. Figures B2A** and **B2B** show that the calculated hydrated mass of WPM was nearly half of that of the PPM. This might be attributed to the 2× lower size of the

WPM particles compared to PPM. Also, it is important to highlight that the %desorption after the rinsing step was significantly higher in the case of the WPM (16%) as compared to that PPM (5.2%) suggesting that PPM had a higher affinity towards the gold surface as compared to WPM. The differences in adsorption and desorption are schematically illustrated in **Figure B2.** In non-microgelled systems, the hydrated adsorbed mass of whey protein and pea protein has been found to be similar when using the gold substrate, unless the proteins are thermally-treated (Zembyla et al., 2021) when the amount of whey protein adsorbed is similarly approximately half that of pea protein, *i.e.*, as for the thermally treated microgels here (see **Figure B2**). This suggests that differences between the proteins or their microgels are the result of the differences in their response to heating. Of more importance, an adsorbed protein molecule (mono)layer is typically 2 to 3 mg m$^{-2}$ (Graham and Phillips, 1979). However, as one might expect, the hydrated mass of microgels were not proportionately high and were still in the same orders of magnitude as those of non-microgelled systems. This suggests that the coverage of the microgel particles on gold surface irrespective of the protein type is far from monolayer and seems to be extremely patchy and flattened out during adsorption.

The final (*i.e.*, at the end of the adsorption time studied) values of the ratio of dissipation to frequency , -ΔD/Δf , were calculated: 0.04 for WPM and 0.02 for PPM. The value of –ΔD/Δf  characterizes the 'degree' of viscoelasticity: higher values represent more viscous and less elastic films, where the time to dissipate energy is increased (Zembyla et al., 2021, Xu et al., 2020). By this measure, although the WPM may be more rigid than the PPM, the adsorbed PPM layer is apparently less viscous and more rigid than the adsorbed WPM layer.  This seems to agree with the lower tendency for the PPM particles to desorb on exchange with water, discussed above, so that they appear to be more rigidly adhered to gold surface.  This greater adhesion was also confirmed by AFM measurements (**Figures B3A and B3B**), which showed a 9× higher adhesion force against the silicon AFM probe for the PPM as compared to WPM. Thus it would appear that the softer PPM microgels are abler to slowly restructure (possibly flattening out, interpenetrating and cross-linking with each other) to form an adsorbed film that becomes more rigid and more strongly adhering to the surface. In contrast, the individual WPM particles are more rigid but because of this are less able to cross-link with their neighboring particles and form such a resilient film, as schematically indicated in **Figure B2B**.

It is worth noting that dilute concentration of microgel dispersions (2.0 vol%) were used to make the W/W emulsions. Hence, as one might expect, the apparent viscosity of the microgel

dispersions was negligible and did not vary between the two microgel types; both WPM and PPM at 2.0 vol% showed Newtonian fluid characteristics with viscosity $\approx$ 1 mPa s (**Figure 5.3C**). Thus, the likelihood of these microgel dispersion contributing to the viscosity of the W/W emulsions stabilized by the microgels can be considered to be negligible. It is important to note that non-microgelled whey protein offers better lubricity than pea protein, where the latter has been demonstrated to jam the contact and increase boundary friction between poly-dimethylsiloxane (PDMS)-PDMS surfaces (Kew et al., 2021). Therefore, a key factor was to investigate the differences in lubrication performance when these two proteins were converted into microgels (see **Figure 5.3C** for results). As expected, water showed minimal reduction in the friction coefficient ($\mu$) at very low entrainment speed (U) in the boundary regime (at U < 5 mm s$^{-1}$) followed by reduction of $\mu$ in the mixed regime (U = 100–1000 mm s$^{-1}$), in line with previous findings (Sarkar et al., 2017a). Both WPM and PPM showed a more marked decrease in $\mu$ with an increase in U. Strikingly, PPM gave a significantly lower $\mu$ in the boundary regime compared to WPM and indeed was lower across the entire experimental window ($p < 0.05$) (see statistical differences in **Table B1A.** Thus, converting pea protein into microgels converts it from being high friction-generating material to a lubricating system that outperforms WPM, exactly opposite to the case of the non-microgelled proteins where $\mu$ for whey protein << pea protein.

To sum it up, both WPM and PPM appear to enter the gap between ball and disk and form a hydrated film that helps to separate the tribo-surfaces and reduce friction. However, the WPM particles, that we assume to have a rigidity $G'$ two orders of magnitude higher than the PPM (see **Figure 5.2A**), because they are less deformable, less hydrated and easier to desorb in the tribological regime than the PPM, are less able to form a coherent film keeping the surfaces apart (see schematic in **Figure 5.3C**).

## 5.3.3. Water-in-water emulsion systems
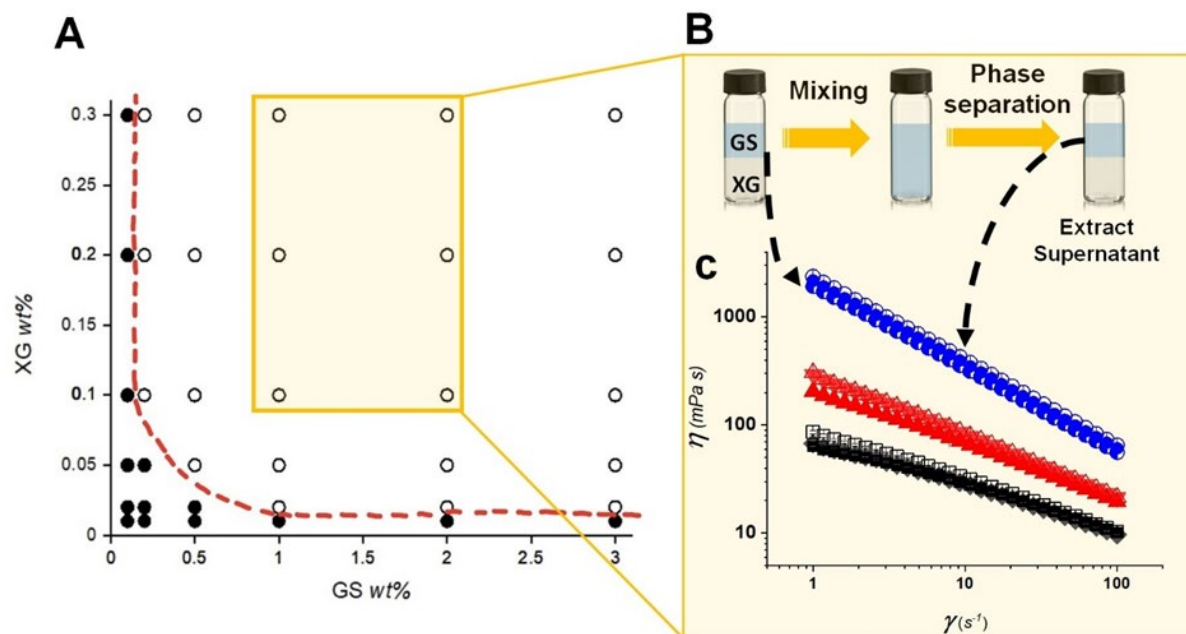


**Figure 5.4. Phase diagram and rheological behaviour of biphasic systems**. Phase diagram (A) of the xanthan gum (XG) + gelatinized starch (GS) system and viscosity curves (B) of mixtures and their corresponding separate phases. In (A), the estimated binodal is shown by the dashed red line (---) and the single phase and biphasic regions are indicated by the filled (●) and unfilled symbols (○), respectively. (B) Schematic diagram of the sampling method to confirm phase separation. (C) The mean apparent viscosity ($\eta$) as a function of shear rate ($\dot{\gamma}$) for XG alone at 0.1, 0.2, and 0.3 wt% (■, ▲, and ●, respectively); the upper phase of the phase separated mixtures of 0.1 wt% XG + 1.0 wt% GS (□), 0.1 wt% XG + 2.0 wt% GS (◆), and 0.2 wt% XG + 1.0 wt% GS (△), 0.2 wt% XG + 2.0 wt% GS (▼), and 0.3 wt% XG + 1.0 wt% GS (○) and 0.3 wt% XG + 2.0 wt% GS (◑). The error bars represent standard deviations for at least three measurements on experiments performed in triplicates (n = 3 × 3).

Having demonstrated that PPM alone reduces friction more than WPM alone, it was then relevant to test whether these same effects occur when the microgels are adsorbed at the W-W interface of a phase separating biopolymer system (Murray and Phisarnchananan, 2016, You et al., 2023). **Figure 5.4** shows the phase diagram of GS + XG mixtures, illustrating the concentration regions where the system is mono- or biphasic. The diagram is typical of others published elsewhere, though details vary slightly due to the variations in the molecular weight distributions of the polysaccharides, due to their origin and processing. Mixtures that showed no phase separation after two months of storage were considered to lie in the monophasic region.

The apparent viscosity of the upper phase separated layers at various concentrations of the mixtures (0.1 wt% XG + 1.0 wt% GS, and 2.0 wt% GS, 0.2 wt% XG + 1.0 wt% GS, and 2.0 wt% GS, and 0.3 wt% XG + 1.0 wt% GS and 2.0 wt% GS) was measured and compared the viscosity of each of the pure XG (0.1, 0.2 and 0.3 wt%) phases, shown in **Figure 5.4B**. **Figure 5.4C** confirms that the viscosities of the upper layers and that of the corresponding pure XG solutions were almost identical for all mixtures tested, highlighting that the phase separation resulted in an almost pure XG-rich phase at the top. This is in close accordance with previous experiments on phase separation, showing phase diagrams between GS and other polysaccharides; XG, $\kappa$-carrageenan, or guar gum, locust bean gum, and galactomannan gums (You et al., 2023, Murray and Phisarnchananan, 2016, Murray and Phisarnchananan, 2014). The other, lower phase, may therefore be fairly safely assumed to be largely starch-rich. The concentrations of W/W emulsions showing no phase separation within a week were further chosen for microstructural, rheological and tribological analyses.

### 5.3.3.1.      Microstructure of microgel-laden W/W emulsions

To investigate the role of WPM or PPM on the microstructure of W/W emulsions formed under the same conditions (2 wt% GS + 0.2 wt% XG) in the biphasic region (**Figure 5.4C**), the microstructure was monitored across a range of length scales. To our knowledge, one study has shown cryo-SEM evidence of WPM with no study on the presence of PPM at the interface of W/W emulsion droplets to date (You et al., 2023), although cryo-SEM remains a standard technique to visualize microgels at the oil-water interface in the case of oil-in-water emulsions (Zhang et al., 2021b, Xu et al., 2021a, Ji et al., 2022, Destribats et al., 2014). Cryogenic scanning electron microscopy (cryo-SEM) observations for microgels at 10,000× magnification (**Figure 5.5A** and **5.5B**) revealed the separated GS- and XG-rich regions as a 'nested architecture', with a fairly uniform distribution of polyhedral volumes.
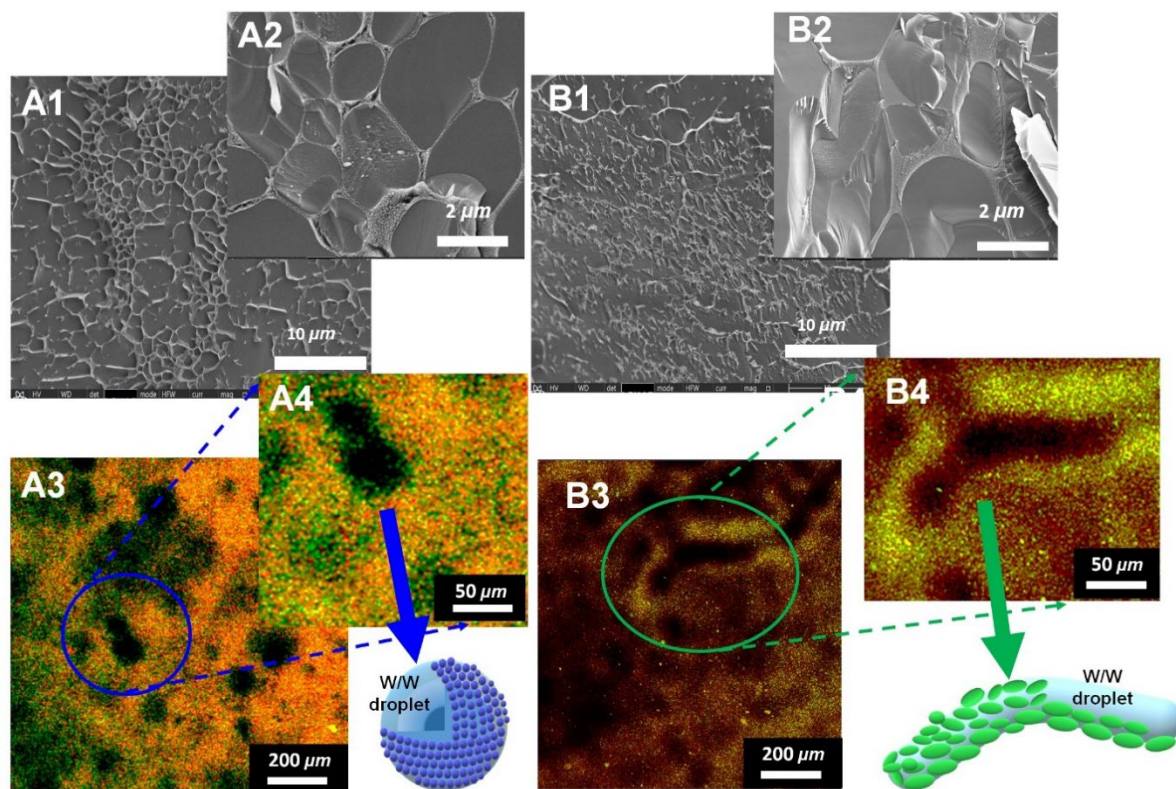
**Figure 5.5. Microstructure of W/W emulsions.** Cryo-SEM images at different magnifications of 2.0 wt% GS + 0.2 wt% XG W/W emulsions with WPM (A1 and A2) and PPM (B1 and B2). CLSM micrographs at two different magnifications of the same systems with WPM (A3 and A4) WPM and PPM (B3 and B4) are also shown. GS, WPM and PPM were fluorescently labelled with Rhodamine B ($\lambda \approx 546$ nm), Acridine Orange ($\lambda \approx 502$ nm), and Fast green ($\lambda \approx 633$ nm), respectively. The schematics alongside the confocal images illustrate the proposed differences in microstructure of WPM and PPM surrounding the water droplets.

We assume that these structures are the water droplets that form, rich in one of the biopolymers. The thickness of the lamellar region separating the water droplets containing interstitial WPM or PPM (see zoomed images in **Figures B4A** and **B4B**) appears to be in the range of hundreds of nm, in line with the microgel sizes reported in **Figures 5.3A2** and **5.3B2.** Many of the particles seem aggregated in the bulk, but a major fraction of the PPM does appear to be situated at the interface. Therefore, this is the first evidence that PPM can stabilize water droplets similar to the behaviour found in oil droplets, which has been previously reported (Zhang et al., 2020a, Zhang et al., 2021b). Noteworthy, there do seem to be differences in the droplet microstructure stabilized by WPM or PPM. In the presence of WPM, more polyhedral

water cells with microgels are evident, for example, in the zoomed-in region of **Figure 5.5A2**. The PPM systems seem to show a similar but more ´broken´ network structure, with the shape of water droplets appearing more irregular and non-uniform than those stabilized by WPM, as seen in **Figure 5.5B2**.

The fabricated microgels could affect the characteristics of W/W emulsions through various mechanisms, for example, particle−solvent interactions, osmotic pressure gradients, particle−particle interactions and particle-interface interactions (Saxena et al., 2014). Taking these in turn, the microgels may change their particle size (swelling or shrinking) according to which of the two phases they are located and the osmotic pressure of these phases, which in turn will vary according to the local evolving biopolymer concentrations. At the same time, the kinetics of evolution of the phase separating structures will be affected by the propensity of the microgel to rapidly adsorbed to the W/W interface and the strength of the attractive interactions between them, causing them form a more continuous and thick microgel layer at this interface. Connected with this is the deformability of the microgels, since softer, more deformable microgels may be able to 'unfold', change their shape and form a contiguous microgel layer more quickly and more easily (Wellert et al., 2015). The greater the magnitude of the interfacial tension (although all the tension values will be low) will also add to the strength of the driving force causing microgel adsorption and unfolding, whilst a higher tension will push the evolving phase separating discontinuous phases structures to adopt more spherical shapes (Shum et al., 2010). Gonzalez-Jordan et al. (2016) showed that by using heated solutions of $\beta$-lactoglobulin under various conditions, one might fabricate protein fibrils, microgels, and fractal aggregates. The effect of protein particle morphology was thus important to dictate the shape of the water droplet, but also the stability of W/W emulsions. Unfortunately, we are not yet in a position to define the relative balance of these different mechanisms, whereas our focus is on the practical implications for the lubricity effects.

Confocal laser scanning microscopy (CLSM) of the W/W emulsions provided further information about the microstructural features, free from the possibility of artefacts introduced *via* the preparation procedures of cryo-SEM. **Figures 5.5A3** and **5.5A4** show water droplets (that appear as dark, unstained areas) completely surrounded by WPM, stained with Acridine Orange (AO), confirming the ability of WPM to act as good Pickering stabilizers of   W/W emulsion systems (Vis et al., 2015a, Beldengrun et al., 2018, Hazt et al., 2020) (see **Figure B5** for additional CLSM images). The PPM-loaded W/W emulsions show a different architecture

(**Figure 5.5B3)**. Numerous non-spherical water regions appear to be surrounded by Fast Green stained PPM (see zoomed image with schematic in **Figure 5.5B4)** but here the water droplets have a more deformed shape, reminiscent of spinodal decomposition structures. One might question the apparent difference in size of the droplets observed between Cryo-SEM and CLSM images. The cryo-SEM specifically focused on lower-sized droplets to allow visualization of the droplets together with the interfacial microgels (**Figure B4**). In addition, the sample preparation (free-fracture) may cause significant changes in the size of the droplets, whereas sample preparation is minimal in the case of CLSM and one necessary focuses on larger sized droplets due to the lower resolution of CLSM and to avoid blurring due to Brownian motion. The next question is whether these different structures perform differently in rheological and tribological regimes and this is addressed below.
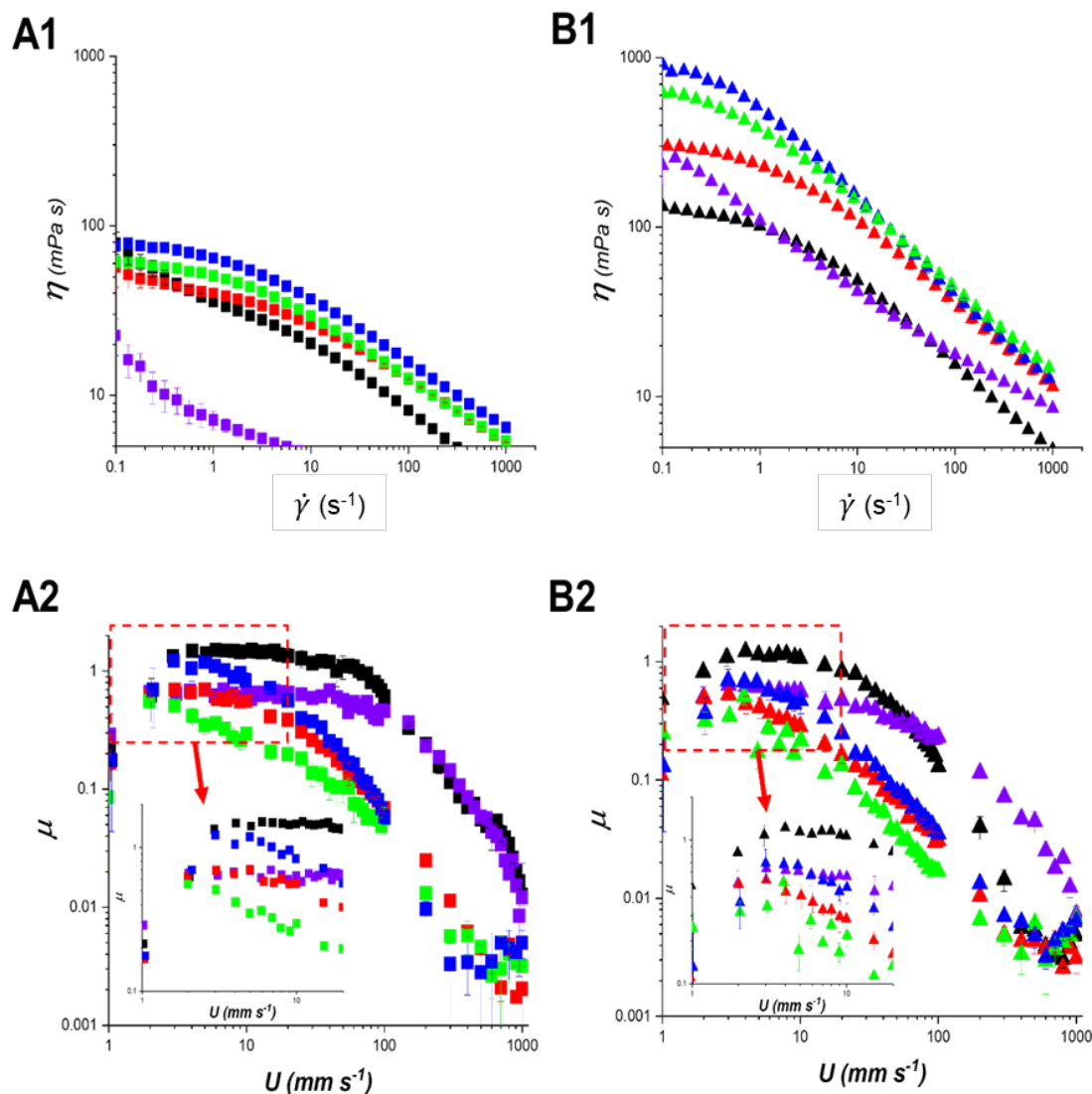
**Figure 5.6. Rheological and tribological properties of W/W emulsions.** Mean apparent viscosity ($\eta$) as a function of shear rate ($\dot{\gamma}$) (A1 and B1) and mean friction coefficient ($\mu$) *versus* entrainment speed ($U$) (A2 and B2) of lower concentration (square) with 1.0 wt% GS and 0.1 wt% XG and higher concentration emulsions (triangle) with 2.0 wt% GS and 0.2 wt% XG; GS (Black, ■ or ▲), XG (purple, ■ or ▲), emulsion (red, ■ or ▲), and WPM-loaded emulsion (Blue, ■ or ▲), and PPM-loaded emulsion (green, ■ or ▲) ), with magnified graph on boundary regime. Error bars represent standard deviations for at least three measurements on experiments performed in triplicates (n = 3 × 3).

## 5.3.3.2.    Rheological properties of Pickering-like W/W emulsions

Since the lubrication properties of biopolymeric systems are often determined by their bulk viscosity, particularly in the high shear rate ($\dot{\gamma}$) regimes (Andablo-Reyes et al., 2019,

Soltanahmadi et al., 2022), the apparent viscosities ($\eta$) of the W/W emulsions were measured, prepared with 2.0 vol% WPM or PPM at lower (1.0 wt% GS + 0.1 wt% XG) and higher (2.0 wt% GS + 0.2 wt% XG) biopolymer concentrations.   The results are shown in **Figures 5.6A1** and **5.6B1**, respectively, alongside controls of the same concentrations of the pure samples of GS and XG. Looking first at the W/W emulsions prepared without microgels, the emulsions were rheologically different to either GS or XG alone, and had non-Newtonian, shear-thinning properties at both concentrations.

At the lower biopolymer concentration (1.0 wt% GS + 0.1 wt% XG), the viscosity of the $\eta_{emulsion}$ appeared to be much closer to the viscosity of the GS ($\eta_{GS}$) than that of the XG ($\eta_{XG}$) at all $\dot{\gamma}$ (**Figure 5.6A1**). However, when the concentrations were doubled, $\eta_{emulsion}$ was considerably higher than the corresponding values of $\eta_{XG}$ or $\eta_{GS}$ alone, as might be expected from the added structuring of the system as observed in **Figure 5.5**. In the case of microgel-laden W/W emulsions, as seen in **Figure 5.6 A1 and B1,** the microgels enhanced $\eta_{emulsion}$ significantly, compared to the systems without microgels. It is noteworthy that the systems with WPM had a higher $\eta_{emulsion}$ than the ones with PPM at lower $\dot{\gamma}$. This might reflect the greater amount of structuring in the WPM systems evident in the cryo-SEM images (**Figure 5.5**). The adsorbed layers of PPM are possibly easier to deform under shear (visible even in the cryo-SEM images) and this inhibits interactions between the droplets and leads to lower $\eta_{emulsion}$ overall than with WPM.

### 5.3.3.3.        Lubrication performance of Pickering W/W emulsions

**Figures 5.6A2** and **5.6B2** show the evolution of friction coefficient ($\mu$) as a function of entrainment speed (*U*) of the W/W emulsions at the lower and higher biopolymer concentrations, respectively, stabilized by WPM or PPM and alongside the corresponding results for just GS and XG alone. **Figure 5.6A2** shows that the behaviour of the W/W emulsions without microgels at the lower biopolymer concentration (1.0 wt% GS + 0.1 wt% XG) has a totally different trend as compared to the corresponding GS and XG. The friction coefficients of the W/W emulsions ($\mu_{emulsion}$) in mixed and hydrodynamic regimes were much lower than those for GS ($\mu_{GS}$) or XG ($\mu_{XG}$) alone - although XG seemed to dominate the behaviour in the boundary regime. Without microgels at the higher biopolymer concentration (2.0 wt% GS + 0.2 wt%

XG) $\mu_{emulsion}$ in the boundary regime showed a rather similar trend as with the lower concentration of biopolymers (**Figure 5.6B2**), but in hydrodynamic regime (U > 500 mm s$^{-1}$) $\mu_{emulsion}$ seemed to be closer to that of $\mu_{GS}$.

One key question is whether or not the water droplets could become entrained and form a hydration film in the contact region between the ball-and-disk (You et al., 2021b). Considering the reduction of friction observed in **Figure 5.6**, it is certain that the droplets were entrained, nevertheless most likely deformed under tribo-shear as such large droplets if intact (**Figure 5.5**) would not be able to enter the contact zone where film thickness lies often in the order of tens to hundreds of nanometers (Torres et al., 2018). You et al. (2023) demonstrated that the tribological behaviour of such water droplets is governed by their size, morphology and volume fraction, depending on the biopolymer concentration. The higher biopolymer concentrations seem to give larger droplets and droplets with more non-spherical shapes, whereas the lower concentrations seem to give smaller droplets but with more well-defined spherical shapes. The microscopy results clearly show that the type of microgel added also influences the morphology and structure of the water droplets. In the case of the microgel-laden W/W emulsions, *i.e.*, W/W systems with 2.0 vol% WPM or PPM, **Figures 5.6A2** and **5.6B2** show that the presence of the different types of microgels also influenced the lubrication behaviour at both biopolymer concentrations. Specifically, the friction coefficient of the WPM-laden W/W emulsion was higher than the value of $\mu_{emulsion}$ without WPM and even XG alone in boundary regime ($p < 0.05$) (see statistical differences in **Tables B1B** and **B1C**). Earlier it was shown that WPM cannot lower $\mu_{WPM}$ in boundary regime as compared to PPM (**Figure 5.3D**). Also, Sarkar et al. (2017a) showed that low volume fractions of WPM give relatively poor lubrication properties - because WPM cannot bear the normal load and overcome the adhesion of PDMS-PDMS surfaces.

The most interesting and unprecedented behaviour was shown in $\mu$ for the PPM-stabilized droplets, which was lower than $\mu_{emulsion}$ (without PPM or containing WPM) and even XG alone in the boundary regime ($p < 0.05$) (see statistical differences in **Table B1**). As discussed previously, PPM alone decreased $\mu$ significantly in the boundary regime (see **Figure 5.3D**), so that this feature was mirrored when PPM was also present in the W/W emulsion system (**Figures 5.6A2** and **B2).** This suggests that both the non spherical-shaped droplets and/or the presence of soft, adhesive PPM on the surface of these droplets or in the interstices between them (**Figures 5.5B3** and **5.5B4**) are better able to squeeze into the tribological gap

and reduce the friction efficient, as compared to the more spherical and less deformable water droplets and associated WPM.

Contrary to expectations, the lubrication performance of the pea protein microgels (PPM) and corresponding PPM-stabilized W/W emulsions was in sharp contrast to the behaviour of the parent non-microgelled pea protein (Kew et al., 2021, Zembyla et al., 2021), since pea protein alone is known to increase friction compared to whey protein alone. This difference is probably related to the complex changes in the structure of the pea protein in its conversion to PPM, due to the applied heat and shear (Zhang et al., 2020a, Moreno et al., 2020). PPM indeed showed higher hydrated mass at a gold surface and higher adhesive forces than WPM. In addition, the PPM appeared to stabilized more distorted, non-spherical W/W emulsion droplets which enhanced the lubrication performance of PPM, unlike the more typical, spherical WPM-stabilized water droplets. Also, the size could be key factor in affecting lubricity as smaller WPM being nearly of half of the diameter of that of PPM can be expected to squeeze into the contact region more easily. However, once entrained larger volumes ($8\times$) will be able to support more load in case of PPM as compared to WPM. Hence, these differences in lubricity might be related to the PPM being softer than the WPM and also the differences in protein affinity, particle size and adhesiveness are crucial in the observed lubricity difference. We believe that this is the first time that such effects have been reported in the literature.

## 5.4. Conclusions

Using a comprehensive suite of multiscale techniques, including microscopy, light scattering, rheology, tribology, and surface adsorption measurements, we have demonstrated two key findings. (1) Soft proteinaceous microgels, made from 2 very different protein sources (pea and whey), can both stabilize Pickering-like water-in-water (W/W) emulsions, though with various morphologies and bulk viscosities as compared to W/W emulsions. (2) Sustainable plant-based (pea) protein microgels outperform the animal (whey) protein microgels in terms of lubricity on their own as well as the lubricity of the microgel-laden W/W emulsions. Strikingly, the microgel and W/W emulsion performance are in sharp contrast to the behaviour of the parent proteins, where pea protein is known to result in increased friction as compared to whey protein. Such differences are attributed to the increased size, lower viscoelasticity, enhanced degree of adsorption, and enhanced adhesive properties of pea protein microgels as

compared to whey protein. In turn, these differences lead to different morphology of the Pickering emulsions, the pea protein microgels leading to more distorted, less spherical water droplets which are possibly more easily entrained within the tribological gap. These novel insights pave the way forward for designing water-based sustainable bio-lubricants from plant proteins which should have applications in food, pharmaceutical, personal care and allied sectors. Further development should investigate the sensory response to such systems in order to validate whether the frictional data translates to the oral or skin regimes in terms of mouthfeel or skinfeel.

## References

AIREY, G. D., RAHIMZADEH, B. & COLLOP, A. C. 2002. Linear viscoelastic limits of bituminous binders. *Asphalt Paving technology,* 71**,** 89-115.

ALMDAL, K., DYRE, J., HVIDT, S. & KRAMER, O. 1993. Towards a phenomenological definition of the term 'gel'. *Polymer gels and networks,* 1**,** 5-17.

ANDABLO-REYES, E., YERANI, D., FU, M., LIAMAS, E., CONNELL, S., TORRES, O. & SARKAR, A. 2019. Microgels as viscosity modifiers influence lubrication performance of continuum. *Soft Matter,* 15**,** 9614-9624.

AUFDERHORST-ROBERTS, A., BAKER, D., FOSTER, R. J., CAYRE, O., MATTSSON, J. & CONNELL, S. D. 2018. Nanoscale mechanics of microgel particles. *Nanoscale,* 10**,** 16050-16061.

BABAULT, N., PAñZIS, C., DELEY, G., GUёRIN-DEREMAUX, L., SANIEZ, M.-H., LEFRANC-MILLOT, C. & ALLAERT, F. A. 2015. Pea proteins oral supplementation promotes muscle thickness gains during resistance training: a double-blind, randomized, Placebo-controlled clinical trial vs. Whey protein. *Journal of the International Society of Sports Nutrition,* 12**,** 3.

BATCHELOR, H., VENABLES, R., MARRIOTT, J. & MILLS, T. 2015. The application of tribology in assessing texture perception of oral liquid medicines. *International Journal of Pharmaceutics,* 479**,** 277-281.

BELDENGRUN, Y., ARAGON, J., PRAZERES, S. F., MONTALVO, G., MIRAS, J. & ESQUENA, J. 2018. Gelatin/maltodextrin water-in-water (w/w) emulsions for the preparation of cross-linked enzyme-loaded microgels. *Langmuir,* 34**,** 9731-9743.

BUREY, P., BHANDARI, B., HOWES, T. & GIDLEY, M. 2008. Hydrocolloid gel particles: formation, characterization, and application. *Critical reviews in food science and nutrition,* 48**,** 361-377.

CAI, H., LI, Y. & CHEN, J. 2017. Rheology and tribology study of the sensory perception of oral care products. *Biotribology,* 10**,** 17-25.

CARVALHO-DA-SILVA, A. M., VAN DAMME, I., TAYLOR, W., HORT, J. & WOLF, B. 2013. Oral processing of two milk chocolate samples. *Food & function,* 4**,** 461-469.

CHEN, J. & STOKES, J. R. 2012. Rheology and tribology: Two distinctive regimes of food texture sensation. *Trends in Food Science & Technology,* 25**,** 4-12.

DAVID-BIRMAN, T., MACKIE, A. & LESMES, U. 2013. Impact of dietary fibers on the properties and proteolytic digestibility of lactoferrin nano-particles. *Food Hydrocolloids,* 31**,** 33-41.

DESTRIBATS, M., ROUVET, M., GEHIN-DELVAL, C., SCHMITT, C. & BINKS, B. P. 2014. Emulsions stabilised by whey protein microgel particles: towards food-grade Pickering emulsions. *Soft matter,* 10**,** 6941-6954.

DICKINSON, E. 2019. Particle-based stabilization of water-in-water emulsions containing mixed biopolymers. *Trends in food science & technology,* 83**,** 31-40.

DIMAKOPOULOS, Y., PAVLIDIS, M. & TSAMOPOULOS, J. 2013. Steady bubble rise in Herschel–Bulkley fluids and comparison of predictions via the augmented Lagrangian method with those via the Papanastasiou model. *Journal of Non-Newtonian Fluid Mechanics,* 200**,** 34-51.

DUNëR, G., THORMANN, E. & DĖDINAITĖ, A. 2013. Quartz Crystal Microbalance with Dissipation (QCM-D) studies of the viscoelastic response from a continuously growing grafted polyelectrolyte layer. *Journal of colloid and interface science,* 408**,** 229-234.

ESQUENA, J. 2016. Water-in-water (W/W) emulsions. *Current Opinion in Colloid & Interface Science,* 25**,** 109-119.

GONZALEZ-JORDAN, A., NICOLAI, T. & BENYAHIA, L. 2016. Influence of the protein particle morphology and partitioning on the behavior of particle-stabilized water-in-water emulsions. *Langmuir,* 32**,** 7189-7197.

GRAHAM, D. & PHILLIPS, M. 1979. Proteins at liquid interfaces: II. Adsorption isotherms. *Journal of Colloid and Interface Science,* 70**,** 415-426.

HAZT, B., BASSANI, H. P., ELIAS-MACHADO, J. P., BUZZO, J. L. A., SILVEIRA, J. L. & DE FREITAS, R. A. 2020. Effect of pH and protein particle shape on the stability of amylopectin–xyloglucan water-in-water emulsions. *Food Hydrocolloids,* 104**,** 105769.

JI, Y., HAN, C., LIU, E., LI, X., MENG, X. & LIU, B. 2022. Pickering emulsions stabilized by pea protein isolate-chitosan nanoparticles: fabrication, characterization and delivery EPA for digestion in vitro and in vivo. *Food Chemistry,* 378**,** 132090.

JIAO, B., SHI, A., WANG, Q. & BINKS, B. P. 2018. High-internal-phase pickering emulsions stabilized solely by peanut-protein-isolate microgel particles with multiple potential applications. *Angewandte Chemie,* 130**,** 9418-9422.

JIN, Z., ZHENG, J., LI, W. & ZHOU, Z. 2016. Tribology of medical devices. *Biosurface and Biotribology,* 2**,** 173-192.

KABOORANI, A. & BLANCHET, P. 2014. Determining the linear viscoelastic region of sugar maple wood by dynamic mechanical analysis. *BioResources,* 9**,** 4392-4409.

KEATING, C. D. 2012. Aqueous phase separation as a possible route to compartmentalization of biological molecules. *Accounts of chemical research,* 45**,** 2114-2124.

KELESSIDIS, V., MAGLIONE, R., TSAMANTAKI, C. & ASPIRTAKIS, Y. 2006. Optimal determination of rheological parameters for Herschel–Bulkley drilling fluids and impact on pressure drop, velocity profiles and penetration rates during drilling. *Journal of Petroleum Science and Engineering,* 53**,** 203-224.

KEW, B., HOLMES, M., STIEGER, M. & SARKAR, A. 2021. Oral tribology, adsorption and rheology of alternative food proteins. *Food Hydrocolloids,* 116**,** 106636.

KHEMISSI, H., BASSANI, H., ASCHI, A., CAPRON, I., BENYAHIA, L. & NICOLAI, T. 2018. Exploiting complex formation between polysaccharides and

protein microgels to influence particle stabilization of W/W emulsions. *Langmuir,* 34**,** 11806-11813.

KOGA, S., WILLIAMS, D. S., PERRIMAN, A. W. & MANN, S. 2011. Peptide–nucleotide microdroplets as a step towards a membrane-free protocell model. *Nature chemistry,* 3**,** 720-724.

KORNET, R., SHEK, C., VENEMA, P., VAN DER GOOT, A. J., MEINDERS, M. & VAN DER LINDEN, E. 2021. Substitution of whey protein by pea protein is facilitated by specific fractionation routes. *Food Hydrocolloids,* 117**,** 106691.

LEE, H. J., HOLLENBECK, R. G., MORGAN, J. A., KRUGER HOWARD, A., SIDDIQUI, A., SAYEED, V. A., SELEN, A. & HOAG, S. W. 2022. A method for the tribological assessment of oral pharmaceutical liquids. *Drug Development and Industrial Pharmacy,* 48**,** 198-210.

LI, X., MURRAY, B. S., YANG, Y. & SARKAR, A. 2020. Egg white protein microgels as aqueous Pickering foam stabilizers: Bubble stability and interfacial properties. *Food Hydrocolloids,* 98**,** 105292.

LIANG, H.-N. & TANG, C.-H. 2014. Pea protein exhibits a novel Pickering stabilization for oil-in-water emulsions at pH 3.0. *LWT-Food Science and Technology,* 58**,** 463-469.

LIMBERT, G., MASEN, M. A., POND, D., GRAHAM, H. K., SHERRATT, M. J., JOBANPUTRA, R. & MCBRIDE, A. 2019. Biotribology of the ageing skin—Why we should care. *Biotribology,* 17**,** 75-90.

LIU, F., OU, S.-Y. & TANG, C.-H. 2017. Ca2+-induced soy protein nanoparticles as pickering stabilizers: Fabrication and characterization. *Food Hydrocolloids,* 65**,** 175-186.

LIU, F. & TANG, C.-H. 2013. Soy protein nanoparticle aggregates as pickering stabilizers for oil-in-water emulsions. *Journal of agricultural and food chemistry,* 61**,** 8888-8898.

LIU, F. & TANG, C.-H. 2014. Emulsifying properties of soy protein nanoparticles: influence of the protein concentration and/or emulsification process. *Journal of Agricultural and Food Chemistry,* 62**,** 2644-2654.

LIU, S. X. & KIM, J.-T. 2009. Application of Kevin—Voigt model in quantifying whey protein adsorption on polyethersulfone using QCM-D. *JALA: Journal of the Association for Laboratory Automation,* 14**,** 213-220.

MA, L., GAISINSKAYA-KIPNIS, A., KAMPF, N. & KLEIN, J. 2015. Origins of hydration lubrication. *Nature communications,* 6**,** 1-6.

MANN, A. & TIGHE, B. 2016. Ocular biotribology and the contact lens: surface interactions and ocular response. *Biomaterials and regenerative medicine in ophthalmology.* Elsevier.

MESHULAM, D. & LESMES, U. 2014. Responsiveness of emulsions stabilized by lactoferrin nano-particles to simulated intestinal conditions. *Food & function,* 5**,** 65-73.

MORENO, H. M., DOMINGUEZ-TIMON, F., DïAZ, M. T., PEDROSA, M. M., BORDERïAS, A. J. & TOVAR, C. A. 2020. Evaluation of gels made with different commercial pea protein isolate: Rheological, structural and functional properties. *Food Hydrocolloids,* 99**,** 105375.

MURRAY, B. S. & PHISARNCHANANAN, N. 2014. The effect of nanoparticles on the phase separation of waxy corn starch+ locust bean gum or guar gum. *Food Hydrocolloids,* 42**,** 92-99.

MURRAY, B. S. & PHISARNCHANANAN, N. 2016. Whey protein microgel particles as stabilizers of waxy corn starch+ locust bean gum water-in-water emulsions. *Food Hydrocolloids,* 56**,** 161-169.

NICOLAI, T. & MURRAY, B. 2017. Particle stabilized water in water emulsions. *Food Hydrocolloids,* 68**,** 157-163.

NOSONOVSKY, M. & BHUSHAN, B. 2010. Green tribology: principles, research areas and challenges. The Royal Society Publishing.

OH, J. K., DRUMRIGHT, R., SIEGWART, D. J. & MATYJASZEWSKI, K. 2008. The development of microgels/nanogels for drug delivery applications. *Progress in polymer science,* 33**,** 448-477.

PEDDIREDDY, K. R., NICOLAI, T., BENYAHIA, L. & CAPRON, I. 2016. Stabilization of water-in-water emulsions by nanorods. *ACS Macro Letters,* 5**,** 283-286.

PERRO, A., COUDON, N., CHAPEL, J.-P., MARTIN, N., BёVEN, L. & DOULIEZ, J.-P. 2022. Building micro-capsules using water-in-water emulsion droplets as templates. *Journal of Colloid and Interface Science,* 613**,** 681-696.

SARKAR, A., ADEMUYIWA, V., STUBLEY, S., ESA, N. H., GOYCOOLEA, F. M., QIN, X., GONZALEZ, F. & OLVERA, C. 2018. Pickering emulsions co-stabilized by composite protein/polysaccharide particle-particle interfaces: Impact on in vitro gastric stability. *Food Hydrocolloids,* 84**,** 282-291.

SARKAR, A., ANDABLO-REYES, E., BRYANT, M., DOWSON, D. & NEVILLE, A. 2019. Lubrication of soft oral surfaces. *Current Opinion in Colloid & Interface Science,* 39**,** 61-75.

SARKAR, A., KANTI, F., GULOTTA, A., MURRAY, B. S. & ZHANG, S. 2017. Aqueous lubrication, structure and rheological properties of whey protein microgel particles. *Langmuir,* 33**,** 14699-14708.

SARKAR, A. & KROP, E. M. 2019. Marrying oral tribology to sensory perception: A systematic review. *Current Opinion in Food Science,* 27**,** 64-73.

SAXENA, S., HANSEN, C. E. & LYON, L. A. 2014. Microgel mechanics in biomaterial design. *Accounts of chemical research,* 47**,** 2426-2434.

SELWAY, N. & STOKES, J. R. 2013. Insights into the dynamics of oral lubrication and mouthfeel using soft tribology: Differentiating semi-fluid foods with similar rheology. *Food Research International,* 54**,** 423-431.

SHAO, Y. & TANG, C.-H. 2016. Gel-like pea protein Pickering emulsions at pH 3.0 as a potential intestine-targeted and sustained-release delivery system for β-carotene. *Food research international,* 79**,** 64-72.

SHUM, H. C., ABATE, A. R., LEE, D., STUDART, A. R., WANG, B., CHEN, C. H., THIELE, J., SHAH, R. K., KRUMMEL, A. & WEITZ, D. A. 2010. Droplet microfluidics for fabrication of non-spherical particles. *Macromolecular rapid communications,* 31**,** 108-118.

SILVёRIO, S. C., RODRïGUEZ, O., TAVARES, A. P., TEIXEIRA, J. & MACEDO, E. 2013. Laccase recovery with aqueous two-phase systems: enzyme partitioning and stability. *Journal of Molecular Catalysis B: Enzymatic,* 87**,** 37-43.

SOLTANAHMADI, S., MURRAY, B. S. & SARKAR, A. 2022. Comparison of oral tribological performance of proteinaceous microgel systems with protein-polysaccharide combinations. *Food Hydrocolloids,* 129**,** 107660.

STOKES, J. R., BOEHM, M. W. & BAIER, S. K. 2013. Oral processing, texture and mouthfeel: From rheology to tribology and beyond. *Current Opinion in Colloid & Interface Science,* 18**,** 349-359.

TANG, T.-Y. D., VAN SWAAY, D., DEMELLO, A., ANDERSON, J. R. & MANN, S. 2015. In vitro gene expression within membrane-free coacervate protocells. *Chemical Communications,* 51**,** 11429-11432.

TORRES, O., ANDABLO-REYES, E., MURRAY, B. S. & SARKAR, A. 2018. Emulsion microgel particles as high-performance bio-lubricants. *ACS applied materials & interfaces,* 10**,** 26893-26905.

VIS, M., OPDAM, J., VAN'T OOR, I. S., SOLIGNO, G., VAN ROIJ, R., TROMP, R. H. & ERNë, B. H. 2015. Water-in-water emulsions stabilized by nanoplates. *ACS Macro Letters,* 4**,** 965-968.

WANG, Y., YUAN, J., ZHAO, Y., WANG, L., GUO, L., FENG, L., CUI, J., DONG, S., WAN, S. & LIU, W. 2022. Water-in-water emulsions, ultralow interfacial tension, and biolubrication. *CCS Chemistry,* 4**,** 2102-2114.

WELLERT, S., RICHTER, M., HELLWEG, T., VON KLITZING, R. & HERTLE, Y. 2015. Responsive microgels at surfaces and interfaces. *Zeitschrift für physikalische Chemie,* 229**,** 1225-1250.

XU, F., LIAMAS, E., BRYANT, M., ADEDEJI, A. F., ANDABLO-REYES, E., CASTRONOVO, M., ETTELAIE, R., CHARPENTIER, T. V. & SARKAR, A. 2020. A self-assembled binary protein model explains high-performance salivary lubrication from macro to nanoscale. *Advanced Materials Interfaces,* 7**,** 1901549.

XU, Q., QI, B., HAN, L., WANG, D., ZHANG, S., JIANG, L., XIE, F. & LI, Y. 2021a. Study on the gel properties, interactions, and pH stability of pea protein isolate emulsion gels as influenced by inulin. *Lwt,* 137**,** 110421.

XU, X., SHARMA, P., SHU, S., LIN, T.-S., CIAIS, P., TUBIELLO, F. N., SMITH, P., CAMPBELL, N. & JAIN, A. K. 2021b. Global greenhouse gas emissions from animal-based foods are twice those of plant-based foods. *Nature Food,* 2**,** 724-732.

XUE, L.-H., XIE, C.-Y., MENG, S.-X., BAI, R.-X., YANG, X., WANG, Y., WANG, S., BINKS, B. P., GUO, T. & MENG, T. 2017. Polymer–protein conjugate particles with biocatalytic activity for stabilization of water-in-water emulsions. *ACS Macro Letters,* 6**,** 679-683.

YOU, K. M., MURRAY, B. S. & SARKAR, A. 2021. Rheology and tribology of starch+ κ-carrageenan mixtures. *Journal of texture studies,* 52**,** 16-24.

YOU, K. M., MURRAY, B. S. & SARKAR, A. 2023. Tribology and rheology of water-in-water emulsions stabilized by whey protein microgels. *Food Hydrocolloids,* 134**,** 108009.

ZEMBYLA, M., LIAMAS, E., ANDABLO-REYES, E., GU, K., KROP, E. M., KEW, B. & SARKAR, A. 2021. Surface adsorption and lubrication properties of plant and dairy proteins: A comparative study. *Food hydrocolloids,* 111**,** 106364.

ZHANG, S., HOLMES, M., ETTELAIE, R. & SARKAR, A. 2020. Pea protein microgel particles as Pickering stabilisers of oil-in-water emulsions: Responsiveness to pH and ionic strength. *Food Hydrocolloids,* 102**,** 105583.

ZHANG, S., MURRAY, B. S., SURIYACHAY, N., HOLMES, M., ETTELAIE, R. & SARKAR, A. 2021. Synergistic interactions of plant protein microgels and cellulose nanocrystals at the interface and their inhibition of the gastric digestion of Pickering emulsions. *Langmuir,* 37**,** 827-840.

# Chapter 6
# General Discussion

## 6.1.  Introduction

The primary objective of this thesis was to examine the rheological and tribological characteristics of biopolymer mixtures, with a particular emphasis on comprehending the interrelationship between the two constituents and its impact on the general performance of water-in-water (W/W) emulsions. Briefly, all the chapter-wise results are summarized in this chapter in **Figure 6**. This thesis also shows constructing biocompatible particles that may be used to stabilize ultra-stable Pickering-like W/W emulsions, as well as to determine how the presence of such particles at the W/W interface provides lubricity in addition to stability. A key focus was to quantify lubricating behaviour of mixed hydrocolloid systems, with a focus on the until now unreported Pickering-like W/W emulsions stabilised by microgel particles providing structure-function relationship. This knowledge was achieved via the use of a comprehensive suite of characterization techniques such as rheology, tribology, quartz crystal microbalance with dissipation monitoring, light scattering and microscopy across length scales *i.e.* confocal laser scanning microscopy, cryogenic scanning electron microscopy and atomic force microscopy. The findings present a novel route to the design of green, stable aqueous lubricants for the future. Finally, the implications of the current findings are discussed as well as the recommendations for future work.
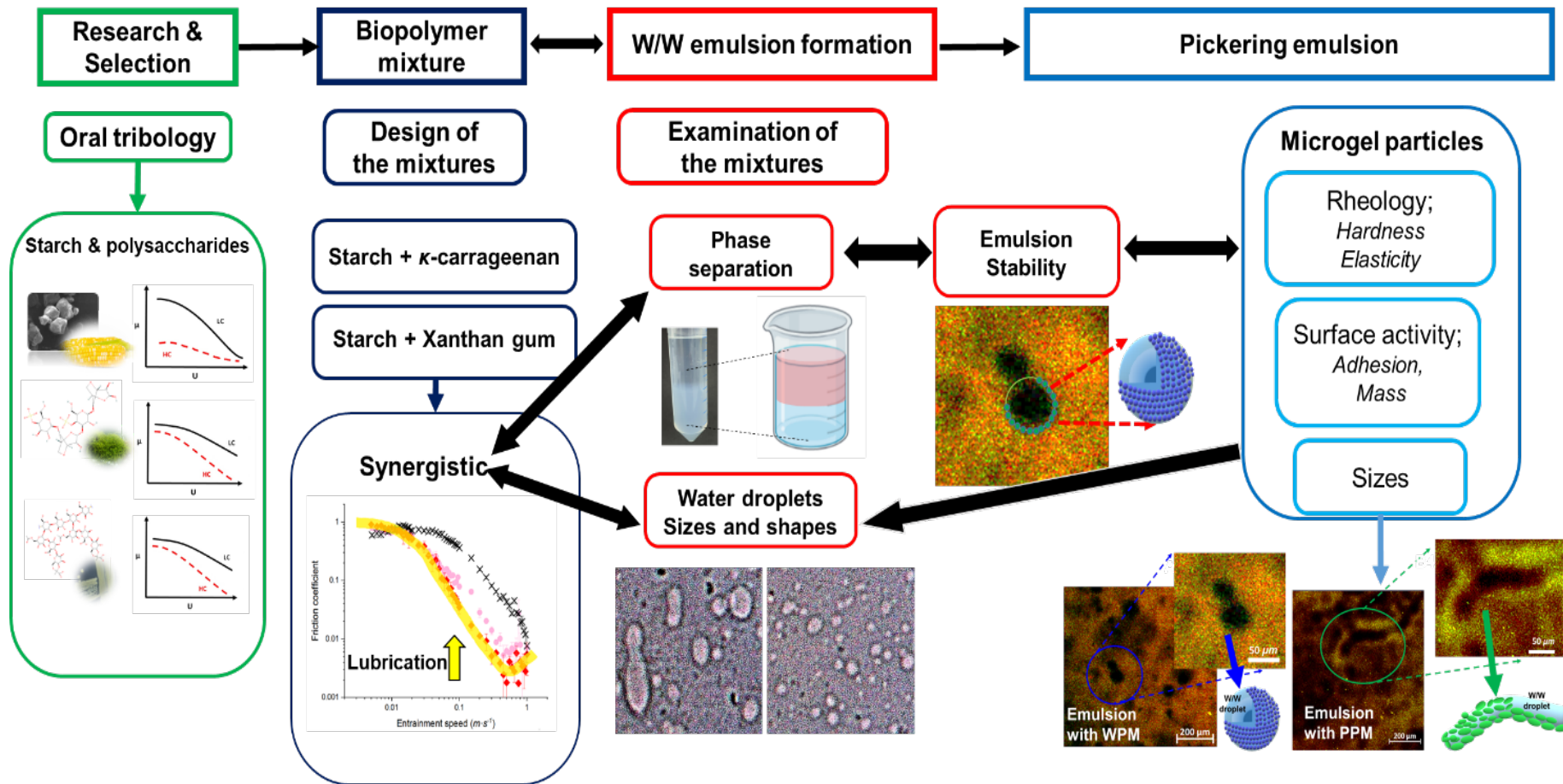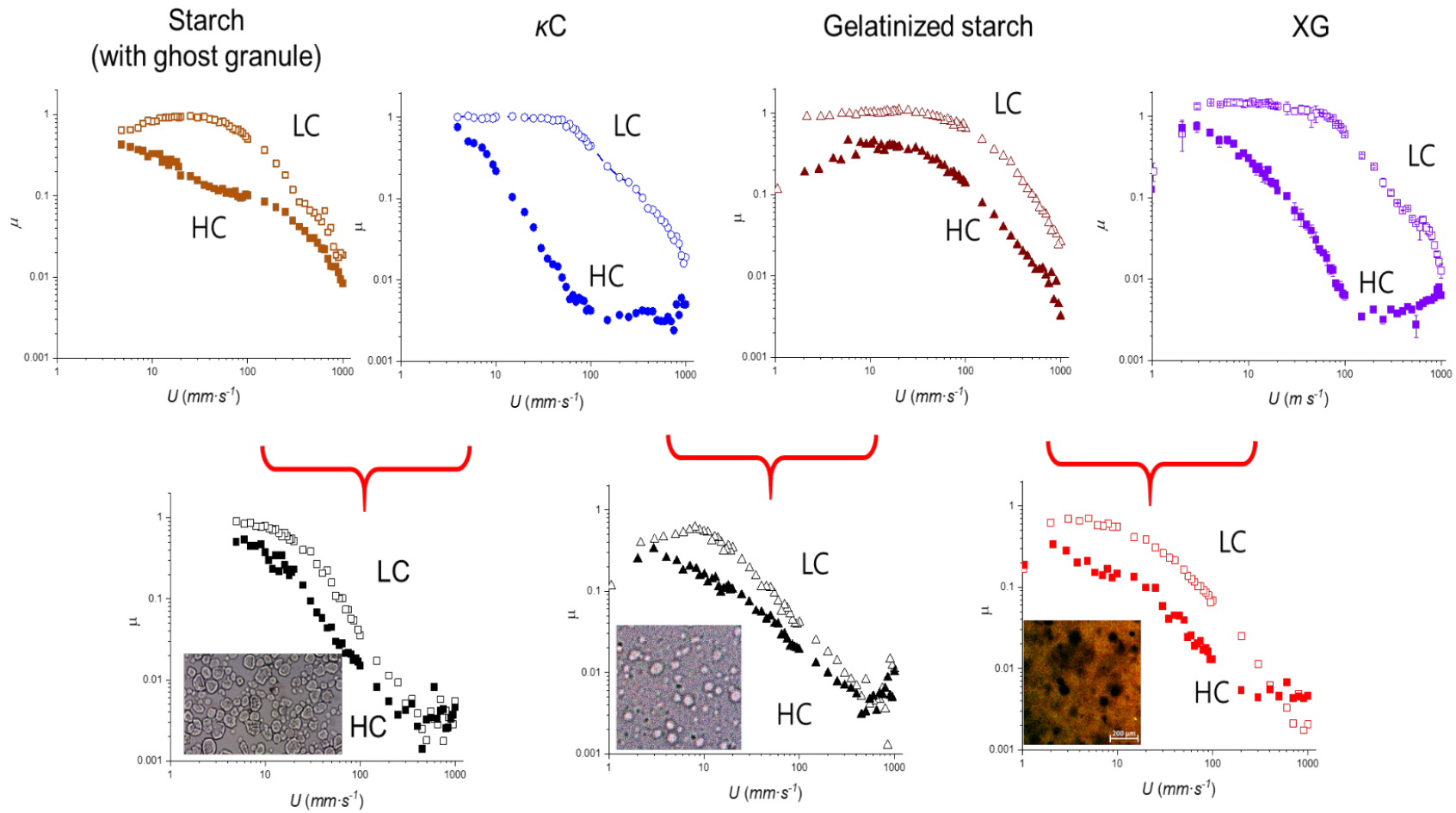
**Figure 6.1.** A schematic framework of the thesis.

**Figure 6.2.** Tribological properties of hydrocolloids and the mixtures in this thesis. LC and HC represent the lowest and highest concentrations of starch, $\kappa$-carrageenan, xanthan gum, and the mixtures.

## 6.2.    Summary of the main results

**Figure 6.1** shows the overall illustration of the results obtained in the entire thesis using tribology, rheology and microscopy. In this thesis, we first research the overall tribological characteristics of hydrocolloids, including starch and non-starch polysaccharides, followed by their characterizing their tribological properties in low concentration (liquid-like systems) and high concentrations (gel-like conditions,) as well as their mixtures. In processed foods, various hydrocolloids have been studied in oral processing particularly with regards to rheology and viscosity modification (**Chapter 2**). However, little has been reported on tribology of hydrocolloids. Furthermore, work on biopolymer mixtures, which can have infinite combinations of hydrocolloids have not reported the tribological characteristics. In the context of processed food products, it is often insufficient for a single hydrocolloid to provide the necessary properties and functionalities required for optimal performance (Gao et al., 2017). Hence, comprehending the properties of mixed hydrocolloid systems, encompassing their molecular interplays, phase conduct, microstructures, and consequently properties and functionalities, holds significance in broadening the applications of current hydrocolloids and conferring innovative functionalities for enhanced product formulation. Therefore, we started investigating the tribological properties of mixtures of hydrocolloids and compared with those of individual hydrocolloids.

Firstly, we study hydrocolloids *i.e.* starch and non-starch polysaccharides, having different results when these two hydrocolloids are combined (Kim and Yoo, 2006, de Vries, 2002, Haug et al., 2004, Murray and Phisarnchananan, 2014, Murray and Phisarnchananan, 2016, Lundin et al., 2000, Jin et al., 2015). We have chosen waxy corn starch with/ without gelatinization, and $\kappa$-carrageenan ($\kappa$C) and xanthan gum (XG) from non-starch polysaccharides category following experiments. According to the concentration of hydrocolloids, they could be liquid and/or gel-like. In this thesis, we wanted to focus on lubrication in liquid conditions, so we limited to lower concentrations of biopolymers. In **Chapter 3**, we started investigating the rheology and tribology of pure hydrocolloids, two types of waxy corn starch with ghost granule or not, and $\kappa$C. By increasing the concentration of the polymers, they showed different trends of tribological characteristics (**Figure 6.2**). Interestingly, starch with ghost granules helped to decrease friction coefficient ($\mu$) in boundary regimes, which has never been reported in literature to date. In the case of $\kappa$C, they show decreasing $\mu$ dramati-

cally by increasing concentration in boundary and hydrodynamic regimes (**Figure 6.2**). Following scaling tribology data to second plateau shear viscosity, we can also notice $\kappa$C could be affected by apparent viscosity in liquid conditions, but starch itself can affect tribological properties *via* ghost granules. By using the tribological information, we designed the mixtures by choosing two different concentrations within the liquid regime having lower and higher lubrication performance. Surprisingly, the mixtures decreased $\mu$ in all regimes regardless of the concentration, sharing characteristics each of the starch and the $\kappa$C; *i.e.* not only decreased $\mu$ in boundary regimes by starch but also in mixed and hydrodynamic regimes (**Figure 6.2**). Furthermore, the mixture with GS and $\kappa$C showed lower $\mu$ in the boundary regime, compared with the mixture with starch including ghost granules and $\kappa$C (**Figure 6.2**).

Following these results, we attempted to understand the phenomenon of lubrication of biopolymer mixtures without starch granules in **Chapter 4**. In the case of the mixtures with GS and $\kappa$C without ghost granules, they showed phase separation with the passage of time, and previous experiments showed a similar phenomenon when mixing two or more biopolymers (Lundin et al., 2000, Murray and Phisarnchananan, 2014, Firoozmand et al., 2009, Jin et al., 2015). Therefore, using phase diagram, we confirmed that phase separation occurred between GS and $\kappa$C at specific concentrations (**Figure 4.1**). Evidenced by microscopy, different concentrations of mixtures showed different shapes and sizes of water-in-water (W/W) emulsion droplets (Esquena, 2016, Beldengrun et al., 2018, Murray and Phisarnchananan, 2016, Perro et al., 2022, Dickinson, 2019), which had interesting lubrication performance (**Figure 4.2**). However, the key problem of W/W emulsions is poor stability (Esquena, 2016, Dickinson, 2019), so we used microgel particles to stabilise the emulsion to create Pickering-like W/W emulsions (Murray and Phisarnchananan, 2016, Esquena, 2016). And **Figure 5.6** showed the possibility that a small amount of microgel particles can help increase lubrication performance, as well as help stabilizing the W/W emulsion droplets. Then the key question was whether the type of microgel mattered in lubricity of W/W emulsion droplets

Hence, we experiment on the two types of microgel particles; animal protein (whey protein, WPM), and plant protein (Pea protein, PPM) **Figure 5.1** and characterized using oscillation test, tribology, AFM and QCM-D. **Figure 5.2** showed the difference in elasticity and hardness between whey and pea protein-based parent hydrogels from, which these mi-

crogel particles are fabricated via controlled shearing. Various surface characteristics including sizes & shapes, adhesion, hydrodynamic mass and lubrication properties showed differences between WPM and PPM. To confirm the role of the microgel particles in the lubricity of W/W emulsion system, we used tribology, rheology and also microscopies such as CLSM and cryo-SEM. Interestingly, **Figure 5.5** shows different shapes and sizes of water droplets formed when using WPM or PPM; WPM could result in formation of spherical water droplets whilst worm-like droplets were formed by PPM. **Figures 5.6** show the evolution of $\mu$ as a function of the entrainment speed ($U$) of W/W emulsions stabilized by WPM or PPM. PPM-stabilised emulsion had lower friction coefficients than those without PPM and WPM stabilised emulsion. This suggests that both the more worm-like shaped droplets and/or the presence of soft, adhesive PPM on the surface or in the interstices between them are better able to squeeze into the tribological gap and reduce friction efficiently.

## 6.3. Concluding Remarks and future directions

## 6.3.1. Concluding remarks

A schematic overview of the approach of this thesis was presented at the beginning of this chapter, highlighting the main outcome of this thesis: tribology and rheology of biopolymer mixture and W/W emulsion droplets stabilised by microgel particles (**Figure 6.1**). The use of a biopolymer mixture with hydrocolloids has the potential to expand the applications of current hydrocolloids and add new and innovative functionalities to product formulations. By studying their molecular interactions, phase behaviour, microstructures, and resulting quantification of lubricity in addition to viscosity, we can create even better products with just-right mouthfeel.

Oil droplets' lubrication has a significant impact on sensory perception, specifically on sensory descriptors such as "cream", "fatty", and "smooth". The substitution of oil droplets with aqueous solutions can pose a challenge. In addition, emulsions that claim to be 'oil-free' exhibit inadequate kinetic stability. Low-molecular-weight surfactants do not provide sufficient stabilisation due to the significantly lower interfacial tension in comparison to a standard oil-water interface. Hence, the application of particles as stabilisers, such as microgel particles, *via* Pickering stabilisation, presents a potentially effective approach to enhance stability. In the thesis, the results showed optimisation of type and concentration of hydrocol-

loids for water-in-water emulsion to provide lubrication performance. To summarise, the results offer comprehensive understanding of the lubrication characteristics of mixed hydrocolloid systems, with a particular focus on Pickering-like water-in-water emulsions that are stabilised by microgel particles. This particular system has not yet been documented in existing literature. The knowledge obtained in this thesis is especially important for the design and application of these emulsions in oral processing context, especially how this affects tribological performance and mouthfeel.

### 6.3.2. Future directions

This thesis has illustrated the potential of W/W emulsion, formulated with specific starch and non-starch hydrocolloids and biocompatible particles, to serve as a viable substitute for fat in food systems, exhibiting favourable lubricity and stability properties. The aforementioned results suggest that additional investigation is needed to fully realise the practical utility of these emulsion systems in relation to oral processing. This may encompass an exploration of factors such as sensory mouth sensation, response to saliva *ex vivo* and *in vivo*, and the utilisation of different hydrocolloid combinations, which remain unexplored.

• ***Characterisation techniques.*** In this thesis, we have used a range of rheological and tribological techniques to characterize the lubrication performance of the W/W emulsions. As a next step, one might consider investigating multiscale tribological properties of these emulsions. For instance, it is known that tribology is not scalable. Proteins have shown that tribological properties may differ significantly when studied at macroscale (Kew et al., 2021, Zembyla et al., 2021) versus nanoscale (Liamas et al., 2023, Liamas et al., 2021), where adhesion matters significantly. Also, the lubrication properties might change significantly if tongue-like rough, hydrophilic surface is employed (Andablo-Reyes et al., 2020, Wang et al., 2021). Hence, it is important to detail further characterization of tribological properties of W/W emulsions at multiple length scales as well as using tongue-like set ups to give indications about their real oral processing behvaviour.

• ***Investigation on the reaction between W/W emulsion with human saliva.*** Human saliva has amylase which catalyses the first step in the digestion of starch, a main source of carbohydrates in the human diet. In this thesis, we made the W/W emulsions system with starch and non-starch polysaccharides. Especially α-amylase, could be a key factor that may

affect the stability of these starch-based emulsion system. Conducting experiments to observe the reaction of emulsions with human saliva can provide confirmation regarding the potential use of an oil-free W/W emulsion system as a fat replacer. Human saliva is composed of electrolytes and proteinaceous compounds, including both large and small molecular weight proteins such as mucin, lactoferrin, and amylase, dispersed in a water medium (Sarkar et al., 2019c, Schipper et al., 2007, Xu et al., 2020). It serves a crucial function in oral activities such as speech, chewing, and swallowing, by providing lubrication to oral tissues and facilitating food bolus formation, disintegration, and swallowing (Ramasubbu et al., 1993, Aguirre et al., 1989, Xu et al., 2020, Sarkar et al., 2019c). There are no experiments in literature on the lubrication performance of W/W emulsion containing starch when reacting with model/ real human saliva. Therefore, it should be valuable to study further to confirm the synergistic or antagonistic interactions by various factors such as the digestion of starch, surface activities of large and small proteins on the W—W interface, *etc*. Detailed controlled experiments should be conducted on oral processing of emulsions in presence of mucins, α-amylase, lactoferrin, statherins *etc* individually as well as in combination to provide information on the breakup as well as entrainment of the emulsions in tribological contacts. Also interaction with stimulated and unstimulated saliva will give information of how lubricity of these W/W emulsions may change when the saliva contains certain protein groups.

• *Sensory testing.* Oral tribology analyses have emerged as a valuable mechanical technique to comprehend the physical mechanism underlying perceived texture. This technique enables the determination of lubrication and friction of oral surfaces in relative motion (Sarkar and Krop, 2019a, Stokes et al., 2013, Laguna et al., 2017a, Sarkar et al., 2021). Nevertheless, a limited number of investigations have employed this approach to replicate practical oral processing circumstances (Krop et al., 2019a, Stribițcaia et al., 2021). Of more importance, often tribometers are unable to differentiate subtle difference in sensorial perception such as between full-fat and skimmed milk even in the presence of saliva. Hence, it is crucial to combine objective and also temporal sensory tests with tribological analyses to comprehend how such mechanical phenomena result in perception (Stribițcaia et al., 2020, Stokes et al., 2013, Wang and Chen, 2017). Therefore, investigating W/W emulsion systems using instrumental characterization and identifying whether such textural properties attributed to different factors, *i.e*, combined ratio, types, microgel particles, and water droplets,

can then be sensorially discriminated and perceived by trained (quantitative descriptive analysis) and consumers (untrained panellists) using tests such as RATA (rate-all-that-apply).

• *Application of various designs of biopolymer mixtures.* In this thesis, we only used limited hydrocolloids to focus on the lubrication performance of the mixtures. However, there are a wide range of hydrocolloids, including starch, protein, and non-starch polysaccharides, and their infinite combinations under liquid or gel conditions can result in a range of food structure with unique properties (**Figure 6.3**).
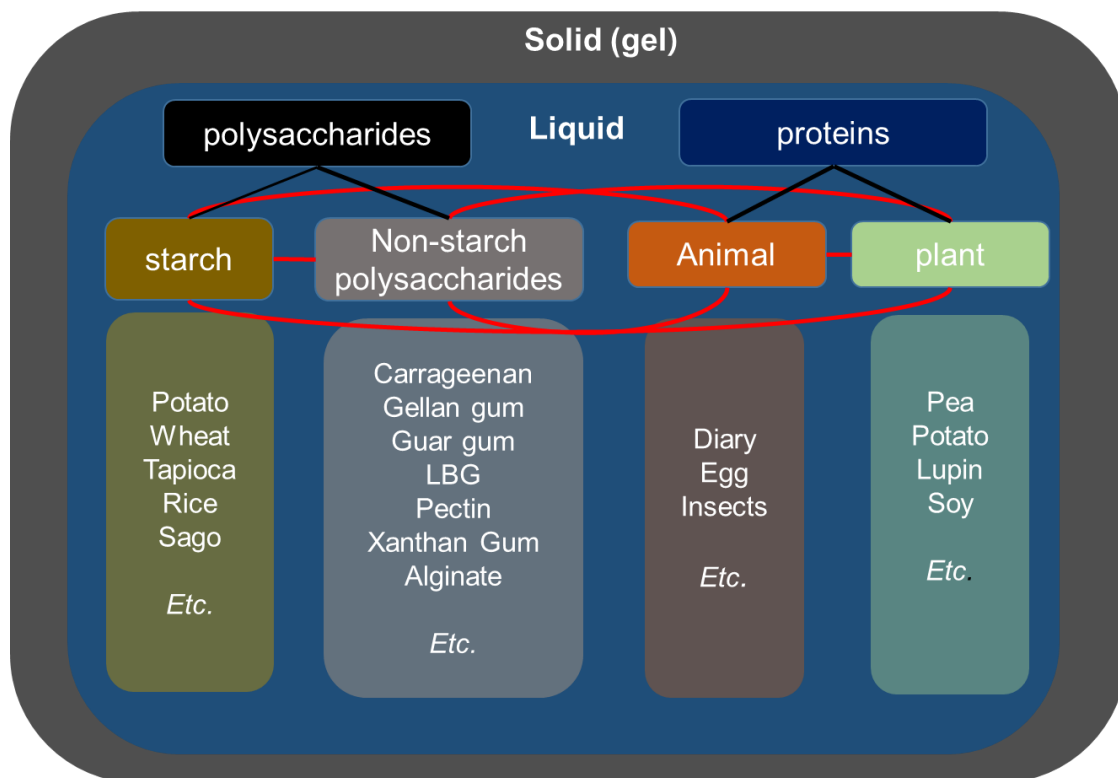


**Figure 6.3.** Schematic of design of the mixtures by various hydrocolloids.

There are already various experiments of hydrocolloids about additives, *i.e.*, stabilizers, gelling, thickeners, and rheological characteristics (Williams and Phillips, 2021, Dickinson, 2009). Experiments using biopolymer mixtures have shown a well-established set of synergistic interactions with a range of viscosity modification ability (Hemar et al., 2001, Murray and Phisarnchananan, 2014, Murray and Phisarnchananan, 2016, Soltanahmadi et al., 2022, Zhang et al., 2021b, Scholten et al., 2004, Lundin et al., 2000, Jin et al., 2015, Firoozmand et al., 2009). Nevertheless, hydrocolloids and biopolymer mixture can also act as lubricant, which could offer high moisturising capacity suitable for designing food for elderly (Araiza-Calahorra et al., 2022) and/or strong ability to stay on biological

surfaces providing relief from oral pathologies such as dry mouth (Hu et al., 2021). By using various combinations of hydrocolloids, further experiments could help developing not only new food products but also oral and pharmaceutical products with optimized tribological performance (Cai et al., 2017, Wang and Chen, 2017).

In summary, this thesis offers novel findings on tribology of biopolymer mixtures and W/W emulsions, which we hope will inspire future oral processing and sensory work to allow design of next generation of aqueous lubricants using hydrocolloids for fat mimetic, food for specialized nutrition and allied applications.

# References

AGUIRRE, A., MENDOZA, B., LEVINE, M., HATTON, M. & DOUGLAS, W. 1989. In vitro characterization of human salivary lubrication. *Archives of oral biology,* 34**,** 675-677.

ANDABLO-REYES, E., BRYANT, M., NEVILLE, A., HYDE, P., SARKAR, R., FRANCIS, M. & SARKAR, A. 2020. 3D biomimetic tongue-emulating surfaces for tribological applications. *ACS Applied Materials & Interfaces,* 12**,** 49371-49385.

ARAIZA-CALAHORRA, A., MACKIE, A. R., FERRON, G. & SARKAR, A. 2022. Can tribology be a tool to help tailor food for elderly population? *Current Opinion in Food Science***,** 100968.

BELDENGRUN, Y., ARAGON, J., PRAZERES, S. F., MONTALVO, G., MIRAS, J. & ESQUENA, J. 2018. Gelatin/maltodextrin water-in-water (w/w) emulsions for the preparation of cross-linked enzyme-loaded microgels. *Langmuir,* 34**,** 9731-9743.

CAI, H., LI, Y. & CHEN, J. 2017. Rheology and tribology study of the sensory perception of oral care products. *Biotribology,* 10**,** 17-25.

DE VRIES, J. 2002. Interaction of carrageenan with other ingredients in dairy dessert gels. *Special Publication-Royal Society of Chemistry,* 278**,** 201-210.

DICKINSON, E. 2009. Hydrocolloids and emulsion stability. *Handbook of hydrocolloids.* Elsevier.

DICKINSON, E. 2019. Particle-based stabilization of water-in-water emulsions containing mixed biopolymers. *Trends in food science & technology,* 83**,** 31-40.

ESQUENA, J. 2016. Water-in-water (W/W) emulsions. *Current Opinion in Colloid & Interface Science,* 25**,** 109-119.

FIROOZMAND, H., MURRAY, B. S. & DICKINSON, E. 2009. Interfacial structuring in a phase-separating mixed biopolymer solution containing colloidal particles. *Langmuir,* 25**,** 1300-1305.

GAO, Z., FANG, Y., CAO, Y., LIAO, H., NISHINARI, K. & PHILLIPS, G. O. 2017. Hydrocolloid-food component interactions. *Food hydrocolloids,* 68**,** 149-156.

HAUG, I. J., DRAGET, K. I. & SMIDSRúD, O. 2004. Physical behaviour of fish gelatin-κ-carrageenan mixtures. *Carbohydrate Polymers,* 56**,** 11-19.

HEMAR, Y., TAMEHANA, M., MUNRO, P. & SINGH, H. 2001. Viscosity, microstructure and phase behavior of aqueous mixtures of commercial milk protein products and xanthan gum. *Food Hydrocolloids,* 15**,** 565-574.

HU, J., ANDABLO-REYES, E., MIGHELL, A., PAVITT, S. & SARKAR, A. 2021. Dry mouth diagnosis and saliva substitutes—A review from a textural perspective. *Journal of Texture Studies,* 52**,** 141-156.

JIN, W., SONG, R., XU, W., WANG, Y., LI, J., SHAH, B. R., LI, Y. & LI, B. 2015. Analysis of deacetylated konjac glucomannan and xanthan gum phase separation by film forming. *Food Hydrocolloids,* 48**,** 320-326.

KEW, B., HOLMES, M., STIEGER, M. & SARKAR, A. 2021. Oral tribology, adsorption and rheology of alternative food proteins. *Food Hydrocolloids,* 116**,** 106636.

KIM, C. & YOO, B. 2006. Rheological properties of rice starch–xanthan gum mixtures. *Journal of Food Engineering,* 75**,** 120-128.

KROP, E. M., HETHERINGTON, M. M., HOLMES, M., MIQUEL, S. & SARKAR, A. 2019. On relating rheology and oral tribology to sensory properties in hydrogels. *Food Hydrocolloids,* 88**,** 101-113.

LAGUNA, L., FARRELL, G., BRYANT, M., MORINA, A. & SARKAR, A. 2017. Relating rheology and tribology of commercial dairy colloids to sensory perception. *Food & function,* 8**,** 563-573.

LIAMAS, E., CONNELL, S. D. & SARKAR, A. 2023. Frictional behaviour of plant proteins in soft contacts: unveiling nanoscale mechanisms. *Nanoscale Advances,* 5**,** 1102-1114.

LIAMAS, E., CONNELL, S. D., ZEMBYLA, M., ETTELAIE, R. & SARKAR, A. 2021. Friction between soft contacts at nanoscale on uncoated and protein-coated surfaces. *Nanoscale,* 13**,** 2350-2367.

LUNDIN, L., ODIC, K., FOSTER, T. & NORTON, I. 2000. Phase separation in mixed carrageenan systems. *Supramolecular and Colloidal Structures in Biomaterials and Biosubstrates.* World Scientific.

MURRAY, B. S. & PHISARNCHANANAN, N. 2014. The effect of nanoparticles on the phase separation of waxy corn starch+ locust bean gum or guar gum. *Food Hydrocolloids,* 42**,** 92-99.

MURRAY, B. S. & PHISARNCHANANAN, N. 2016. Whey protein microgel particles as stabilizers of waxy corn starch+ locust bean gum water-in-water emulsions. *Food Hydrocolloids,* 56**,** 161-169.

PERRO, A., COUDON, N., CHAPEL, J.-P., MARTIN, N., BëVEN, L. & DOULIEZ, J.-P. 2022. Building micro-capsules using water-in-water emulsion droplets as templates. *Journal of Colloid and Interface Science,* 613**,** 681-696.

RAMASUBBU, N., THOMAS, L. M., BHANDARY, K. K. & LEVINE, M. J. 1993. Structural characteristics of human salivary statherin: a model for boundary lubrication at the enamel surface. *Critical Reviews in Oral Biology & Medicine,* 4**,** 363-370.

SARKAR, A. & KROP, E. M. 2019. Marrying oral tribology to sensory perception: A systematic review. *Current Opinion in Food Science,* 27**,** 64-73.

SARKAR, A., SOLTANAHMADI, S., CHEN, J. & STOKES, J. R. 2021. Oral tribology: Providing insight into oral processing of food colloids. *Food Hydrocolloids,* 117**,** 106635.

SARKAR, A., XU, F. & LEE, S. 2019. Human saliva and model saliva at bulk to adsorbed phases–similarities and differences. *Advances in Colloid and Interface Science,* 273**,** 102034.

SCHIPPER, R. G., SILLETTI, E. & VINGERHOEDS, M. H. 2007. Saliva as research material: biochemical, physicochemical and practical aspects. *Archives of oral biology,* 52**,** 1114-1135.

SCHOLTEN, E., VISSER, J. E., SAGIS, L. M. & VAN DER LINDEN, E. 2004. Ultralow interfacial tensions in an aqueous phase-separated gelatin/dextran and gelatin/gum arabic system: A comparison. *Langmuir,* 20**,** 2292-2297.

SOLTANAHMADI, S., MURRAY, B. S. & SARKAR, A. 2022. Comparison of oral tribological performance of proteinaceous microgel systems with protein-polysaccharide combinations. *Food Hydrocolloids,* 129**,** 107660.

STOKES, J. R., BOEHM, M. W. & BAIER, S. K. 2013. Oral processing, texture and mouthfeel: From rheology to tribology and beyond. *Current Opinion in Colloid & Interface Science,* 18**,** 349-359.

STRIBIȚCAIA, E., GIBBONS, C., SIER, J., BOESCH, C., BLUNDELL, J., FINLAYSON, G. & SARKAR, A. 2021. Effects of oral lubrication on satiety, satiation and salivary biomarkers in model foods: A pilot study. *Appetite,* 165**,** 105427.

STRIBIȚCAIA, E., KROP, E. M., LEWIN, R., HOLMES, M. & SARKAR, A. 2020. Tribology and rheology of bead-layered hydrogels: Influence of bead size on sensory perception. *Food Hydrocolloids,* 104**,** 105692.

WANG, Q., ZHU, Y. & CHEN, J. 2021. Development of a simulated tongue substrate for in vitro soft "oral" tribology study. *Food Hydrocolloids,* 120**,** 106991.

WANG, X. & CHEN, J. 2017. Food oral processing: Recent developments and challenges. *Current Opinion in Colloid & Interface Science,* 28**,** 22-30.

WILLIAMS, P. A. & PHILLIPS, G. O. 2021. Introduction to food hydrocolloids. *Handbook of hydrocolloids.* Elsevier.

XU, F., LIAMAS, E., BRYANT, M., ADEDEJI, A. F., ANDABLO-REYES, E., CASTRONOVO, M., ETTELAIE, R., CHARPENTIER, T. V. & SARKAR, A. 2020. A self-assembled binary protein model explains high-performance salivary lubrication from macro to nanoscale. *Advanced Materials Interfaces,* 7**,** 1901549.

ZEMBYLA, M., LIAMAS, E., ANDABLO-REYES, E., GU, K., KROP, E. M., KEW, B. & SARKAR, A. 2021. Surface adsorption and lubrication properties of plant and dairy proteins: A comparative study. *Food hydrocolloids,* 111**,** 106364.

ZHANG, S., MURRAY, B. S., SURIYACHAY, N., HOLMES, M., ETTELAIE, R. & SARKAR, A. 2021. Synergistic interactions of plant protein microgels and cellulose nanocrystals at the interface and their inhibition of the gastric digestion of Pickering emulsions. *Langmuir,* 37**,** 827-840.

# Appendix A

# Supporting information for Chapter 3
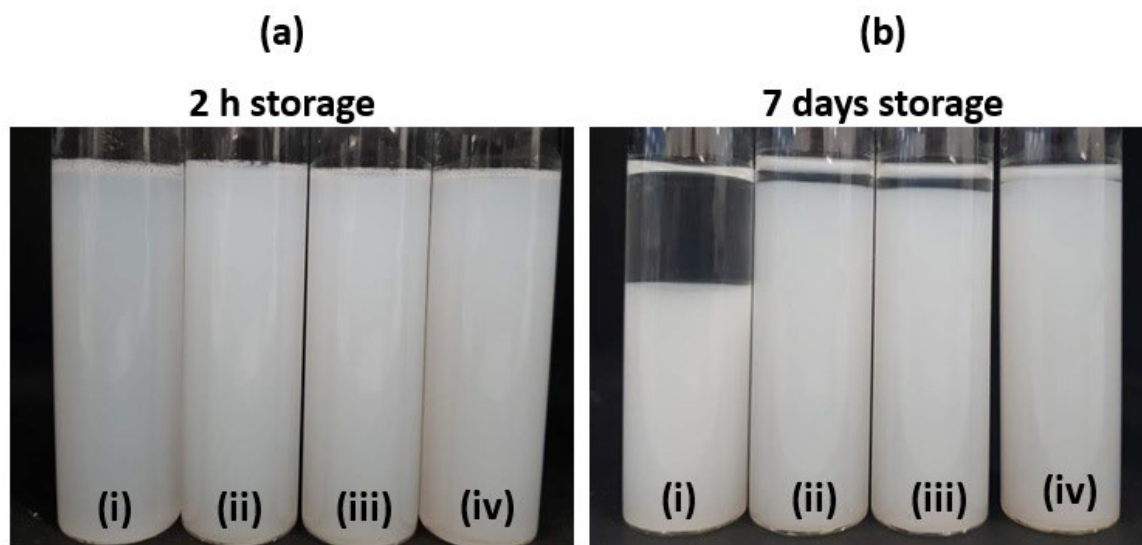


**Figure A1.** Visual iamges of 2.5 wt% CS1 + $\kappa$C mixtures containing (i) 0.025 wt% $\kappa$C, (ii) 0.05 wt% $\kappa$C, (iii) 0.15 wt% $\kappa$C, (iv) 0.25 wt% $\kappa$C after (a) 2 h and (b) 7 days of storage at ambient conditions.
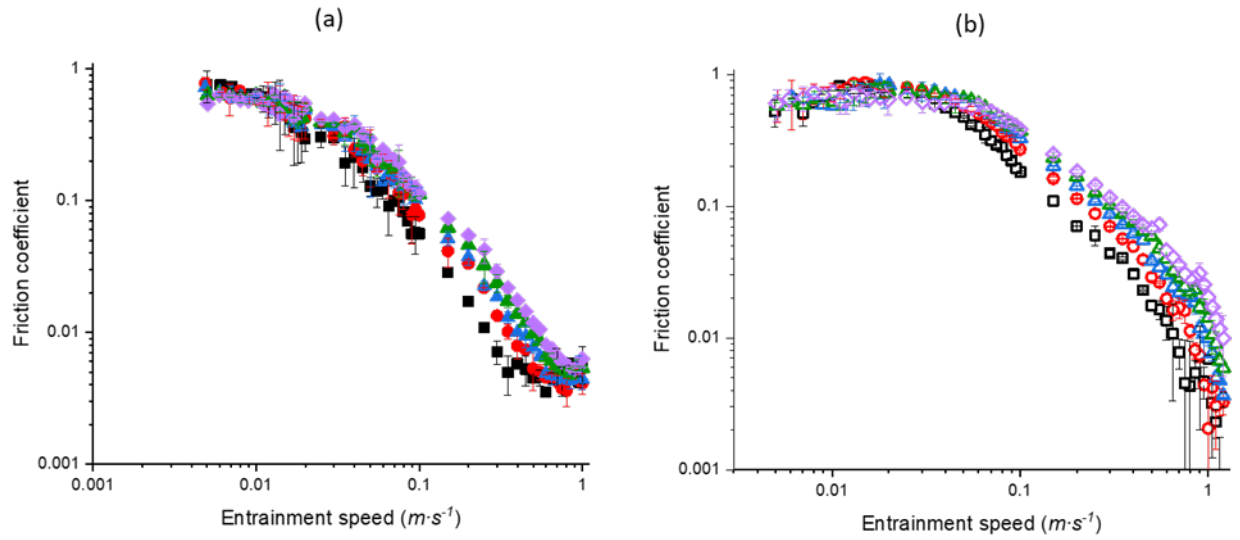
**Figure A2.** Friction coefficient ($\mu$) of (a) 0.5 wt% $\kappa$C (closed symbols) and (b) 5 wt% G-CS (open symbols) as a function of entrainment speed ($U$) at loads ranging from 1 (■, □), 2 (●, ○), 3 (▲, △), 4 (▼, ▽) to 5 (◆, ◇) N, respectively.

**Table A1.** Mean and standard deviation (SD) of the friction coefficients in the boundary and mixed regimes of $\kappa$C (a), CS1 (b), the $\kappa$C + CS1 mixtures with respective concentrations of $\kappa$C and CS1 (c) and the $\kappa$C + CS2 mixtures compared with $\kappa$C + CS1 mixtures with respective concentrations of $\kappa$C, CS1 and CS2 (d). Different lower case letters in the same column indicate a statistically significant difference ($p < 0.05$).

| (a) | Friction coefficient of $\kappa$C | | | | | |
|---|---|---|---|---|---|---|
| | Boundary lubrication regime (0.005 m s$^{-1}$) | | Mixed lubrication regime (0.05 m s$^{-1}$) | | Mixed lubrication regime (0.1 m s$^{-1}$) | |
| | Mean | SD | Mean | SD | Mean | SD |
| $\kappa$C 0.05 wt% | 1.0440[a] | 0.0400 | 0.9320[a] | 0.0710 | 0.4480[a] | 0.0400 |
| $\kappa$C 0.1 wt% | 1.0665[a] | 0.2000 | 0.3826[b] | 0.0013 | 0.0916[b] | 0.0116 |
| $\kappa$C 0.5wt% | 0.8514[a] | 0.0139 | 0.0486[c] | 0.0003 | 0.0128[bc] | 0.0011 |
| $\kappa$C 1.0wt% | 0.5053[b] | 0.1041 | 0.0107[c] | 0.0001 | 0.0294[bc] | 0.0232 |
| **(b)** | **Friction coefficient of CS1** | | | | | |
| | Boundary lubrication regime (0.005 m s$^{-1}$) | | Mixed lubrication regime (0.05 m s$^{-1}$) | | Mixed lubrication regime (0.1 m s$^{-1}$) | |
| | Mean | SD | Mean | SD | Mean | SD |
| CS1 0.5 wt% | 0.6486[a] | 0.1163 | 0.8137[a] | 0.0638 | 0.5009[a] | 0.0662 |
| CS1 1.0 wt% | 0.6907[a] | 0.0113 | 0.7859[a] | 0.1906 | 0.5552[ab] | 0.0617 |
| CS1 2.0 wt% | 0.4542[a] | 0.1291 | 0.6717[a] | 0.0307 | 0.3984[ac] | 0.0323 |
| CS1 3.0 wt% | 0.2015[b] | 0.0554 | 0.6221[a] | 0.0306 | 0.3637[ac] | 0.0186 |
| CS1 5.0 wt% | 0.1169[b] | 0.0099 | 0.1080[b] | 0.0345 | 0.0810[d] | 0.0394 |
| **(c)** | **Friction coefficient of 1.65 wt% $\kappa$C +CS1 mixtures with pure $\kappa$C or CS1** | | | | | |
| | Boundary lubrication regime (0.005 m s$^{-1}$) | | Mixed lubrication regime (0.05 m s$^{-1}$) | | Mixed lubrication regime (0.1 m s$^{-1}$) | |
| | Mean | SD | Mean | SD | Mean | SD |
| CS1 1.5 wt% + $\kappa$C 0.15 wt% | 0.9110[ab] | 0.0086 | 0.1598[b] | 0.0424 | 0.0351[b] | 0.0056 |
| CS1 1.5 wt% | 0.6907[a] | 0.0113 | 0.7859[a] | 0.1906 | 0.5552[a] | 0.0617 |
| $\kappa$C 0.15 wt% | 1.0665[b] | 0.2000 | 0.3826[b] | 0.0013 | 0.0916[b] | 0.0116 |
| **(d)** | **Friction coefficient of 2.75 wt% $\kappa$C +CS2 or 2.75 wt% $\kappa$C +CS1 mixtures with pure $\kappa$C or CS1 or CS2** | | | | | |
| | Boundary lubrication regime (0.005 m s$^{-1}$) | | Mixed lubrication regime (0.05 m s$^{-1}$) | | Mixed lubrication regime (0.1 m s$^{-1}$) | |
| | Mean | SD | Mean | SD | Mean | SD |
| CS1 2.5 wt% + $\kappa$C 0.25 wt% | 0.4973[a] | 0.1714 | 0.0444[a] | 0.0022 | 0.0149[a] | 0.0011 |
| CS2 2.5 wt% + $\kappa$C 0.25 wt% | 0.4389[a] | 0.0186 | 0.1405[a] | 0.0055 | 0.0664[a] | 0.0093 |
| CS1 2.5 wt% | 0.4542[a] | 0.1291 | 0.6717[b] | 0.0307 | 0.3984[b] | 0.0323 |
| CS2 2.5 wt% | 0.6907[ab] | 0.0104 | 0.7859[b] | 0.1361 | 0.5707[c] | 0.0270 |
| $\kappa$C 0.25 wt% | 0.9589[b] | 0.1036 | 0.2156[a] | 0.0007 | 0.0522[a] | 0.0061 |

**Table A2.** Mean and standard deviation (SD) of the apparent viscosity at 50 s$^{-1}$ shear rate of $\kappa$C (a), CS1 (b), the $\kappa$C + CS1 mixtures with respective concentrations of $\kappa$C and CS1 (c). Different lower case letters in the same column indicate a statistically significant difference ($p < 0.05$).

| (a) | Apparent viscosity of $\kappa$C | |
|---|---|---|
| | Shear rate (50 s$^{-1}$) | |
| | Mean | SD |
| $\kappa$C 0.05 wt% | 0.0011[a] | 0.0000 |
| $\kappa$C 0.1 wt% | 0.0011[a] | 0.0000 |
| $\kappa$C 0.5wt% | 0.0142[a] | 0.0003 |
| $\kappa$C 1.0wt% | 0.2466[b] | 0.0106 |
| **(b)** | **Apparent viscosity of CS1** | |
| | Shear rate (50 s$^{-1}$) | |
| | Mean | SD |
| CS1 0.5 wt% | 0.0008[a] | 0.0000 |
| CS1 1.0 wt% | 0.0017[a] | 0.0000 |
| CS1 2.0 wt% | 0.0025[a] | 0.0001 |
| CS1 3.0 wt% | 0.0210[b] | 0.0027 |
| CS1 5.0 wt% | 0.1137[c] | 0.0112 |
| **(c)** | **Apparent viscosity of 1.65 wt% $\kappa$C + CS1 mixtures and 2.75 wt% $\kappa$C + CS1 mixtures with pure $\kappa$C or CS1** | |
| | Shear rate (50 s$^{-1}$) | |
| | Mean | SD |
| CS1 1.5 wt% + $\kappa$C 0.15 wt% | 0.0244[a] | 0.0009 |
| CS1 1.5 wt% | 0.0021[b] | 0.0001 |
| $\kappa$C 0.15 wt% | 0.0078[c] | 0.0002 |
| CS1 2.5 wt% + $\kappa$C 0.25 wt% | 0.0808[d] | 0.0001 |
| CS1 2.5 wt% | 0.0211[a] | 0.0027 |
| $\kappa$C 0.25 wt% | 0.0150[e] | 0.0023 |

# Appendix B

# Supporting information for Chapter 5
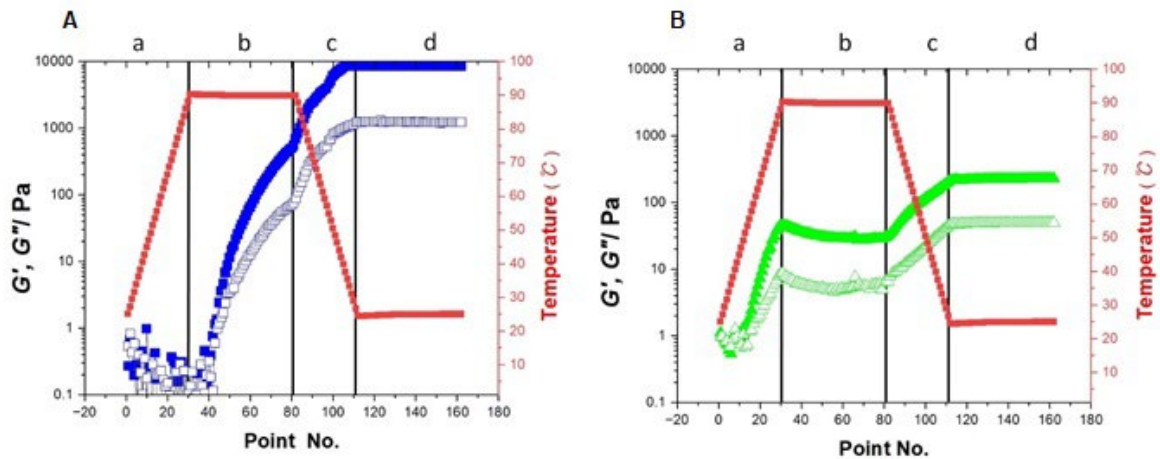


**Figure B1. Viscoelasticity during and after *in situ* gelation**. Development of viscoelastic parameters during thermal processing of 12.0 wt% whey protein (■) (A) and pea protein (■) (B) hydrogels. Closed symbols = *G'* and open symbols = *G''*. The different regions of the thermal processing cycle are heating a. from 25 to 90 °C at a rate of 0.08 °C/s, b. holding at 90 °C for 10 min, c.    cooling from 90 °C to 25 °C at a rate of 0.08 °C/s where a frequency sweeps of 0.1-100 rad/s at a strain of 0.1% was initialized, and d) holding at 25 °C for 10 min. The storage and loss moduli, G' and G", at 1 Hz are plotted against time.
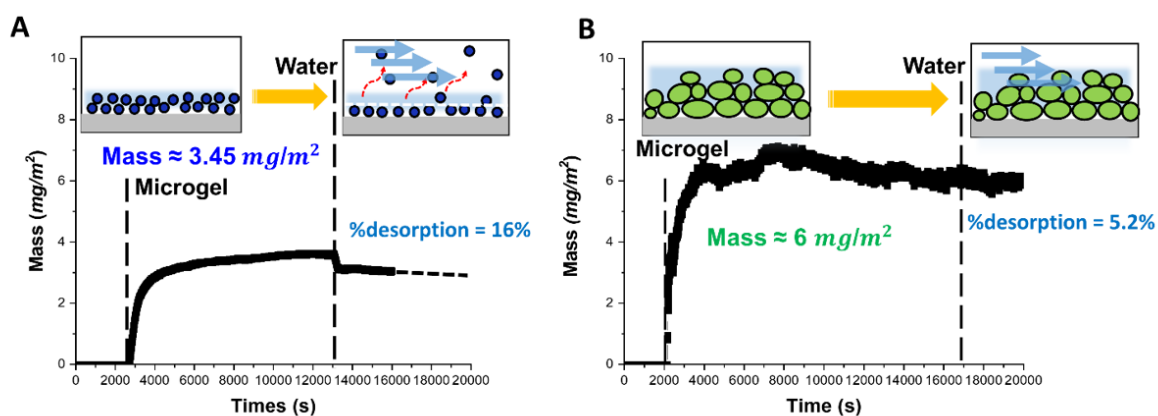
**Figure B2. Hydrated mass on hydrophilic gold sensor**. Hydrated mass of WPM (A) or PPM (B) once adsorbed onto gold surface with schematics showing the proposed adsorption and desorption of the adsorbed layers of microgels. WPM is shown in blue whilst and PPM is shown in green, the size and shape of the microgels are informed by the AFM, DLS and the rheology results. Mass is calculated by fitting to Voigt's viscoelastic model and %desorption is calculated based on desorption upon rinsing with water.
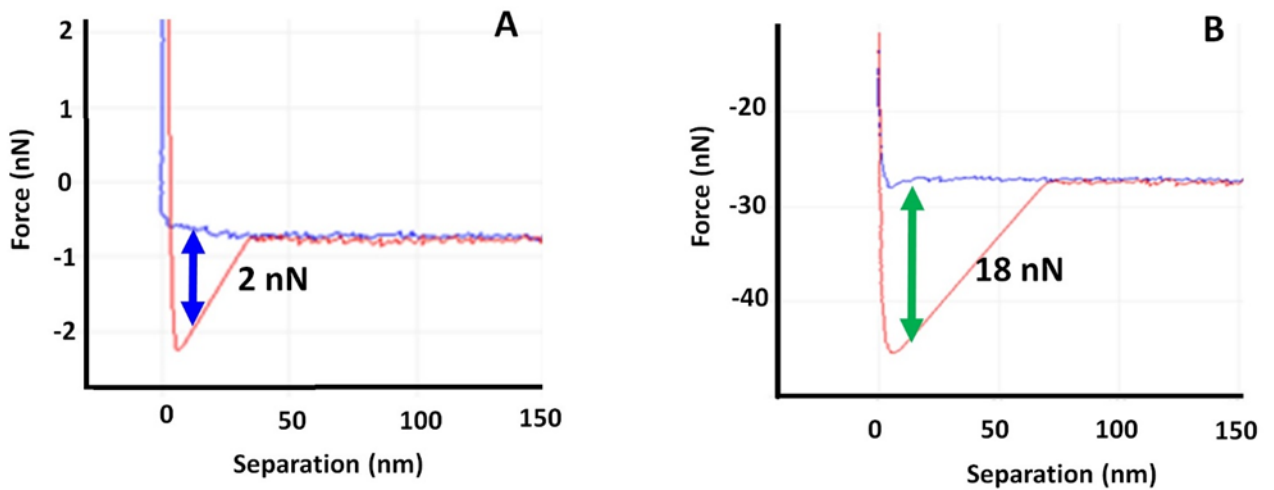
**Figure B3. Comparison of adhesion forces.** Characteristic force distance curves between the AFM cantilever tip and silicon surface in the presence of WPM (A) or PPM (B), respectively. Blue line represents the tip approaching the sample (Right-left), while the red line shows retraction (left-to-right).
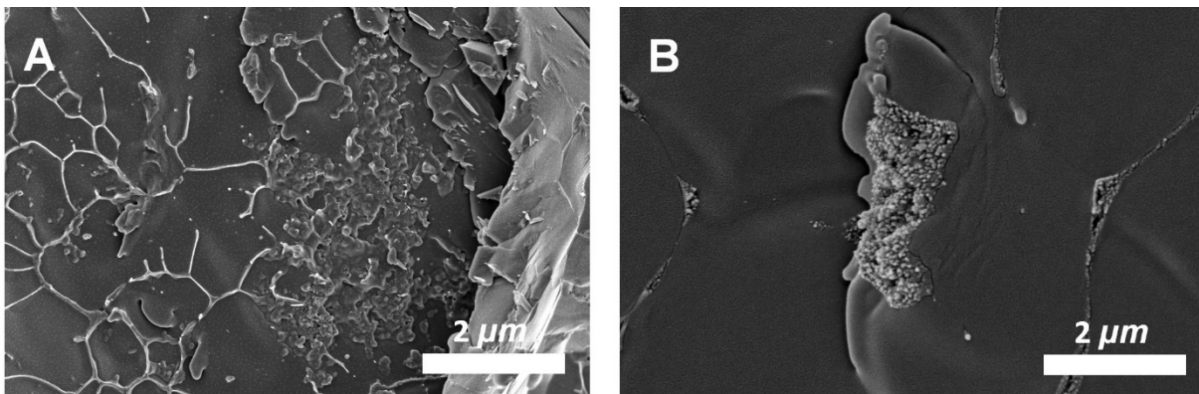
**Figure B4. Visualization of microgels at interface of W/W emulsions.** Cryo-SEM images showing the microstructure and morphology of 2.0 wt% GS + 0.2 wt% XG W/W emulsions with WPM (A) or PPM (B) at the interface.
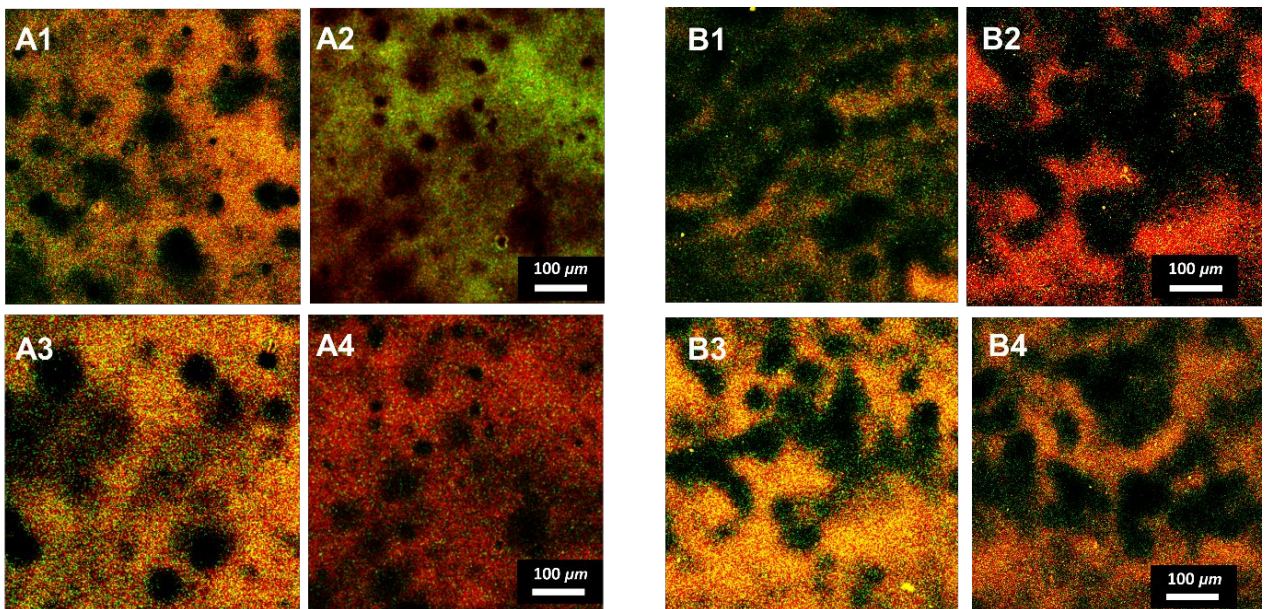
**Figure B5. Microstructure showing microgels at the surface of Pickering-like W/W emulsion droplets.** Additional CLSM micrographs of the 2.0 wt% GS + 0.2 wt% XG W/W emulsions stabilized by WPM (A1-A4) or PPM (B1-B4) at different areas of the sample. GS, WPM and PPM are fluorescently labelled by Rhodamine B ($\lambda \approx 546$ nm), Acridine Orange ($\lambda \approx 502$ nm), and Fast green ($\lambda \approx 633$ nm), respectively. Schematics show the corresponding droplets beside the CLSM images.
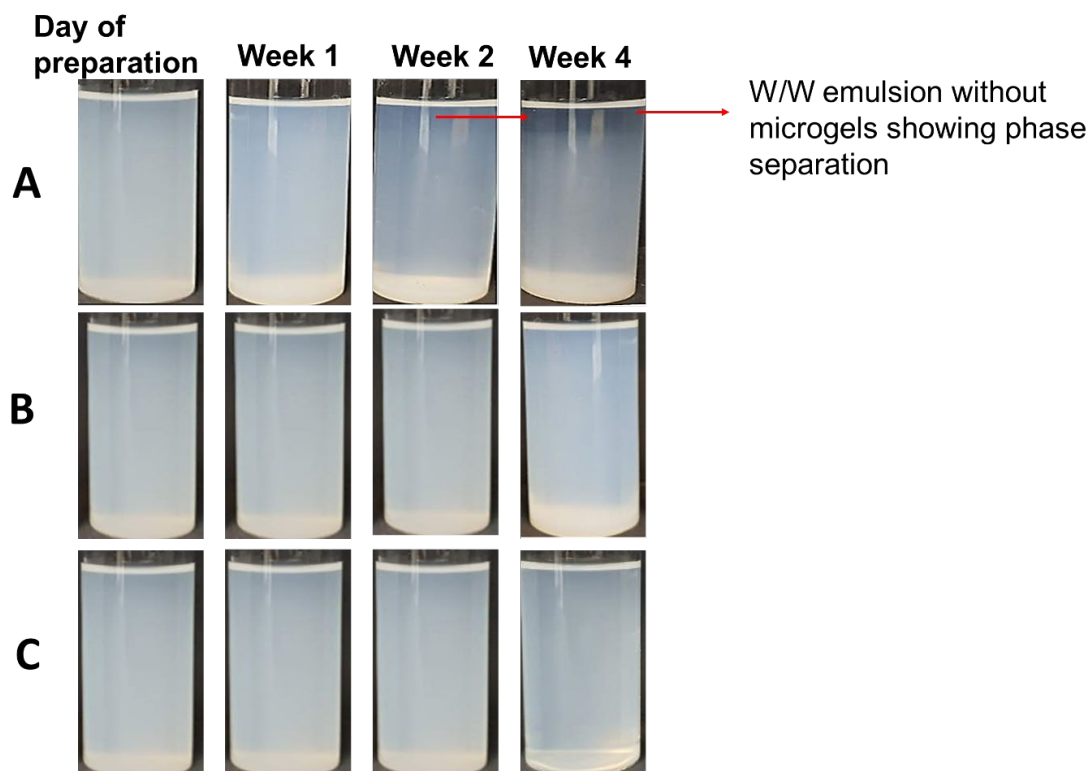
**Figure B6. Stability of Pickering-like W/W emulsions.** Visual appearance of W/W emulsions upon preparation and after 1, 2 and 4 weeks of storage containing 1 wt% starch +0.1 wt% XG (A), and the Pickering-like emulsion with 2.0 vol% WPM (B) or 2.0 vol% PPM (C). The W/W emulsions with microegls show phase separation within 2 weeks whereas the emulsions stabilized with WPM or PPM show no phase separation after 4 weeks of storage.

**Table B1. Statistical differences in friction coefficients.** Means and standard deviations (SDs) of friction coefficient of (A) WPM and PPM in Figure 3C, (B) 1.0 wt% GS + 0.1 wt% XG emulsion without or with WPM and PPM in Figure 6B1, and (C) 2.0 wt% GS + 0.2 wt% XG emulsion without or with PPM in Figure 6B2 at boundary, mixed and hydrodynamic regimes. Different lower case letters in the same column indicate a statistically significant difference (p < 0.05).

| (A) | Statistical differences in lubricity between WPM and PPM (Figure 3C) | | | | | |
|---|---|---|---|---|---|---|
| | Boundary lubrication regime | | Mixed lubrication regime | | Hydrodynamic lubrication regime | |
| | $(5\text{-}10 \text{ mm s}^{-1})$ | | $(80\text{-}100 \text{ mm s}^{-1})$ | | $(700\text{-}900 \text{ mm s}^{-1})$ | |
| | Mean | SD | Mean | SD | Mean | SD |
| MilliQ water | 1.298[a] | 0.0392 | 0.764[a] | 0.0035 | 0.030[a] | 0.0027 |
| 2.0 vol% WPM | 1.411[b] | 0.0292 | 0.134[b] | 0.0022 | 0.005[b] | 0.0011 |
| 2.0 vol% PPM | 0.505[c] | 0.0369 | 0.057[c] | 0.0082 | 0.005[b] | 0.0006 |
| (B) | Statistical differences in lubricity of 1.0 wt% GS + 0.1 wt% XG emulsions without or with microgels (Figure 6B1) | | | | | |
| | Boundary lubrication regime | | Mixed lubrication regime | | Hydrodynamic lubrication regime | |
| | $(5\text{-}10 \text{ mm s}^{-1})$ | | $(80\text{-}100 \text{ mm s}^{-1})$ | | $(700\text{-}900 \text{ mm s}^{-1})$ | |
| | Mean | SD | Mean | SD | Mean | SD |
| emulsion without microgels | 0.596[a] | 0.0257 | 0.079[a] | 0.0039 | 0.003[a] | 0.0005 |
| WPM-stabilized emulsion | 1.000[b] | 0.0728 | 0.078[a] | 0.0056 | 0.005[a] | 0.0010 |
| PPM-stabilized emulsion | 0.311[c] | 0.0348 | 0.056[b] | 0.0010 | 0.003[a] | 0.0015 |
| (C) | Statistical differences in lubricity of 3.0 wt% GS + 0.3 wt% κC emulsions without or with WPM (Figure 6B2) | | | | | |
| | Boundary lubrication regime | | Mixed lubrication regime | | Hydrodynamic lubrication regime | |
| | $(5\text{-}10 \text{ mm s}^{-1})$ | | $(80\text{-}100 \text{ mm s}^{-1})$ | | $(700\text{-}900 \text{ mm s}^{-1})$ | |
| | Mean | SD | Mean | SD | Mean | SD |
| emulsion without microgels | 0.337[a] | 0.0460 | 0.036[a] | 0.0026 | 0.004[a] | 0.0006 |
| WPM-stabilized emulsion | 0.531[b] | 0.0600 | 0.041[a] | 0.0020 | 0.005[a] | 0.0005 |
| PPM-stabilized emulsion | 0.214[c] | 0.0265 | 0.018b[b] | 0.0005 | 0.004[a] | 0.0008 |